THE UNIVERSITY *of* EDINBURGH

Understanding the balance between osteogenesis and bone marrow adipogenesis in the aetiology of bone disease in experimental chronic kidney disease

WORACHET PROMRUK

This thesis is presented for the degree of Doctor of Philosophy at The University of Edinburgh

Doctor of Philosophy – The University of Edinburgh – 2025

Declaration

I hereby declare that this thesis represents an original account of my research and has been composed entirely by me. It has not been submitted, either in whole or in part, for any previous academic degree or professional qualification. All experimental work presented in this thesis was carried out by me unless otherwise stated.

The proteomic data described in Chapter 5 were generated through experiments conducted in collaboration with Chartinun Chutoe and Professor Alexander von Kriegsheim at the Edinburgh Cancer Research UK Centre, Institute of Genetics and Cancer, University of Edinburgh. I played a principal role in the design, preparation, and execution of these experiments, while the subsequent data analysis and interpretation were performed independently by me. Any collaborative inputs, including technical calibration and experimental assistance, have been fully acknowledged and appropriately referenced as detailed in the associated publication.

All sources of information, data, and ideas from the work of others have been properly cited and acknowledged throughout this thesis.

Worachet Promruk

November, 2025

Acknowledgement

I would like to sincerely express my gratitude to my best supervisor, Professor Colin Farquharson, who has greatly supported, encouraged and mentored me throughout my PhD. I also thank my co-advisors, Dr William Cawthorn, Prof. Katherine Staines, and Dr Louise Stephen, who have helped shape me and provided incredible and valuable guidance. I have learned so much from this degree, and all these experiences will be beneficial for my future career.

My thanks also to all members in Farquharson's lab, including Lewis Shun-Neng Hsu, a previous lovely PhD student who has helped me during my first year, Dr Soher Jayash, a generous core scientist who has helped me lots throughout my PhD, Aine Pears, Charlotte Clews, and Rachel Wade have been more than just lab mates; they have fulfilled my ideal PhD experience and provided constant mental support throughout my PhD, especially during all the wine nights and various activities we've shared. I would also like to thank all the kind and helpful staff at the Roslin Institute building who provided me with excellent technical support and valuable assistance over these four years, including Heather Warnock, Lee McManus, Kanchan Phadwal, Lucie Bourne, Colin Wood, Anna Raper, Paul Tang, Kuan-Chan Chen, April Tan, and Donald Dunbar.

Moreover, I would like to thank all my mental supporters and dear friends throughout my PhD journey, including Pla, Plern, Parusk, Mild, Piano, Sun, Eye, Nattapong, Art, Mac, Nui, and Keng—special thanks to Mild (Chartinun), who has helped and collaborated with me on my paper. I would also like to express my appreciation to those who have been my Edinburgh family, supporting me both physically and mentally, including Auntie Chu, KhunMae Pom, Khun Len, Auntie Gay, and all the staff at Nok's Kitchen.

Furthermore, I truly appreciate my family—super grandpa, super mum, beloved brother and sister-in-law, and my lovely niece and nephew—as well as my aunties, who always support me unconditionally. More importantly, I cherish my beloved partner, Sutipong Jongrak (MyTonhom), who consistently supports me both physically and mentally, encouraging me to pursue this dream and standing by my side in every situation I have faced.

Abstract

Chronic kidney disease–mineral and bone disorder (CKD-MBD) involves irreversible renal impairment that disrupts mineral balance and leads to skeletal complications collectively known as renal osteodystrophy (ROD). Increased bone marrow adipose tissue (BMAT) is a consistent feature in both patients and animal models of CKD, although its regulation remains unclear. Elevated levels of the Wnt signalling inhibitors sclerostin and dickkopf-1 (DKK1) have been implicated, as they suppress osteogenesis while promoting adipogenesis.

This study examined the relationship between BMAT accumulation and bone structure in CKD, with a focus on whether disease progression alters bone marrow mesenchymal stromal cell (BMSC) fate commitment to osteogenic or adipogenic precursors and their subsequent differentiation into mature osteoblasts or adipocytes. I further examined the effects of CKD-related factors—including parathyroid hormone (PTH), fibroblast growth factor 23 (FGF23), phosphate, sclerostin, and indoxyl sulfate—on BMSC differentiation. Furthermore, I evaluated whether dual inhibition of sclerostin and DKK1 with a bispecific antibody could prevent bone loss and limit BMAT expansion in a CKD mouse model.

Eight-week-old male C57BL/6J mice were fed a 0.2% adenine-supplemented diet for up to 5-weeks to induce CKD, while control mice received the same diet without adenine. CKD onset was confirmed by elevated plasma blood urea nitrogen, creatinine, PTH and FGF23 from week 3. After 5-weeks, trabecular bone mineral density and microarchitecture were significantly reduced, and cortical bone area and thickness declined as early as week 3. BMAT in the proximal tibia increased progressively, showing a significant rise by week 5 and was negatively correlated with trabecular bone volume. In early CKD (weeks 1–2), BMSCs exhibited greater adipogenic capacity, although the proportions of osteogenic and adipogenic progenitors were unchanged. *In vitro*, low doses of PTH enhanced osteogenesis, while indoxyl sulfate impaired both osteogenic and adipogenic differentiation; FGF23, phosphate, and sclerostin had no direct effects. Treatment with a bispecific antibody targeting sclerostin and DKK1 for 6-

weeks improved trabecular and cortical bone parameters and prevented BMAT expansion in CKD mice.

In summary, BMAT accumulation during CKD progresses with disease duration and is not driven by early changes in precursor populations. Systemic CKD factors may modulate stromal cell fate over time, and dual inhibition of sclerostin and DKK1 represents a potential therapeutic strategy for the maintenance of bone health in CKD-MBD.

Lay summary

Chronic kidney disease (CKD) not only affects the kidneys but also disrupts the body's mineral balance, leading to bone loss that has been called as renal osteodystrophy. One striking feature seen in both CKD patients and animal studies is the build-up of fat inside the bone marrow, called bone marrow adipose tissue (BMAT). BMAT develops from bone marrow stromal cells and is found inside bones. It exists in a stable form located mainly in the fatty (yellow) marrow and a more flexible form found in the blood-forming (red) marrow. The flexible form can increase with ageing and metabolic condition such as cancer, obesity and caloric restriction. However, why bone marrow fat accumulates in CKD and how it affects bone health are not fully understood. In this study, I examined how bone marrow fat changes as CKD progresses and how this relates to bone loss. I also investigated whether substances that accumulate in the blood during CKD — including parathyroid hormone (PTH), fibroblast growth factor 23 (FGF23), phosphate, sclerostin, and indoxyl sulfate — influence how bone marrow stromal cells develop into bone-forming cells or fat cells. Finally, I tested whether blocking two proteins that inhibit bone formation and found increased in CKD, sclerostin and DKK1, could protect bone loss in mice with CKD. Using adenine-induced CKD mouse model, I found that bone marrow fat increased over time and appeared before bone loss. In early CKD, bone marrow cells were more likely to develop into fat cells, although the overall balance of precursor cells remained unchanged. Laboratory experiments showed that low levels of PTH supported bone formation, while indoxyl sulfate impaired both bone and fat cell development. Other CKD substances tested had no effect. Importantly, treatment with an antibody that blocks both sclerostin and DKK1 improved bone strength and prevented fat accumulation in the bone marrow. These findings suggest that BMAT expansion in CKD is linked to disease progression and circulating factors in the blood. Targeting sclerostin and DKK1 may offer a promising strategy to protect bone health in CKD.

Publications

Promruk W, Cawthorn WP, Bourne LE, Jayash SN, Pears A, Staines KA, Stephen LA and Farquharson C (2025) Bone marrow adipose tissue expansion and bone loss in experimental chronic kidney disease is independent of altered bone marrow stromal cell lineage determination. *Front. Endocrinol*. 16:1666681. doi: 10.3389/fendo.2025.1666681

Jayash SN, Duff T, Tanveer Q, **Promruk W**, Farquharson C (2025) Osteoblasts sense extracellular levels of phosphate to control the local expression of phosphatases for matrix mineralisation. *Bone Rep*. 30;26:101863. doi: 10.1016/j.bonr.2025.101863.

Worachet Promruk, Soher N Jayash, Chartinun Chutoe, Hua Zhu Ke, Xiaofeng Liu, Alexander von Kriegsheim, William P Cawthorn, Katherine A Staines, Louise A Stephen, Colin Farquharson. Bispecific antibody against sclerostin and DKK1 improves bone health and reduces bone marrow adipose tissue accumulation in experimental chronic kidney disease. https://doi.org/10.21203/rs.3.rs-7788058/v1 Under review for *Bone Research* (Submitted)

Invited talk

Worachet Promruk, William P Cawthorn, Katherine A Staines, David Ke, Xiaofeng Liu, Louise Stephen, Colin Farquharson. Bispecific antibody for sclerostin and DKK1 improves bone health and prevent bone marrow adipose tissue accumulation in chronic kidney disease mouse model. Bone Research Society Annual Meeting, U.K, July 2025.

Abbreviations

3D	Three-dimensional
ABM	Adipocyte basal medium
ACN	Acetonitrile
ACP	Amorphous calcium phosphate
AD	Adynamic bone disease
AD	Adynamic bone disease
AGC	Automatic gain control
AGEs	Advanced glycation end-products
AhR	Aryl hydrocarbon receptor
AIM	Adipocyte induction medium
ALP	Alkaline Phosphatase
ANK	Ankylosis protein
ANOVA	Analysis of variance
APC	Adipogenic progenitor cell
ARS	Alizarin red staining
ATP	Adenosine triphosphate
BMAT	Bone marrow adipose tissue
BMD	Bone mineral density
BMPs	Bone morphogenetic proteins
BMSCs	Bone marrow stomal cells
BRC	Bone remodelling compartment
BSA	Bovine serum albumin
BUN	Blood urea nitrogen
BV/TV	Bone volume/tissue volume
C/EBP	CCAAT/enhancer binding protein
Ca^{2+}	Calcium ion
CaSR	Calcium-sensing receptor
cBMAT	Constitutive BMAT
cDNA	Complementary DNA
CKD	Chronic kidney disease
CKD-MBD	CKD–mineral and bone disorder
CR	Caloric restriction
CS	Calf serum
CXCL1	C-X-C motif chemokine ligand 1
dH2O	Distilled water
DKK1	Dickkopf
DMEM	Dulbecco's Modified Eagle Medium
DMSO	Dimethyl sulfoxide
dNTP	Deoxyribonucleotide triphosphate

E.Pm	Endosteal perimeter
ECM	Extracellular matrix
EDTA	Ethylenediaminetetraacetic acid
eGFR	Estimated glomerular filtration rate
ELISA	Enzyme-linked immunosorbent assay
ENPP1	Ectonucleotide pyrophosphatase/phosphodiesterase-1
FBS	Foetal bovine serum
FGF23	Fibroblast growth factor 23
FMO	Fluorescence minus one
GC	Glucocorticoids
GP to T/F J	Growth plate to tibia/fibula junction
GSEA	Gene Set Enrichment Analysis
gWAT	Gonadal WAT
IBMX	3-isobutyl-1-methylxanthine
IGF-1	Insulin-like growth factor-1
IS	Indoxyl sulfate
iWAT	Inguinal WAT
KDIGO	The Kidney Disease Improving Global Outcomes
LCN	Lacunae-canalicular network
LepR	Leptin receptor
M	Mineralisation
M-CSF	Monocyte/macrophage colony-stimulating factor
Med.Ar	Medullary area
MMI max	Maximum moment of inertia
MMI min	Minimum moment of inertia
MS	Mass spectrometry
MUO	Mixed uremic osteodystrophy
MV	Matrix vesicle
n	Number
NACWO	Named animal care and welfare officer
NBF	Neutral-buffered formalin
NF-κB	Nuclear factor κB
NFATc1	Nuclear factor of activated T-cells 1
NVS	Named veterinary surgeon
OCN	Osteocalcin
ocSSC	Osteochondrogenic SSC
OF	Osteitis fibrosa
OM	Osteomalacia
OPC	Osteochondrogenic progenitor cell
OPG	Osteoprotegerin

OPN	Osteopontin
ORO	Oil red O
P.Pm	Periosteal perimeter
P/S	Penicillin/streptomycin
PBS	Phosphate-buffered saline
PCS	p-cresyl sulfate
Pdgfrα	Platelet-derived growth factor α
Pi	Phosphate
Ppar	Peroxisome proliferator-activated receptor
PPi	Pyrophosphate
Proxi Epi	Top of the proximal bone to the growth plate
PTH	Parathyroid hormone
PTH1R	PTH receptor 1
pvSSC	Perivascular SSC
qPCR	Quantitative polymerase chain reaction
RANKL	Receptor activator of nuclear factor κB (NF-κB) ligand
rBMAT	Regulated BMAT
rbsAb	Sclerostin/Dkk1 antibody
ROD	Renal osteodystrophy
S.E.M.	Standard error of the mean
Sca1	Stem cell antigen-1
Scl-Ab	Sclerostin antibody
scRNAseq	Single-cell RNA sequencing
SHPT	Secondary hyperparathyroidism
SMAD	SMA and MAD protein
***Sost*$^{-/-}$**	*Sost*-deficient
SSC	Skeletal stem cell
T	Bone turnover
T/F J to End	Tibia/fibula junction to the end of the distal bone
Tb	Trabecular
Tb. Conn Dn	Trabecular connectivity density
Tb. N	Trabecular number
Tb. Sp	Trabecular separation
Tb. Th	Trabecular thickness
TD NMR	Time-Domain Nuclear Magnetic Resonance
TFA	Trifluoroacetic acid
TFEB	Transcription Factor EB
TGF-β	Transforming growth factor - beta
TNAP	Tissue non-specific alkaline phosphatase
V	Bone volume

VOI	Volume of interest
WAT	White adipose tissue
αMEM	Minimum essential medium alpha
βGP	β-glycerophosphate
μCT	Micro computed tomography

Contents

List of Figures

List of Tables

Chapter 1

Introduction and Background

1.1. Chronic Kidney Disease (CKD)

1.1.1. Definition, diagnosis and cause of CKD

Chronic Kidney Disease (CKD) is characterised by longstanding damage to the structural and/or functional aspects of the kidneys. Structural anomalies encompass tumours, cysts, and any congenital malformations detectable via imaging techniques. An alternative operational definition of CKD involves an estimated glomerular filtration rate (eGFR) of less than 60 mL/min/1.73 m² persisting for over three months. Such alterations diminish the kidneys' capacity to excrete waste products from the bloodstream (Webster et al., 2017), which can typically be identified through elevated serum creatinine and blood urea nitrogen (BUN) levels. In advanced cases, proteins such as albumin may be detectable in the urine of CKD patients. The Kidney Disease Improving Global Outcomes (KDIGO) guidelines categorise CKD patients into various stages based on estimated eGFR and the degree of albuminuria (Figure 1.1). These parameters are employed for classification because eGFR serves as a reliable indicator of renal filtration efficiency, while albuminuria indicates glomerular barrier dysfunction. These two metrics are inversely correlated and provide dependability in CKD staging (Charles & Ferris, 2013).

CKD results from various causes that share common pathological processes, including glomerulosclerosis, tubulointerstitial fibrosis, ongoing inflammation, and progressive nephron loss. Diabetes mellitus, the leading global reason for CKD, causes kidney damage through chronic hyperglycaemia, the formation of advanced glycation end-products (AGEs), glomerular hyperfiltration caused by altered SGLT2-mediated sodium handling, podocyte loss, and transforming growth factor - beta (TGF-β)–triggered extracellular matrix protein accumulation and mesangial expansion (Alicic et al., 2017; Chagnac et al., 2019; Kumar Pasupulati et al., 2016; Schena & Gesualdo, 2005). Hypertension, the second most common cause, leads to glomerular damage by raising intraglomerular pressure, causing vascular remodelling, renal ischemia, and activating the renin–angiotensin–aldosterone system. This activation increases oxidative stress, inflammation, and fibrosis in the kidney (Arendshorst et al., 2024; Costantino et al., 2021; Sun et al., 2020). Although these conditions originate differently, they eventually activate

similar pathways leading to nephron loss and fibrosis. The diseased kidney results in mineral imbalance leading to a myriad of hormonal changes in an attempt to restore physiological levels of calcium and phosphate (Pi). This manifestation of CKD is referred to as CKD–mineral and bone disorder (CKD-MBD) (Bello et al., 2017) and can lead to cardiovascular disease, bone loss and the accumulation of bone marrow adipose tissue (Badr et al., 2023; Woods et al., 2018). The bone loss and the accumulation of bone marrow adipocytes are the main focus of this study.

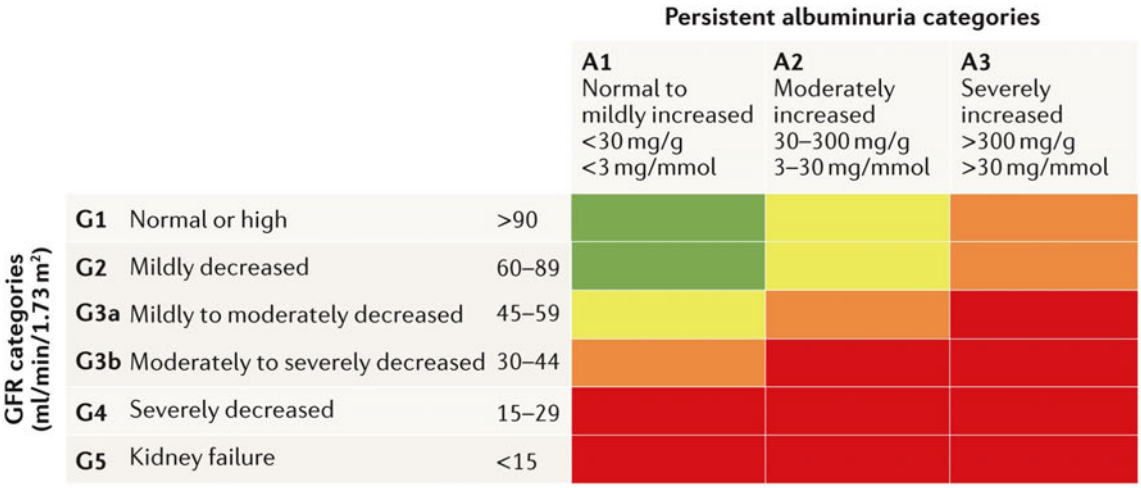

Figure 1.1. KDIGO classifies several stages of CKD, followed by decreased GFR and the amount of albumin found in urine. Different colours represent different risks of kidney dysfunction: green is low risk, yellow is moderately increased risk, orange is high risk, and red is very high risk. (Romagnani et al., 2017).

1.1.2. Impact of CKD on the incidence of osteopenia/osteoporosis

A systematic study revealed that 697.5 million people worldwide, especially those in the ageing population, suffer from CKD, and 1.2 million died with CKD complications in 2017 (Bikbov et al., 2020). Moreover, the mortality rate has been predicted to increase by 2.2 million by 2040 (Bikbov et al., 2020). Progressive loss of kidney function leads to disturbances in mineral metabolism resulting in hyperphosphatemia, secondary hyperparathyroidism and increased fibroblast growth factor 23 (FGF23) levels (Moe et al., 2006) (section 1.1.4). These changes in circulating factors are recognised indicators

for the diagnosis of CKD-MBD which can lead to cardiovascular disease including ectopic mineralisation and skeletal complications (Fang et al., 2014).

Currently, the incidence of osteopenia and osteoporosis in CKD patients (aged 18 years-of-age and over), is 45.91% and 23.29%, respectively, in both developed and developing countries (Tariq & Sulaiman, 2020). In addition, the progression of CKD together with ageing increases the incidence of fracture 5-fold compared to non-CKD individuals (Naylor et al., 2015). Moreover, sex also affects the incidence of fracture in CKD patients which is two-fold higher in women than in men (Pimentel et al., 2021). Skeletal abnormalities in patients with CKD are a global problem that needs to be addressed. The increased fracture risk leads to poor life quality and potentially death in the ageing population. In addition, the financial burden to health services is high and therefore further mechanistic insight into the aetiology of the low bone mass observed in CKD is required in order that preventative treatments can be identified (Kemmak et al., 2020).

1.1.3. Type of bone manifestation of CKD-MBD

The skeletal defects associated with CKD-MBD, commonly known as renal osteodystrophy (ROD), are classified based on a system that assesses bone turnover (T), mineralisation (M), and bone volume (V) - collectively called TMV (Ott, 2008). Turnover indicates the normal rate of bone remodelling, which involves evaluating bone formation and resorption. Bone volume measures the amount of bone in a given volume, while mineralisation refers to how osteoid/collagen becomes calcified during bone formation. The TMV classification system helps identify several types of bone abnormalities as follows (Figure 1.2, (Moe et al., 2006)):

- Adynamic bone disease (AD) is characterised by low bone turnover with normal mineralisation and reduced bone volume. It usually results from excessive suppression of parathyroid hormone (PTH), often caused by overuse of calcium-based phosphate binders, vitamin D analogues, or calcimimetics. Histologically, it shows minimal osteoblastic activity and decreased osteoid and bone formation rates, contributing to fragile bones (Bover et al., 2014; Moe et al., 2006).

- Osteitis fibrosa (OF) features high bone turnover with normal mineralisation, and bone volume varies depending on the disease duration. It is usually caused by elevated PTH levels, as observed in secondary hyperparathyroidism (SHPT) in CKD patients. Histologically, it shows increased osteoclastic and osteoblastic activity, resulting in woven bone and marrow fibrosis (Aguilar et al., 2023; Hruska et al., 2017; Moe et al., 2006)
- Osteomalacia (OM) is mainly a problem with bone mineralisation. Bone volume can vary from low to medium based on the severity, duration, and other influences on bone health. It often results from low vitamin D levels, aluminium toxicity, or specific medications. Under the microscope, it presents as a buildup of unmineralised bone matrix (osteoid) with inadequate calcium and Pi deposition, causing the bones to soften (Moe et al., 2006)
- Mixed uremic osteodystrophy (MUO) is characterised by both high bone turnover, known as osteitis fibrosa, and defective mineralisation (osteomalacia). Microscopically, it presents a complex bone pathology with both increased bone resorption and impaired mineralisation occurring at the same time (Moe et al., 2006).
- Mild hyperparathyroid-related bone disease is categorised separately, but it actually encompasses a spectrum of abnormalities along a continuum of medium to high turnover, with bone volume depending on disease duration (Moe et al., 2006).

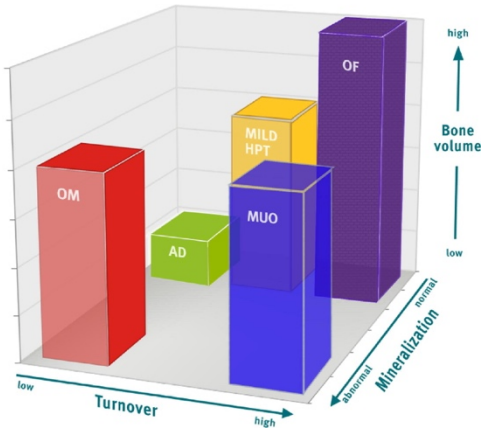

Figure 1.2. The TMV classification system for bone histomorphometry. This visual example demonstrates how the TMV system offers more detailed information compared to traditional classification methods. Each axis corresponds to a specific descriptor within the TMV system: turnover rate (ranging from low to high), mineralization status (from normal to abnormal), and bone volume (from low to high) (Moe et al., 2006).

1.1.4. Altered bone metabolism in response to CKD

The cause of the disordered bone metabolism in CKD-MBD is complex and not completely understood. Several organs are involved in the aetiology of the disease, including bone, parathyroid gland, gut and kidneys. A decrease in renal function in CKD leads to serum Pi accumulation or hyperphosphatemia. The effects of hyperphosphatemia on bone structure and integrity are poorly understood, but an association between a high level of Pi and risk of fracture in CKD patients has been reported (Block et al., 2004; Campos-Obando et al., 2017). Furthermore, the increased serum Pi concentration enhances the production of FGF23 by osteocytes in an attempt to maintain Pi homeostasis through increased Pi excretion in the urine (phosphaturia) (Prié et al., 2009) since FGF23 is known to enhance Pi excretion (Courbebaisse & Lanske, 2018; Gattineni et al., 2009). This compensation leads to elevated FGF23 levels, which can promote bone loss by several diverse mechanisms. FGF23 can indirectly induce bone loss in CKD-MBD by inducing the expression of sclerostin and Dickkopf (DKK1), recognised inhibitors of the Wnt-signalling pathway, which is critical for osteoblast differentiation and bone formation (Carrillo-López et al., 2016). Moreover, it has been reported that circulating sclerostin and osteocyte sclerostin expression are increased in CKD patients (Hernandez et al., 2018). Additionally, FGF23 can inhibit the production of calcitriol (1,25-dihydroxycholecalciferol), the active form of vitamin D in the kidneys leading to a decrease in calcium and Pi absorption in the intestine (Dhayat et al., 2016). In addition, nephron damage/loss in CKD can also result in decreased calcitriol production (Gal-Moscovici & Sprague, 2007). The nephron is a source of 1alpha hydroxylase enzyme, which is responsible for converting the inactive vitamin D precursor 25-dihydroxycholecalciferol to active calcitriol (Mac Way et al., 2012).

The resulting hypocalcaemia, stimulates the production of PTH, resulting in SHPT. SHPT contribute to bone loss by increasing bone resorption and decreasing bone formation (Hruska et al., 2017). Several clinical and experimental studies have reported that SHPT in CKD is positively correlated to fracture risk, which is caused by decreased cortical bone mass and density rather than defects to the trabecular bone (Jadoul et al., 2006; Marques et al., 2017; Nickolas et al., 2013). However, other studies have reported

trabecular and cortical bone defects prior to the onset of SHPT (Bacchetta et al., 2010; Metzger et al., 2020). The role of SHPT in the high bone turnover phase of ROD is well recognised, but uremic toxins such as indoxyl sulfate (IS), which accumulate in the blood of CKD patients, are linked to the earlier, low bone turnover phase of ROD characterised by skeletal PTH resistance, as shown in Figure 1.3 (Hsu et al., 2020). Evidence indicates that IS directly inhibits bone formation by reducing osteoblast Wnt/β-catenin signalling (W. C. Liu et al., 2018; Nii-Kono et al., 2007; Watanabe et al., 2017). Moreover, IS affects ROD through effects on mitochondrial dysfunction and mitophagy in osteocytes, which can be mitigated with antioxidants and charcoal absorption (Hsu et al., 2025). Similar mitochondrial abnormalities are seen in other bone diseases such as osteoporosis (Behera et al., 2022; Yan et al., 2023). The evidence also indicates that very low serum PTH levels are associated with adynamic bone disease and a higher risk of fractures (Coco & Rush, 2000; Massy & Drueke, 2017). This growing body of evidence suggests that low bone turnover is the primary type of ROD in the early stages of CKD, representing an optimal window for implementing targeted therapies (Massy & Drueke, 2017).

Bone marrow adipose tissue (BMAT) expansion has been observed in various skeletal syndromes and ageing, and it has also been detected in ROD (Hardouin et al., 2016; Hosain & Clinkenbeard, 2024; Li & Rosen, 2023; Woods et al., 2018). The exact mechanisms are not fully understood but may involve Wnt/β-catenin signalling, which can enhance adipogenesis and the expression of adipocyte-specific genes in white adipose tissue (de Winter & Nusse, 2021; Okamura et al., 2009). Recent clinical and preclinical studies agree that BMAT increases in CKD and correlates with disease severity, while showing an inverse relationship with bone mass and quality indices (Hosain & Clinkenbeard, 2024; Moorthi et al., 2015; Woods et al., 2018). However, the limitation of most previous studies is that they were cross-sectional, investigated bone health only at the end of the study, and were unable to monitor the temporal progression of bone loss in CKD-MBD. Accordingly, to observe the temporal pathophysiology of bone in CKD, longitudinal studies are required.

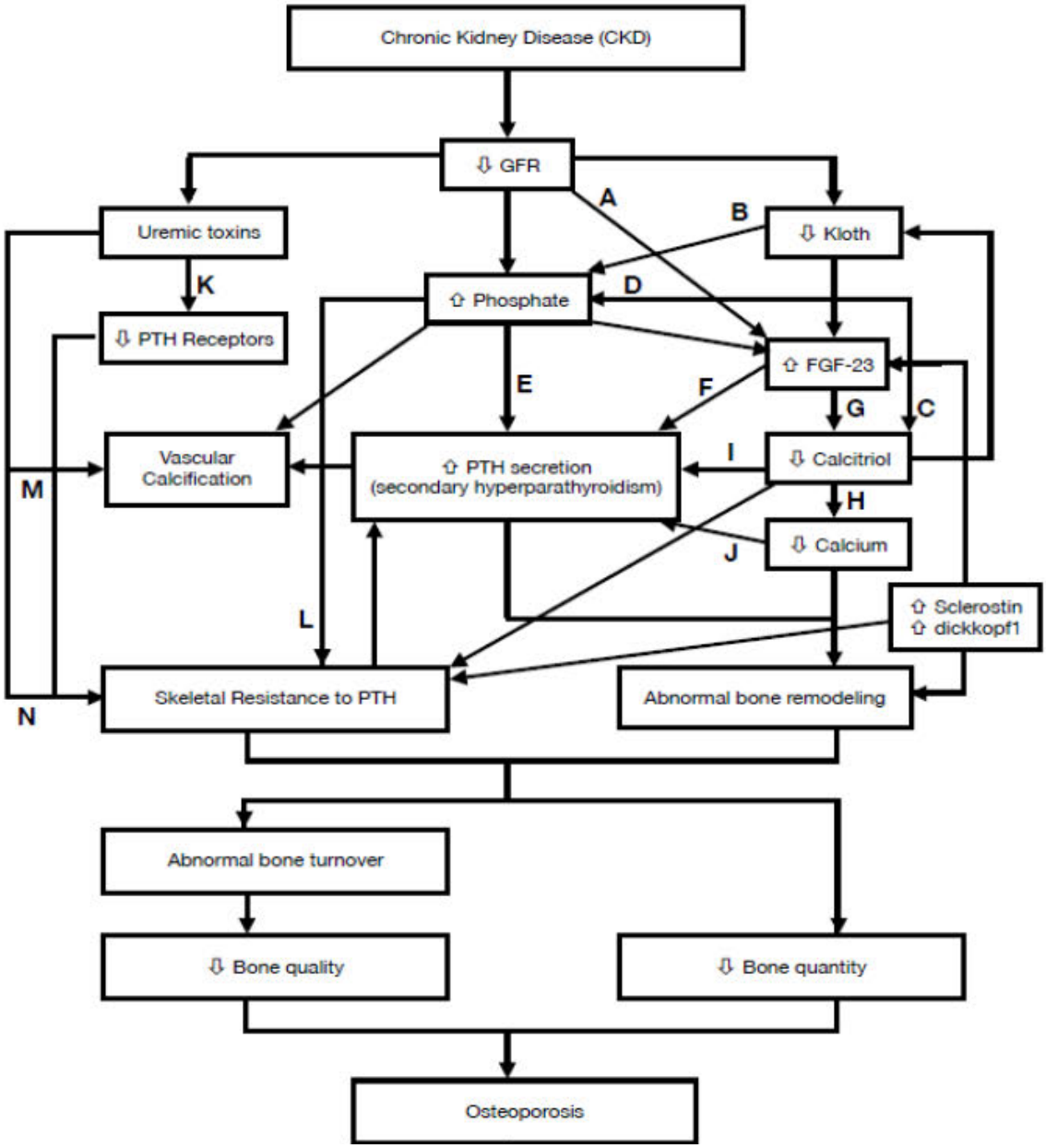

Figure 1.3. The summary of possible CKD mechanisms that contribute to bone loss or osteoporosis. The mechanism involves multiple steps: (A) decreased clearance of FGF23; (B) reduced phosphaturic effect of FGF23; (C) inhibition of 1α-hydroxylase in the proximal tubule of the kidney; (D) increased renal tubular Pi resorption; (E) induction of hypocalcemia, decreased calcitriol levels, increased PTH gene expression, and PTH secretion; (F) diminished inhibitory effect due to reduced FGFR1 and kloth protein; (G) further inhibition of 1α-hydroxylase; (H) reduced intestinal calcium absorption and decreased calcium release from bone; (I) lowered number of VDRs in parathyroid cells, weakening its inhibitory effect on the parathyroid gland; (J) increased PTH mRNA levels and decreased expression of calcium-sensing receptor (CaSR) in the parathyroid; (K)

indoxyl sulfate reduces PTH1 receptor expression; (L) Pi and calcium precipitate physicochemically, potentially causing skeletal resistance to PTH; (M) indoxyl sulfate promotes CpG hypermethylation of the Kloth gene; (N) P-cresyl sulfate causes osteoblastic dysfunction (Hsu et al., 2020).

1.1.5. Current CKD-MBD management

Management of CKD–MBD currently and the prevention of ROD, focuses on correcting disturbances in Pi, calcium, vitamin D, and PTH (Bellorin-Font et al., 2022; Hu et al., 2022; Zaimi & Grapsa, 2024). KDIGO recommends lowering elevated serum Pi towards the normal range in CKD G3a–G5 (Fig. 1.1), using a combination of dietary Pi restriction and Pi-binding agents (Beto et al., 2019). Pi binders are prescribed when dietary measures are insufficient. Calcium-based binders (calcium carbonate, calcium acetate) have long been standard but can exacerbate hypercalcemia and contribute to vascular and valvular calcification (Block et al., 2007; Wilson & Copley, 2017). KDIGO therefore advises limiting the dose of calcium-based binders, especially in patients with hypercalcemia, low PTH, or extensive vascular calcification (Beto et al., 2019). Non-calcium binders such as sevelamer and lanthanum carbonate effectively reduce Pi, and trials suggest they attenuate coronary and aortic calcification compared with calcium-based binders and may improve survival in selected subgroups (Jamal et al., 2013; Suki et al., 2007). In advanced CKD patients with persistent SHPT, active vitamin D sterols or analogues like calcitriol and paricalcitol are used to suppress PTH and improve bone health (Coyne et al., 2013; Obi & Kalantar-Zadeh, 2016), but KDIGO recommends restricting their use mainly to CKD G4–G5 (Fig. 1.1) with severe SHPT due to risks of hypercalcemia, hyperphosphatemia, and oversuppression of bone turnover (Beto et al., 2019; Han et al., 2013).

SHPT is a key driver of high-turnover ROD (osteitis fibrosa) (Aguilar et al., 2023; Moe et al., 2006). For CKD G5D patients with high or rising PTH, KDIGO recommends three PTH-lowering therapies, which are calcimimetics, calcitriol, and vitamin D analogues, used alone or together, based on calcium and Pi levels. (Beto et al., 2019). Calcimimetics (calcium-sensing receptor agonists) such as cinacalcet and etelcalcetide

enhance the sensitivity of the calcium-sensing receptor on parathyroid cells, thereby lowering PTH, serum calcium, and often Pi (Akizawa et al., 2016; Pereira et al., 2018; Shigematsu et al., 2018). Meta-analyses show that cinacalcet effectively reduces PTH and biochemical markers of high-turnover bone disease; clinical trials suggested possible reductions in some cardiovascular events, although the primary composite outcome was not significantly improved in the intention-to-treat analysis (Block et al., 2004; Chertow et al., 2012). Etelcalcetide is as effective as cinacalcet in lowering PTH when given thrice weekly post-haemodialysis, potentially boosting adherence (Block et al., 2017). Recent data suggest that cinacalcet may reduce cardiovascular events compared with conventional therapy, but this confounding cannot be ruled out (Abdelrahman et al., 2025). Subtotal parathyroidectomy remains a key option for SHPT when other treatments fail, enhancing biochemical control, alleviating bone pain, pruritus, and sometimes extending survival (Ketteler et al., 2025). For patients with low-turnover or adynamic bone disease, the priority is to avoid further PTH suppression treatment to permit a moderate rise in PTH while maintaining safe calcium and Pi levels (Ketteler et al., 2025). This turnover-directed strategy primarily depends on bone biopsy, but since biopsies are often limited by availability and invasiveness, treatment then is usually guided by biochemical markers like PTH and bone-specific alkaline phosphatase, along with clinical context (Srisuwarn et al., 2024; Thompson et al., 2025).

Osteoporosis pharmacotherapy is increasingly considered for CKD patients, especially those with stages G3–G4 (Figure 1.1) (Hara et al., 2021; Khairallah & Nickolas, 2018). Bisphosphonates, osteoclast inhibitors, are generally safe and effective in early CKD (stages G1-G3), but require careful consideration in advanced stages (G4-G5) due to concerns about adynamic bone complications and increased risk of CKD progression (Liu et al., 2013; Nitta et al., 2017; Robinson et al., 2021). Denosumab, a receptor activator of nuclear factor κB (NF-κB) ligand (RANKL) inhibitor that is not cleared by the kidneys, is effective across all CKD stages but has a high risk of hypocalcemia, especially in advanced disease (Bird et al., 2024; Cowan et al., 2023; Sun et al., 2025). Anabolic agents such as teriparatide (PTH agonist) and romosozumab (sclerostin inhibitor) might help certain patients with low-turnover bone disease, although evidence for their use in advanced-stage CKD is still limited, as shown by potentially increased risk

of hypocalcemia (Brandenburg et al., 2019; Cejka, 2021; Sabaghian et al., 2024). Despite existing treatments, the incidence of fractures and vascular calcification remains elevated. Currently, most therapies address biochemical irregularities rather than the fundamental cellular processes underlying ROD. This emphasises the need for interventions that more directly target osteoblast and osteoclast activity, as well as Wnt signalling pathways, such as sclerostin and Dkk1 inhibitors

1.2. Bone structure and (re)modelling

1.2.1. Bone anatomy and function

Bone is a highly specialised, dynamic connective tissue that provides mechanical support and soft tissue protection, facilitates locomotion, and acts as a reservoir for essential minerals such as calcium and Pi. Mammalian bones come in various shapes and forms and are characterised as long bones (e.g., femur and tibia), flat bones (e.g., skull and sternum), short bones (e.g., carpals (wrist bones) and tarsals (ankle bones), and irregular bones (e.g., vertebrae and sacrum). Every bone is composed of two distinct but complementary types of tissue, cortical bone and trabecular bone, which differ in structure, function, and remodelling dynamics but together maintain skeletal integrity and metabolic homeostasis. Cortical bone, also known as compact bone, forms the dense outer shell of most bones and accounts for approximately 80% of the total skeletal mass. It provides the primary structural support necessary for movement, protection of internal organs, and resistance to mechanical stress (Peretti & Domenicucci, 2022). Microscopically, cortical bone is organised into structural units called osteons or Haversian systems, which consist of concentric lamellae, orientated in alternating directions, of mineralised collagen surrounding a central Haversian canal containing blood vessels and nerves (Maggiano et al., 2016; Peretti & Domenicucci, 2022) (Figure 1.4). Lacunae where osteocytes locate are found between the individual lamellae. The osteons are interconnected by transverse Volkmann's canals, forming a vascular network that facilitates nutrient delivery and waste removal. This highly organised architecture allows cortical bone to resist bending and torsional forces, making it essential for weight-bearing functions, particularly in the shafts of long bones such as the femur and tibia

(Maggiano et al., 2016). In humans and larger mammals, cortical bone undergoes remodelling throughout their lives, leading to the development of secondary osteons and expansive areas on interstitial lamellae, while, smaller animals like rats and mice lack Haversian systems; however, intracortical remodelling still occurs in these species (Barak, 2024; Lad, 2023; Maggiano et al., 2016).

Trabecular bone, also known as cancellous or spongy bone, constitutes approximately 20% of the skeletal mass but has a disproportionately large role in mineral metabolism and mechanical strength (Seeman, 2013). It is predominantly found at the ends of long bones, in vertebral bodies, and is involved in active bone remodelling (Peretti & Domenicucci, 2022). Structurally, trabecular bone is composed of a three-dimensional lattice of rod- and plate-like structures oriented along lines of mechanical stress to efficiently absorb and distribute applied forces (Ding et al., 2002; Peretti & Domenicucci, 2022). Histologically, (Figure 1.4) trabecular bone is organised into lamellae adjacent to marrow spaces filled with haematopoietic tissue and mesenchymal stem cells that can differentiate into several cell types including osteoblasts, chondrocytes, and adipocytes. The trabecular surface is covered by lining cells, osteoblasts, and osteoclasts, where bone remodelling occurs to maintain bone strength and mineral homeostasis (Peretti & Domenicucci, 2022). Because of its open architecture and high remodelling rate, trabecular bone is more responsive—and thus more vulnerable—to systemic hormonal fluctuations and metabolic disturbances than cortical bone (Li et al., 2017).

1.2.2. Bone formation and development

Bone formation, or ossification, is a tightly regulated process that begins during embryogenesis and continues throughout life as part of skeletal growth, maintenance, and repair. The vertebrate skeleton develops through two distinct but interconnected pathways: intramembranous ossification and endochondral ossification. Both processes involve the differentiation of bone mesenchymal stromal cells (BMSCs) into osteogenic lineages under the control of multiple signalling pathways, transcription factors, and hormonal cues.

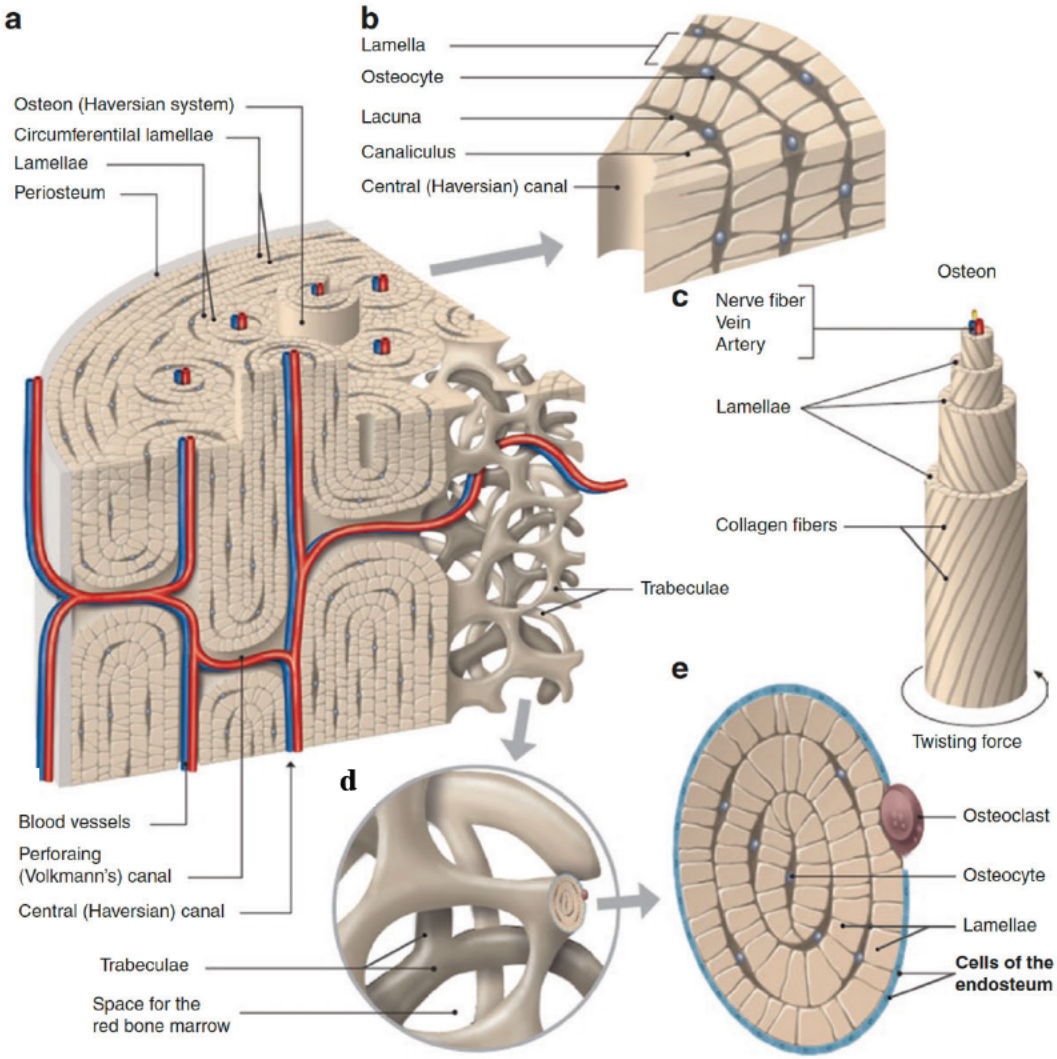

Figure 1.4 Structure of cortical and trabecular bone. (a): osteons of cortical bone consisting of circumferential lamellar bone surrounding Haversian and Volkmann's canals, which contain blood vessels and nerves. (b & c), osteocytes within their lacunae of alternating collagenous lamellae surrounding the central Haversian canal. trabecular bone alignment in bone marrow cavity (d), and cross-section of trabecular bone consisting of lamellae and osteocytes with an osteoclast situated on the endosteum (e). Modified from (Peretti & Domenicucci, 2022).

Intramembranous ossification is the direct process of bone formation from mesenchymal condensations without a cartilage intermediary. This mechanism primarily gives rise to flat bones of the skull, mandible, and clavicle. During intramembranous

ossification (Figure 1.5a), BMSCs within a fibrous membrane are loosely arranged to form a thin avascular area (Jabalee & Franz-Odendaal, 2015; Zhu et al., 2021). The BMSCs inside the condensed area are induced by cytokines such as bone morphogenetic proteins (BMPs), which upregulate osteoblast transcription factors, Runt-related transcription factor 2 (*Runx2*) and osterix *(Sp7),* which differentiate the BMSCs into osteoprogenitor cells and subsequently into osteoblasts (Xu et al., 2015; Zhu et al., 2021). Mature osteoblasts secrete osteoid, the non-mineralised type I-collagen-rich organic matrix of bone, with blood vessels penetrating (Percival & Richtsmeier, 2013; Zhu et al., 2021). Upon osteoid mineralisation, some osteoblasts become encased within the matrix, differentiating into osteocytes. The mesenchymal tissue, rich in blood vessels, condenses around the mineralised matrix and eventually forms the periosteum (Percival & Richtsmeier, 2013). Beneath the periosteum, the spongy bone is compressed, resulting in the formation of compact bone (Zhu et al., 2021).

In contrast, endochondral ossification involves the replacement of a pre-existing cartilage template with bone and is responsible for forming the majority of the axial and appendicular skeleton, including long bones such as the femur, tibia, and humerus. The process (Figure 1.5b) begins when mesenchymal cells condense and differentiate into chondrocytes, forming a cartilage template enriched with collagen type II and proteoglycans such as aggrecan (Mwale et al., 2002; Spath et al., 2018). The chondrocytes undergo proliferation and after the cessation of cell division the chondrocytes secrete collagen type X and increase their size to ~10x that of the proliferating chondrocytes (Cheung et al., 2001; Ionescu et al., 2004). The collagenous matrix surrounding the enlarged hypertrophic chondrocytes is mineralised and VEGF produced by the chondrocyte attracts blood vessels and osteoprogenitor cells into the cartilage anlage (Duan et al., 2015; Horner et al., 1999). Osteoblasts derived from these progenitors then deposit collagen type 1 rich bone matrix on the remnants of calcified cartilage, forming the primary ossification centre in the diaphysis. Secondary ossification centres later

appear in the epiphyses, allowing for longitudinal growth via the epiphyseal growth plate until puberty when the growth plate closes (Setiawati & Rahardjo, 2018; Zhu et al., 2021).

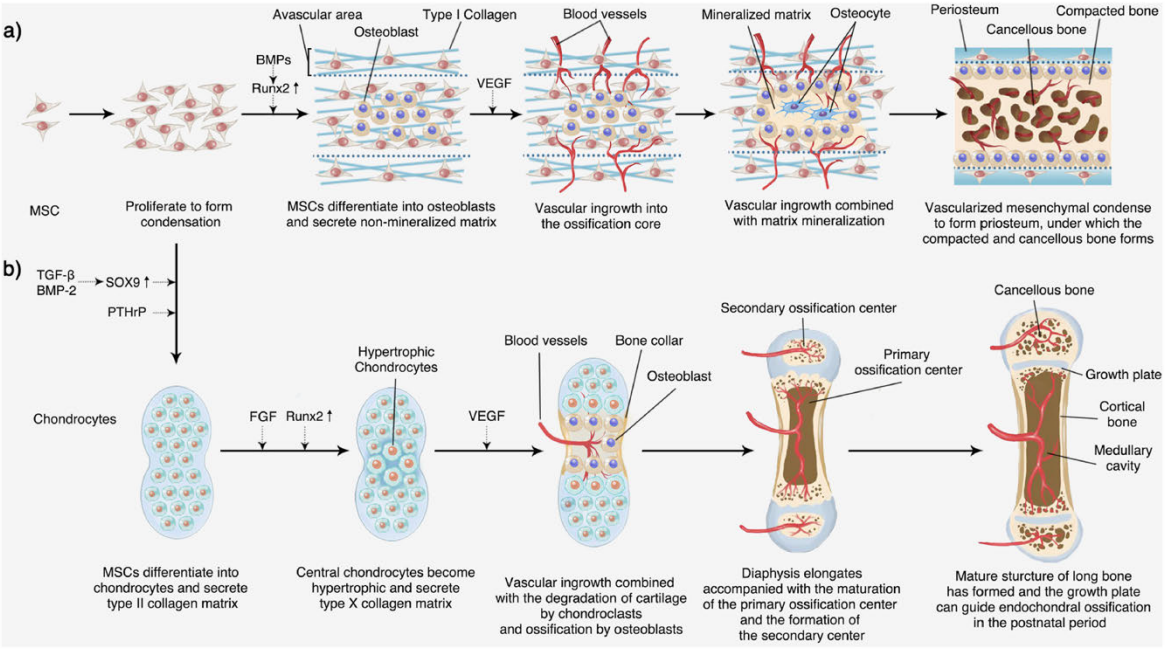

Figure 1.5 Embryonic bone development: a) intramembranous ossification process and b) endochondral ossification process (Zhu et al., 2021).

1.2.3. Bone remodelling process and associated cells

Bone modelling and remodelling are two fundamental yet distinct biological processes that shape, maintain, and adapt the skeleton throughout life. Both involve the coordinated activities of bone-forming osteoblasts and bone-resorbing osteoclasts, but they differ markedly in their spatial coordination, timing, and physiological purpose. Bone modelling alters the size and shape of bone by forming and resorbing bone on different surfaces, allowing the skeleton to grow and adapt to mechanical demands; unlike remodelling, these processes are not spatially or temporally coupled (Barak, 2024; Roberts et al., 2004). In contrast, bone remodelling is a tightly coordinated renewal process in which osteoclasts remove old bone and osteoblasts replace it at the same site, preserving bone quality and mineral homeostasis (Henriksen et al., 2009; Kular et al., 2012; Sims & Martin, 2015).

Bone remodelling is a dynamic, lifelong process that maintains skeletal integrity, repairs microdamage, and also maintains systemic calcium and Pi homeostasis levels (Peterson & Riggs, 2010; Siddiqui & Partridge, 2016). In humans, ~10% of the skeleton is remodelled every year (Valdés-Flores et al., 2013). Bone remodelling occurs within discrete basic multicellular units (BMUs) composed of osteoclasts, which resorb bone, and osteoblasts, which subsequently form new bone in the same location (Andersen et al., 2009; Raggatt & Partridge, 2010). The process is tightly coordinated to ensure that bone resorption and formation remain balanced *i.e.* the amount of bone removed by osteoclasts is replaced by the same amount of new bone by osteoblasts (Raggatt & Partridge, 2010; Siddiqui & Partridge, 2016). Disruption of this coupling, whether through hormonal imbalance, ageing, disease *e.g.* CKD-MBD and inflammatory bowel disease and drug induced *e.g.* corticosteroids can lead to net bone loss, thereby compromising bone structure and strength (Bolamperti et al., 2022; Feng & McDonald, 2011). Bone remodelling is characterised by five sequential but overlapping phases (Henriksen et al., 2009; Li et al., 2024; Raggatt & Partridge, 2010) (Figure 1.6):

1. Activation phase: it is currently unclear how osteoclasts are recruited to the site of damaged bone but a role for the osteocyte has been proposed. Osteocyte apoptosis in response to fatigue microdamage, and/or endocrine/inflammatory cues release signals to neighbouring healthy osteocytes to produce osteoclastogenic cytokines (Al-Dujaili et al., 2011; Jilka et al., 2013). This triggers the recruitment of pre-osteoclasts (monocytes) and the stimulation of a remodelling site (Al-Dujaili et al., 2011). The pre-osteoclasts are recruited from the bone marrow or blood vessels to the site of damaged bone – the bone remodelling compartment (BRC). The BRC at this stage is still covered by bone lining cells (Andersen et al., 2009; Khosla et al., 2010).

2. Resorption phase: pre-osteoclasts differentiate to mature osteoclasts in response of monocyte/macrophage colony-stimulating factor (M-CSF) and RANKL. The mature and functional osteoclasts excavate a resorption lacunae (Howships Lacunae) removing the damaged area of bone. This involves the dissolution of inorganic mineral via the production of protons and the resulting low pH, whereas the degradation of the

organic matrix is mediated by collagenases, gelatinases, cathepsin K and other hydrolytic enzymes.

3. Reversal phase: during this phase, bone resorption ceases and there is a shift to bone formation. Reversal cells (including mononuclear cells, bone lining cells) prepare the bone surface for new formation, remove debris, and release coupling factors that stimulate osteoblast differentiation from BMSCs.

4. Formation phase: osteoblasts deposit osteoid (unmineralised matrix) which subsequently becomes mineralised with carbonated hydroxyapatite. The active bone formation continues until the resorption cavity is refilled.

5. Termination/Quiescence phase: once new osteoid is laid down and mineralised, the bone surface becomes quiescent. Some osteoblasts become bone-lining cells, others become osteocytes, or undergo apoptosis. The site remains inactive until the next activation cycle.

In healthy adults, the remodelling of bone ensures that old bone is replaced by new bone of similar volume and mechanical competence. However, in various pathologic states, including ageing, post-menopausal osteoporosis, and CKD, the coupling between resorption and formation is broken. For example, in post-menopausal osteoporosis the decrease in circulating oestrogen leads to decreased osteoblastic activity but increased osteoclastic activity. This excessive resorption and insufficient formation leads to net bone loss and structural weakness (Bolamperti et al., 2022; Thapa et al., 2022). From a structural standpoint, the remodelling cycle occurs more rapidly in trabecular bone than cortical bone, and the specific architecture of the BMU differs between these compartments (Delaisse et al., 2020). Understanding this cycle in detail and specifically, endocrine factors, local signalling pathways (e.g., RANK/RANKL/OPG, Wnt/β-catenin, sclerostin/Dkk1), osteocyte apoptosis, and cell fate decisions, is crucial for interpreting how systemic diseases (such as CKD) disrupt bone homeostasis and increase fracture risk (Feng & McDonald, 2011; Raggatt & Partridge, 2010; Wang et al., 2022).

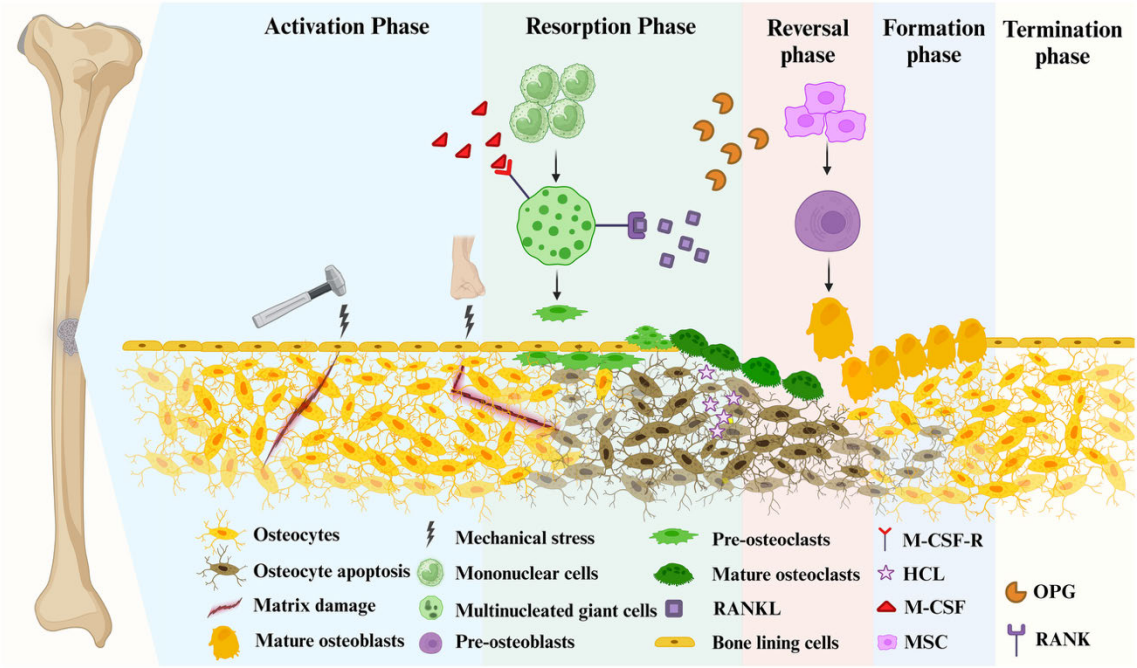

Figure 1.6 Bone remodelling composes of 5 distinct phases but overlapping phases. Phase 1 (Activation phase): activation of bone remodelling and the formation and of the bone remodelling compartment. Phase 2 (Resorption phase): M-CSF and osteoblasts induce osteoclast differentiation to resorb damaged bone together with activating osteoblast differentiation. Phase 3 (Reversal phase): bone remodelling process shift from resorption to formation. Phase 4 (Formation phase): osteoblasts finish osteoid secretion trapping some osteoblasts within the matrix. Phase 5 (Termination phase): osteoid mineralises and osteocytes become fully differentiated (Li et al., 2024).

1.2.3.1. Osteoblasts

Osteoblasts originate from MSCs under the influence of key transcription factors, most notably *Runx2* and *Sp7* (osterix). *Runx2* initiates the osteogenic programme, while *Sp7* drives the maturation of pre-osteoblasts into matrix-synthesising osteoblasts. Several morphogenetic pathways (*e.g.*, BMPs, Wnt,) as well as mechanical and microenvironmental cues guide the transition from MSCs to pre-osteoblasts and also pre-osteoblasts to mature osteoblasts (Komori, 2010; Zhu et al., 2024). Histologically, mature osteoblasts are a cuboidal shape and attach on the surface of both trabecular and cortical bone (Pazzaglia et al., 2014) (Figure 1.7). The active mature osteoblasts synthesise and

secrete type I collagen and specialised non-collagenous matrix proteins, such as osteocalcin (OCN, vitamin-K dependent Ca binding protein specific to bone), tissue non-specific alkaline phosphatase (TNAP) and PHOSPHO1 (essential for mineral deposition) and osteopontin (OPN) which together with other collagenous and non-collagenous proteins constitute the bone extracellular matrix (ECM) (Bala et al., 2013; Schlesinger et al., 2020; Zhu et al., 2024). The ECM is first secreted in a form of unmineralised osteoid in which the collagen fibrils become mineralised by the incorporation of carbonated hydroxyapatite which is composed of mainly calcium and Pi (Bala et al., 2013; Zhu et al., 2024)(see section 1.2.4). In addition to forming bone, osteoblasts together with osteocytes also have the ability to control osteoclast formation and function through distinct molecular mechanisms (Kim et al., 2020; Robling & Bonewald, 2020).

Research has identified three primary pathways through which osteoblasts exert this control. First, osteoblasts utilise the RANKL/RANK/osteoprotegerin (OPG) signalling axis, where membrane-bound RANKL on osteoblasts interacts with RANK receptors on osteoclast precursors to promote their differentiation, while OPG acts as a decoy receptor to inhibit this process (Katagiri & Takahashi, 2002; Martin, 2004). The RANKL/OPG ratio is an important indicator of normal bone remodelling. Second, direct cell-to-cell contact occurs through specific ligand-receptor pairs, such as ephrin/Eph and semaphorin/plexin interactions, enabling immediate communication between osteoblasts and osteoclasts. Ephrin B2 is expressed on osteoclasts and interacts with the EphB4 receptor on osteoblasts, enabling bidirectional signalling between these cells. This communication pathway regulates bone remodelling by promoting osteoblast differentiation through forward signalling (osteoclast to osteoblast) and inhibiting osteoclastogenesis through reverse signalling (osteoblast to osteoclast). Osteoclasts also express semaphorin 4D on their surface, which binds to plexin-B1 receptor on osteoblasts. This signalling pathway negatively regulates bone formation by suppressing osteoblast differentiation. (Boyce, 2013; Chen et al., 2018; Kim et al., 2020). Third, osteoblasts influence osteoclast activity through the secretion and regulation of cytokines and growth factors, including TGF-β and various inflammatory mediators that modulate osteoclast function (Chen et al., 2018). Osteoblasts also respond to systemic hormones (PTH, 1,25-dihydroxyvitamin D, insulin-like growth factor-1 (IGF-1), oestrogen, glucocorticoids

(GC)) and mechanical loading. While PTH and vitamin D stimulate osteoblastic activity, GC, inflammatory cytokines, oxidative stress and AGEs can impair osteoblast differentiation and function (Iantomasi et al., 2023; Kuriwaka-Kido et al., 2013; Park et al., 2021). Mechanical loading induced strain and intermittent PTH down-regulates osteocyte-derived sclerostin and thereby releasing a brake on Wnt/β-catenin signalling and enhancing osteoblast activity and bone formation (Bellido et al., 2005; Costa et al., 2011; Turner et al., 2009). Osteoblasts therefore serve as the effector cells of bone formation and key nodes in the coupling between formation, resorption and mechano-sensing.

After the ECM is secreted by osteoblasts and becomes mineralised, some osteoblasts embedded in the mineralised ECM differentiate into osteocytes. Other mature osteoblasts that remain on the bone surface transform into quiescent bone lining cells, which can be activated into active osteoblasts if needed (Infante & Rodriguez, 2018; Kular et al., 2012).

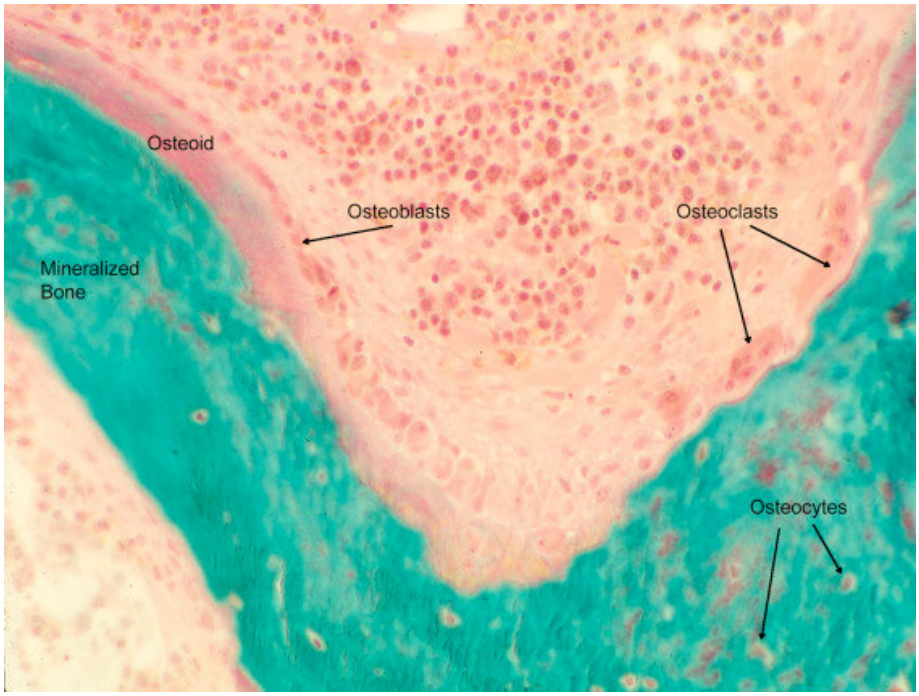

Figure 1.7 A photomicrograph of Masson's trichrome staining of bone showing osteoblasts, osteoclasts and osteocytes (Ott, 2017).

1.2.3.2. Osteocytes

Among the diverse cell types that constitute the bone tissue, the osteocyte occupies a unique niche. Originating from osteoblasts that become embedded in the mineralised matrix (Figure 1.7), osteocytes are the most abundant bone cell type (~95% of all bone cells) and form an extensive, interconnected network within the bone matrix (Dallas et al., 2013). This transition involves morphological changes, a including reduction of cell volume, elongation of dendritic processes, and establishment of the lacunae-canalicular network (LCN) that connects them together, with bone surface cells, and with vascular spaces (Figures 1.7 and 1.8). The network enables not only structural integration but also biochemical and mechanical signalling across the bone tissue (Dallas et al., 2013; Kollmannsberger et al., 2017). One of the central roles of osteocytes is mechano-sensing: detection of mechanical strain, microdamage, fluid shear within the LCN, and subsequent transduction into cellular responses that regulate bone remodelling (Choi et al., 2021). The sensing of mechanical strain or micro damage by osteocytes affect the secretion of several mediators, including prostaglandins, nitric oxide, Wnt ligands, and others (Cao et al., 2020). Through their dendritic processes and gap-junction connectivity, they coordinate responses across bone surfaces and deeper matrix zones. Furthermore, osteocyte apoptosis (for example, due to unloading or microdamage) triggers recruitment of osteoclast precursors and initiation of bone resorption (Bellido, 2014). Thus, osteocytes serve as the "orchestrators" of adaptation: responding to mechanical and microenvironmental cues to regulate bone formation and resorption for the maintenance of maintain skeletal integrity. Beyond mechano-sensation, osteocytes hold a regulatory influence over osteoblasts and osteoclasts. In genetically engineered mice in which the RANKL gene (*Tnfsf11*) was globally knockout, there is reduced osteoclastogenesis, resulting in a decrease in bone resorption and osteopetrosis (Kong et al., 1999). In addition, osteocytes also secrete RANKL's decoy receptor OPG to regulate osteoclastogenesis and bone resorption (Cao et al., 2020; Kong et al., 1999). Thus, osteocytes can initiate targeted bone remodelling through modulation of osteoclast lineage activity. In addition, osteocytes produce various osteocyte-derived factors such as sclerostin (encoded by *Sost*), which acts as a potent inhibitor of Wnt/β-catenin signalling in osteoblasts, thereby limiting bone formation. Osteocytes also secrete FGF23, which

regulates systemic Pi and vitamin D metabolism via renal actions (Dallas et al., 2013). In summary, osteocytes integrate mechanical, hormonal and paracrine signals to coordinate bone mass and mineral homeostasis which are disrupted in CKD resulting in abnormal systemic levels of sclerostin and FGF23 (Agoro et al., 2020; Delgado-Calle & Bellido, 2022; Laster et al., 2023; Mace et al., 2020)

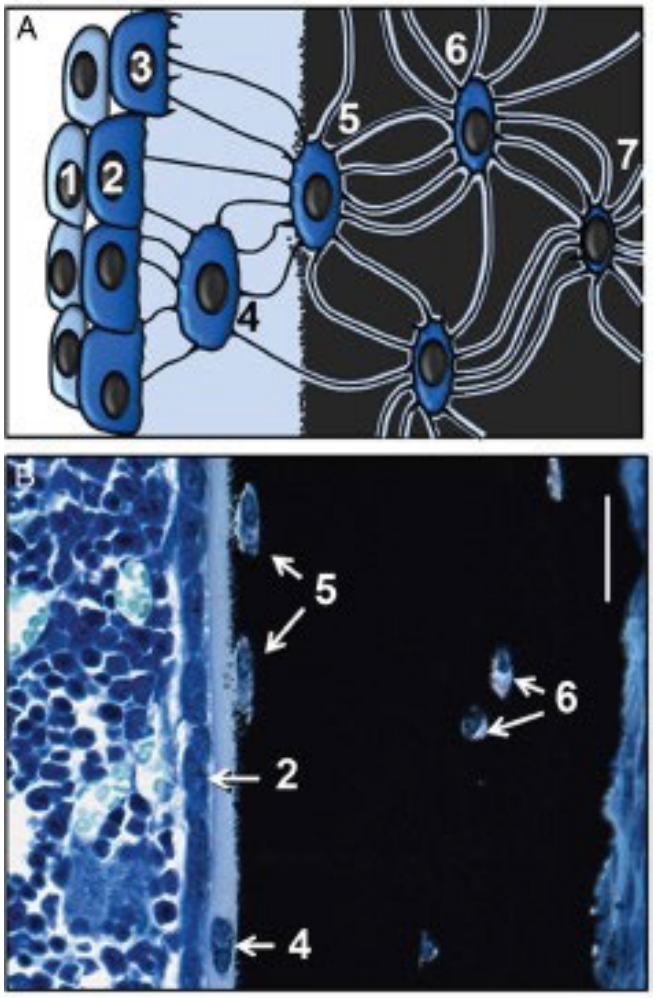

Figure 1.8 Osteocyte differentiation. (A) The illustration shows the stages that osteoblasts pass through as they become mature osteocytes. Throughout this transformation, both cell size and the number of organelles are reduced. The numbered labels indicate: 1, preosteoblast; 2, osteoblast; 3, embedding osteoblast; 4, osteoid osteocyte; 5, mineralising osteocyte; 6 and 7, mature osteocytes. (B) A tetrachrome-stained section from an adult mouse tibia highlights various transitional forms between osteoblasts and osteocytes as outlined in panel A (scale bar: 25 μm) and modified from (Dallas et al., 2013).

1.2.3.3. Osteoclasts

Osteoclasts are multinucleated (Figure 1.7), highly specialised cells responsible for degrading mineralised bone matrix, a process essential for skeletal renewal, microdamage repair, and calcium–phosphate homeostasis. Osteoclasts originate from haematopoietic stem cells of the monocyte–macrophage lineage (Ikeda & Takeshita, 2016). Their differentiation (Figure 1.9) is primarily driven by two cytokines: M-CSF, which promotes proliferation and survival of precursors, and RANKL, which induces commitment to the osteoclast lineage (Boyle et al., 2003). RANKL binds to its receptor RANK on osteoclast progenitors, triggering downstream activation of NF-κB, c-Fos, and nuclear factor of activated T-cells 1 (NFATc1) — the master regulator of osteoclastogenesis (Takegahara et al., 2024). Osteoclastogenesis through the RANKL signalling pathway is controlled by OPG, a decoy receptor which is produced mainly by osteoblasts and osteocytes, to sequester RANKL (Cao et al., 2020). As differentiation proceeds, mononuclear precursors fuse to form multinucleated osteoclasts that adhere tightly to bone surfaces. These cells develop a sealing zone composed of actin filaments and integrins along with a ruffled border formed by vesicular trafficking, both of which enable bone resorption (Luxenburg et al., 2007; Takito & Nakamura, 2020; Touaitahuata et al., 2014). Within the resorption lacunae, vacuolar H-ATPases secrete protons to lower the pH and dissipate the hydroxyapatite, while cathepsin K and matrix metalloproteinases degrade the organic collagenous matrix (Cao et al., 2020; Zaidi et al., 2003). The products of resorption are endocytosed, transcytosed in which vesicles internalise, transport across the cytoplasm and release out the other side of the cell, and released into the extracellular space, completing the degradation cycle (Cao et al., 2020). Bone homeostasis depends on the coupling of osteoclastic resorption and osteoblastic formation. This communication is mediated by molecular cross-talk within the BMU (Kim & Kim, 2020; Sims & Martin, 2015). Osteoblasts and osteocytes regulate osteoclast differentiation through the RANKL/RANK/OPG axis, while osteoclasts, in turn, secrete factors known as clastokines (e.g., sphingosine-1-phosphate, cardiotrophin-1, and complement C3a) that stimulate osteoblast recruitment and differentiation (Kim et al., 2020; Matsuoka et al., 2014). RANKL-induced activation of NFATc1 integrates calcium signalling, MAPK, and PI3K–AKT pathways to orchestrate the expression of osteoclast-specific genes. These pathways

also ensure cytoskeletal reorganisation and cell survival (Lee & Kim, 2003; Moon et al., 2012; Park et al., 2017). Excessive activation of RANKL or NFATc1 signalling promotes pathological bone loss, as seen in osteoporosis and inflammatory bone destruction, whereas defective activation results in osteopetrosis and impaired remodelling (Sun et al., 2021; Teitelbaum, 2007). Thus, osteoclast regulation must remain tightly controlled to maintain skeletal integrity.

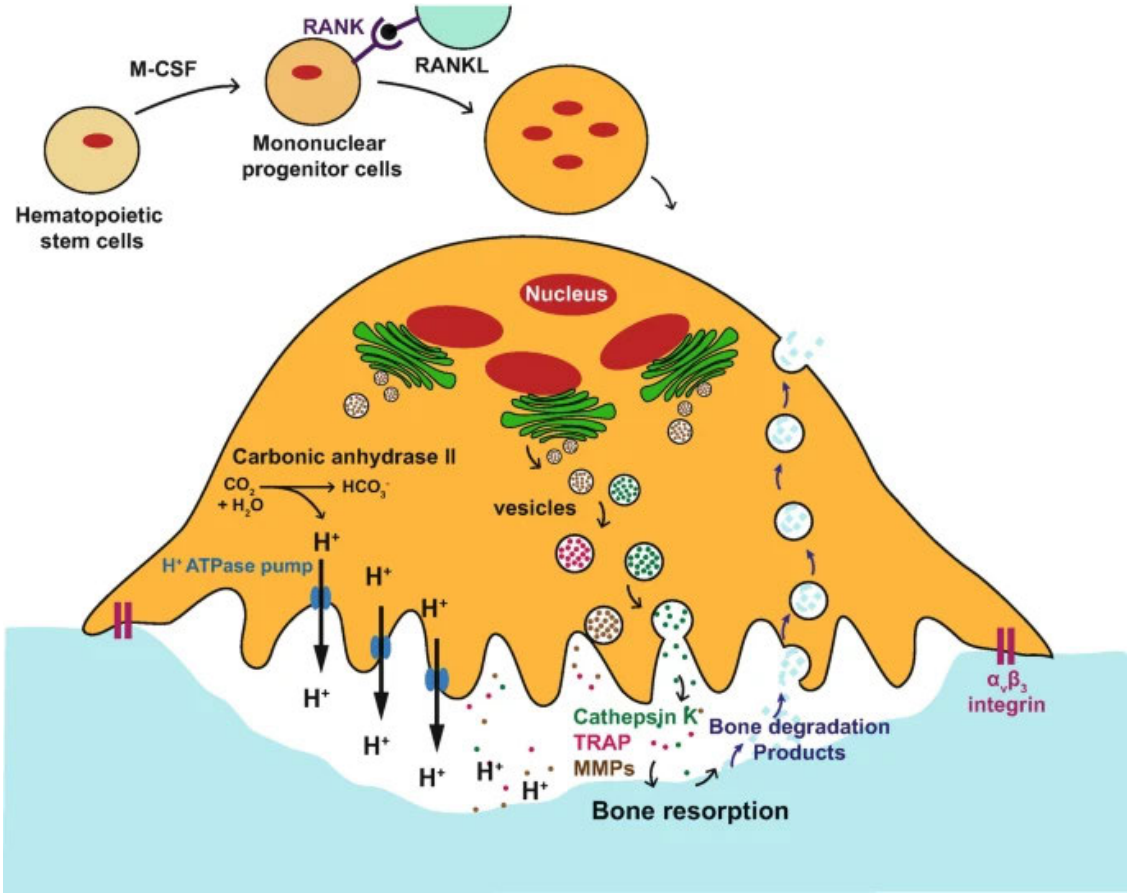

Figure 1.9 Multinucleated osteoclasts develop when single-nucleus precursors, originating from haematopoietic stem cells, fuse together. This process is driven by signals such as M-CSF and the binding of RANKL from neighbouring cells (*i.e.* osteoblast lineage cells and T cells) to RANK receptors on the precursor cell surface. Once formed, these multinucleated cells anchor to bone using αvβ3 integrin, creating a sealed area for bone resorption. The ruffled border of the osteoclast uses a vacuolar-type H^+-ATPase to acidify the space beneath it. Enzymes—such as cathepsin K, TRAP, and MMPs—are secreted to break down the bone matrix. The breakdown products are taken up by the osteoclast, processed inside the cell, and then moved out through the opposite side (Ansari & Sims, 2020).

1.2.4. Bone mineralisation

The process of bone mineralisation begins with the secretion of an ECM by osteoblasts, followed by the subsequent mineralisation of that matrix through carefully orchestrated cellular activities and enzymatic processes (Bourne et al., 2021). The process is carried out by osteoblasts, which form osteoid (unmineralised ECM), and the osteoid mineralises through a balanced biphasic process. Osteoblasts initially release matrix vesicles (MVs) containing amorphous calcium phosphate(Lovdel et al.) (Yamada, 1976) and/or hydroxyapatite , which serve as nucleation sites for primary mineralisation along with other proteins and enzymes. Key components for their function include phospholipids, calcium channels, and annexins, as well as essential phosphatases such as TNAP and PHOSPHO1 (Dillon et al., 2019; Hessle et al., 2002). The mechanism involves PHOSPHO1 generating Pi from membrane-bound phospholipid substrates (Dillon et al., 2019), and TNAP releasing Pi from inorganic pyrophosphate (PPi), which is transported into the MVs by type III Na/Pi co-transporter (PiT-1/SLC20A1/Glvr1) (Yadav et al., 2016)(Figure 1.10). Lack of either phosphatase alone leads to hypomineralised bones, while missing both phosphatases results in embryonic death and total skeletal mineralisation failure (Yadav et al., 2011). Calcium ion (Ca^{2+}) enters the MVs via annexins A (Genge et al., 1990; Pei et al., 2022) and once Ca^{2+} and Pi supersaturate within MVs, ACP and/or hydroxyapatite nucleation occurs (Figure 1.9) (Hohling et al., 1976; Roohani et al., 2022). Hydroxyapatite or ACP bursts out of the MVs and deposits within, and on the collagen fibrils, representing secondary mineralisation outside MVs. Numerous Ca^{2+}- and Pi-binding proteins facilitate biomineralisation by controlling the quantity and size of hydroxyapatite crystals formed (Millan & Whyte, 2016).

Proper regulation of bone mineralisation relies on two main inhibitors: ectonucleotide pyrophosphatase/phosphodiesterase-1 (ENPP1) (Clews et al., 2025; Hajjawi et al., 2014; Roberts et al., 2019) and the progressive ankylosis protein (ANK) (Kim et al., 2010; Moochhala et al., 2008). ENPP1 generates PPi, a potent inhibitor of mineralisation, from adenosine triphosphate (ATP) (Millan & Whyte, 2016). Mutations in the ENPP1 gene, have been associated with chondrocalcinosis arthropathy in both humans and mice (Babij et al., 2009; Takei et al., 2025). The ANK protein, a transmembrane

channel transports PPi from inside the cell into the ECM (Ho et al., 2000) although this has recently been disputed (Szeri et al., 2022). As PPi is a substrate for TNAP this phosphatase is essential for the regulation of the Pi/PPi ratio which in turn is vital for physiological biomineralisation. This process, together with calcium-binding proteins, is crucial for bone mineralisation within the ECM.

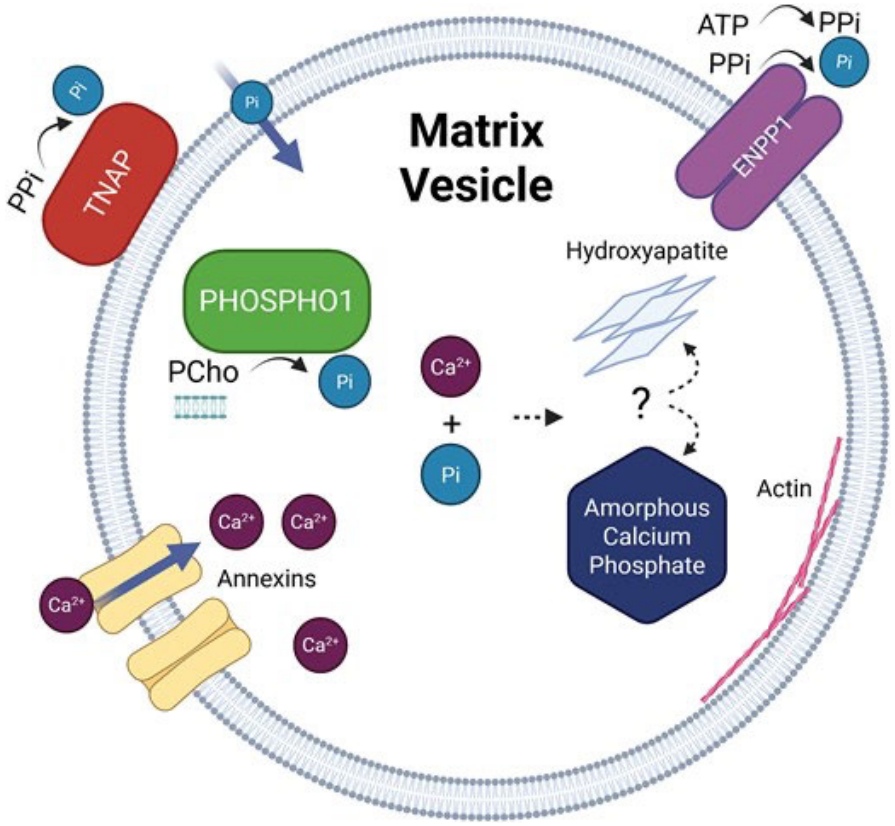

Figure 1.10. A schematic illustrating the current understanding of particular mineralisation components within MV. The key proteins involved are PHOSPHO1, TNAP, and ENPP1 (Clews et al., 2025).

1.3. Bone marrow stromal cells (BMSCs)

BMSCs are multipotent stromal progenitors residing in the bone marrow microenvironment and play a pivotal role in skeletal homeostasis. These cells are capable of self-renewal and differentiation into osteoblasts, adipocytes, and chondrocytes, thereby serving as a fundamental source of progenitors for osteogenesis and bone marrow adipogenesis (Pittenger et al., 2019). Published studies have shown that the BMSC

genome has significant overlap in binding sites for key transcriptional regulators like RUNX2 and CCAAT/enhancer binding protein beta (C/EBPβ). These sites, which decrease epigenetically during differentiation, display high plasticity (Henriquez et al., 2011; Hochmann et al., 2023). This flexibility allows BMSCs to trans-differentiate between adipocytes and osteoblasts. Thus, their lineage fate decisions are central to the balance between bone formation and marrow adiposity (Wu et al., 2017).

BMSCs display surface markers such as CD73, CD90, and CD105, but lack endothelial marker CD31 and haematopoietic marker CD45, (Brown et al., 2019). Previous studies have reported that all skeletal MSCs differentiating into osteoblasts or chondrocytes are marked by Osx1 in neonatal bone (Mizoguchi et al., 2014). In adult bone, similar cells express Nestin- an indicator of neural stem cells- and Leptin receptor (LepR), which is typically found on adipocytes (Mendez-Ferrer et al., 2010; Zhou et al., 2014). Moreover, the entire marrow adipocyte population derives from overlapping groups of cells expressing Prx1, Osx1, LepR, and adiponectin (Ambrosi et al., 2017; Y. Liu et al., 2013; Zhou et al., 2017; Zhou et al., 2014). Thus, identifying the defined population of skeletal stem cells could help gain more understanding of BMSC differentiation lineages.

Recent advances in single-cell RNA sequencing (scRNAseq) have offered a deeper understanding of the heterogeneity in the bone marrow microenvironment and the variety of cell types within subpopulations of all stem cells (Baccin et al., 2020; Baryawno et al., 2019; Tikhonova et al., 2019; Wolock et al., 2019). Lineage-tracing mouse models have identified the specific population and localisation of BMSCs that differentiate into osteoblasts, chondrocytes, and adipocytes within the bone marrow environment. For example, Mouse strains carrying Cre recombinase driven by lineage-specific promoters (Vav1 for hematopoietic cells; Cdh5 and Tek/Tie2 for endothelial cells; Prx1 and PDGFRα for mesenchymal cells; and AdipoQ for adipocytes) were bred with the mTmG reporter line, which expresses membrane-localized tdTomato and GFP. Following Cre-dependent recombination, the tdTomato cassette is removed, resulting in a switch to green fluorescent protein (GFP) expression. (Ambrosi & Schulz, 2017; Ambrosi et al., 2017; Ambrosi et al., 2021; Chan et al., 2015). In the postnatal long bones of mice, there are at

least two types of BMSC populations that exhibit genuine skeletal stem cell (SSC) characteristics. Osteochondrogenic SSC (ocSSC, characterised by CD45$^-$Ter119$^-$Tie2$^-$CD51$^+$Thy1$^-$6C3$^-$CD105$^-$, Figure 1.11A) gives rise to bone, cartilage, and stromal lineages but not to BMAT (Ambrosi et al., 2021; Chan et al., 2015). Another population of BMSC is called perivascular SSC (pvSSC). This population lacks expression of CD31 and CD45 but expresses stem cell antigen-1 (Sca1), platelet-derived growth factor α (Pdgfrα), and CD24. These cells differentiate into two distinct unilaterally committed populations: osteochondrogenic progenitor cells (characterised by CD31$^-$CD45$^-$Sca1$^-$Pdgfrα$^+$) and adipogenic progenitor cells (characterised by CD31$^-$CD45$^-$Sca1$^+$Pdgfrα$^+$CD24$^-$), both *in vitro* and *in vivo* (Figure 1.11B) (Ambrosi et al., 2017; Ambrosi et al., 2021). The pvSSC population of BMSCs could be a determinant of the balance between adipogenesis and osteogenesis during physiological and pathological conditions.

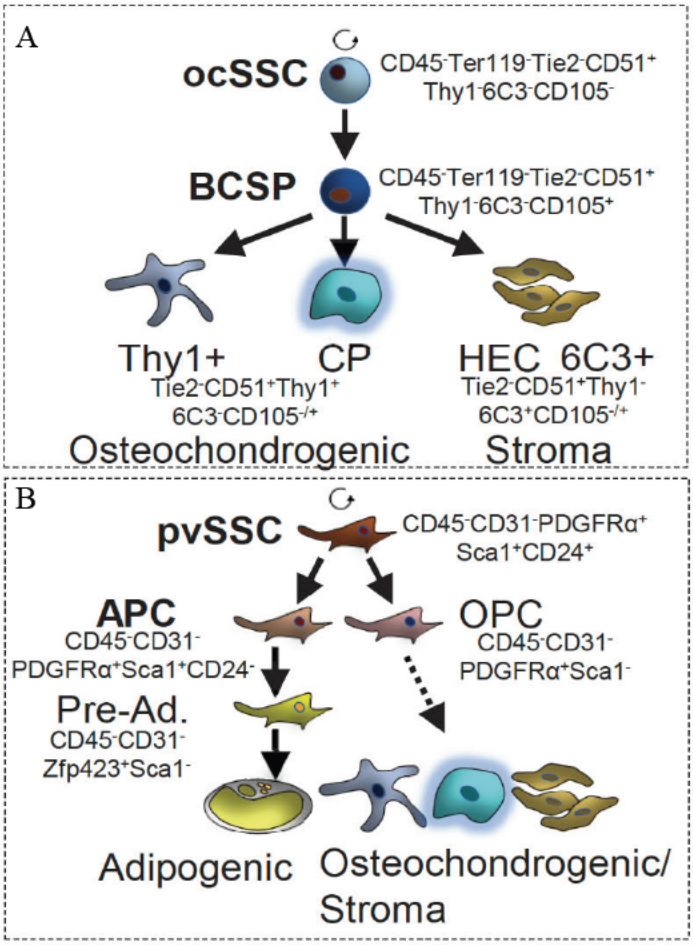

Figure 1.11 The diagram illustrates two previously described skeletal stem cell (SSC) populations and their downstream lineages, which are characterised by distinct cell

surface protein expression patterns. (A) Shows the SSC lineage tree of the osteochondral SSC (ocSSC), which generates bone, cartilage, and stromal cells. (B) Depicts the lineage tree of the perivascular SSC (pvSSC), which can give rise to bone, cartilage, adipose tissue, and stromal cells. Abbreviations: BCSP (bone cartilage stroma progenitor), CP (cartilage progenitor), APC (adipogenic progenitor cell), Pre-Ad. (pre-adipocyte), and OPC (osteochondrogenic progenitor cell). Modified from (Ambrosi et al., 2021).

When BMSCs commit to the osteoblast lineage, a complex network of signalling pathways and transcriptional regulators is engaged. A key early regulator is the transcription factor Runx2 widely regarded as the "master" osteogenic regulator: its expression is up-regulated during BMSC commitment and is required for osteoblast differentiation (Pierce et al., 2019; Zhu et al., 2024). Downstream of *Runx2* is another essential factor, *Sp7* (osterix), which further drives the osteoblast phenotype (matrix production and mineralisation) (Komori, 2017; Nakashima et al., 2002). Mutation of both *Runx2* or *Sp7* genes leads to poor skeletal development (Baek et al., 2014; Nakashima et al., 2002). Among signalling pathways regulating osteoblast differentiation, the canonical Wnt/β-catenin pathway is central (Figure 1.12) (Hill et al., 2005; Rossini et al., 2013). Activation of Wnt ligands (*e.g.*, Wnt10b) binding to Frizzled/LRP5/6 receptors leads to β-catenin stabilisation and nuclear translocation, where it cooperates with TCF/LEF transcription factors and interlocks with Runx2/Sp7 expression to drive osteoblastogenesis (MacDonald & He, 2012; McCarthy & Centrella, 2010; Rodda & McMahon, 2006), while simultaneously suppressing adipogenesis underscoring the reciprocal nature of the lineage decision (Huang et al., 2024; M. Wu et al., 2017). Another major pathway is the BMP/TGF-β signalling pathway particularly BMP2 and BMP4 among the BMP family, which engage SMA and MAD protein (SMAD)1/5/8 phosphorylation, bind SMAD4, and enhance osteoblast differentiation (Chen et al., 2012; Nishimura et al., 1998). The mechanical/actin cytoskeleton–RhoA/ROCK axis and mTOR pathway are also contributing pathways for osteogenesis through cytoskeletal tension and mechano-transduction (Arnsdorf et al., 2009; Lewis et al., 2020; Wang et al., 2012). During matrix production, osteoblasts express a characteristic set of proteins including type I collagen, osteocalcin, TNAP, osteopontin and bone sialoprotein (Dacic et al., 2001; Komori, 2019).

In contrast, when BMSCs commit to the adipocyte lineage, a different set of transcriptional regulators is activated. The nuclear receptor peroxisome proliferator-activated receptor gamma (*Pparg*), together with the C/EBP family (*Cebpa, Cebpb, Cebpg, and Cebpd*), orchestrate the adipogenic programme (Hardouin et al., 2016; Qian et al., 2010), driving the formation of cytoplasmic lipid droplets in adipocytes and expressing a number of genes related to lipid storage (i.e., *Plin1, Fabp4*), fatty acid metabolism (i.e., *Fasn*, *Pnpla2* and *Lipe*), and adipocyte function as adipokines (i.e., *Adipoq* and *Lep*) (Pierce et al., 2019; Tencerova et al., 2018). In addition, they can also induce each other's expression and can each act independently to promote fat cell differentiation (Madsen et al., 2014; Rosen et al., 2002). Inhibiting *Pparg* in the BMS2 bone marrow stromal cell line hinders the formation of fat cells but enhances the differentiation into osteoblasts (Gimble et al., 1996). In mouse models, lacking *Pparg* leads to defective development of adipose tissue when exposed to a high-fat diet (Jones et al., 2005). It has also been demonstrated that an isoform of *Cebpb,* which lacks the transcriptional binding domain, can activate *Runx2* and stimulate osteogenesis in mouse BMSCs (Hata et al., 2005). Additionally, mice deficient in C/EBP exhibit reduced adipogenesis and decreased insulin sensitivity (Linhart et al., 2001; Rosen et al., 2002; Zuo et al., 2006). Moreover, *Cebpb*-deficient mice present with lower bone mineral density (BMD) and fewer trabeculae compared to control mice (Staiger et al., 2009; Zanotti et al., 2009). These results highlight the critical involvement of C/EBPs in the early stages of mesenchymal stem cell differentiation and commitment (Tominaga et al., 2008).

Notably, many of the osteogenic signalling pathways act as reciprocal inhibitors of adipogenesis. For example, Wnt/β-catenin activation suppresses *Pparg* and *Cebpa*, thereby inhibiting adipocyte differentiation (Kang et al., 2007; H. X. Li et al., 2008). On the other hand, inhibition of Wnt/ β-catenin via antagonists such as DKK1 and sclerostin promotes adipogenic differentiation (Figure 1.12) (Christodoulides et al., 2006; Fairfield et al., 2018). This is a crucial conceptual framework, "see-saw" model of BMSC fate: promotion of osteogenesis tends to suppress adipogenesis and vice versa (Atashi et al., 2015; James, 2013). This "see-saw" fate of BMSC differentiation may drive bone loss and BMAT accumulation noted in CKD patients and experimental models of CKD

(Sirimongkolchaiyakul et al., 2021; Woods et al., 2018). This will be addressed in this thesis (Chapter 5).

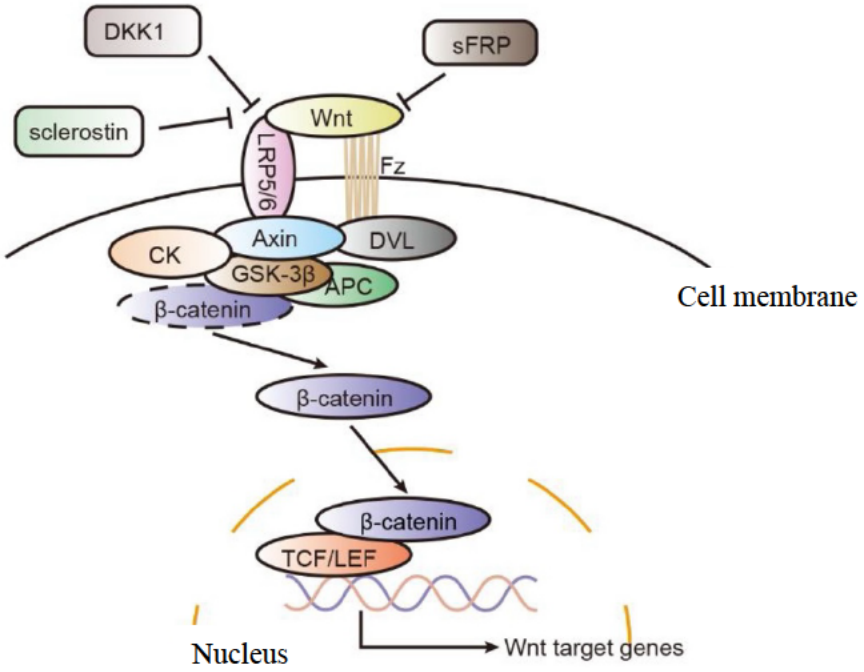

Figure 1.12 The canonical Wnt signalling pathway involves several regulators, including inhibitors such as sFRP, DKK1, and sclerostin. Wnt proteins interact with receptors Fz and LRP 5/6, leading to the activation of DVL and the inactivation of the destruction complex. This process results in the release of cytoplasmic β-catenin, which then translocates to the nucleus. Once inside, β-catenin binds to TCF/LEF transcription factors, thereby controlling the expression of Wnt target genes (Bao et al., 2021)

1.4. Bone marrow adipose tissue (BMAT)

1.4.1. BMAT characterisation

BMAT is differentiated from mesenchymal stem cells. These stem cells can also differentiate into chondrocytes, and osteoblasts (Bianco & Robey, 2015). There are two types of BMAT based on their location in the bone marrow space and functionally they are either constitutive BMAT (cBMAT) or regulated BMAT (rBMAT) (Tavassoli, 1976). cBMAT is the yellow marrow and located in the distal region of long bones whereas rBMAT is interspersed among haematopoietic bone marrow in the proximal part of long

bones (Figure 1.13) (Scheller et al., 2015). During the expansion of haematopoietic tissue, the fat cells within red bone marrow are reduced whereas in the yellow bone marrow the number of fat cells remain constant (Craft et al., 2018). Moreover, during haematopoietic cell depletion, rBMAT but not cBMAT are decreased (Tavassoli, 1976). These pieces of evidence suggest that rBMAT is more labile while cBMAT is more stable when compared to each other. Furthermore, cBMAT spontaneously develops and accumulate after the postnatal developmental period in vertebrates whereas rBMAT volume gradually increase with ageing (Li et al., 2018; Zhang et al., 2024). Also, the fat cells of cBMAT are larger and more densely packed than those of rMBAT (Craft et al., 2018; Scheller et al., 2014).

Functionally, rBMAT, located among several cell types such as haematopoietic, endothelial and bone cells, are thought to be involved in energy production to support their neighbouring cells (Ziru Li et al., 2022; Robles et al., 2019). While cBMAT is also recognised as an energy providing tissue there is a limited number of surrounding cells to support. In addition, they have been proposed as the last energy storage during the final stages of starvation (Devlin, 2011; Zhou et al., 2017). Indeed, BMAT have been defined as an endocrine organ that can secret several adipokines including leptin and adiponectin. These are essential for metabolic homeostasis (Jennifer H. Stern et al., 2016).

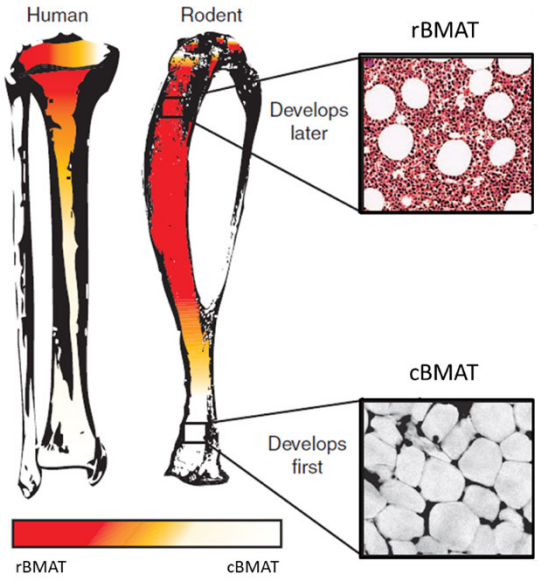

Figure 1.13 Graphical and histological picture representing subtypes of BMAT; rBMAT and cBMAT in human and mouse bone. rBMAT; regulated BMAT, cBMAT; constitutive BMAT. Adapted from Scheller et al., 2015.

1.4.2. BMAT and its regulators

It is well recognised that PPARγ is a master signalling regulator of adipogenesis and contributes to BMAT development (Hardouin et al., 2016; Tencerova & Kassem, 2016). There is supporting evidence that *Pparg* ablation reduces BMAT numbers and increases bone mass in mice, with the researchers stating that its deletion "largely recapitulates high–bone mass phenotypes" (Li et al., 2022). Pharmacological use of the PPARγ antagonist, bisphenol-A-diglycidyl ether, also significantly increased bone volume and improved bone quality, accompanied by decreased marrow adiposity in mature male mice (Duque et al., 2013). In contrast, the overexpression of *Pparg* results in more BMAT and less bone (Tencerova & Kassem, 2016). In addition, there are other transcription factors and secreted products that are crucial for bone marrow adipogenesis, such as fatty acid binding protein 4 (*Fabp4*), leptin and adiponectin (Tencerova & Kassem, 2016).

Leptin and adiponectin are primarily secreted by adipocytes and can regulate adipogenesis (Kajimura et al., 2013; Turner et al., 2013). An *in vitro* study demonstrated that leptin suppresses adipogenesis while promoting osteoblastogenesis in human marrow stromal cells (Thomas et al., 1999). Conversely, mice lacking leptin (ob/ob) and those deficient in LepR (db/db) show increased bone marrow fat accumulation and reduced bone density (Turner et al., 2013). The main effects of leptin on bone are centrally mediated through the sympathetic nervous system (Ducy et al., 2000), as shown by the fact that selective inhibition of the LepR in osteoblasts has no effect on bone mass, whereas its inhibition in the hypothalamus results in a phenotype similar to that of ob/ob mice (Shi et al., 2008). Furthermore, leptin inhibits the activity of extramedullary adipocytes, impairing their ability to respond to insulin, metabolise lipids, and reducing lipogenesis (Harris, 2014). Circulating adiponectin levels rise during caloric restriction (CR) in both animals and humans (Coppola et al., 2009; Delporte et al., 2003), and this increase was found to be secreted from BMAT rather than peripheral white adipose tissue (Cawthorn et al., 2014). This indicates that BMAT significantly contributes to circulating adiponectin, as BMAT expands during CR (Cawthorn et al., 2014). Adiponectin suppresses the differentiation of BMSC into adipocytes (Yokota et al., 2002), promotes

osteoblast differentiation, proliferation, and maturation through a cyclooxygenase 2 (Cox2)-dependent pathway and inhibits osteoclast formation (Lee et al., 2009; Oshima et al., 2005). Nevertheless, the *in vivo* effects of adiponectin on bone mass are more complex. Adiponectin has opposing effects on bone metabolism: it inhibits osteoblast proliferation and promotes apoptosis locally, while reducing sympathetic tone via hypothalamic neurons to increase bone mass (Kajimura et al., 2013).

Moreover, there are several endocrine regulators that can modulate BMAT development. GC are a class of steroid hormones produced by the adrenal gland that can increase BMAT and enhance bone loss after administration of cortisol or corticosterone (Suchacki et al., 2016). In agreement, BMAT is increased in Cushing's patients who have excessive GC production by the adrenal glands (Maurice et al., 2018). On the other hand, administration of leptin prevents the expansion of BMAT by decreasing adipocyte size and number (Ambati et al., 2010). It has also been proposed that leptin may attenuate the effect of GC leading to decreased BMAT accumulation (Perry et al., 2014). Furthermore, removing the GC receptor from bone marrow adipocytes has a minor effect on bone health, and this receptor is not necessary for BMAT accumulation during CR (Schill et al., 2024). Moreover, PTH administration in men and postmenopausal women can decrease the expansion of BMAT (Cohen et al., 2013; Fan et al., 2017; Yang et al., 2016). Additionally, in animal models, PTH administration and also the overexpression of the PTH receptor in transgenic mice can suppress BMAT accumulation (Calvi et al., 2001; Costa et al., 2019). A recent study discovered a novel pathway where PTH regulates osteogenesis and suppresses adipogenesis through the production of Zfp467 in a feed-forward, PTH receptor 1(PTH1R)-cyclic AMP pathway-dependent manner in mesenchymal progenitor cells (Figure 1.14) (Liu et al., 2023). These data emphasise the importance and ability of various regulators to control adipocyte formation and BMAT modulation. However, the underlying mechanism(s) involved in BMAT development are still unclear in both physiological and pathological conditions including CKD that might contribute to bone loss.

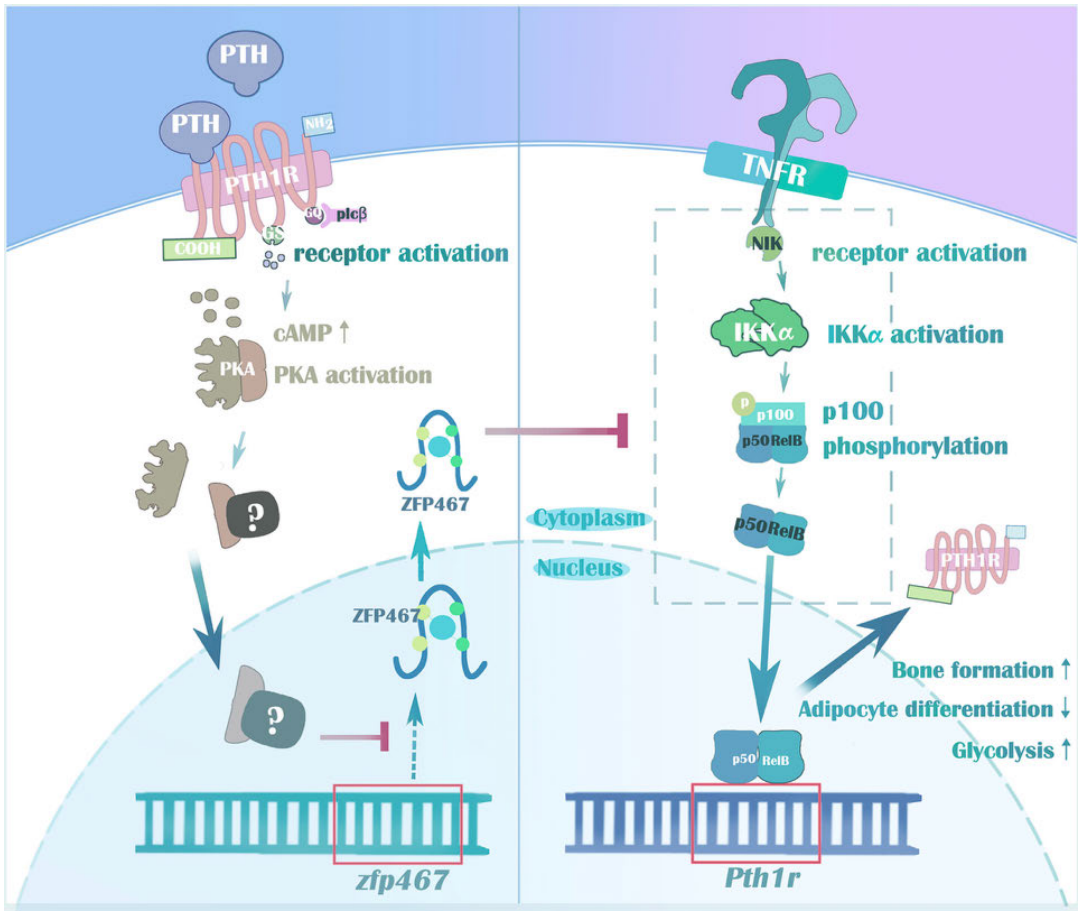

Figure 1.14 PTH regulates osteogenesis and suppresses adipogenesis through Zfp467 in a feed-- forward, PTH1R-- cyclic AMP-dependent manner in mesenchymal progenitor cells (Liu et al., 2023).

1.4.3. BMAT and bone metabolism

Bone and BMAT are products of the same skeletal stem cells (Bianco & Robey, 2015). It has been proposed that BMAT may provide mechanical support to bone but it may also play a role in facilitating bone formation as shown in the armadillo where fluctuations in BMAT positively associated with bone formation (Craft & Scheller, 2017; Simkin, 2018). However, as BMAT and bone are differentiated from the same skeletal stem cells, any increase of adipocyte formation could have a negative effect on osteoblast formation which may result in reduced bone formation and increased fracture incidence. Most studies report an inverse relationship between BMAT and bone in both healthy and

disease conditions (Veldhuis-Vlug & Rosen, 2018). For example, the inverse relationship between BMAT and bone mass has been shown in healthy white women aged 18-80 years (Shen et al., 2007). Additionally, longitudinal studies have reported that higher BMAT levels contribute to age-related bone loss in elderly women. (Griffith et al., 2011). Postmenopausal women with osteoporosis have demonstrated an increase in BMAT (in size and amount of adipocytes) while a decrease in BMD (Beekman et al., 2019). In addition, the clinical relationship between osteoporosis and BMAT accumulation has also been investigated. Bisphosphonates and oestrogen not only improved bone quality but also decreased BMAT in osteoporotic women and men (Fan et al., 2017; Yang et al., 2016) as well as in animal models (Costa et al., 2019). Moreover, the increase in BMAT has also been associated with poor bone integrity and increased fracture risk (Schellinger et al., 2001). Furthermore, a preclinical study found that BMAT depletion increases local bone formation and protects mice from CR- and OVX-induced bone loss (Li et al., 2022). Whilst the inverse relationship between bone mass and BMAT volume is well accepted, the underlying mechanisms need to be further investigated. Additionally, there was a study in elderly people (both sexes, average age around 80 years old) reported that the increase in saturated BMAT is associated with negative bone outcomes such as reduced BMD and increased risk of both existing and future vertebral fractures. In contrast, unsaturated BMAT is linked to better bone health and reduced fracture risk of vertebral bone. These findings indicate that saturated and unsaturated BMAT exert distinct, independent and opposing influences on bone health which will need further investigation on the underlying mechanism (Woods et al., 2022). Recently, several studies have reported that factors secreted by bone marrow adipocytes can modulate osteoblast and osteoclast differentiation and function. For example, BMAT secreted extracellular vesicles contain adipogenic RNA that can attenuate osteoblast function (Sulston & Cawthorn, 2016). Additionally, BMAT can secrete signalling molecules, including RANKL and CXCL1; molecules that can contribute to osteoclast differentiation and result in increased bone resorption (Fan et al., 2017; Sulston & Cawthorn, 2016).

1.4.4. Relationship between BMAT and bone mass in humans or experimental animals with CKD

Recently, an accumulation of BMAT in CKD patients in comparison to healthy adults has been reported, and this elevation was associated with the severity of CKD (Moorthi et al., 2015; Woods et al., 2018). In addition, children with CKD have increased BMAT and a high bone turnover rate (high serum concentration of PTH and TNAP activity). The inverse relationship between a reduced bone formation rate and an increased adipocyte number was also found in CKD children with high bone remodelling (Sirimongkolchaiyakul et al., 2021). Moreover, patients with advanced CKD (G4-5) who received one healthy kidney transplant have higher BMAT amounts after one year of transplantation which was inversely correlated to bone health (Hernandez et al., 2018). In experimental studies, the induction of CKD by nephrectomy and dietary adenine resulted in the elevation of BMAT (Ni et al., 2019; Wang et al., 2017). These data have led to the hypothesis that BMAT accumulation in CKD may be a result of altered bone marrow-derived skeletal stem cell differentiation which would lead to compromised bone formation. However, the underlying mechanism of BMAT accumulation together with bone loss in CKD is poorly understood and requires further investigation.

1.5. Possible mechanisms of dietary adenine-induced CKD in animal models

There are a number of experimental animal models available to study the aetiology of CKD (Yang et al., 2024). These include 5/6 nephrectomy (Lair et al., 2024; Vaziri et al., 2013; Watanabe et al., 2013) diabetic nephropathy (Alicic et al., 2017; Reidy et al., 2014; Wada & Makino, 2013), hypertension-induced renal injury (Ku et al., 2019; Udani et al., 2011), primary glomerular nephropathy (Arif et al., 2016; Bertani et al., 1986) and adenine-induced CKD (Hsu et al., 2025; Lair et al., 2024; Yokozawa et al., 1986) which was used in this thesis. The adenine-induced CKD model has been used for several years and is a well-established non-invasive technique to induce CKD in animals, including mice and rats. This model exhibits higher serum levels of PTH, FGF23, Pi, creatinine and BUN which reflect the malfunction of the kidney in adenine-treated mice compared to controls (Diwan et al., 2018; Hsu et al., 2022; Hsu et al., 2025; Rahman et al., 2018).

Table 1. Summary of advantages and disadvantages of CKD animal models. (Bao et al., 2018; Liang & Liu, 2023)

Models	Advantages	Disadvantages	References
5/6 nephrectomy	- Mimic progressive glomerulosclerosis and interstitial fibrosis - Common model for renal failure	- Highly invasive technique - High mortality rate - Not ideal for studying early stages of CKD	Lair et al., 2024; Vaziri et al., 2013; Watanabe et al., 2013
Diabetic nephropathy	- Gene modified - Commercially available	- Expensive - Confounding effect of diabetes - Take long time to develop advanced CKD	Alicic et al., 2017; Reidy et al., 2014; Wada & Makino, 2013
Hypertension-induced renal injury	- Genetic modified - Useful to study angiotensin II effect over kidney	- Confounding effect of hypertension - High cost - Slow CKD progression	Ku et al., 2019; Udani et al., 2011
Primary glomerular nephropathy	- Widely used - Induce podocyte injury	- Highly depends on species and strains - Toxic for most other cells (drug induced) - Resistant in C57BL6 mice	Arif et al., 2016; Bertani et al., 1986
Adenine-induced CKD	- Mimics human chronic tubulointerstitial nephropathy - produces the range of CKD stages - non-invasive technique	- causes severe animal weight loss - not a direct model of genetic CKD	Hsu et al., 2025; Lair et al., 2024; Yokozawa et al., 1986

The adenine-induced model offers specific benefits not found in other models. Firstly, adenine is a nucleobase and purine derivative that provides an environmentally safe option and poses no risk during standard laboratory procedures. Unlike the 5/6 nephrectomy model, adenine induction is delivered through simple methods such as gavage or dietary feeding, making it a non-surgical and non-invasive procedure for the

animal. Third, the adenine induction technique enables the creation of a range of CKD severity from mild to severe, which exhibit a consistent progression of the disease and are produced with a high success rate, with outcomes influenced by the dosage of adenine and the length of treatment (Diwan et al., 2018; Diwan et al., 2013). The adenine model consistently replicates the progression of kidney disease in both male and female animals, providing valuable insights into gender-specific differences that reflect the clinical presentation of CKD affecting both sexes (Bairey Merz et al., 2019; Diwan et al., 2014; Melsom et al., 2022). Nevertheless, the adenine-induced model of chronic kidney disease has certain limitations. One such limitation is the uncertainty regarding adenine's effects on reproductive and other organ systems, as no specific biomarkers for adenine-induced CKD have been identified. Additionally, although this model primarily damages renal tubules, the detailed molecular and biochemical pathways responsible for nephron injury caused by adenine remain unclear.

There are several lines of evidence that support the mechanisms by which supplementary dietary adenine can induce CKD progression. In the gastrointestinal tract, adenine is absorbed and normally metabolized by adenine phosphoribosyltransferase to form adenosine monophosphate, which serves as a precursor for several purine metabolites, including adenosine, inosine monophosphate, hypoxanthine, and xanthine. Xanthine is subsequently converted into uric acid, which is eliminated by the kidneys. Adenine can also be metabolized by xanthine oxidase, producing 2,8-dihydroxyadenine, a compound excreted in urine, which can be highly accumulated in the kidney after prolong administration (Yang et al., 2024). The 2,8-dihydroxyadenine can cause kidney tubulointerstitial fibrosis as indicated by renal histopathology and the upregulation of inflammatory and fibrotic genes in adenine-treated mice, leading to CKD (Jia et al., 2013; Yang et al., 2024). Inroads have been made towards an understanding of the cellular mechanisms responsible for the observed renal interstitial fibrosis in adenine-induced mice (Jia et al., 2013; Yuan et al., 2021). Autophagy of tubular epithelial cells has been proposed as the underlying mechanism for the development of interstitial fibrosis which is reliant on the mechanism Transcription Factor EB (TFEB) (Yuan et al., 2021). TFEB protein is increased in renal tubular epithelial cells of adenine-fed mice, and this leads to a cascade of downstream effects on regulators of the autophagy process, which include

Beclin-1, the autophagy activator of phagophore formation and LC3, an autophagosome membrane-associated protein (Ren et al., 2024; Yuan et al., 2021). Interestingly, the expression of TFEB and LC3 proteins are also upregulated in renal tubular epithelial cells of CKD patients (Nakamura et al., 2020). This evidence strongly supports a role for TFEB and autophagy induced tubulointerstitial fibrosis in the aetiology of CKD in the dietary adenine mouse model (Yuan et al., 2021).

1.6. Project Rationale and Objectives

Although a few studies have reported an increase in BMAT in CKD patients and animal models, the cell and molecular mechanisms in how BMAT accumulation relates to bone loss in CKD are unclear. Moreover, a previous RNA-seq study in my host laboratory has revealed that in CKD mouse bone the expression of genes associated with bone formation were decreased whereas genes associated with adipocyte formation were increased (Hsu et al., 2025). These data suggest that BMAT may increase in CKD mice due to the mesenchymal stem cells switching from osteoblast differentiation to adipocyte differentiation.

In addition, previous publications report cross-sectional data that cannot inform on disease progression and associated bone loss and BMAT accumulation. Therefore, to identify the factors contributing to BMAT accumulation, analysis of tissues with increasing CKD severity would be beneficial. Such mechanistic information will potentially benefit intervention strategies and drug development that may prevent bone loss in CKD patients by inhibiting adipogenesis in the bone marrow.

Therefore, in this study, I set out to examine the hypothesis that bone deterioration in CKD mice may be the result of an imbalance between adipogenesis and osteoblastogenesis, leading to BMAT accumulation in this mouse model. To address this hypothesis, the specific aims for my PhD research were:

Aim 1: To establish a CKD mouse model by feeding adult male mice a diet supplemented with 0.2% adenine and analyse blood and tissues taken at early (1 week), mid (3 weeks) and advanced (5 weeks) stages of CKD.

Aim 2: To evaluate the bone phenotype and BMAT accumulation in experimental CKD progression in relation to systemic levels of PTH, FGF23, adiponectin, leptin, and corticosterone.

Aim 3: To evaluate, via *in vitro* experimentation, the ability of PTH, FGF23, indoxyl sulfate, sclerostin and Pi to differentiate BMSC to the osteoblast or adipocyte lineages

Aim 4: To determine if bone loss and BMAT accumulation in experimental CKD can be prevented with a bispecific antibody to sclerostin and DKK1.

Chapter 2

Materials and methods

2.1. Reagents and solutions

Chemicals were acquired from Sigma Aldrich (Dorset, U.K.) unless specified otherwise. Tissue culture flasks, cell culture plates, and reagents were obtained from Thermo Fisher Scientific (Northumberland, U.K.), unless otherwise specified. PCR primers were obtained from Primerdesign (Camberley, UK) and Sigma-Aldrich (Dorset, UK).

2.2. Animals and tissue collections

Male C57BL/6J strain mice were purchased from Charles River Laboratories (Margate, Kent, UK) and used in all studies. Male mice were used throughout this study to avoid potential variability associated with the oestrous cycle in females, which could introduce hormonal influences on bone remodelling and metabolism. All animal studies were approved by the Roslin Institute's named veterinary surgeon (NVS) and named animal care and welfare officer (NACWO), with animals maintained in accordance with the Home Office code of practice (for the housing and care of animals bred, supplied or used for scientific purposes). The number of animals used in each experiment was determined based on previous studies (Hsu et al., 2025). All mice were maintained at the Roslin Institute BRF, University of Edinburgh, unless otherwise stated.

2.2.1. Study 1: BMAT accumulation and bone phenotypes in different stages of CKD

A group of 36 seven-week-old mice were acclimatised for 1 week after arrival and then randomly assigned to either a CKD (n=18) or a control (n=18) group. The mice in the CKD group were fed a casein-based diet containing 0.6% calcium, 0.9% Pi, 1.5% Vitamin Mix (AIN-76A, containing vitamin D_3), and 0.2% adenine (Envigo, Teklad Co. Ltd, Cat# TD.140290). Control mice received the same diet without adenine supplementation (Envigo, Teklad Co. Ltd, Cat# TD.138898). Body weights were recorded every 2 days until termination.

Six control and CKD mice were sacrificed after 1, 3 and 5 weeks of CKD induction. Blood was collected by cardiac puncture under anaesthesia for evaluation of biochemistry (calcium, Pi, BUN, and creatinine) and hormone levels (PTH, FGF23, leptin, adiponectin, and corticosterone). Tibiae and femora were collected, processed and

stored accordingly. Left tibiae were collected and fixed with 10% neutral-buffered formalin (NBF) to evaluate BMD and also trabecular and cortical bone architecture by using micro computed tomography (μCT) (section 2.6). Thereafter, the bones were stained with osmium tetroxide to allow the quantification of adipocyte accumulation inside bone marrow (section 2.5). Right tibiae and femora were dissected and the proximal and distal epiphysis was cut apart to remove the articular and growth plate cartilage. The bones were placed in a cut-pipette tip inserted in a 1.5 mL Eppendorf and centrifuged at 13,000 rpm, 1 minute at 4 °C to separate bone marrow tissue and bone. Bone marrow and bone tissue of tibiae and femora were flash-frozen in liquid nitrogen and stored at -70 °C and analysed separately to evaluate the expression of genes that are recognised to be involved in osteoblast and bone marrow adipocyte differentiation (sections 2.10.2).

2.2.2. Study 2: Food intake and body composition evaluation by Time-Domain Nuclear Magnetic Resonance (TD NMR)

Sixteen seven-week-old mice were used in this study. Mice were acclimatised for 1 week and then singly housed and assigned to either the control (n=6) or CKD (n=10) groups. The mice were fed ad lib according to their respective diet for 5 weeks. Food and water intake were monitored and recorded every day. This study was conducted at the Little France, University of Edinburgh, animal facility.

The plan for this study was to evaluate body composition (fat, muscle and bone) at baseline, 1, 3 and 5 weeks after CKD induction by using the TD NMR (section 2.3). Unfortunately, after two weeks of induction, the adenine-fed mice lost more than 30% of their initial weight, and, considering welfare grounds, this study was terminated. Therefore, only baseline and 1-week-old data were obtained.

2.2.3. Study 3: BMSCs, osteoblast (OPC) and adipocyte (APC) precursor cells populations in the early stages of CKD (1 and 2 weeks of CKD induction)

Twenty-four seven-week-old male mice were used in this study. The mice were acclimatised for 1 week after arrival before being randomly assigned to either a CKD or a control group. The CKD and control mice were fed with their respective diets for 1 or 2 weeks and the body weight of each mouse was recorded every 2/3 days.

Blood was collected by cardiac puncture under anaesthesia for the quantification of BUN and creatinine levels. Peripheral white adipose tissue (WAT), including inguinal and gonadal WAT, was collected and weighed. To collect the marrow cells, the tibiae and femora were dissected and the proximal and distal epiphysis was cut apart to remove the articular and growth plate cartilage. The bones were placed in a cut-pipette tip inserted in a 1.5 mL Eppendorf and centrifuged at 13,000 rpm, 1 minute at 4 °C. The marrow cells from the tibia and femur of each mouse were pooled together for flow cytometry analysis to evaluate the BMSC, APC, and OPC populations (section 2.7).

2.2.4. Study 4: Pair-feeding study

This study was conducted over three separate trials. The first trial involved 26 seven-week-old male mice. The mice were acclimatised for one week after arrival prior to being single housed and randomly assigned to either control, CKD, or pair-fed groups. The control (n=6) and CKD mice (n=10) were fed *ad-libitum* with normal and adenine diets, respectively whereas the pair-fed mice (n=10) received the same amount of normal diet that their "paired" CKD mouse consumed the previous day. These mice were expected to be treated with their respective diets for more than three weeks. Unfortunately, the CKD mice lost over 30% of their initial body weight during the first week of induction. Consequently, the study was terminated on animal welfare grounds and no results were obtained. This rapid loss of bodyweight was also seen in the single-housed CKD mice of study 2, and after discussions with our NVS and NACWO, it was considered that single housing was causing extra stress, leading to excess body weight loss. Therefore, in a 2nd study, male mice aged six weeks were acclimatised in the rodent facility at the Roslin Institute, for one week in group housing and then for another week in single housing. They were then randomly assigned to control, CKD, and pair-fed groups, but the CKD mice again lost more than 30% of their initial body weight within the first two weeks of induction. As a result, this study was also terminated without any results.

Although group housing is not ideal for a pair-fed study, it was judged that housing 2 mice in one cage may be a compromise and workable solution. Therefore, the final trial was performed by housing 2 mice/cage. Twenty-six seven-week-old male mice were used in this study. They were acclimatised for 1 week after arrival before being housed in pairs

and randomly assigned to control (n = 6, 3 pairs), CKD (n = 10, 5 pairs) or pair-fed (n = 10, 5 pairs) groups. Control and CKD mice were fed *ad-libitum* with normal and adenine diet, respectively whereas the pair-fed group were fed the same amount of normal diet consumed by its paired cage (CKD cage) the previous day. The mice were fed their respective diets for 3 weeks and body weight was recorded every day. After the sacrifice, the tibiae were collected and BMAT was stained with osmium and evaluated by μCT.

2.2.5. Study 5: Potential differentiation of BMSCs to either adipocyte or osteoblast lineages of CKD mice

Eight male mice at 7-weeks of age were used in this study. The mice were acclimatised for 1 week and then randomly assigned equally to either a CKD group or a control group. CKD mice were fed an adenine-supplemented diet, while control mice received the same diet without adenine supplementation. The mice were maintained on their respective diets for 4 weeks to induce CKD. The study was terminated at this point because CKD mice had lost nearly 30% of their initial body weight. At the termination date, the mice were sacrificed, and the tibiae, femora, humeri, and iliac bones were isolated. The adhering muscle and connective tissues were quickly removed and the cleaned bones were subjected to BMSCs isolation as described in section 2.9.1.

2.2.6. Study 6: Effect of sclerostin and DKK1 antibodies neutralisation on bone phenotype and BMAT accumulation

Forty 7-week-old male mice were used in this study. The mice were acclimatised for 1-week and then randomly assigned to either a CKD group, which were fed with an adenine-supplemented diet *ad-libitum*, or a control group, which were fed the same diet *ad-libitum* without adenine supplementation. In this study, the CKD induction regimen was modified from the standard protocol in which an adenine supplemented diet was offered 7 days per week to a 5 days on/2 days off protocol. In summary, the CKD mice were fed the adenine diet for 5 days and then switched to a normal diet for the remaining 2 days of each week. Control mice were fed a normal diet throughout the study period. This protocol was continued for 6-weeks and no mouse lost more than 30% bodyweight. This modification of the previous protocol was based on the studies of Lair and colleagues and introduced to induce CKD but avoid pathological weight loss (Hsu et al., 2022; Lair

et al., 2024) Each of the 10 mice in both the control and CKD groups was treated with either vehicle (phosphate-buffered saline, PBS) or Sclerostin/Dkk1 antibody (rbsAb). This antibody is a bispecific antibody that binds specifically to both sclerostin and Dkk1 proteins. It was kindly provided by Angitia Biopharmaceuticals, Guangzhou, China. The control and CKD mice received intraperitoneal injections of either PBS or rbsAb at a dose of 30 mg/kg body weight on days 0, 7, 14, 21, 28, and 35. Their body weights were recorded every other day.

After 6 weeks, the mice were sacrificed, and blood was collected by cardiac puncture under anaesthesia for the quantification of serum levels of calcium, Pi, BUN, creatinine, PTH, sclerostin and DKK1. Gonadal WAT (gWAT), inguinal WAT (iWAT), tibiae, femora and lumbar vertebrae 4 (L4) were dissected, processed and stored accordingly. gWAT and iWAT were measured and normalised to their respective body weights. The left tibiae were used to evaluate bone structure and mineral density using μCT. Thereafter, they were decalcified and stained with osmium tetroxide for BMAT evaluation by μCT. The right tibiae were used for proteomics analysis (n = 5), and the other half of the group (n = 5) was used for RT-qPCR gene expression in cortical bone and bone marrow tissue. The right femora were used for 3-point bending analysis. L4 were collected for structural analysis by μCT and compression testing.

2.3. Time domain nuclear magnetic resonance (TD-NMR)

The TD-NMR (Bruker) measurement offers details on mice body fat, lean mass, and free fluid. It enables non-invasive body composition analysis using radio-frequency energy, allowing the entire sample volume to be analysed without harm. Mice are placed in plastic tubes supplied by Bruker, then gently pushed to the end with an inserter that locks onto the tube to ensure safety. The tube is inserted into the TD-NMR machine for about 20-30 seconds. After scanning, the results for body fat, lean mass, and free fluid are displayed as absolute masses. The tube is then removed from the scanner and opened above the cage to release the mouse.

2.4. Blood biochemistry

Heparin-coated tubes were used to collect the blood, approximately 0.5-0.9 ml from each mouse. Plasma was obtained by centrifugation at 2500 x g for 10 min at 4°C. The plasma was aliquoted (200 µL) into micro Eppendorf tubes and creatinine, BUN, Pi and calcium concentrations were evaluated immediately using a chemical analyser (Beckman Coulter AU480, Olympus). This service was done by colleagues at Easter Bush Pathology, The Royal (Sadick et al.) School of Veterinary Studies, University of Edinburgh. The remaining plasma was stored at -80 °C.

2.5. Enzyme-linked immunosorbent assay (Bacchetta et al.)

ELISA kits were used to quantify PTH (Immutopics, Cat# 60-2305), FGF23 (Kainos Laboratories, Inc. Japan, Cat# CY4000), adiponectin (Sigma-Aldrich, Inc., Cat# A6354), leptin (R&D, Cat# MOB00), corticosterone (Enzo, Cat# ADI-900-097), sclerostin (R&D, Cat# MSST00) and DKK1 (R&D, Cat# MKK100) in each plasma sample. All ELISAs used in this study were colorimetric competitive enzyme immunoassays, and each ELISA was performed following the manufacturer's instructions.

2.6. Osmium tetroxide staining

Tibiae were fixed in 10% NBF for 24 hours before µCT scanning for the analysis of bone structure (section 2.7). The bones were then decalcified in 10% ethylenediaminetetraacetic acid (EDTA, pH 7.4) at 4°C with constant agitation for 14 days. The EDTA solution was changed every 2-3 days. The decalcified bones were washed with Sorensen's buffer and stored in a 1.5 mL Eppendorf tubes containing 400 µL of Sorensen's buffer. To stain the decalcified bones, 400 µL of 2% osmium tetroxide (Clinisciences Ltd, Cat# 23310-10) was added to each tube, and then 400 µL of Sorensen's buffer was added to make a final concentration of 1% osmium tetroxide. The decalcified bones were incubated at room temperature for 48 hours and thereafter the bones were washed for 1 hour with 2-3 changes of Sorensen's buffer. The 1% osmium solution and all the plastics that came into contact with osmium were deactivated with corn oil before normal cleaning or disposal. As osmium tetroxide is a very toxic reagent, the entire osmium staining process was done in a fume hood following the standard operating

procedure. The stained bones were stored in Sorensen's buffer at 4°C, and the BMAT was quantified by μCT.

2.7. Micro computed tomography (μCT)

The calcified (tibia and L4 vertebrae) and decalcified osmium stained bone were scanned by μCT (Skyscan 1172 X-ray microtomography, Bruker, Kontich, Belgium) to quantify bone architecture and BMAT accumulation. Briefly, these samples were scanned at high resolution with an isotropic voxel size of 5 μm (60 kV, 167 μA and 0.5 mm filter, 0.6° rotation angle). Next, the slices acquired from the scanner were reconstructed using the NRecon 1.7.3.0 program (Bruker, Kontich, Belgium). Then, CTAn software 1.15.4.0 (Skyscan) was used to visualise and evaluate bone structural parameters and BMAT volume from the reconstructed image sets. Three-dimensional (3D) images were created using CTVol software (Skyscan).

To analyse tibia architecture, each bone was aligned along its longitudinal axis and the volume of interest (Bellorin-Font et al.) of the whole bone was selected. The trabecular (Tb) VOI in the proximal tibial metaphysis was selected from the bottom of the growth plate, excluding cortical bone and extended distally 50 slides (250 μm) from the growth plate. A total of 250 slices beneath this slice were selected to analyse trabecular bone to obtain the following parameters using CTAn software (Skyscan, Belgium); trabecular bone volume/tissue volume (BV/TV; %), trabecular thickness (Tb. Th; mm), trabecular number (Tb. N; 1/mm), trabecular separation (Tb. Sp; mm), and trabecular connectivity density (Tb. Conn Dn; $1/mm^3$). Hydroxyapatite phantoms of known hydroxyapatite densities - 0.25 and 0.75 g/cm^3 - were scanned and reconstructed as described, allowing the calculation of BMD. For the analysis of tibial cortical bone, 2D analysis of the entire tibia (10-90% of the whole bone length, Figure 2.1) was conducted by using CTAn software (Skyscan, Belgium), and the following parameters were measured; cortical bone area (B.Ar; mm^2), thickness (mm), maximum moment of inertia (MMI max; mm^4), minimum MMI (MMI min; mm^4), polar MMI (J; mm^4), medullary area (Med.Ar; mm^2), periosteal perimeter (P.Pm; mm), endosteal perimeter (E.Pm; mm) and porosity (%). The data from the diaphysis (10 – 90% of the tibial length, Figure 2.1) was analysed using R Studio (Bourne et al., 2024; Javaheri et al., 2020).

To analyse the structure of the L4 vertebra, a 300-slice section through the middle of the vertebral body was examined. The analysis included calculating trabecular parameters *i.e.* BMD (g/cm^3), bone volume/tissue volume (BV/TV; %), thickness (Tb. Th; mm), number (Tb. N; 1/mm), and separation (Tb. Sp; mm) and cortical parameters including BMD (g/cm^3), bone volume (BV; mm^3), and thickness (Th; mm).

To analyse BMAT volume, osmium-stained bones were scanned and aligned along their longitudinal axis. The distribution of BMAT along the tibia length (10 - 90% of tibia length, Fig. 2.1) was examined with (Chapter 3 and 5) /without (Chapter 5) normalisation to the marrow cavity by R Studio (Bourne et al., 2024; Javaheri et al., 2020). Moreover, the tibia was divided into three anatomical regions to analyse the distribution of BMAT in the proximal epiphysis, which is from the top of the proximal bone to the growth plate (Proxi Epi), the growth plate to tibia/fibula junction (GP to T/F J), which contains regulated BMAT (rBMAT) and the tibia/fibula junction to the end of the distal bone (T/F J to End) which contains constitutive BMAT (cBMAT). BMAT volume in each region of the bone was analysed and normalised with the size of the bone marrow cavity (Chapters 3 and 5). Bones and BMAT accumulation in Chapter 5 (Study 6: Sclerostin and DKK1 antibody neutralisation) were scanned with the new µCT (NeoScan N80, Mechelen, Belgium) under the same conditions as described above. All slides of all the samples were reconstructed with the NRecon 1.7.3.0 program (Bruker, Kontich, Belgium) under the same conditions. 3D images were created using the Neoscan80 software package (NeoScan).

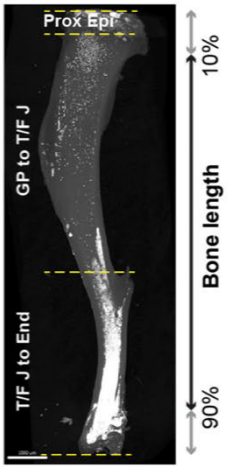

Figure 2.1 Image of the whole length of a decalcified tibia stained with osmium. This figure shows the three anatomical regions of the diaphysis (10- 90 % of the entire tibial

length) in which BMAT accumulation was analysed - . the top of the proximal bone to the growth plate (Proxi Epi); the growth plate to tibia/fibula junction (GP-T/F J); and the tibia/fibula junction to the end of the distal bone (T/F J-End).

2.8. Flow cytometry

BMSCs were isolated from the tibiae and femora of control and CKD mice at 1 and 2 weeks post-CKD induction, as described in section 2.2.3. Cells from each mouse were pooled and suspended in 1 mL of cold cell-suspension buffer containing 2% foetal bovine serum (FBS) and 100 U/mL penicillin/streptomycin (P/S) in PBS. Hematopoietic cells were depleted using ammonium-chloride-potassium lysis buffer for 5 minutes. The cells were then resuspended in cell-suspension buffer and blocked for 30 minutes with 2% rabbit serum in PBS to prevent non-specific binding. Subsequently, the cells were incubated for 1 hour with fluorochrome-conjugated monoclonal antibodies (from Thermo Fisher Scientific, UK): anti-CD45 (Cat# 11-0451-82), CD31 (Cat# 11-0311-82), Sca1 (Cat# 17-5981-82), Pa (Cat# 12-1401-81), and CD24 (Cat# 47-0242-82). Zombie Violet (BioLegend, USA, Cat# 423113) served as a dead cell marker. A fluorescence minus one (FMO) control was used for each antibody to establish gating boundaries. Flow cytometry was conducted on a BDLRSFortessa™ instrument, and cells were identified with FlowJo software based on the following surface marker profiles: BMSC (CD31–CD45–Sca1+Pa+CD24+), APC (CD31–CD45–Sca1+Pa+CD24–), and OPC (CD31–CD45–Sca1–Pa+) (Ambrosi et al., 2021).

2.9. Mechanical property analysis

2.9.1. Three-point bending analysis

Three-point bending tests were performed on the femur diaphysis using an LS5 Lloyds materials testing machine equipped with NEXYGEN Plus software (Ametek, Leicester, UK) and a 100 N load cell. The goal was to assess bone stiffness and breaking strength. The testing setup involved placing the femora on an anvil in a consistent anteroposterior orientation, with a span length of 10 mm. The crosshead pressed down perpendicular to the bone at a speed of 10 mm/min. Data collection commenced after each increment of 0.2 N in load and 0.1 mm in displacement. The bones were subjected to load until they fractured. For each sample, a load-displacement curve was plotted and analysed.

Key biomechanical parameters such as stiffness, maximum load, yield load, work to fracture, and post-yield displacement were calculated, as illustrated in Figure 2.2.

2.9.2. Compression analysis

For compression testing, the spinal processes were removed from the vertebral body and prepared to have flat and parallel ends, which were obtained using a polishing wheel. It was then bonded to a fixed bottom plate with cyanoacrylate glue. A 500N load cell, moving downward at a speed of 10 mm/min, compressed the vertebra until it permanently broke. The load-displacement curve was generated, and data were recorded after every 0.2 N change in load until bone deformation occurred. The load-displacement curve for each bone was analysed and calculated to obtain the following parameters: stiffness, maximum load, yield load, work to fracture and post-yield displacement as shown in Fig. 2.2.

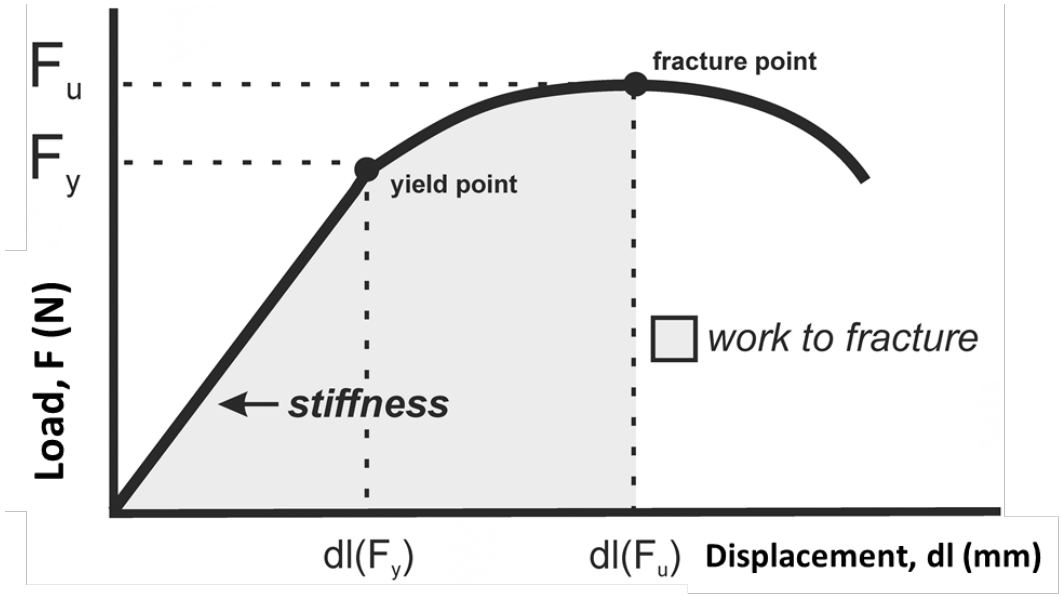

Figure 2.2 The illustration of a typical load-displacement curve used to assess the biomechanical characteristics of a single bone in a three-point bending test and compression. The force at the initial point of damage (Suchacki et al.) indicates the maximum strength of the bone under elastic conditions, while F_u represents the minimum load required to break the bone, reflecting its structural strength. The grey square area denotes the energy needed to fracture the bone. The displacements shown include dl (Suchacki et al.), which is the maximal elastic deformation at the yield point, and dl (F_u), the deformation at fracture. Stiffness is determined from the linear section of the curve, calculated as the ratio of load to displacement (Pawlak et al., 2016).

2.10. *In vitro* study

2.10.1. Primary mesenchymal stromal cells culture and maintenance

Primary BMSCs were collected from tibiae, femora and iliac bones of normal male mice aged 8-9 weeks old to assess the ability of CKD-associated systemic factors (*i.e.* Pi, PTH, FGF23, sclerostin and IS) to directly influence the differentiation of BMSCs to the adipocyte or osteoblast phenotype. Primary BMSCs from study 5 were isolated from the tibiae, femora, humeri and ilia of CKD and control mice after 4 weeks on their respective diets. For BMSCs isolation, the proximal and distal ends of the bones were removed and placed in a cut-pipette tip inserted into a 1.5 ml Eppendorf tube containing BMSC basal media [minimum essential medium alpha (αMEM, Life Technologies, Cat# 22561021), 10% foetal bovine serum (FBS, Life Technologies, Cat# 10500064), and 1% penicillin/streptomycin (P/S; Life Technologies, Cat# 11528876)]. The bones were then centrifuged at 10,000 rpm for 1 minute at room temperature to pull down the BMSC into the culture media. and the pipette tips and bone were discarded. A 1 ml syringe fitted with a 25 G needle was used to disperse any clump of cells. The mix of BMSCs and haematopoietic cells was expanded in BMSC basal media in T175 flasks (Thermo Scientific, Cat# 159910) at 37 °C with 5% CO_2 for 48 hours. Next, cells were trypsinised with 0.25% trypsin-EDTA (Thermo Scientific, Cat# 25-200-056) under agitation at 37 °C for 5 minutes. BMSCs (250,000 cells) were plated in 6-well plates (Corning B.V Life Sciences, Cat# 3516) and maintained until they reached 80-90 % confluence for further experiments. Culture media was changed every other day during maintenance.

2.10.1.1. BMSC culture in differentiation media

Upon confluency (designated as day 0), the BMSC basal medium was replaced with either osteogenic or adipogenic differentiation media, depending on the intended lineage commitment. For osteogenic differentiation, confluent BMSCs were cultured for 21 days in osteogenic medium comprising 8 mM L-ascorbic acid and 1 mM β-glycerophosphate (βGP) in BMSC basal medium. The osteogenic medium was refreshed every two to three days. Following confluence, BMSCs were exposed to adipocyte induction medium (AIM), comprising 0.5 mM 3-isobutyl-1-methylxanthine (IBMX), and

1 µM dexamethasone in adipocyte basal medium (ABM; 10% FBS, 1% penicillin/streptomycin, 20 µM Rosiglitazone, and 2µM insulin in high-glucose Dulbecco's Modified Eagle Medium (DMEM)), for 48 hours. This medium was then replaced with fresh AIM for an additional 48 hours. On day 4, the AIM was substituted with ABM, and the cells were maintained in ABM until day 7, with medium changes every other day (Maridas et al., 2018).

2.10.2. MLO-Y4 cell line culturing and maintaining

MLO-Y4 cell line (a kind gift from Lynda Bonewald) is a murine late osteoblast/preosteocyte cell line that is usually used to investigate the osteoblast-to-osteocyte differentiation, mineralisation processes, and the effects of mechanical loading on bone cells, contributing significantly to our understanding of bone biology and related pathologies.

All flasks and multi-well plates used to culture the MLO-Y4 cells were coated with sterile collagen (rat tail type I collagen, Sigma-Aldrich, Cat# C3876). The collagen powder was dissolved in 0.02M acetic acid to prepare a working solution at a concentration of 0.15 mg/mL. This solution was then used to coat all the flasks and plates before conducting the experiments. All plates and flasks were coated for 1 hour at room temperature, and after removing the collagen solution, the plates were dried at room temperature under sterile conditions. The coating solution was kept at 4 °C and can be reused 6 times. The dried plates/flasks can be kept for 1-2 months at 4 °C. Prior to culture, the dried plates/flasks were rinsed with PBS.

A cryovial of MLO-Y4 cells were quickly thawed after removal from liquid nitrogen and cultured at 37 °C in the media, αMEM containing 5% heat-activated (at 56°C for 30 mins) FBS, 5% heat-activated (at 56°C for 30 mins) bovine calf serum (CS: Thermo Scientific, Cat# 26010074) and 1% P/S for 1-2 days. Thereafter, the cells were changed to maintenance media (αMEM media containing 2.5% heat-activated FBS, 2.5 % heat-activated CS and 1 % P/S) in a T75 flask at 37 °C with 5% CO_2 until cells were fully confluent. Cells were then expanded in T175 flasks and finally seeded in 6-well plates for the experiments with an initial density of 1.0×10^4 cells/cm^2. Culture media was changed

every 2-3 days until cells reached full confluence (day 0). After this point, experimental treatments were applied for each experiment.

2.11. RNA extraction

2.11.1. Isolation of RNA from primary BMSCs and MLO-Y4

Following completion of the challenge experiments, the culture media was removed and the cells were rinsed with 1 mL of PBS. Cells were then scraped into 1 ml of Qiazol reagent (Qiagen, Cat# 79306) and homogenized using a Rotor-Stator Homogenizer (Ultra-Turrax T10). The homogenates were incubated at room temperature for 5 minutes to facilitate the dissociation of nucleoprotein complexes. Subsequently, 200 µl of chloroform (Scientific Laboratory Supplies, Cat# che1576) was added to each sample, followed by thorough mixing to promote optimal phase separation. Samples were centrifuged at 13,000 rpm for 15 minutes at 4°C. This process generated three distinct layers: an upper aqueous phase containing RNA, an interphase, and a lower organic phase. The upper aqueous phase (~500 µl) was carefully collected to minimise cross-contamination. RNA was then isolated and purified using the Qiagen RNeasy Mini Kit (Qiagen, Cat# 74106) in conjunction with RNase-Free DNase I treatment (Qiagen, Cat# 79254), according to the manufacturer's protocol. RNA purification relied on a specialised buffer system and silica membrane technology. Ethanol (70%) was added to facilitate RNA binding, and contaminants were eliminated through sequential washes and centrifugation steps. RNA concentration (A260/A280) and purity (A260/A230) were assessed using a NanoDrop spectrophotometer (ND-1000; Thermo Fisher Scientific, Loughborough, UK).

2.11.2. Isolation of RNA from mouse tissues

Tissues were pulverized in RNase-free 2 ml microtubes (VWR, Part of Avantor, Cat# 0030120094) containing 1 ml of cold Qiazol lysis reagent (Qiagen, Cat# 79306) using a Rotor-Stator homogenizer, applying three cycles of 10-second homogenization. Total RNA was isolated, purified and concentration determined as described in section 2.11.1.

2.11.3. Reverse transcription of RNA

Prior to reverse transcription, the concentration of RNA in each sample was equal to the lowest concentration among all samples using RNase-free water. Reverse transcriptase was employed to synthesise complementary DNA (cDNA) from the diluted RNA templates. For each reaction, 10 µL of RNA was combined with 2 µL of random primers (50 ng/µL) and incubated in a Dyad PCR system DNA Engine Peltier thermal cycler (MJ Research) at 70°C for 10 minutes. Subsequently, a master mix consisting of 4 µL 5X First-Strand Buffer (Life Technologies, Cat# 18064-014), 2 µL dithiothreitol (DTT; 0.1 M, Life Technologies, Cat# 18064-014), 1 µL deoxyribonucleotide triphosphate (dNTP; 10 mM, Life Technologies, Cat# 18427-013), and 1 µL Superscript II RNase reverse transcriptase (Life Technologies, Cat# 18064-014) was prepared. An aliquot of 8 µL of this master mix was added to each sample. Reverse transcription was performed on the Dyad PCR thermal cycler under the following conditions: 25°C for 10 minutes, 42°C for 50 minutes, 70°C for 15 minutes, and a final hold at 4°C. Resulting cDNA samples were diluted to 5 ng/µL with RNase-free water and stored at −20°C until subsequent analyses.

2.11.4. Real-time quantitative polymerase chain reaction (qPCR) and quantification

Each sample was prepared by combining 10 µL of SYBR Green reagent (appropriate for Stratagene platforms and Agilent Aria 2.1 system, Primerdesign, Cat# PPLUS-MX-SY, or Biosystems, Cat# PB20.15-51), 1 µL of primer mix, and 4 µL of RNase-free water. For each quantitative PCR reaction, 15 µL of the master mix was combined with 5 µL of diluted complementary cDNA. Gene expression analysis was conducted using SYBR Green detection chemistry on a Stratagene Mx3000P real-time qPCR system (Agilent Technologies, Santa Clara, USA) for the data reported in chapters 3 and 4 and an Agilent Aria 2.1 real-time qPCR system (Agilent Technologies, Cheadle, UK) for the data reported in chapter 5.

The qPCR thermal cycling protocol began with an initial denaturation at 95°C for 2 minutes. This was followed by 40 cycles, each comprising: 60°C for 1 minute, 95°C for 1 minute, 55°C for 30 seconds, and 95°C for 30 seconds. Reactions were performed in

duplicate using separate RNA samples. Negative controls included reactions with 5 µL of nuclease free water and 15 µL of master mix instead of cDNA. Gene expression was quantified relative to the housekeeping gene *Ppia* (Sigma-Aldrich). Primer specificity was verified by a single peak in the melting curve. Data analysis used standard curves and amplification plots, which showed fluorescence intensity versus cycle number, with the baseline normalised to the ROX dye. Relative expression levels were calculated using the ΔΔCt method (Livak & Schmittgen, 2001) and reported as fold changes relative to housekeeping genes. The primer sequences used in this thesis are listed in Appendix I.

2.12. Cell-based assays and staining

2.12.1. Alkaline phosphatase (Cohen et al.) activity and alizarin red staining (ARS)

The osteogenic differentiation potential of primary BMSCs from CKD mice (Chapter 3) was evaluated using an ALP activity assay kit (Sigma-Aldrich, Cat# MAK447) and alizarin red staining. After 21 days of differentiation into osteoblasts, the cells were washed with PBS and lysed with 0.2% Triton X-100 to extract both the intracellular ALP enzyme and total protein. The ALP activity was measured according to the manufacturer's protocol, utilizing p-nitrophenyl phosphate as the substrate, with the resulting p-nitrophenol detected by absorbance at 405 nm (Mushtaq et al., 2002). After cell lysis for ALP, the mineralised cell layer in each well was stained with 1 mL of 2% ARS solution at pH 4.2 at room temperature for 5 minutes with gentle agitation. Afterwards, the stain was removed and the wells were rinsed several times with distilled water until the water ran clear. The calcium-bound stain was then solubilised in 10% cetylpyridinium chloride, and the optical density of the resulting eluted solution was measured using a BioTek Synergy Microplate Reader at 570 nm (Hsu et al., 2022).

2.12.3. Oil red O (ORO) staining

The adipogenic differentiation potential of primary BMSCs from CKD mice (Chapter 3) was assessed by ORO staining. Cells were fixed in 10% neutral buffer formalin at room temperature for 30 minutes. The fixed cells were rinsed with distilled water and incubated in 60% isopropanol (in distilled water) for 5 minutes at room temperature. The adipocytes were stained with ORO working solution (a mixture of 3

parts of 0.35% ORO in isopropanol with 2 parts of 60% isopropanol) for 5 minutes at room temperature under gentle agitation. The stained adipocytes were washed 3 times with distilled water. The bound stain was solubilised in isopropanol and spectrophotometric measurement of the eluate's optical density was performed at a wavelength of 490 nm (Maridas et al., 2018).

2.13. Protein methods

2.13.1. Protein extraction from primary cells

After ORO staining, cells were rinsed with PBS and cellular proteins were extracted with fixed-cell lysis buffer containing 300 mM Tris-HCl (pH 8), 2% SDS, 2X protease and phosphatase inhibitor cocktail (Kawashima et al., 2014; Sadick et al., 2016). The amount of total cellular protein from adipocytes (after ORO staining) and osteoblasts (total lysate after ALP activity, Section 2.11.1) was determined by the Quick Start Bradford protein assay (Bio-Rad, UK, Cat# 5000201) according to the manufacturer's instructions. The total protein was used to normalise ALP activity, ARS and ORO staining in their respective groups.

2.13.2. Protein extraction from tissue and proteomic analysis

Protein phenotypes of bone and bone marrow tissue from CKD and CKD treated with rbsAb were determined by proteomic analysis. Both proximal and distal ends of the right tibial bone (n=5) were cut and placed into a cut pipette tip inserted within a 1.5 mL Eppendorf tube, and subjected to centrifugation at 13,000 rpm for 5 minutes at 4°C to separate bone marrow from bone. Tibial cortical bone and bone marrow tissue were homogenised separately by a Rotor-Stator Homogeniser in 100 µL of lysis buffer containing 5% sodium deoxycholate, 100 mM Tris-HCl (pH 8.5), 1 mg/mL chloroacetamide, and 1.5 mg/mL tris(2-carboxyethyl)phosphine. The lysates were subsequently heated at 95°C for 15 minutes. Protein capture and digestion from plasma, bone and bone marrow lysates were performed according to a previously published protocol (Batth et al., 2019), using an automated KingFisher Flex system (Thermo Fisher Scientific). Proteins were captured using MagReSyn HILIC magnetic microspheres (MR-HLC002, ReSyn Biosciences). Protein-bound beads were then digested with 0.5 µg of

MS-grade trypsin (90057, Thermo Fisher Scientific) in 50 mM triethylammonium bicarbonate buffer (18597, Sigma-Aldrich) at 37°C. The tryptic peptides were sequentially washed with 95% (v/v) acetonitrile (ACN) and 70% ethanol. Digestion was terminated by acidification with 2% formic acid. Peptides were subsequently desalted using a C18-based desalting procedure, eluted with 0.1% trifluoroacetic acid (TFA) in 50% ACN, and dried by speed vacuum. Thereafter, dried peptides were reconstituted in 0.1% TFA for subsequent mass spectrometry analysis.

One microgram of peptide was subjected to electrospray ionisation for mass spectrometry (MS) analysis using an Orbitrap Fusion Lumos mass spectrometer (Thermo Fisher Scientific). Liquid chromatography was performed using mobile phase A (0.5% acetic acid and 2% ACN in LC-MS grade water) and mobile phase B (0.5% acetic acid and 80% ACN in LC-MS grade water). For MS1 acquisition, the scan range was set to 200–2,000 m/z, with a normalised automatic gain control (AGC) target of 1000% and an injection time of 50 ms. For MS2 acquisition, the scan range was set to 350–1,650 m/z, with a resolution of 120,000, an AGC target of 1000%, and an IT of 60 ms. Data acquisition employed higher-energy collisional dissociation with a normalised collision energy of 28. The data were analysed utilising DIA-NN 2.0 software, where spectral matching was carried out against the Mus musculus UniProt protein database (Demichev et al., 2020). Normalisation was achieved by assessing the total peptide abundance across different LC-MS runs. Gene Set Enrichment Analysis (GSEA) was performed using GSEA software version 4.4.3 from the Broad Institute, USA. The proteomics data including raw files and search results have been deposited to the ProteomeXchange Consortium via the PRIDE partner repository with the dataset identifier PXD 069117.

2.13 Statistics

Data is presented as mean ± standard error of the mean (S.E.M.). The precise number (n) is indicated in the relevant figure legends. The correlation between the individual parameters was conducted by using Pearson's correlation. Statistical analysis was performed using a Student's t-test, one-way analysis of variance (ANOVA) followed by Tukey's range test, or two-way ANOVA, as appropriate. Non-normally distributed data were analysed using the Mann–Whitney test with Bonferroni correction for multiple

comparisons. Statistical analysis was performed using GraphPad Prism software (GraphPad Software, Inc., USA), and statistical significance is denoted as follows: * $p < 0.05$, ** $p < 0.01$, and *** $p < 0.001$. For the analysis of the proteomic differential expression, data processing was carried out using Perseus software (Tyanova et al., 2016). The data underwent $\log_2$ transformation, and missing values were estimated by assuming a normal distribution. To compare groups, pairwise two-sample t-tests were performed. Proteins were deemed significantly different if they had a p-value below 0.05 and a fold-change exceeding 1.5.

Chapter 3

Bone marrow adipose tissue expansion and bone loss in experimental chronic kidney disease is independent of altered bone marrow stromal cell lineage determination

Published in ***Frontiers in Endocrinology***

22 September 2025

DOI 10.3389/fendo.2025.1666681

Introduction

CKD affects more than 10% of the global population, accounting for approximately 800 million individuals worldwide (Kovesdy, 2022). In 2017 alone, an estimated 1.2 million people died as a result of CKD (Bikbov et al.,2020). Without effective intervention, the global mortality burden is projected to rise to nearly 2.2 million deaths by 2040 (Bikbov et al., 2020). CKD is an irreversible, progressive disorder characterised by structural abnormalities and a gradual decline in renal function. Clinically, CKD is defined by an eGFR below 60 mL/min/1.73 m^2. To differentiate CKD from acute kidney injury, reduced eGFR and/or elevated urinary albumin excretion must persist for at least 90 days in repeated assessments (Kovesdy, 2022).

The progression of CKD disrupts systemic mineral and hormonal homeostasis—particularly involving calcium, Pi, PTH, and FGF23, which collectively contribute to skeletal complications. This altered mineral status, known as CKD-MBD, includes ROD and is characterised by low bone density (osteopenia) that can progress to osteoporosis (Sprague et al., 2016). The prevalence of osteopenia and osteoporosis in CKD patients has been reported to be approximately 45% and 23%, respectively, across both developed and developing regions (Tariq & Sulaiman, 2020). Furthermore, as CKD advances, particularly in older adults, the risk of bone fracture increases nearly fivefold compared with age-matched individuals without CKD (Naylor et al., 2015). Fractures in CKD patients represent a major clinical concern, as they significantly compromise quality of life and elevate mortality risk (Hsu et al., 2020).

The mechanisms underlying CKD-MBD are complex and multifactorial. Impaired renal function in CKD often results in Pi retention and subsequent hyperphosphatemia. Although the direct impact of hyperphosphatemia on bone structure remains unclear, several clinical studies have demonstrated a positive correlation between elevated serum Pi levels and increased fracture risk in CKD patients (Geoffrey A. Block et al., 2004; Campos-Obando et al., 2017). In response to hyperphosphatemia, osteocytes increase the secretion of FGF23, promoting Pi excretion through the kidneys and thereby attempting to maintain Pi balance (Prié et al., 2009). However, excessive FGF23 contributes to bone deterioration by upregulating DKK1, a potent Wnt/β catenin

signalling inhibitor that suppresses osteoblast differentiation (Carrillo-López et al., 2016). Sclerostin, another Wnt/β catenin signalling inhibitor, is also found to be increased in CKD condition (Moe et al., 2015; Neto et al., 2021). Prolonged hypocalcemia also ensues in the presence of elevated FGF23 due to the down regulation of hormonally active vitamin D_3 (1,25-dihydroxycholecalciferol) and this stimulates PTH secretion, leading to SHPT, a condition that accelerates bone resorption and diminishes bone formation (Hruska et al., 2017). Several clinical and experimental investigations have demonstrated a positive association between SHPT and increased fracture risk in CKD patients (Jadoul et al., 2006; Marques et al., 2017; Nickolas et al., 2013).

BMAT has been recognised for decades as a distinct and metabolically active fat depot within the bone microenvironment. Its formation is primarily driven by the transcription factor PPARγ, a key regulator of adipogenic differentiation (Akune et al., 2004). Other adipogenic markers, including C/EBPα, Fabp4, and adiponectin, also contribute to the regulation of BMAT expansion (Tencerova & Kassem, 2016). Several endocrine factors strongly influence BMAT development under various physiological and pathological conditions. For instance, glucocorticoid excess, as seen in Cushing's syndrome, promotes BMAT accumulation (Maurice et al., 2018), and the administration of cortisol or corticosterone in animal models produces similar effects (Suchacki et al., 2016). Notably, elevated circulating glucocorticoids have also been reported in CKD patients and animal models (Sagmeister et al., 2022; Uslar et al., 2025). Conversely, leptin and PTH have been shown to suppress BMAT expansion (Ambati et al., 2010; Costa et al., 2019).

Beyond serving as a fat reservoir, BMAT is increasingly recognised as an endocrine organ that secretes adipokines such as leptin and adiponectin, which play key roles in systemic metabolic regulation (J. H. Stern et al., 2016). Factors released by marrow adipocytes can also influence local bone remodelling processes. For example, BMAT-derived extracellular vesicles carrying adipogenic RNAs have been shown to suppress osteoblast function (Sulston & Cawthorn, 2016). Moreover, bone marrow adipocytes can produce RANKL and C-X-C motif chemokine ligand 1 (CXCL1), both

of which stimulate osteoclast differentiation and increase bone resorption (Cawthorn et al., 2016; Fan et al., 2017).

It's well known that BMSCs possess multipotent differentiation potential, giving rise to osteoblasts, chondrocytes, myoblasts, and adipocytes (Bianco & Robey, 2015). Osteoblast and adipocyte lineages are thought to share a reciprocal, "seesaw-like" relationship in which activation of one lineage suppresses the other (James, 2013). Consequently, enhanced adipogenic differentiation of BMSCs often occurs at the expense of osteogenesis, contributing to reduced bone formation. Numerous studies have documented this inverse relationship between BMAT accumulation and bone mass in metabolic conditions such as ageing, diabetes, and caloric restriction (Ali, Tencerova, et al., 2022; Bredella et al., 2009; Devlin et al., 2010; Guimaraes et al., 2024; Justesen et al., 2001) (Veldhuis-Vlug & Rosen, 2018). Importantly, and relevant to the work of this thesis, several clinical and experimental studies have also reported increased BMAT content in CKD, which correlates positively with disease severity (Moorthi et al., 2015; Woods et al., 2018). In paediatric CKD, an inverse relationship between bone formation rate and marrow adipocyte number has been observed, particularly in children with high bone turnover (Sirimongkolchaiyakul et al., 2021). Moreover, both lower eGFR and decreased bone mineral density have been shown to correlate inversely with BMAT volume in CKD patients (Borelli et al., 2023). Experimental CKD induced by nephrectomy or adenine-supplemented diets consistently demonstrate BMAT expansion alongside bone loss (Ni et al., 2019; Wang et al., 2017).

Collectively, this evidence suggests that BMAT accumulation in CKD may contribute to skeletal deterioration either by skewing mesenchymal stem cell differentiation toward adipogenesis at the expense of osteoblastogenesis, or through direct paracrine effects that promote bone resorption. Despite growing recognition of this relationship, the mechanistic basis underlying BMAT expansion and its interaction with bone metabolism during CKD progression remains poorly defined. Furthermore, most existing studies have been cross-sectional, providing only static snapshots rather than capturing the temporal sequence of bone and BMAT changes. To address this gap, the present study was designed to investigate the mechanistic link between BMAT

development and bone pathology during the progression of adenine-induced CKD in mice, employing a longitudinal experimental design to better reflect the dynamic nature of bone alterations in CKD.

The published paper from this study had a number of co-authors who contributed to the laboratory work and writing. However, I can confirm that I wrote the first draft of the paper and completed all laboratory work. I was assisted by Soher N. Jayash and Aine Pears on the *in vitro* experiments and flow cytometry, respectively. Lucie E. Bourne kindly helped me with whole cortical bone analysis using R Studio, and I have adapted her technique for my own work.

frontiers | Frontiers in Endocrinology

TYPE Original Research
PUBLISHED 22 September 2025
DOI 10.3389/fendo.2025.1666681

OPEN ACCESS

EDITED BY
Ciro Menale,
University of Naples Federico II, Italy

REVIEWED BY
Sarah E. Little-Letsinger,
Duke University, United States
Giulia Battafarano,
Bambino Gesù Children's Hospital (IRCCS), Italy

*CORRESPONDENCE
Worachet Promruk
W.Promruk@sms.ed.ac.uk
Colin Farquharson
colin.farquharson@roslin.ed.ac.uk

RECEIVED 15 July 2025
ACCEPTED 25 August 2025
PUBLISHED 22 September 2025

CITATION
Promruk W, Cawthorn WP, Bourne LE, Jayash SN, Pears A, Staines KA, Stephen LA and Farquharson C (2025) Bone marrow adipose tissue expansion and bone loss in experimental chronic kidney disease is independent of altered bone marrow stromal cell lineage determination.
Front. Endocrinol. 16:1666681.
doi: 10.3389/fendo.2025.1666681

Bone marrow adipose tissue expansion and bone loss in experimental chronic kidney disease is independent of altered bone marrow stromal cell lineage determination

Worachet Promruk[1,2*], William P. Cawthorn[3], Lucie E. Bourne[4], Soher N. Jayash[1], Aine Pears[1], Katherine A. Staines[4], Louise A. Stephen[1] and Colin Farquharson[1*]

[1]Functional Genetics Division, The Roslin Institute and Royal (Dick) School of Veterinary Studies, University of Edinburgh, Edinburgh, United Kingdom, [2]Chulabhorn Royal Academy, Bangkok, Thailand, [3]Institute for Neuroscience and Cardiovascular Research, Edinburgh Bioquarter, University of Edinburgh, Edinburgh, United Kingdom, [4]Centre for Lifelong Health, School of Applied Sciences, University of Brighton, Brighton, United Kingdom

Introduction: Chronic kidney disease-mineral bone disorder is the irreversible loss of kidney function leading to altered mineral homeostasis and bone loss, commonly referred to as renal osteodystrophy. Bone marrow adipose tissue (BMAT) accumulates in clinical CKD and animal models of this disease, but the mechanism(s) responsible are unclear. This study sought to determine the relationship between BMAT distribution and bone structure and to establish whether disease progression directly affected: 1) the commitment of bone marrow mesenchymal stromal cells (BMSCs) to osteoblastic (OPC) and adipogenic (APC) precursor cells, and 2) the differentiation of BMSCs to mature adipocytes and osteoblasts.

Methods: Eight-week-old male C57BL/6J mice received a diet supplemented with 0.2% adenine for ≤5 weeks to induce CKD. Control mice received the same diet without adenine. Serum biochemistries were quantified using a biochemistry analyzer and plasma hormone levels by ELISA. Bone phenotypes were evaluated by μCT. The same bones were decalcified and stained with 1% osmium tetroxide and BMAT quantified using μCT. Precursor cell populations in bone marrow were quantified by flow cytometry.

Results: The development of CKD during the early stages of the disease was confirmed by elevated serum concentrations of blood urea nitrogen and creatinine from 3-weeks' induction. After 5-weeks' induction, trabecular bone microarchitecture including bone mineral density was compromised whereas cortical bone area and thickness were decreased in CKD tibiae after 3- and 5-weeks' induction. Compared to age-matched controls, proximal tibial BMAT tended to increase in CKD mice by 3 weeks' induction and this reached statistical significance after 5-weeks where there was a negative correlation between regulated BMAT accumulation and trabecular bone loss. BMAT accumulation was not due to calorie deficiency and was positively correlated with circulating adiponectin, but not with circulating leptin or corticosterone. During CKD onset

10.3389/fendo.2025.1666681

(weeks 1-2) of CKD, BMSCs from CKD mice had enhanced adipogenic potential but the proportions of OPCs and APCs within the bone marrow were unchanged. **Conclusions:** In experimental CKD, BMAT expansion depends on CKD duration and does not appear to be driven by hypoleptinemia or hypercorticosteronemia, or by altered precursor cell differentiation during CKD onset.

KEYWORDS

chronic kidney disease, renal osteodystrophy, bone marrow adipocytes, adipokines, bone, corticosteroids

Introduction

Chronic kidney disease (CKD) is irreversible and results in the gradual loss of kidney function. Globally, more than ~800 million individuals world-wide present with CKD symptoms (1) and the mortality rate attributed to CKD is expected to reach ~2.2 million by 2040 (2). The progression of CKD leads to CKD–mineral bone disorder (CKD–MBD) which is characterized by disrupted mineral (calcium and phosphate) and hormonal (parathyroid hormone - PTH and fibroblast growth factor 23 - FGF-23) homeostasis, leading to cardiovascular disease and renal osteodystrophy (ROD) – the skeletal pathology component of the CKD-MBD syndrome (3).

The mechanism(s) responsible for the development of ROD are poorly understood but causative roles for hyperphosphatemia, hyperparathyroidism and elevated FGF-23 levels have been proposed (4). Indeed, increased systemic phosphate concentrations have been correlated with increased fracture risk in CKD patients (5). Also, FGF-23 is induced by hyperphosphatemia and this phosphaturic hormone can directly promote bone loss by inducing the expression of the Wnt/β-catenin signaling pathway inhibitor, Dickkopf-1 (6). Additionally, FGF-23 inhibits calcitriol production by the kidney, leading to decreased intestinal calcium absorption, secondary hyperparathyroidism and increased osteoclastic bone resorption (7). Clinical studies have reported that secondary hyperparathyroidism in CKD-MBD is positively correlated with fracture risk (8, 9).

Nevertheless, clinical and animal studies offer an alternative contributory explanation for the development of ROD. Bone marrow mesenchymal stromal cells (BMSC) can differentiate into various cell types, and osteoblast and adipocyte lineages are considered to have a 'seesaw' relationship with each requiring their own specific transcription factors (10). Therefore, the observation that bone marrow adipose tissue (BMAT) accumulation is inversely related to bone mass in CKD patients suggests a possible switch in stem cell commitment in CKD, resulting in a deficit of osteoblasts and thus bone formation (11). In experimental studies, the induction of CKD by nephrectomy or dietary adenine also results in BMAT accumulation and bone loss (12, 13).

In addition to peroxisome proliferator-activated receptor γ (PPARγ), a transcription factor essential for BMAT development, there are also a number of endocrine factors such as glucocorticoids, leptin and PTH that can influence BMAT accumulation (14, 15). Therefore, altered transcription factor expression and/or changes in the endocrine milieu that are characteristic of CKD may favor bone marrow adipogenesis rather than a commitment towards the osteoblast lineage. It is also possible that BMAT-secreted factors, such as leptin and adiponectin (16), can modulate osteoblast and osteoclast differentiation and cellular function (17). For example, BMAT secretes receptor activator of nuclear factor kappa beta ligand (RANKL) and C-X-C motif chemokine ligand 1 (CXCL1), which promote osteoclast differentiation and bone resorption (18, 19).

As the mechanisms responsible for BMAT accumulation in CKD and its relationship to bone loss is unclear, this study was undertaken to address this gap in our knowledge. Specifically, using a dietary adenine-induced CKD mouse model, we evaluated bone marrow adipocyte (BMAd) accumulation, bone structure and circulating adipokine concentrations during the early stages of CKD as well as quantifying BMSC, osteoblastic (OPC) and adipogenic (APC) precursor cell populations during CKD onset.

Materials and methods

Mice

All mouse studies were approved by the University of Edinburgh Animal Welfare and Ethical Review Board and were conducted under project licenses granted by the UK Home Office. Animal studies were conducted and are reported in line with the ARRIVE guidelines.

C57BL/6JCrl mice were obtained from Charles River Laboratories (Margate, Kent, UK). Seven-week-old male mice were acclimatized for 1-week after arrival into the animal facility prior to the start of the study. The animals were randomly assigned to control or CKD groups. The 8-week-old mice were subsequently fed their respective diet for up to 5 weeks: CKD mice received a casein-based diet containing 0.6% calcium, 0.9% phosphate, 1.5% Vitamin Mix, AIN-76A (containing vitamin D3), and 0.2% adenine

(Envigo, Teklad Co. Ltd, Cat# TD.140290). Control mice received the same diet without adenine (Envigo, Cat# TD.138898) (20). Body weights were obtained from mice at the start of the experiment, and then at sacrifice after 1-, 3- and 5-weeks of induction.

For paired-feeding experiments, control and CKD mice were singly housed to facilitate the measurement of food intake by each mouse. This approach resulted in a rapid bodyweight loss (≥ 30% with ~ 1-week) in the adenine-fed mice, possibly due to enhanced stress of single housing. This study was therefore terminated for welfare reasons. Further attempts to prevent the rapid loss of body weight with increased bedding and acclimatization time were unsuccessful. Therefore, to complete the pair-feeding study, 6-week-old mice were acclimatized for 1-week in group housing, acclimatized in pairs for another 1-week and then randomly assigned to one of three groups: (1) *ad-lib* control diet, (2) *ad-lib* CKD diet and (3) paired-fed control diet for 3 weeks. Food intake of all cages was recorded daily. The amount of adenine diet consumed by both mice in each cage of group 2 was equal to the amount of control diet offered to its respective "paired" cage in group 3 the next day. In addition to their control or adenine-supplemented diet, mice were offered a gel pot (ClearH2O, USA, Cat# 7235022) for 2 days at the end of weeks 1 and 2. Over the 3-week duration of this study, this strategy was successful in preventing the adenine-fed mice breaching 30% body weight loss, which is the maximum allowed by our animal research license from the UK Home Office.

Serum biochemistry

Control and CKD mice were sacrificed after 1-, 3-, and 5-weeks of induction and blood was collected by cardiac puncture under terminal anesthesia. Serum creatinine, blood urea nitrogen (BUN), were quantified using a biochemistry analyzer (Beckman Coulter AU480). Intact PTH (Immutopics International, USA, Cat# 60-2305), FGF-23 (Kainos Laboratories, Inc. Japan, Cat# CY4000), adiponectin (Sigma-Aldrich, UK Cat# A6354), leptin (R&D Systems, UK Cat# MOB00) and corticosterone (Enzo Life Sciences, UK, Cat# ADI-900-097) were measured by ELISA according to the manufacturers' instructions.

Micro-computed tomography

The left tibiae from control and CKD-mice, culled after 1-, 3-, or 5-weeks, were fixed in 10% formaldehyde for 24 hours prior to the evaluation of bone architecture and bone mineral density (BMD) by microCT (Skyscan 1172 X-ray microtomography, Bruker, Kontich, Belgium). Briefly, the bones were scanned with an isotropic voxel size of 5 µm (60 kV, 167 µA and 0.5 mm filter, 0.6° rotation angle) and the scans were reconstructed using the NRecon 1.7.3.0 program (Bruker) to remove artefacts, including beam-hardening and ring artefacts. CTAn software 1.15.4.0 (Skyscan) was used to visualize and evaluate bone histomorphometric parameters. Three-dimensional (3D) images were created using CTVol software (Skyscan).

To analyze the tibia architecture, each bone was aligned along its longitudinal axis and the trabecular volume of interest (VOI) in the proximal metaphysis was a 1000-µm section of the metaphysis, 250 µm subjacent to the growth plate (21). The following parameters were quantified: trabecular bone volume/tissue volume (BV/TV; %), trabecular thickness (Tb. Th; mm), trabecular number (Tb. N; 1/mm), trabecular separation (Tb. Sp; mm), and Tb. connectivity density (Tb. Conn Dn; $1/mm^3$). The cortical VOI was between 10 and 90% of the entire tibial length, as previously described (22). The proximal and distal 10% portions of tibial length were digitally cropped to exclude the epiphysis, growth plates and trabecular bone from the analysis. Cortical thickness (Th; mm), bone area (B.Ar; mm^2), moment of inertia maximum (MMI max; mm^4) and minimum (MMI min; mm^4) and polar moment of inertia (*J*; mm^4) were determined. Hydroxyapatite phantoms of known densities (0.25 and 0.75 g/cm^3) were scanned and reconstructed under identical conditions as the experimental samples to allow the calculation of BMD. R studio was used to create the line graph of the cortical bone parameters along the tibia length (23).

White adipose mass

Gonadal (gWAT) and inguinal (iWAT) fat depots were dissected from mice sacrificed after 1- and 3-weeks of induction. The weight of each peripheral fat depot was calculated as a % of body weight.

Quantification of BMAT

After microCT scanning the tibiae were decalcified in 14% ethylenediaminetetraacetic acid pH 7.4 for 14 days at 4°C under agitation, with the solution changed every 2 - 3 days. The bones were stained with osmium tetroxide to evaluate BMAT accumulation within the bone marrow cavity (24). Briefly, the decalcified bones were washed and stored in 1.5 mL Eppendorf tubes containing 400 µl of Sorensens' buffer (81 mM Na_2HPO_4·H2O, 19 mM KH_2PO_4, pH 7.4). Thereafter, 400 µl of 2% osmium tetroxide (Generon Ltd, Cat# 23310-10) was added to each tube to give a final concentration of 1% osmium tetroxide. After incubation for 48 hours at room temperature the bones were washed 2–3 times for a total of 1 hour with Sorensens' buffer and stored in the same at 4°C.

The osmium-stained bones were re-scanned by microCT and BMAT volume was normalized to the size of the bone marrow cavity. BMAT volume was quantified in the whole tibia and also in 3 distinct anatomical regions: the top of the proximal bone to the growth plate (Proxi Epi); the growth plate to tibia/fibula junction (GP-T/F J), which contains regulated BMAT (rBMAT); and the tibia/fibula junction to the end of the distal bone (T/F J-End), which contains constitutive BMAT (cBMAT) (25). rBMAT is more labile and responds to metabolic challenges such as caloric restriction

10.3389/fendo.2025.1666681

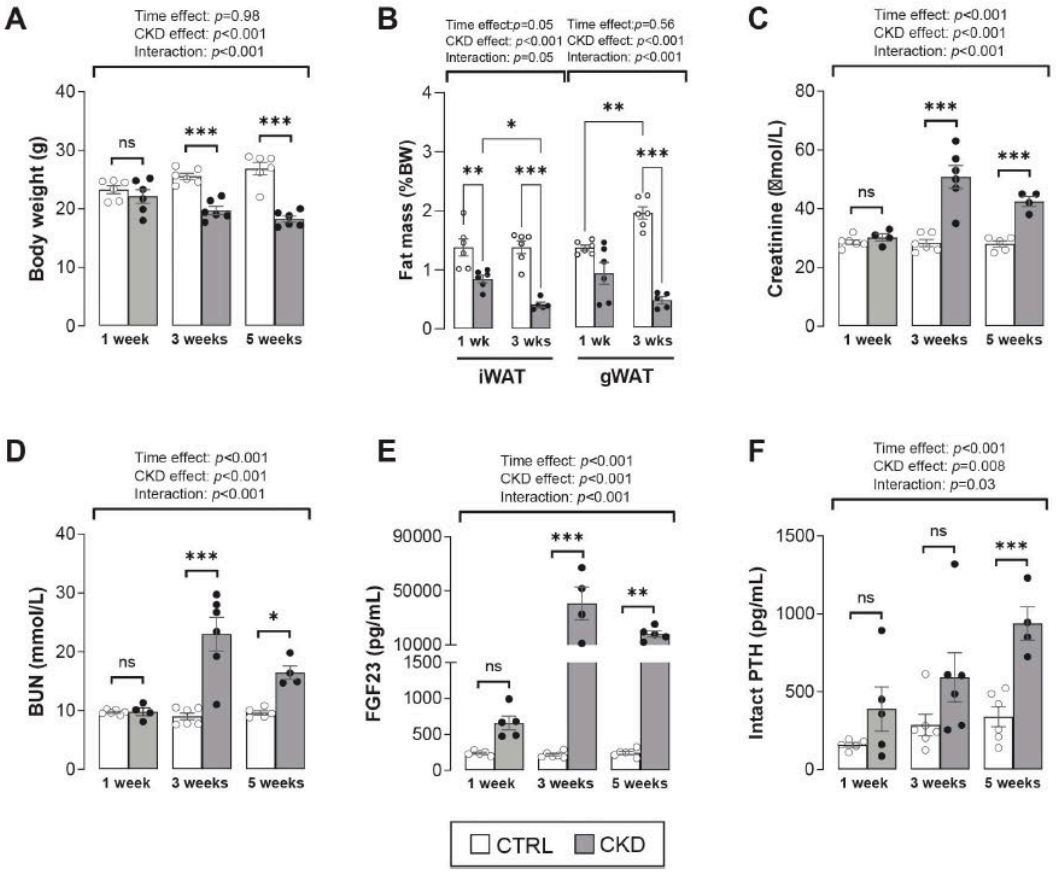

FIGURE 1
Validation of CKD development in adenine-treated mice. **(A)** Body weight of CKD mice was decreased after 3- and 5- weeks' induction. **(B)** Inguinal (iWAT) and gonadal (gWAT) white adipose tissue of CKD mice was decreased after 1- and 3-weeks' induction. **(C–E)** Serum levels of creatinine, blood urea nitrogen (BUN), and fibroblast growth factor 23 (FGF23) were increased from 3-weeks post-induction, whereas **(F)** parathyroid hormone (PTH) serum levels were increase after 5-weeks' induction. The data are presented as mean ± SEM, with each dot representing an individual mouse. ns, not significant, $*P < 0.05$, $**P < 0.01$, $***P < 0.001$.

(CR), diabetes and ageing. R studio was used to create the line graph of BMAT accumulation along the tibia length.

BMSC culture

To investigate the *ex-vivo* differentiation of osteoblast and adipocyte lineages, BMSCs were isolated from the tibiae, femora, humeri and ilia of CKD and control mice after 4-weeks on their respective diets. Briefly, BMSCs were obtained by centrifugation at 13,000x g at room temperature for 1 minute and the cell clump was gently broken-up using a 1-ml syringe with 25 G needle. Bone marrow cells were pooled separately from each group (control and CKD mice) and expanded in minimum essential medium alpha (αMEM, Life Technologies, Cat# 22561021), 10% fetal bovine serum (FBS, Life Technologies, Cat# 10500064), and 1% penicillin/streptomycin (referred to as BMSC medium) for 48 hours. For adipocyte and osteoblast differentiation, BMSCs were seeded in 6-well plates at a density of 5×10^5 cells/well and maintained in BMSC media until the cells reached confluency (day 0). For osteoblast differentiation, confluent BMSCs were cultured in osteoblast differentiation medium (BMSC media containing 50 µg/mL ascorbic acid and 8 mM β-glycerophosphate) for 21 days, with medium replaced in every 2–3 days. For adipocyte differentiation, confluent BMSCs were cultured in adipocyte induction medium, which consisted of adipocyte-basal medium (Dulbecco Modified Eagle Medium, high-glucose, supplemented with 10% FBS, 1% penicillin/streptomycin, 1 µM rosiglitazone and 2 µM insulin) supplemented with 0.5 mM 3-isobutyl-1-methylxanthine and 1 µM dexamethasone. Medium was changed on day 2. On day 4, adipocyte induction medium was switched to adipocyte-basal medium and the cells were cultured for another 5 days, with medium changes every other day (26).

Alkaline phosphatase activity and alizarin red and oil red O staining.

Alkaline phosphatase (ALP) activity and Alizarin Red staining of cultured BMSCs from control or CKD mice were determined on day 21 of osteogenic differentiation. Cells were lysed with 0.2% triton X-100 to release intracellular ALP. The ALP activity assay (Sigma-Aldrich, Cat# MAK447) used p-nitrophenyl phosphate as substrate and the production of p-nitrophenol was measured at an absorbance of 405 nm. The mineralized matrix in each well was stained with a 2% solution of Alizarin Red at pH 4.2 at room temperature for 5 min. After rinsing several times with water, the bound stain was solubilized in 10% cetylpyridinium chloride and the optical density of the resultant eluted solution was measured by spectrophotometry at 570 nm (27). On day 9 of adipogenic differentiation, adipocytes were stained with Oil Red O. Briefly, adipocytes were fixed in 10% neutral buffer formalin for 30 min at room temperature. After rinsing with water, 60% isopropanol was added for 5 mins at room temperature. The adipocytes were stained with Oil Red O solution for 5 min, washed with water and the bound stain solubilized in isopropanol. The optical density of the resultant eluted solution was measured by spectrophotometry at 490 nm. ALP activity, Alizarin Red staining and Oil Red O staining were normalized to total cellular protein, as determined by the Quick start Bradford protein assay (Bio-Rad, UK, Cat# 5000201) according to the manufacturers' instructions.

Flow cytometry

Control and adenine-fed mice were sacrificed after 1- or 2- weeks on their respective diets. Bone marrow from tibiae and femora was isolated by centrifugation as described above and suspended in 1 ml of cold cell-suspension buffer (sterile PBS with 2% FBS and 100 U/ml penicillin/streptomycin). Hematopoietic cells were depleted by the addition of ammonium-chloride-potassium lysis buffer for 5 minutes. Cells were resuspended in cell-suspension buffer, followed by blocking of non-specific protein binding sites using 2% rabbit serum in PBS for 30 minutes. Thereafter, the cells were incubated for 1 hour with the following fluorochrome-conjugated monoclonal antibodies (all from Thermo Fisher Scientific, UK): anti-CD45 (Cat# 11-0451-82), CD31 (Cat# 11-0311-82), Sca1 (Cat# 17-5981-82), Pa (Cat# 12-1401-81) and CD24 (Cat# 47-0242-82). Zombie Violet (BioLegend, USA, Cat# 423113) was used as a dead cell marker. Fluorescence minus one (FMO) was applied for each antibody as a negative control to inform gating boundaries. Flow cytometry was performed on a BD LRSFortessa™ and cells were identified using FlowJo software according to the following surface markers: BMSC, CD31-CD45-Sca1+Pa+CD24+; APC, CD31-CD45-Sca1+Pa+CD24-, and OPC, CD31-CD45-Sca1-Pa+ (28).

Quantitative polymerase chain reaction

Isolated bone and bone marrow were snap frozen in liquid nitrogen and stored at -80^{0}C. Cells were thawed, lysed in 1 ml of Qiazol (Qiagen, Manchester, UK, Cat# 79306) and homogenized with a Rotor-Stator Homogenizer (Ultra-Turrax T10). RNA from both tissues was extracted using a Qiagen RNeasy Mini kit (Qiagen, Cat# 74106) and quantified by nanodrop spectrophotometry (Thermo Fisher Scientific, Loughborough, UK). RNA quality was evaluated by the 260/280 nm ratio. All RNA was diluted to the same concentration and reverse transcribed to cDNA using SuperScript II (Thermo Fisher Scientific, Cat# 18064022). To evaluate gene expression, cDNA was mixed with PrimerDesign PrecisionPlus Master Mix and premixed SYBR Green (PrimerDesign, Chandler's Ford, UK, Cat# PB20.11-05) and assessed by a Stratagene Mx3000P real-time qPCR system (Agilent Technologies, Cheadle, UK). Target gene expression was normalized to a housekeeping gene (*Ppia*) and analyzed using the ΔΔCt method. Oligonucleotide primers (Supplementary Table S1) were obtained from Sigma-Aldrich.

Statistics

Data are presented as mean ± standard error of the mean (S.E.M). Each dot in all bar graphs represents 1 mouse sample in each study. Statistical analysis was performed using a two-way analysis of variance (ANOVA) to determine the effect of time and CKD status on bone and BMAT alterations. Correlations between individual parameters were performed using Spearman correlation. Statistical analysis was implemented using GraphPad Prism software (GraphPad Software, Inc., USA) and R studio (for the whole cortical bone and BMAT analysis) and statistical significance was shown as; * $p<0.05$; ** $p<0.01$ and *** $p<0.001$.

Results

Validation of disease progression in the CKD mouse model

The temporal development of the CKD phenotype in mice fed an adenine-supplemented diet was verified. The body weight of CKD mice decreased from 3-weeks' induction when compared to age-matched control mice (Figure 1A). This coincided with a decrease in fat mass in the gWAT and iWAT depots (Figure 1B). After 1-week of induction, serum creatinine, BUN, FGF-23 and PTH were similar in age-matched control and adenine-fed mice, but after 3- or 5- weeks' induction these analytes were increased in the CKD mice (Figures 1C–F). These data confirm the temporal development of CKD in the experimental mice and suggest that in this model "CKD onset" and the "early stages of CKD" occur after 1 – 2, and 3–5 weeks of induction, respectively (20).

Cortical and trabecular bone structure is impaired in CKD mice

We next investigated how CKD duration impacts cortical and trabecular bone structure. In the CKD mice, cortical bone area was

10.3389/fendo.2025.1666681

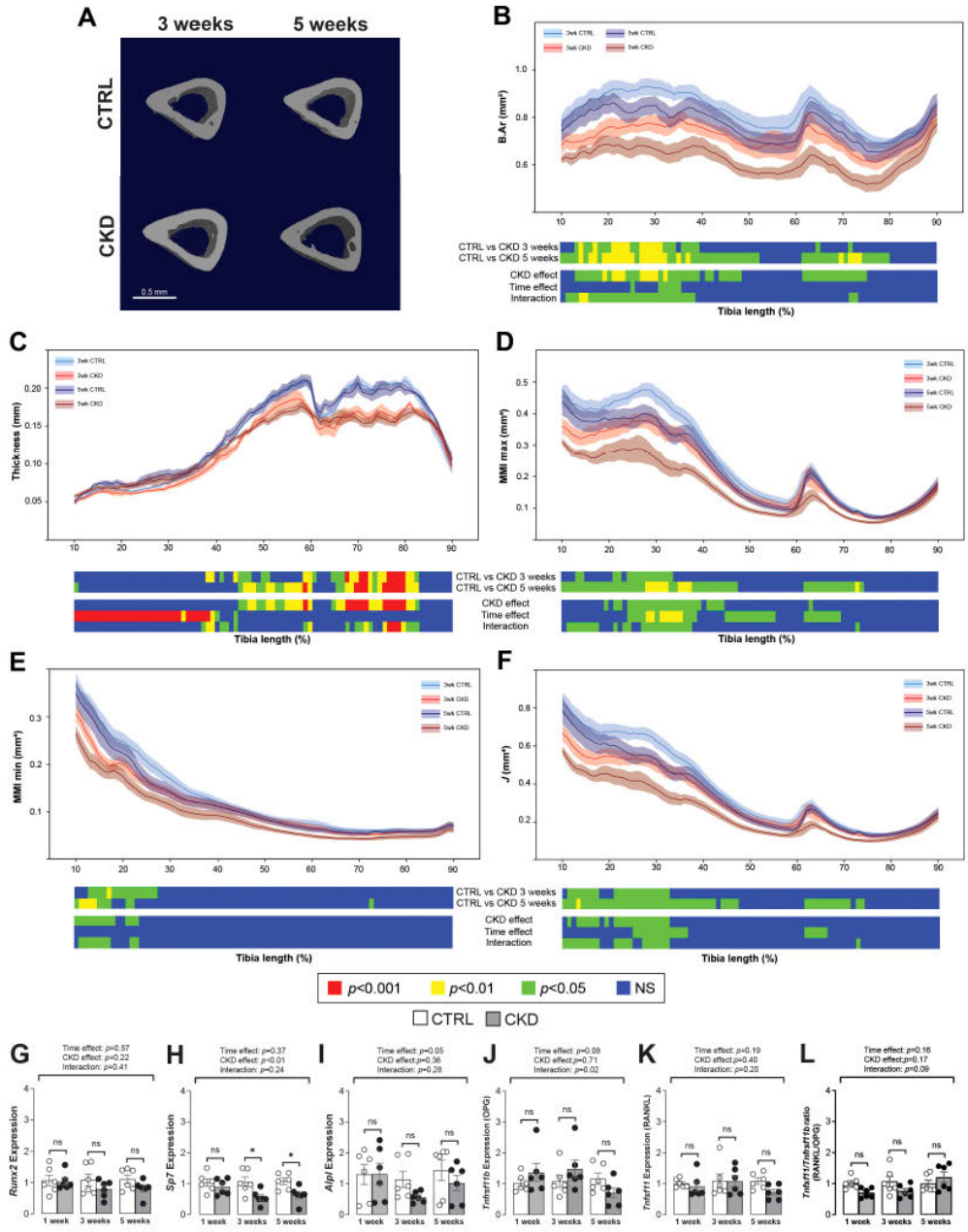

FIGURE 2
Micro-CT analysis and gene expression of tibial cortical bone. **(A)** 3-dimentional images of cortical bone from CTRL and CKD mice after 3- and 5-weeks' induction. Quantification of whole bone analyses of cortical bone between 10 and 90% of total tibial length, excluding proximal and distal metaphyseal bone, of CTRL and CKD tibia after 3- and 5-weeks' induction. **(B)** bone area (B.Ar), **(C)** thickness, **(D)** maximum moment of inertia (MMI max), **(E)** minimum moment of inertia (MMI min), and **(F)** polar moment of inertia **(J)** were all reduced in various regions of the tibia following CKD induction. For clarity, data for 1-week CTRL vs CKD are shown in Supplementary Figure S1. Data are presented as mean ± SEM, n = 5–6 bones per group. The expression of **(H)** *Sp7* was decreased after 3- and 5-weeks' induction whereas the expression of **(G)** *Runx2*, **(I)** *Alpl*, **(J)** *Tnfrsf11b*, and **(K)** *Tnfsf11* as well as the **(L)** *Tnfsf11/Tnfrsf11b* ratio was similar in the tibia from CTRL and CKD mice at all sampling points. The data are presented as mean ± SEM, with each dot representing an individual mouse. ns, not significant, *$P < 0.05$.

decreased in the proximal tibia after 3-weeks' induction but after 5-weeks the bone area of both the proximal and distal bone was reduced (Figure 2A and 2B). Cortical thinning was most evident in the distal tibia of CKD mice (Figure 2C) whereas MMI max and min as well as the polar moment of inertia (*J*) were decreased particularly in the proximal tibia of the CKD mice (Figures 2D–F). No differences for CKD vs control were noted after 1-week of induction (Supplementary Figure S1).

Changes to the trabecular compartment were observed only after 5-weeks' induction. When compared to age-matched controls, bone volume fraction and trabecular BMD, thickness, number and connectivity were all decreased in CKD mice after 5-weeks' induction (Supplementary Figure S2).

Osterix expression in cortical bone is decreased in CKD mice

In cortical bone, the expression of *Runx2* was unaltered whereas *Sp7* was decreased after 3- and 5-weeks' induction (Figures 2G, H). *Alpl*, *Tnfrsf11b* and *Tnfsf11* were similarly expressed in control and CKD cortical bone at all stages of disease progression, with only a weak time-dependent variation observed for *Alpl* (Figures 2I–K). The *Tnfsf11/Tnfrsf11b* ratio was similar in control and CKD cortical bone after 1-, 3- and 5-weeks' induction (Figure 2L).

CKD mice have increased BMAT accumulation

To establish whether altered bone structure in the CKD mice was related to changes in BMAT accumulation and distribution, we next quantified BMAT along the tibia length as visualized by microCT images of osmium-stained adipose tissue (Figures 3A, B). After 5-weeks' induction, rBMAT of CKD mice was increased in the proximal tibia (~10 - 48% region of the tibia length). Similarly, cBMAT of CKD mice was increased in the ~65 - 82% and ~52 - 78% regions of the tibial length after 3- and 5- weeks' induction, respectively (Figures 3C and S3). We next determined if BMAT accumulation within the trabecular compartment was at the expense of juxtaposed bone formation. No differences in trabecular bone structure were noted in CKD mice after 3-weeks' induction (Supplementary Figure S2); a time point when there was increased constitutive and total BMAT and a trend for increased rBMAT (Figures 3C and S3). Correlation analysis revealed an inverse relationship between rBMAT and trabecular bone volume fraction after 5-weeks' induction but not at the earlier time points (Figures 3D–F). These results indicated that rBMAT accumulation tended to occur prior to trabecular bone loss and that there was a negative correlation between rBMAT accumulation and trabecular bone loss during the early stages of CKD.

Hormonal changes and their correlations with BMAT

During calorie restriction (CR), changes in circulating adiponectin, leptin, and glucocorticoids have been proposed as consequences or causes of BMAT expansion (19); hence, we tested these relationships in our CKD model. Plasma levels of adiponectin in CKD mice increased in a time-dependent manner, being higher in CKD mice than in age-matched control mice after 3- and 5- weeks' induction (Figure 4A). In contrast, the concentrations of plasma leptin or corticosterone in CKD mice were lower or higher, respectively, than in control mice at all ages studied (Figures 4B, C).

These results suggest that increased adiponectin is associated with other duration-dependent effects of CKD, including on BMAT, whereas the changes in leptin and corticosterone precede these other CKD effects. To test these relationships, the correlation between rBMAT accumulation and plasma levels of adiponectin, leptin and corticosteroids in control and CKD mice was determined. This revealed that circulating adiponectin was positively correlated with rBMAT accumulation whereas both circulating leptin and corticosterone were not (Figures 4D–F).

BMAT accumulation in CKD is not due to caloric restriction

The altered hormonal profile of the CKD mice was similar to that observed in CR. Therefore, to determine whether increased BMAT in the CKD mice might be caused by CR rather than CKD *per se*, a pair-feeding experiment was carried out. Mice fed the CKD diet *ad-lib* consumed less than those fed the control diet *ad-lib* and this difference in food intake was reflected in their body weights (Supplementary Figures S4A, B). To prevent excessive, pathological weight loss, all mice had *ad-lib* access to a supplementary gel pot diet for 48 h periods at the ends of week 1 and 2 (Supplementary Figures S4A, B, green shading). The CKD mice lost more body weight than the pair-fed mice despite a similar caloric intake over the 3 weeks of the study, suggesting that CKD was having effects beyond those explainable by CR alone (Supplementary Figures S4A, C). Consistent with this, BMAT accumulation was similar between control and pair-fed mice but was greater in CKD mice than in either of these groups (Supplementary Figure S4D). These results suggest that the accumulation of BMAT was a consequence of CKD progression and not of CR *per se*.

Gene expression in bone marrow tissue is altered in CKD mice

To investigate if bone marrow progenitor fate is altered in CKD mice, we next assessed the expression of key transcription factors and phenotype-specific genes in bone marrow tissue from control and CKD mice. For adipogenic markers, there was no effect of CKD on *Pparg2*, *Cebpa* or *Lep* expression whereas two other markers of mature adipocytes, *Fabp4* and *Adipoq*, were significantly increased in the bone marrow of CKD mice at 3- and 5-weeks of disease progression (Figures 5A–E). The expression of the lipolytic genes, *Pnpla2* and *Lipe* was similar in control and CKD bone marrow but tended to be higher in CKD mice after 3-weeks' induction, with this

10.3389/fendo.2025.1666681

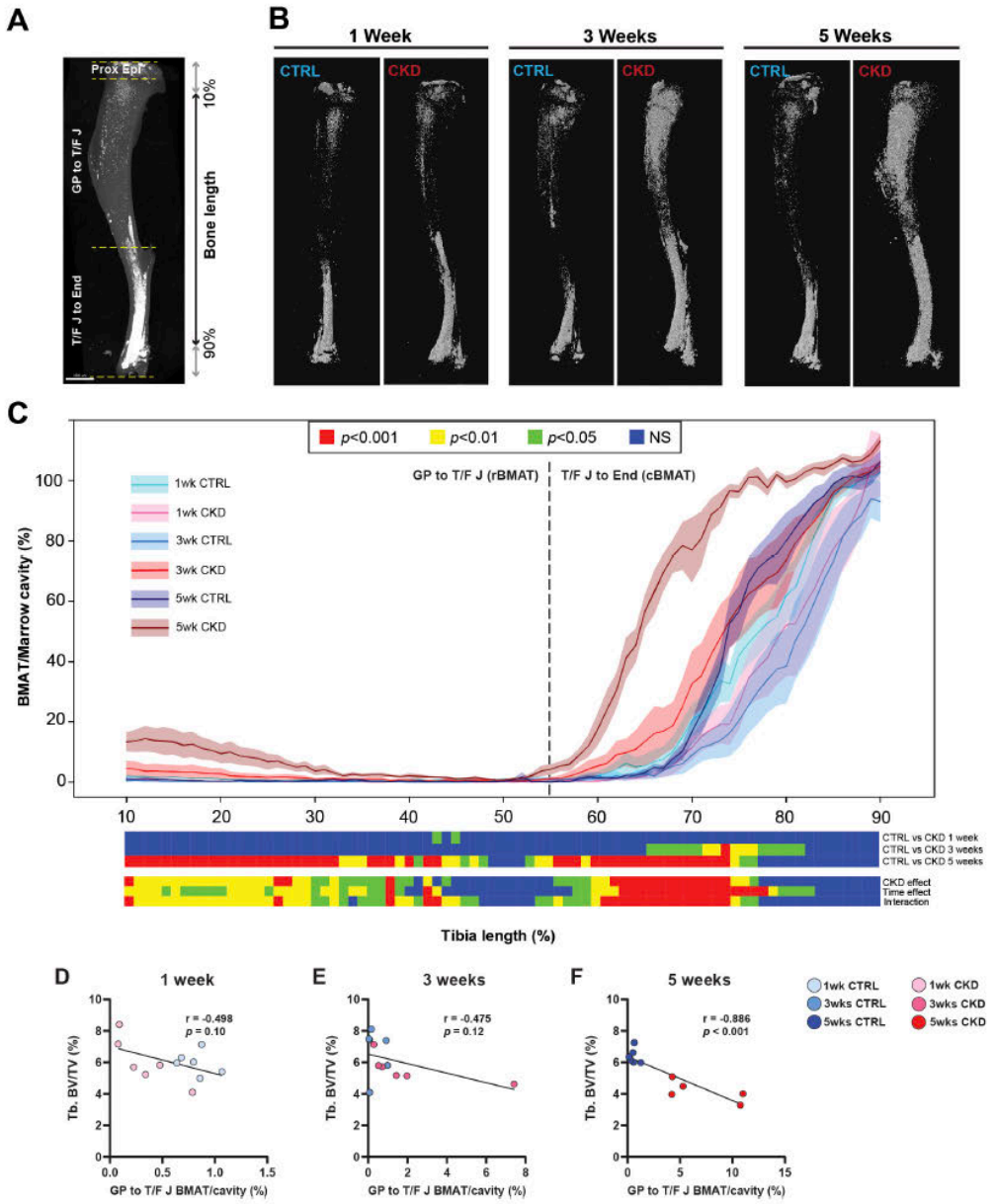

FIGURE 3
BMAT distribution along the tibial bone shaft and its correlation with trabecular bone. Visualization and quantification of bone marrow adipose tissue (BMAT) within the marrow cavity of CTRL and CKD tibia after 1-, 3- and 5-weeks' induction. **(A)** distribution of osmium stained BMAT within the different anatomical regions of the tibia: the top of the proximal bone to the growth plate (Proxi Epi); the growth plate to tibia/fibula junction (GP-T/F J), which contains regulated BMAT (rBMAT); and the tibia/fibula junction to the end of distal bone (T/F J-End), which contains constitutive BMAT (cBMAT). **(B)** distribution and **(C)** quantification of rBMAT and cBMAT in CTRL and CKD mice. cBMAT was increased in CKD mice at 3- and 5-weeks after induction whereas an increase in rBMAT in CKD mice was only noted after 5-weeks' induction. **(D–F)**. The dashed line represents the junction between rBMAT and cBMAT. Data are presented as mean ± SEM, n = 5–6 bones per group. **(D–F)** Correlation analysis between trabecular bone volume fraction (Tb.BV/TV) and rBMAT indicated a negative correlation after 5-weeks' induction but not after 1- or 3-weeks. Each dot represents an individual mouse.

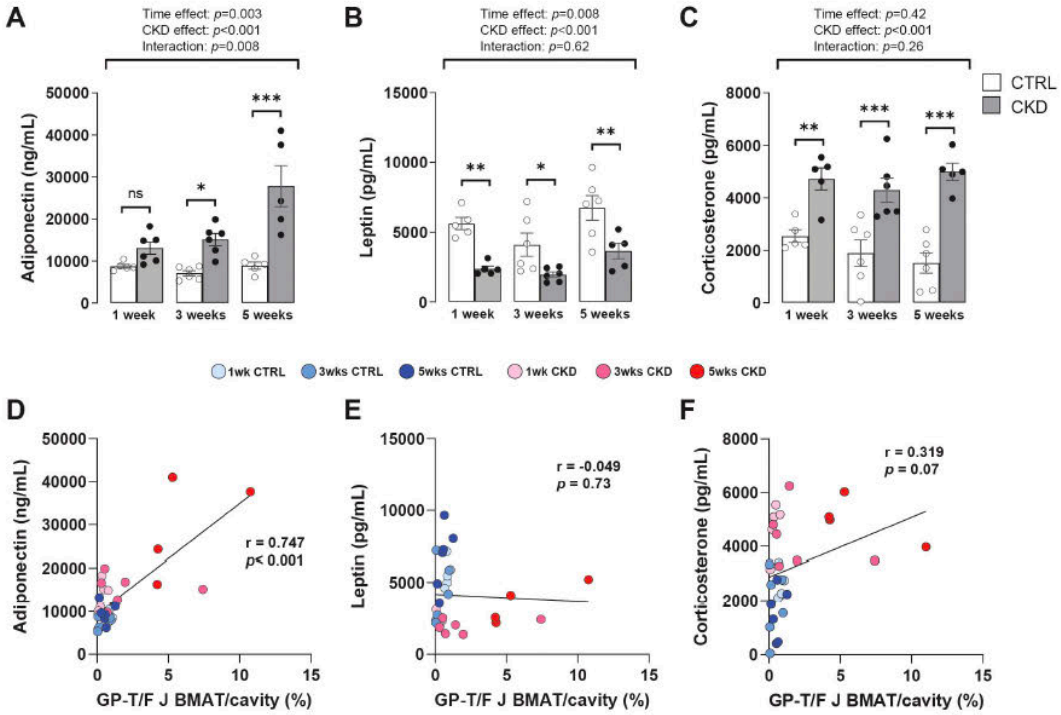

FIGURE 4
Hormonal changes and their correlation with rBMAT accumulation. Serum levels of **(A)** adiponectin **(C)** and corticosterone were increased in CKD mice following 3- and 1- weeks' induction, respectively, whereas **(B)** leptin levels were decreased at all sampling points. Data are presented as mean ± SEM, with each dot representing an individual mouse. ns, not significant, $*P < 0.05$, $**P < 0.01$, $***P < 0.001$. **(D)** Circulating adiponectin exhibited a positive correlation with rBMAT (GP-T/F BMAT) but no such correlation was observed with **(E)** leptin or **(F)** corticosterone.

difference reaching significance for *Lipe* expression (Figures 5F, G). For osteogenic markers, the expression of *Runx2*, *Sp7*, *Alpl* and *Tnfrsf11b* were similar in bone marrow of CKD and control mice, whereas *Tnfsf11* expression was higher in CKD mice after 5-weeks' induction when compared to age-matched controls (Figures 5H–L).

The number of adipocyte and osteoblast progenitor cells are unchanged during CKD onset

The observation that the expression of *Fabp4* and *Adipoq* was higher in CKD bone marrow tissue (Figure 5) and that BMAT in CKD mice started to accumulate from 3-weeks of induction (Figure 3) suggests that in CKD there may be a switch, prior to the 3-week time point, in BMSC commitment towards the adipocyte rather than the osteoblast phenotype. To address this possibility, we used flow cytometry to analyze bone marrow from control and CKD mice, 1- and 2- weeks after induction, to quantify the number of BMSCs, OPCs and APCs (Figure 6A). The BMSC population in CKD bone marrow was reduced from control levels after 1- and 2- weeks' induction whereas the proportions of OPCs and APCs were similar in bone marrow from CKD and control mice at both time points studied (Figure 6B). These results indicate that BMAT accumulation in CKD mice is unlikely to be driven by a prior change in BMSC commitment but it is possible that 1 or 2-weeks of dietary adenine intake was insufficient to program such changes in BMSC lineage commitment.

Expression of *Adipoq* and adipocyte transcription factors is increased in BMSCs from CKD mice

To further explore the effects of CKD on BMSC lineage commitment, we next determined whether disease progression directly affects the differentiation of BMSCs to mature adipocytes and osteoblasts rather than simply their commitment to APCs or OPCs, as studied above (Figure 6). We isolated primary BMSCs from mice that had been on control or CKD diets for 4-weeks, when CKD-induced BMAT accumulation was established (Figure 3). After nine days of adipogenic induction, BMSCs from control and CKD mice had similar oil red O staining and expression of the adipogenic genes *Cebpa*, *Fabp4*, *Adipoq* and *Pparg2* (Figures 7A, B). In contrast, when cultured in BMSC medium the expression of *Cebpa*, *Fabp4* and *Adipoq* but not *Pparg2* was upregulated in CKD

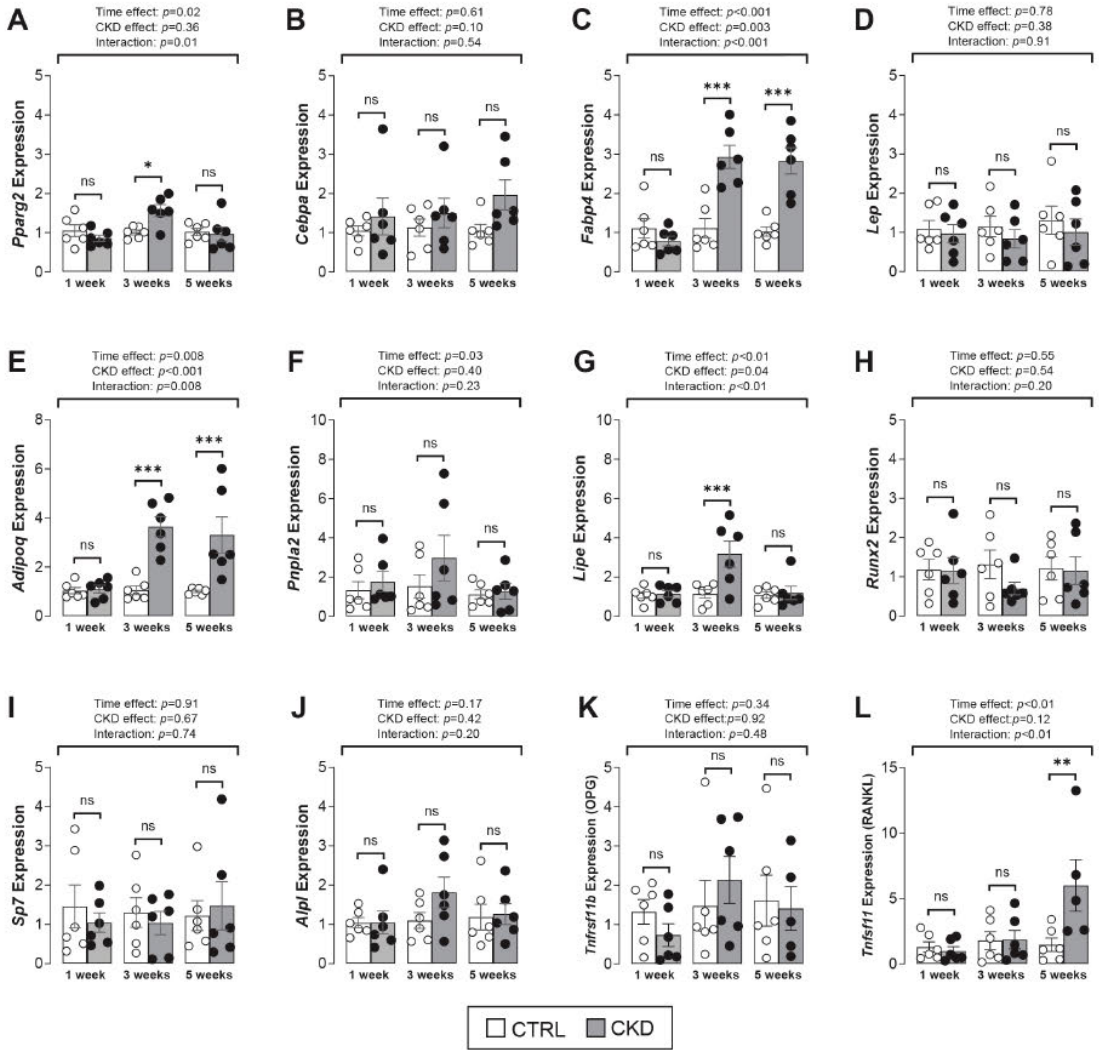

FIGURE 5
Adipogenic and osteogenic gene expression in bone marrow tissue. **(A–E)** The expression of the adipogenic transcription factor genes, *Pparg2* and *Cebpa* were similar in CTRL and CKD samples whereas the mature adipocyte marker genes, *Fabp4* and *Adipoq* but not *Lep* were increased in CKD marrow after 3- and 5-weeks' induction. There was a tendency for an increase in the expression of the lipolytic genes, **(F)** *Pnpla2* and **(G)** *Lipe* after 3-weeks' CKD induction but this difference only reached significance for *Lipe* expression. The expression of the osteogenic transcription factor genes **(H)** *Runx2*, **(I)** *Sp7*, **(J)** *Alpl* and **(K)** *Tnfrsf11b* were similar in CKD and CTRL mice while **(L)** *Tnfsf11* expression was increased in CKD mice after 5-weeks' induction. Data are presented as mean ± SEM, with each dot representing an individual mouse. ns, not significant, $*P < 0.05$, $**P < 0.01$, $***P < 0.001$.

cells compared to control cells (Figure 7B). This incongruity is likely explained by the overpowering capacity of adipogenic medium to induce adipocyte gene expression and dwarf any programming effects of CKD.

For osteoblast differentiation, BMSC from control and CKD mice had similar ALP activity and Alizarin Red staining after 21 days in osteogenic medium (Figures 7C, D) but the expression of *Runx2*, *Alpl*, *Col1a1* and *Tnfsf11* was upregulated in CKD cells compared to control cells (Figure 7E). In contrast, the expression of the osteogenic genes by control and CKD cells cultured in BMSC medium was similar (Figure 7E). The *Tnfsf11*/*Tnfrsf11* gene ratio was similar in control and CKD BMSC cultured in BCM but increased when cultured in OCM (Figure 7F). These discrepant gene expression data may be a result of differences in responsiveness between control and CKD cells to osteogenic medium. It is of course possible that increased sample number and longer culture periods may have revealed further differences in gene expression and in oil red O and alizarin red staining.

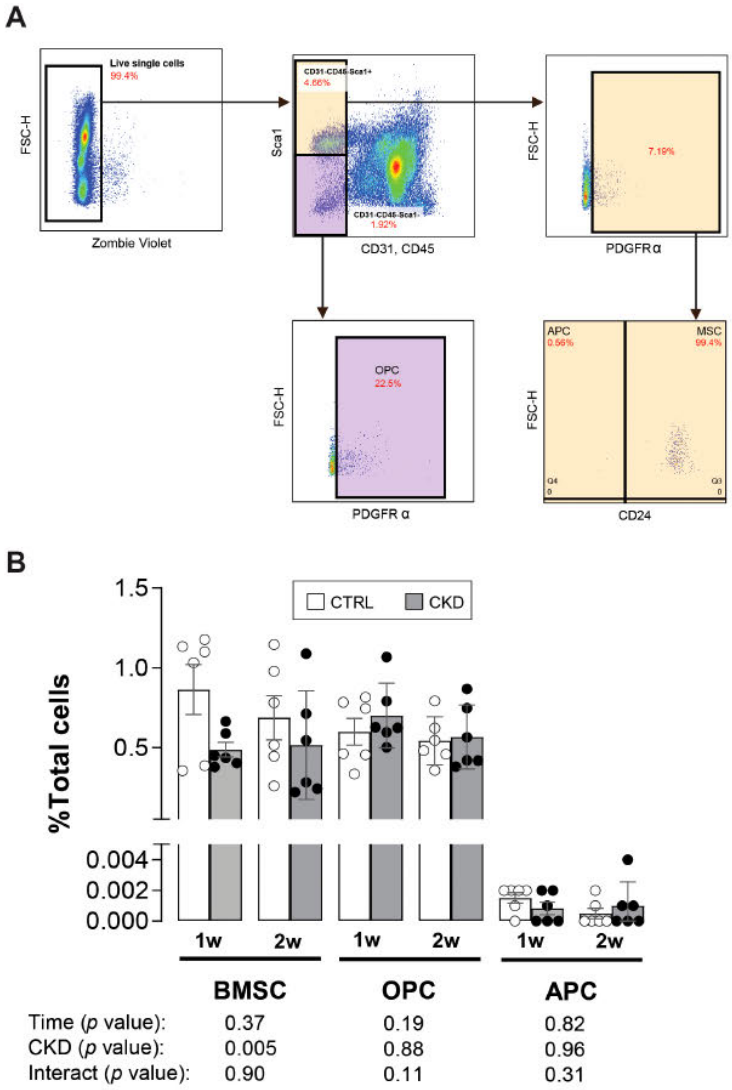

FIGURE 6
APC and OPC populations in CKD and CTRL mice. **(A)** The populations of bone marrow mesenchymal stromal cells (BMSCs), osteoblastic (OPC) and adipogenic (APC) precursor cells from the bone marrow of CTRL and CKD after 1- and 2-weeks induction were gated by CD45-CD31-Sca1+CD24+, CD45-CD31-Sca1+CD24- and CD45-CD31-Sca1-Pa+, respectively. **(B)** The BMSC population as a percentage of all live cells (total cells) was reduced in the CKD mice whereas the OPC and APC populations as a percentage of total cells was unchanged. Data represented as mean ± SEM, with each dot representing an individual mouse. Sca1; stem cell antigen 1, PDGFRα; platelet-derived growth factor-α.

Discussion

It is widely recognized that CKD can lead to bone loss, thereby increasing the risk of osteoporosis and fractures (29). Bone loss and increased serum bone turnover markers have also been noted in a variety of animal models of CKD-MBD and while the precise mechanisms responsible for the development of ROD remains unclear, increased bone resorption due to chronically high PTH levels is regarded as central to its etiology (8, 9, 20). However, other mechanisms such as uremic-toxin-induced mitochondrial abnormalities are likely to also be involved, as increased hip and vertebral fractures have been reported in patients with low circulating PTH (30, 31).

Our finding of increased BMAT in this mouse model of CKD is consistent with previous observations in other animal models (12, 13) and in humans with this disease (32, 33). There are several mechanisms through which increased BMAT may directly contribute to bone loss and fracture risk in CKD. One possibility is that a switch in the commitment of BMSC from the osteoblast to the adipocyte lineage may offer an additional/alternative explanation for

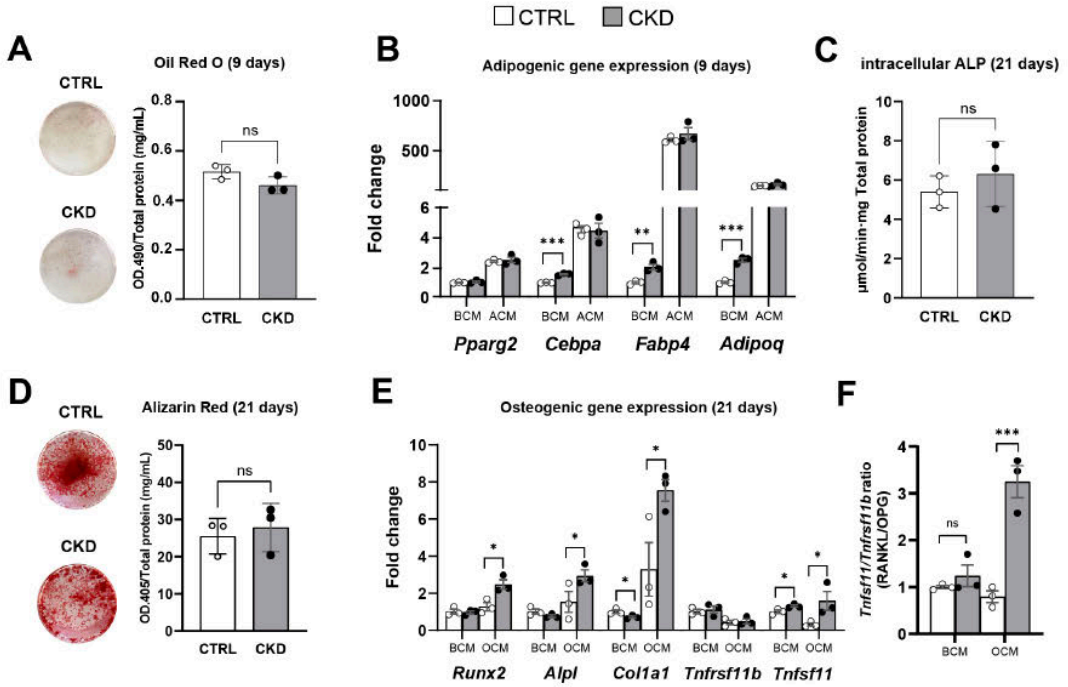

FIGURE 7
Adipocyte and osteoblast differentiation of isolated primary BMSC from control and CKD mice. Primary BMSC from CTRL and CKD mice were cultured in BMSC cell culture media (BCM), adipogenic cell culture media (ACM) for 9 days and osteogenic cell culture media (OCM) for 21 days. **(A)** After 9 days in ACM, oil red O staining of adipocytes was similar in CTRL and CKD cultures. **(B)** Expression of the adipogenic genes, *Cebpa*, *Fabp4* and *Adipoq* were increased in the BMSC from CKD mice cultured in BCM. In contrast, while ACM induced *Pparg2*, *Cebpa*, *Fabp4* and *Adipoq* gene expression in BMSC from both CTRL and CKD mice the expression levels were similar in CTRL and CKD cultures. In primary BMSC cultured in OCM for 21 days, both **(C)** intracellular ALP activity and **(D)** alizarin red staining was similar in CTRL and CKD cultures. **(E)** The expression of osteogenic genes by BMSC cultured in BCM revealed that *Col1a1* was decreased whereas *Tnfsf11* was increased in CKD samples. When primary BMSC were cultured in OCM, osteogenic genes *Runx2*, *Alpl*, *Col1a1* and *Tnfsf11* were increased in CKD samples. **(F)** The *Tnfsf11/Tnfrsf11* ratio was similar in CTRL and CKD BMSC cultured in BCM but increased when cultured in OCM. Data are presented as mean ± SEM with each dot representing an individual culture. ns, not significant, $^{*}P < 0.05$, $^{**}P < 0.01$, $^{***}P < 0.001$.

the development of ROD. A change in mesenchymal cell fate may also explain the higher marrow fat content in patients with osteopenia/osteoporosis (34, 35), ageing (36, 37), obesity (38) and CR (26). An inverse relationship between bone mass and BMAT is observed in the CKD mice of the present study and a CKD-specific determinant of BMAd accumulation could be PTH. When administered intermittently, PTH is anabolic to the skeleton and reduces BMAT in mice and in male and female osteoporotic patients (18). However, the influence of chronically high levels of PTH, as observed in CKD patients and CKD animal models, on BMAT accumulation is unknown. In CKD patients, BMAT accumulation is positively associated with disease severity. For example, Woods et al. showed that BMAT is greater in individuals with an estimated glomerular filtration rate (eGFR) of ≤45 mL/min compared to those with an eGFR of >60mL/min (33) and Borelli and colleagues reported that BMAT accumulation in CKD patients is negatively correlated to eGFR and volumetric BMD (11). Clinical studies in non-CKD patients have also shown that BMAT accumulation correlates with vertebral fracture risk, and in ageing adults this risk is independent of BMD, suggesting that factors released from BMAds such as RANKL may contribute to poor bone quality (39, 40). Moreover, variants in the RANKL gene (*TNFSF11)* are associated with altered bone marrow adiposity in humans (37), further highlighting the links between BMAT and bone remodeling. Whether BMAT is associated with fracture incidence in CKD patients is yet to be determined.

To establish whether BMAT accumulation and bone loss noted in CKD is a result of a switch in BMSC differentiation to favor adipogenesis at the expense of osteoblast formation, we first established a longitudinal mouse model of CKD-BMD to record the temporal relationship between BMAT accumulation and bone mass during disease progression. Our findings reveal an inverse relationship between trabecular bone mass and rBMAT accumulation during the progression of CKD, which is consistent with adult and pediatric CKD data (11, 41).

However, our data also suggest that BMAT accumulation precedes bone loss in CKD. We show that body weight loss and serum CKD markers first become apparent after 3-weeks in CKD mice, by which time there is an increase in total BMAT accumulation and *Fabp4* and *Adipoq* expression in CKD bone marrow tissue but no change in trabecular BMD, BV/TV, number, thickness or connectivity. These

data confirm the complex relationship between BMAT accumulation and bone loss. While an increase in adipogenesis in bone marrow stromal cells and a reduction in osteogenic differentiation occurs in both CR and ageing (26, 42), other studies have reported BMAT accumulation *per se* does not lead to bone loss (43, 44). Also, studies with rabbits have disclosed that during CR, bone loss can occur independently of BMAT accumulation (19). Furthermore, recent studies have identified the presence of two distinct BMSC populations and questioned the mutually exclusive commitment of BMSC to the adipogenic or osteogenic lineages (45). Therefore, more definitive experiments are required which could involve inducible Cre lines that exclusively label pre-commitment cellular population *e.g.* Cxcl12-CreE (46). This approach would allow the visualization of stromal cell populations *in vivo*.

From our data it is possible that additional factors beyond lineage differentiation may contribute to BMAT accumulation in CKD. Nevertheless, we reveal that the proportion of BMSCs decreases during CKD onset and, while this suggests a potential impairment of BMSC proliferation and/or survival, further studies are required to confirm this. Also, the differentiation of primary BMSCs from 4-week-induced CKD mice towards the adipocyte and osteoblast phenotype may be insightful. The increased expression of adipogenic genes in CKD BMSC cultured in BMSC medium suggests an inherent predisposition towards adipogenesis. This may be attributed to long-term exposure to an altered systemic milieu in the CKD mice that may prime BMSCs for adipogenic differentiation. The preferential upregulation of osteogenic genes in CKD BMSC cultured in osteogenic media suggests a potentially heightened, yet potentially dysfunctional, osteogenic response.

Our finding of higher serum levels of adiponectin in the CKD mice mirrors human data where, in CKD individuals, it may act as a biomarker for renal dysfunction (47). The correlation between serum adiponectin and BMAT volume supports the possibility that the accumulated BMAT is the source of the increased adiponectin in the CKD mice, as noted in mouse models of CR (19). Consistent with this, we show that *Adipoq* expression is increased within the bone marrow of CKD mice. However, despite the decrease in iWAT and gWAT mass during CKD onset, it cannot be ruled out that WAT, due to increased production and secretion, is a contributary source to the increased circulating adiponectin in the CKD mice. This, however, is unlikely as in CR, adiponectin expression and secretion from WAT does not increase. Regardless of the source, adiponectin may, through autocrine mechanisms, promote preadipocyte differentiation, but whether such a 'feed-forward' mechanism contributes to BMAT accumulation in CKD is currently unclear (48).

Leptin is produced by WAT and the decrease in circulating levels in CKD mice are a likely consequence of reduced food intake and decreased body fat (49). As leptin-deficient *ob/ob* mice present with increased BMAT and decreased BMD, it is possible that low circulating leptin levels contribute to the BMAT accumulation and bone loss noted in the CKD mice (50). However, CR in female mice can increase BMAT without causing hypoleptinemia, whereas CR of male rabbits leads to decreased systemic leptin without BMAT expansion (19). Thus, it is possible that hypoleptinemia *per se* is neither necessary nor sufficient to promote BMAT expansion in CKD.

In addition to adipokines, cytokines such as RANKL are also secreted from BMAds and we show that expression of *Tnfsf11* expression, but not *Tnfrsf11b*, is increased in CKD mice. Thus, BMAT-derived RANKL may also contribute to the bone loss noted in these mice (51).

The decrease in leptin levels is likely responsible for the increased circulating corticosterone in CKD mice (49, 52) and this observation is consistent with the phenotype of calorie restricted mice and Cushing's disease, where glucocorticoid excess may contribute to BMAT expansion (19, 53). It remains unclear if increased corticosterone in CKD mice contributes to their BMAT accumulation and/or impaired bone health. Indeed, our pair-feeding studies suggest that CR *per se* is not responsible for BMAT accumulation in the CKD mice, suggesting that the mechanisms underlying BMAT expansion likely differ between CKD and CR.

In conclusion, we induced CKD-MBD in mice by feeding them an adenine-supplemented diet for up to 5-weeks. These mice lose both cortical and trabecular bone and accumulate adipocytes within the marrow cavity. BMAT accumulates prior to trabecular bone loss and is negatively correlated with trabecular bone volume fraction, suggesting that BMAT accumulation may contribute to bone loss in CKD. Although the numbers of adipocyte and osteoblast progenitor cells are unchanged during CKD onset, BMSCs from CKD mice have greater expression of adipogenic markers, suggesting enhanced adipogenic potential *in vivo* that may contribute to the increased BMAT in this disease.

These findings will inform future studies into the causes and consequences of BMAT accumulation in CKD, which may help to identify the cellular mechanisms involved and more specifically determine if the expansion of BMAds is at the expense of impaired osteoblast bone formation. Such studies are likely to uncover improved strategies for the clinical management of this condition.

Data availability statement

The original contributions presented in the study are included in the article/Supplementary Files, further inquiries can be directed to the corresponding author/s.

Ethics statement

The animal study was approved by University of Edinburgh Animal Welfare and Ethical Review Board. The study was conducted in accordance with the local legislation and institutional requirements.

Author contributions

WP: Conceptualization, Formal analysis, Funding acquisition, Investigation, Methodology, Project administration, Software, Visualization, Writing – original draft, Writing – review & editing. WC: Conceptualization, Supervision, Validation, Writing – review & editing. LB: Investigation, Methodology, Software, Writing – review & editing. SJ: Formal analysis, Investigation, Methodology, Writing –

review & editing. AP: Formal analysis, Investigation, Methodology, Writing – review & editing. KS: Conceptualization, Supervision, Validation, Writing – review & editing. LS: Conceptualization, Funding acquisition, Supervision, Validation, Writing – review & editing. CF: Conceptualization, Data curation, Formal analysis, Funding acquisition, Project administration, Supervision, Writing – original draft, Writing – review & editing.

Funding

The author(s) declare financial support was received for the research and/or publication of this article. We acknowledge financial support from Chulabhorn Royal Academy to WP and the Biotechnology and Biological Sciences Research Council (BBSRC) for supporting LAS via a Discovery Fellowship (BB/X009904/1) and for Institute Strategic Programme Grant Funding (BBS/E/D/10002071 and BBS/E/RL/230001C) to CF and SJ. We also acknowledge the Medical Research Council for funding to KAS (MR/V033506/1 and MR/R022240/2) and WPC (MR/M021394/1 and MR/S010505/1).

Acknowledgments

We thank Heather Warnock and the staff of the Biological Research Facility (BRF) at the University of Edinburgh for providing invaluable animal support, Colin Wood and the staff at Easter Bush Pathology, Royal (Dick) School of Veterinary Studies, University of Edinburgh for conducting mouse serum biochemistries and also Chartinun Chutoe and Kuan-Chan Chen, Edinburgh University Medical School for help with visualization of the data. For the purpose of open access, the authors have applied a CC-BY public copyright license to any Author Accepted Manuscript version arising from this submission.

Conflict of interest

The authors declare that the research was conducted in the absence of any commercial or financial relationships that could be construed as a potential conflict of interest.

Generative AI statement

The author(s) declare that no Generative AI was used in the creation of this manuscript.

Any alternative text (alt text) provided alongside figures in this article has been generated by Frontiers with the support of artificial intelligence and reasonable efforts have been made to ensure accuracy, including review by the authors wherever possible. If you identify any issues, please contact us.

Publisher's note

All claims expressed in this article are solely those of the authors and do not necessarily represent those of their affiliated organizations, or those of the publisher, the editors and the reviewers. Any product that may be evaluated in this article, or claim that may be made by its manufacturer, is not guaranteed or endorsed by the publisher.

Supplementary material

The Supplementary Material for this article can be found online at: https://www.frontiersin.org/articles/10.3389/fendo.2025.1666681/full#supplementary-material

References

1. Kovesdy CP. Epidemiology of chronic kidney disease: an update 2022. *Kidney Int Suppl.* (2022) 12:7–11. doi: 10.1016/j.kisu.2021.11.003

2. GBD Chronic Kidney Disease Collaboration. Global, regional, and national burden of chronic kidney disease, 1990-2017: a systematic analysis for the Global Burden of Disease Study 2017. *Lancet.* (2020) 395:709–33. doi: 10.1016/S0140-6736(20)30045-3

3. Fang Y, Ginsberg C, Sugatani T, Monier-Faugere MC, Malluche H, Hruska KA. Early chronic kidney disease-mineral bone disorder stimulates vascular calcification. *Kidney Int.* (2014) 85:142–50. doi: 10.1038/ki.2013.271

4. Hsu CY, Chen LR, Chen KH. Osteoporosis in patients with chronic kidney diseases: A systemic review. *Int J Mol Sci.* (2020) 21:1–24. doi: 10.3390/ijms21186846

5. Campos-Obando N, Koek WNH, Hooker ER, van der Eerden BC, Pols HA, Hofman A, et al. Serum phosphate is associated with fracture risk: the rotterdam study and mrOS. *J Bone Mineral Res.* (2017) 32:1182–93. doi: 10.1002/jbmr.3094

6. Carrillo-López N, Panizo S, Alonso-Montes C, Román-García P, Rodríguez I, Martínez-Salgado C, et al. Direct inhibition of osteoblastic Wnt pathway by fibroblast growth factor 23 contributes to bone loss in chronic kidney disease. *Kidney Int.* (2016) 90:77–89. doi: 10.1016/j.kint.2016.01.024

7. Dhayat NA, Ackermann D, Pruijm M, Ponte B, Ehret G, Guessous I, et al. Fibroblast growth factor 23 and markers of mineral metabolism in individuals with preserved renal function. *Kidney Int.* (2016) 90:648–57. doi: 10.1016/j.kint.2016.04.024

8. Jadoul M, Albert JM, Akiba T, Akizawa T, Arab L, Bragg-Gresham JL, et al. Incidence and risk factors for hip or other bone fractures among hemodialysis patients in the Dialysis Outcomes and Practice Patterns Study. *Kidney Int.* (2006) 70:1358–66. doi: 10.1038/sj.ki.5001754

9. Nickolas TL, Stein EM, Dworakowski E, Nishiyama KK, Komandah-Kosseh M, Zhang CA, et al. Rapid cortical bone loss in patients with chronic kidney disease. *J Bone Mineral Res.* (2013) 28:1811–20. doi: 10.1002/jbmr.1916

10. Bianco P, Robey PG. Skeletal stem cells. *Development.* (2015) 142:1023–7. doi: 10.1242/dev.102210

11. Borelli C, Vergara D, Guglielmi R, Aucella F, Testini V, Guglielmi G. Assessment of bone marrow fat by 3-Tesla magnetic resonance spectroscopy in patients with chronic kidney disease. *Quant Imaging Med Surg.* (2023) 13:7432–43. doi: 10.21037/qims-23-530

12. Wang CY, Hsu YJ, Peng YJ, Lee HS, Chang YC, Chang CS, et al. Knee subchondral bone perfusion and its relationship to marrow fat and trabeculation on multi-parametric MRI and micro-CT in experimental CKD. *Sci Rep.* (2017) 7:3073. doi: 10.1038/s41598-017-03059-3

13. Ni LH, Tang RN, Yuan C, Song KY, Wang LT, Zhang XL, et al. Cinacalcet attenuated bone loss via inhibiting parathyroid hormone-induced endothelial-to-adipocyte transition in chronic kidney disease rats. *Ann Transl Med.* (2019) 7:312. doi: 10.21037/atm.2019.06.44

14. Suchacki KJ, Cawthorn WP, Rosen CJ. Bone marrow adipose tissue: formation, function and regulation. *Curr Opin Pharmacol*. (2016) 28:50–6. doi: 10.1016/j.coph.2016.03.001

15. Costa S, Fairfield H, Reagan MR. Inverse correlation between trabecular bone volume and bone marrow adipose tissue in rats treated with osteoanabolic agents. *Bone*. (2019) 123:211–23. doi: 10.1016/j.bone.2019.03.038

16. Stern JH, Rutkowski JM, Scherer PE. Adiponectin, leptin, and fatty acids in the maintenance of metabolic homeostasis through adipose tissue crosstalk. *Cell Metab*. (2016) 23:770–84. doi: 10.1016/j.cmet.2016.04.011

17. Sulston RJ, Cawthorn WP. Bone marrow adipose tissue as an endocrine organ: close to the bone? *Horm Mol Biol Clin Investig*. (2016) p:21–38. doi: 10.1515/hmbci-2016-0012

18. Fan Y, Hanai JI, Le PT, Bi R, Maridas D, DeMambro V, et al. Parathyroid hormone directs bone marrow mesenchymal cell fate. *Cell Metab*. (2017) 25:661–72. doi: 10.1016/j.cmet.2017.01.001

19. Cawthorn WP, Scheller EL, Parlee SD, Pham HA, Learman BS, Redshaw CMH, et al. Expansion of bone marrow adipose tissue during caloric restriction is associated with increased circulating glucocorticoids and not with hypoleptinemia. *Endocrinology*. (2016) 157:508–21. doi: 10.1210/en.2015-1477

20. Hsu SN, Stephen LA, Dillon S, Milne E, Javaheri B, Pitsillides AA, et al. Increased PHOSPHO1 expression mediates cortical bone mineral density in renal osteodystrophy. *J Endocrinol*. (2022) 254:153–67. doi: 10.1530/JOE-22-0097

21. Staines KA, Hopkinson M, Dillon S, Stephen LA, Fleming R, Sophocleous A, et al. Conditional deletion of E11/Podoplanin in bone protects against ovariectomy-induced increases in osteoclast formation and activity. *Biosci Rep*. (2020) 40(1): BSR20190329. doi: 10.1042/BSR20190329

22. Dillon S, Suchacki K, Hsu SN, Stephen LA, Wang R, Cawthorn WP, et al. Ablation of enpp6 results in transient bone hypomineralization. *JBMR Plus*. (2021) 5: e10439. doi: 10.1002/jbm4.10439

23. Bourne LE, Jayash SN, Michels LV, Hopkinson M, Guppy FM, Clarkin CE, et al. Sexually dimorphic effects of prenatal alcohol exposure on the murine skeleton. *Biol Sex Differ*. (2024) 15:51. doi: 10.1186/s13293-024-00626-y

24. Scheller EL, Troiano N, Vanhoutan JN, Bouxsein MA, Fretz JA, Xi Y, et al. Use of osmium tetroxide staining with microcomputerized tomography to visualize and quantify bone marrow adipose tissue *in vivo*. *Methods Enzymol*. (2014) 537:123–39. doi: 10.1016/B978-0-12-411619-1.00007-0

25. Scheller EL, Doucette CR, Learman BS, Cawthorn WP, Khandaker S, Schell B, et al. Region-specific variation in the properties of skeletal adipocytes reveals regulated and constitutive marrow adipose tissues. *Nat Commun*. (2015) 6:7808. doi: 10.1038/ncomms8808

26. Liu L, Le PT, Stohn JP, Liu H, Ying W, Baron R, et al. Calorie restriction in mice impairs cortical but not trabecular peak bone mass by suppressing bone remodeling. *J Bone Miner Res*. (2024) 39:1188–99. doi: 10.1093/jbmr/zjae104

27. Staines KA, Myers K, Little K, Ralston SH, Farquharson C. Proton pump inhibitors inhibit PHOSPHO1 activity and matrix mineralisation *in vitro*. *Calcif Tissue Int*. (2021) 109:696–705. doi: 10.1007/s00223-021-00882-9

28. Ambrosi TH, Sinha R, Steininger HM, Hoover MY, Murphy MP, Koepke LS, et al. Distinct skeletal stem cell types orchestrate long bone skeletogenesis. *Elife*. (2021) 10:e66063. doi: 10.7554/eLife.66063

29. Tariq MH, Sulaiman SAS. Prevalence of osteopenia and osteoporosis among chronic kidney disease patients: A systematic review. *Open Urol Nephrol J*. (2020) 13:5–12. doi: 10.2174/1874303X02013010005

30. Coco M, Rush H. Increased incidence of hip fractures in dialysis patients with low serum parathyroid hormone. *Am J Kidney Dis*. (2000) 36:1115–21. doi: 10.1053/ajkd.2000.19812

31. Hsu SN, Stephen LA, Phadwal K, Dillon S, Carter R, Morton NM, et al. Mitochondrial dysfunction and mitophagy blockade contribute to renal osteodystrophy in chronic kidney disease-mineral bone disorder. *Kidney Int*. (2025) 107:1017–36. doi: 10.1016/j.kint.2025.01.022

32. Moorthi RN, Fadel W, Eckert GJ, Ponsler-Sipes K, Moe SM, Lin C. Bone marrow fat is increased in chronic kidney disease by magnetic resonance spectroscopy. *Osteoporos Int*. (2015) 26:1801–7. doi: 10.1007/s00198-015-3064-7

33. Woods GN, Ewing SK, Sigurdsson S, Kado DM, Ix JH, Hue TF, et al. Chronic kidney disease is associated with greater bone marrow adiposity. *J Bone Miner Res*. (2018) 33:2158–64. doi: 10.1002/jbmr.3562

34. Yeung DK, Griffith JF, Antonio GE, Lee FK, Woo J, Leung PC. Osteoporosis is associated with increased marrow fat content and decreased marrow fat unsaturation: a proton MR spectroscopy study. *J Magn Reson Imaging*. (2005) 22:279–85. doi: 10.1002/jmri.20367

35. Morris DM, Wang C, Papanastasiou G, Gray CD, Xu W, Sjöström S, et al. A novel deep learning method for large-scale analysis of bone marrow adiposity using UK Biobank Dixon MRI data. *Comput Struct Biotechnol J*. (2024) 24:89–104. doi: 10.1016/j.csbj.2023.12.029

36. Shen W, Chen J, Punyanitya M, Shapses S, Heshka S, Heymsfield SB. MRI-measured bone marrow adipose tissue is inversely related to DXA-measured bone mineral in Caucasian women. *Osteoporos Int*. (2007) 18:641–7. doi: 10.1007/s00198-006-0285-9

37. Xu W, Mesa-Eguiagaray I, Morris DM, Wang C, Gray CD, Sjöström S, et al. Deep learning and genome-wide association meta-analyses of bone marrow adiposity in the UK Biobank. *Nat Commun*. (2025) 16:99. doi: 10.1038/s41467-024-55422-4

38. Ambrosi TH, Scialdone A, Graja A, Gohlke S, Jank AM, Bocian C, et al. Adipocyte accumulation in the bone marrow during obesity and aging impairs stem cell-based hematopoietic and bone regeneration. *Cell Stem Cell*. (2017) 20:771–84 e6. doi: 10.1016/j.stem.2017.02.009

39. Schwartz AV, Sigurdsson S, Hue TF, Lang TF, Harris TB, Rosen CJ, et al. Vertebral bone marrow fat associated with lower trabecular BMD and prevalent vertebral fracture in older adults. *J Clin Endocrinol Metab*. (2013) 98:2294–300. doi: 10.1210/jc.2012-3949

40. Rinotas V, Gkikopoulou E, Tzortzis E, Kritikos K, Siatra P, Papadopoulos A, et al. Interplay between bone marrow adiposity and bone resorption in RANKL-mediated modelled osteoporosis. *J Cell Physiol*. (2024) 239:e31434. doi: 10.1002/jcp.31434

41. Sirimongkolchaiyakul O, Pereira RC, Gales B, Bacchetta J, Salusky IB, Wesseling-Perry K. Bone marrow adiposity inversely correlates with bone turnover in pediatric renal osteodystrophy. *Bone Rep*. (2021) 15:101104. doi: 10.1016/j.bonr.2021.101104

42. Kawai M, Rosen CJ. PPARgamma: a circadian transcription factor in adipogenesis and osteogenesis. *Nat Rev Endocrinol*. (2010) 6:629–36. doi: 10.1038/nrendo.2010.155

43. Li Z, Bowers E, Zhu J, Yu H, Hardij J, Bagchi DP, et al. Lipolysis of bone marrow adipocytes is required to fuel bone and the marrow niche during energy deficits. *ELife*. (2022) 11:e78496. doi: 10.7554/eLife.78496.sa2

44. Rosen CJ, Ackert-Bicknell C, Rodriguez JP, Pino AM. Marrow fat and the bone microenvironment: developmental, functional, and pathological implications. *Crit Rev Eukaryot Gene Expr*. (2009) 19:109–24. doi: 10.1615/CritRevEukarGeneExpr.v19.i2.20

45. Deng P, Yuan Q, Cheng Y, Li J, Liu Z, Liu Y, et al. Loss of KDM4B exacerbates bone-fat imbalance and mesenchymal stromal cell exhaustion in skeletal aging. *Cell Stem Cell*. (2021) 28:1057–73 e7. doi: 10.1016/j.stem.2021.01.010

46. Zhong L, Yao L, Tower RJ, Wei Y, Miao Z, Park J, et al. Single cell transcriptomics identifies a unique adipose lineage cell population that regulates bone marrow environment. *Elife*. (2020) 9:e54695. doi: 10.7554/eLife.54695

47. Song SH, Oh TR, Choi HS, Kim CS, Ma SK, Oh KH, et al. High serum adiponectin as a biomarker of renal dysfunction: Results from the KNOW-CKD study. *Sci Rep*. (2020) 10:5598. doi: 10.1038/s41598-020-62465-2

48. Fu Y, Luo N, Klein RL, Garvey WT. Adiponectin promotes adipocyte differentiation, insulin sensitivity, and lipid accumulation. *J Lipid Res*. (2005) 46:1369–79. doi: 10.1194/jlr.M400373-JLR200

49. Perry RJ, Wang Y, Cline GW, Rabin-Court A, Song JD, Dufour S, et al. Leptin mediates a glucose-fatty acid cycle to maintain glucose homeostasis in starvation. *Cell*. (2018) 172:234–48 e17. doi: 10.1016/j.cell.2017.12.001

50. Hamrick MW, Pennington C, Newton D, Xie D, Isales C. Leptin deficiency produces contrasting phenotypes in bones of the limb and spine. *Bone*. (2004) 34:376–83. doi: 10.1016/j.bone.2003.11.020

51. Li Z, Hardij J, Bagchi DP, Scheller EL, MacDougald OA. Development, regulation, metabolism and function of bone marrow adipose tissues. *Bone* (2018) 110:134–40. doi: 10.1016/j.bone.2018.01.008

52. Dubuc PU. Basal corticosterone levels of young og/ob mice. *Horm Metab Res*. (1977) 9:95–7. doi: 10.1055/s-0028-1095550

53. Geer EB, Shen W, Strohmayer E, Post KD, Freda PU. Body composition and cardiovascular risk markers after remission of Cushing's disease: a prospective study using whole-body MRI. *J Clin Endocrinol Metab*. (2012) 97:1702–11. doi: 10.1210/jc.2011-3123

frontiers

Supplementary Material

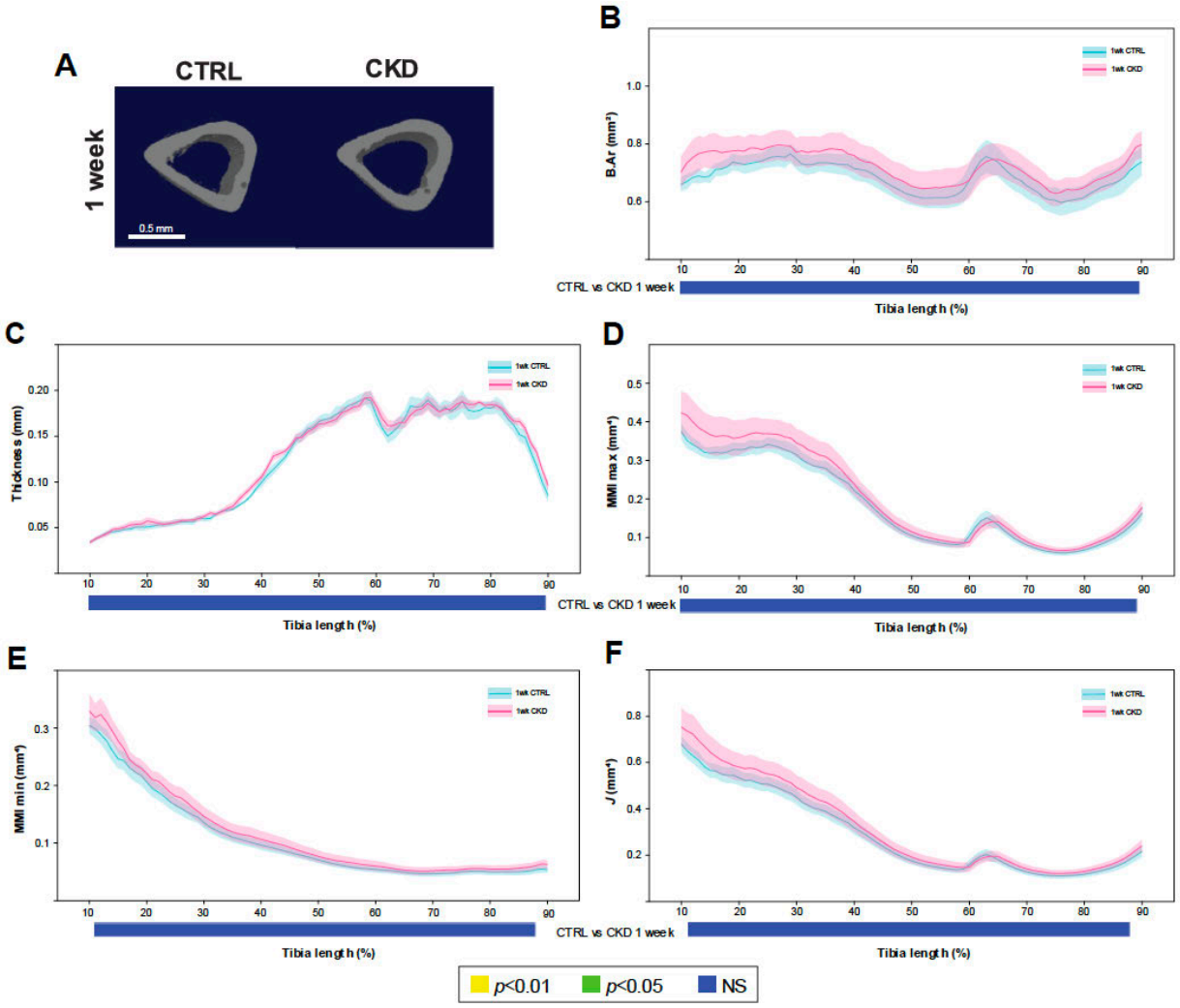

Supplementary Figure 1. Micro-CT analysis of tibial cortical bone. (A) 3-dimentional images of tibial cortical bone compartment. Quantification of whole bone analyses of cortical bone between 10 and 90% of total tibial length, excluding proximal and distal metaphyseal bone, of CTRL and CKD tibia after 1-weeks' induction. (B) cortical bone area (B.Ar), (C) thickness, (D) maximum moment of inertia (MMI max), (E) minimum moment of inertia (MMI min) and (F) and *J* - polar moment of inertia were all similar between control and CKD mice. Data are presented as mean ± SEM, n = 5 - 6 bones per group.

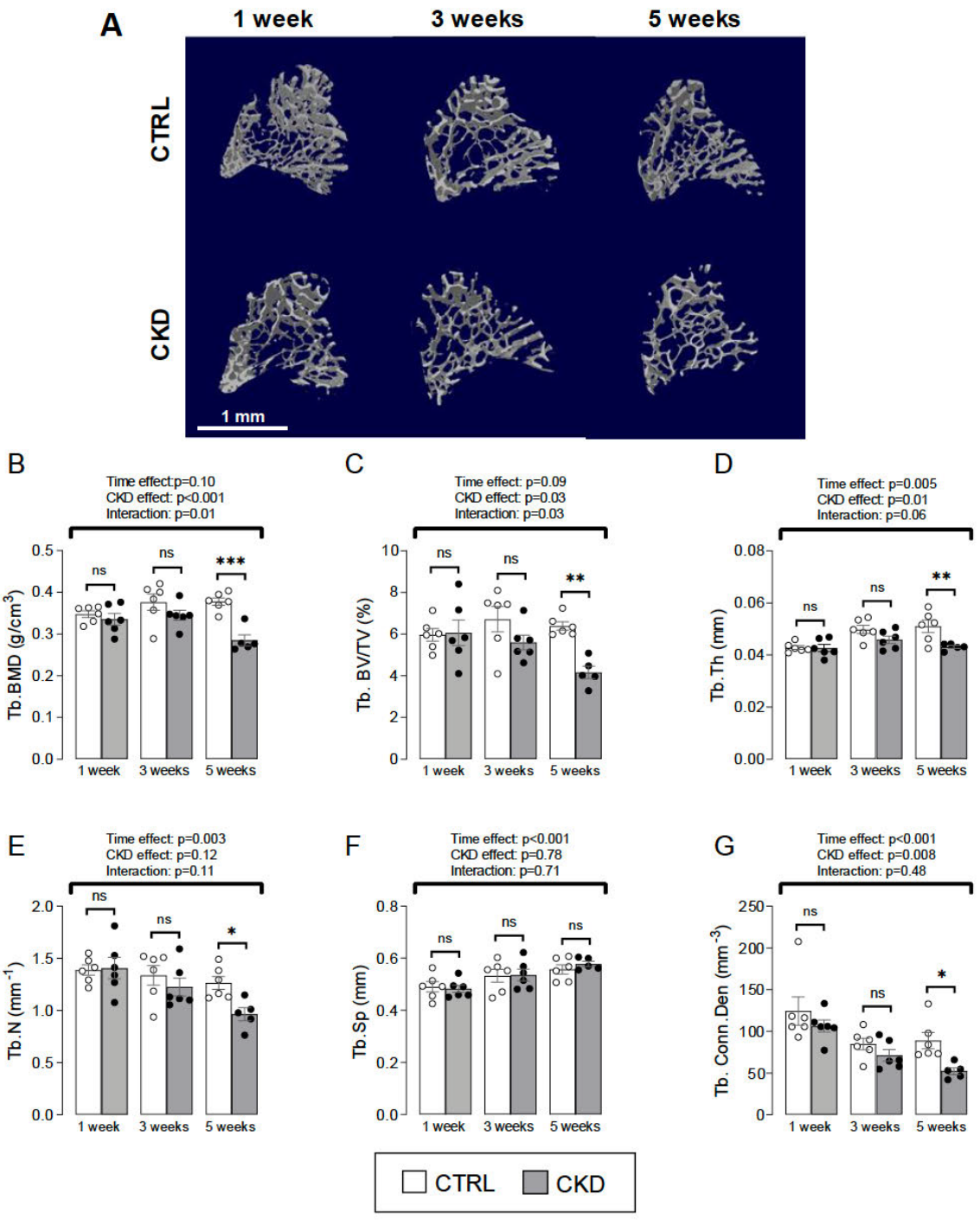

Supplementary Figure 2. Micro-CT analysis of tibial trabecular bone. (A) 3-dimentional images of tibial trabecular bone compartment. Trabecular (B) bone mineral density (Tb.BMD), (C) bone volume fraction (Tb.BV/TV), (D), thickness (Tb.Th), (E) number (Tb.N) and (G) connectivity density (Tb. Conn.Den) but not (F) separation (Tb.Sp) were decreased in CKD mice after 5 weeks' induction. Data are presented as mean ± SEM with each dot representing an individual mouse. ns, not significant, * $P < 0.05$, ** $P < 0.01$, *** $P < 0.001$.

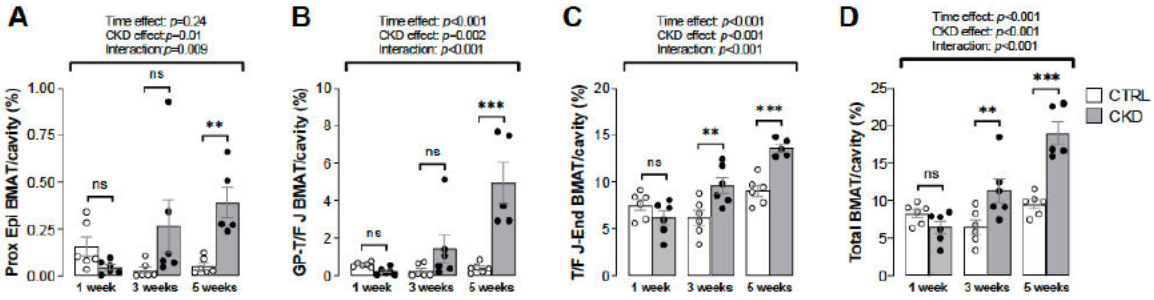

Supplementary Figure 3. Regional quantification of BMAT accumulation in the tibial bone shaft. Bone marrow adipose tissue (BMAT) in CKD mice at (A) proximal epiphysis (Prox Epi) and (B) growth plate to tibia-fibula junction (rBMAT; GP-T/F J) was increased in CKD mice after 5-weeks' induction whereas BMAT in the (C) tibia-fibula junction to distal end region (cBMAT; T/F J-End) and (D) whole tibial cavity was increased after 3- and 5-weeks' induction. Data are presented as mean ± SEM with each dot representing an individual mouse. ns, not significant, ** $P < 0.01$, *** $P < 0.001$.

Supplementary Table 1 Primers for qPCR

Gene	Forward (5`-3`)	Reverse (5`-3`)
Adipoq	AAGAAGGACAAGGCCGTTCTCTT	GCTATGGGTAGTTGCAGTCAGTT
Cebpa	TGGACAAGAACAGCAACGAG	TCACTGGTCAACTCCAGCAC
Fabp4	TGGAAGCTTGTCTCCAGTGA	AATCCCCATTTACGCTGATG
Lep	GACACCAAAACCCTCAT	CAGTGTCTGGTCCATCT
Pparg2	CCAGAGCATGGTGCCTTCGC	TTCCGAAGTTGGTGGGCCAGA
Lipe	CCTTGTGGCTTGCGCTCTGGA	CCGCGCGAACATGACCGAGT
Pnpla2	CGGCTTCCTCGGGGTCTAC	CGCGCTCATGGCAATCAG
Sp7	ATGGCGTCCTCTCTGCTTG	TGAAAGGTCAGCGTATGGCTT
Runx2	ACCATAACAGTCTTCACAAATCCT	CAGGCGATCAGAGAACAAACTA
Tnfrsf11b	CCTTGCCCTGACCACTCTTA	CACACACTCGGTTGTGGGT
Tnfsf11	CAGCATCGCTCTGTTCCTGTA	CTGCGTTTTCATGGAGTCTCA
Col1a1	ACATGTTCAGCTTTGTGGACC	TAGGCCATTGTGTATGCAGC
Alpl	GGGACGAATCTCAGGGTACA	AGTAACTGGGGTCTCTCTC
Pipia	CACCGTGTTCTTCGACATCA	CAGTGCTCAGAGCTCGAAAGT

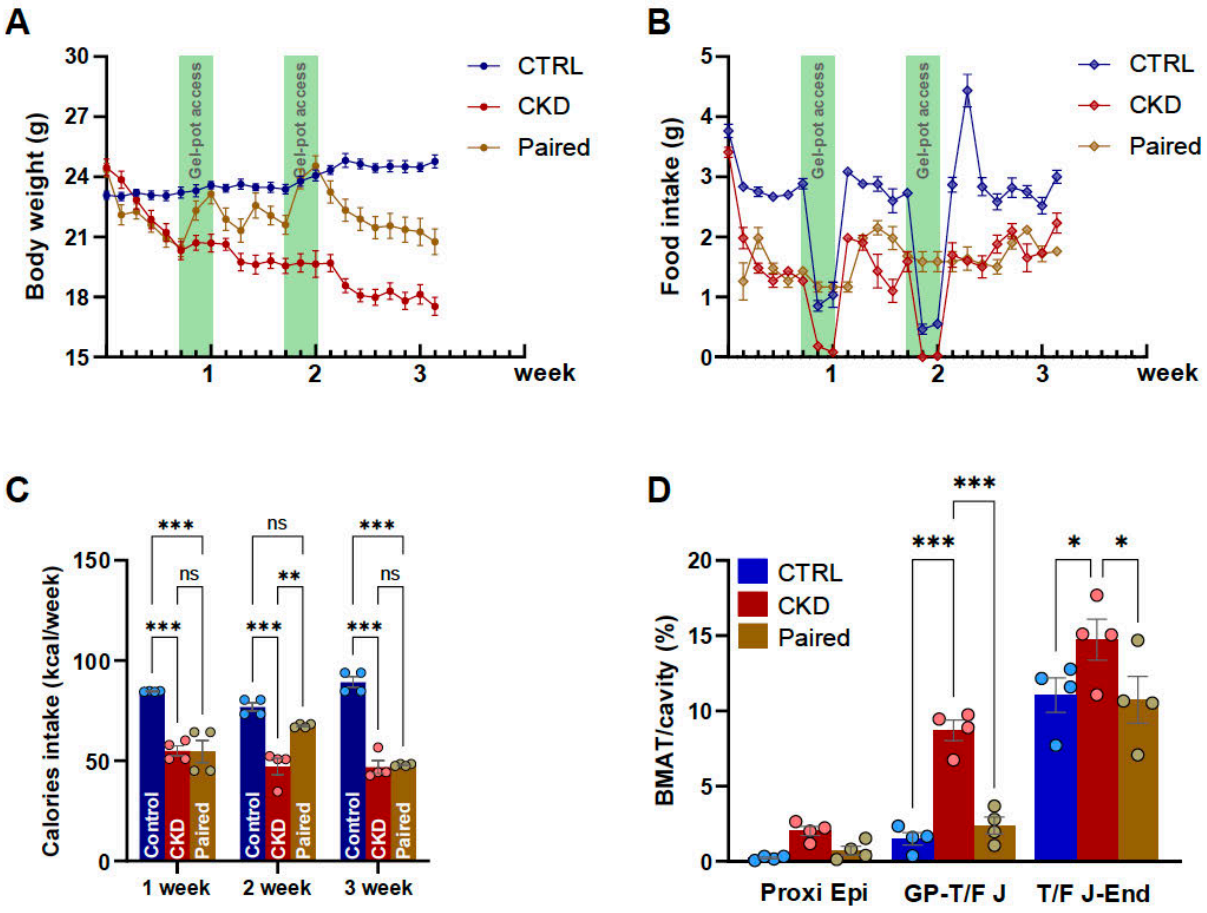

Supplementary Figure 4. Body weight, food and calorie intake and BMAT accumulation in pair-fed mice. (A) Body weight of CTRL and CKD mice increased and decreased, respectively over the experimental period. The CKD mice lost more body weight than the pair-fed mice despite a similar (B) food and (C) caloric intake. (D) Bone marrow adipose tissue (BMAT) accumulation was similar between CTRL and pair-fed mice but was increased in growth plate to the tibia-fibula junction region (rBMAT; GP-T/F J), and the tibia-fibula junction to the distal end (cBMAT; T/F J-End) of the CKD mice. Data are expressed as mean ± SEM, with each data point representing an individual mouse. ns, not significant, * $P < 0.05$, ** $P < 0.01$, *** $P < 0.001$.

Conclusion

This study investigated the underlying mechanisms responsible for BMAT accumulation during CKD progression and its contribution to bone loss by using the adenine-induced CKD mouse model. Male mice were used in this study and were fed an adenine diet for up to 5 weeks. CKD mice were then assessed for BMAT accumulation, bone morphometry, osteogenic and adipogenic gene expression in bone and bone marrow tissue and circulating hormones that may influence BMAT expansion, such as adiponectin, leptin, and corticosterone. Additionally, the populations of BMSCs, APCs, and OPCs at the onset of CKD were also assessed, along with the potential differentiation of BMSCs from CKD mice into either adipogenic or osteogenic lineages. Furthermore, this study investigated whether BMAT accumulation in this CKD model was a consequence of either caloric restriction or progression of the disease. According to the results of this study, the conclusions that could be drawn are as follows:

1. Adenine-induced CKD in these mice was successfully established as a disease model, as demonstrated by increased levels of BUN, creatinine, FGF23, and PTH from 3 weeks of induction.
2. BMAT accumulation began to rise at 3 weeks, preceding trabecular bone loss, which occurred after 5 weeks in CKD mice.
3. Regulated BMAT accumulation was significantly increased at 5 weeks post-CKD induction and was associated with lower trabecular bone volume fraction.
4. Circulating adiponectin and corticosterone levels increased, whereas leptin levels decreased in CKD mice; however, only adiponectin levels were associated with BMAT accumulation.
5. There were limited changes in the expression of osteoblast transcription factors and osteoblast markers in CKD mice. Only Osterix (*Sp7*) expression in the cortical bone of CKD mice was reduced after 3 weeks of induction.
6. The expression of adipogenic transcription factors increased in the bone marrow tissue and BMSCs of CKD mice.
7. The BMSC population decreased, while the APC and OPC populations remained unchanged at the onset of CKD.

8. BMAT accumulation in this model was a consequence of CKD progression and not caloric restriction.
9. BMSCs from CKD mice also exhibited a potential for adipogenic differentiation.

In addition to increased circulating concentrations of PTH, FGF23, this study also revealed (not reported in the paper) increased serum sclerostin concentrations in CKD mice (Figure 3.1). Moreover, BMSCs from CKD mice also exhibited a potential for adipogenic differentiation, which may contribute to BMAT accumulation in CKD. CKD-associated factors may influence BMSC commitment to either adipocyte or osteoblast lineages. Therefore, investigating the effects of these CKD-associated factors, including PTH, FGF23, sclerostin, Pi, and uremic toxins, on BMSC differentiation into either adipocytes or osteoblasts may help better understand the mechanisms underlying BMAT accumulation associated with CKD-MBD.

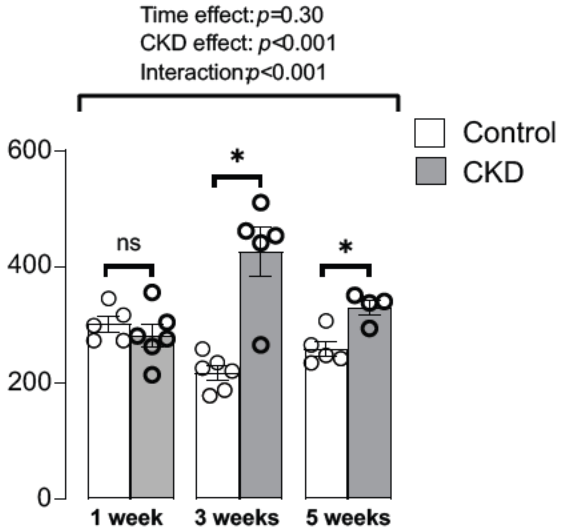

Figure 3.1 Serum level of sclerostin. Circulating sclerostin was increased from 3 weeks of induction. The data are presented as mean ± SEM, with each dot representing an individual mouse. ns, not significant, *P < 0.05.

Chapter 4

Effect of CKD associated systemic factors on primary BMSCs differentiation

4.1. Introduction

Clinically, individuals with CKD-MBD exhibit a marked increase in skeletal fragility and fracture risk, along with an elevation in BMAT, suggesting a complex pathophysiological phenotype (Hosain & Clinkenbeard, 2024; Moe et al., 2006). At the cellular level, BMSCs - multipotent progenitors capable of differentiating into osteoblasts, adipocytes and chondrocytes – may be directly influenced by elevated levels of CKD-MBD associated systemic factors including Pi, FGF23, PTH, sclerostin and uremic toxins. The influence of these factors on BMSC differentiation could contribute to the observations in Chapter 3, where BMSCs from CKD mice were found to have enhanced adipogenic potential *in vivo.* This interplay could potentially lead to impaired osteogenesis and heightened marrow adiposity characteristic of CKD.

Hyperphosphatemia, a hallmark of CKD, has been shown to directly trigger elevations in FGF23, a hormone with detrimental effects on bone health. Evidence suggests that FGF23 actively promotes bone loss by upregulating the Wnt-signalling pathway inhibitor DKK1, leading to a significant reduction in bone formation (Carrillo-López et al., 2016). Research employing nephrectomy and parathyroidectomy in CKD rat models fed a high-Pi diet revealed notable results: decreased serum FGF23 levels, diminished bone formation rates, and compromised osteoblast activity (Ferreira et al., 2013). These findings imply a Pi-mediated mechanism responsible for bone loss that operates independently of PTH (Batista et al., 2010). This raises the compelling hypothesis that an elevated Pi concentration may exert a direct influence on the differentiation and functional capacity of osteoblasts. Supporting this assertion, *in vitro* studies have demonstrated that heightened Pi levels actively promote the differentiation of human bone marrow-derived mesenchymal stem cells into osteoblasts (Lin et al., 2021; Rui et al., 2022). Nevertheless, the potential effects of high Pi on the differentiation of mesenchymal stem cells into adipocytes remain conspicuously underexplored.

While the intermittent administration of PTH (teriparatide (1–34 fragment of PTH)) is widely recognised to enhance bone formation (Thomas, 2006), hyperparathyroidism in the context of CKD typically manifests in the early stages of the disease and persists throughout its progression (Metzger et al., 2025). Prolonged exposure

to elevated PTH levels has been implicated in diminishing osteoblast responsiveness and promoting bone resorption through mechanisms involving osteoblast-mediated osteoclast differentiation (Metzger et al., 2025; Silva & Bilezikian, 2015). While several studies have highlighted the capacity of intermittent PTH treatment to stimulate mesenchymal stromal cells differentiation into osteoblasts while simultaneously inhibiting adipogenesis (Rickard et al., 2006; Yang et al., 2019), the long-term implications of elevated PTH on adipose differentiation remains a topic that warrants further investigation.

Furthermore, the accumulation of uremic toxins, such as p-cresyl sulfate (PCS) and IS - toxic by-products that build up in CKD patients and preclinical animal models, has been implicated in deleterious effects on bone metabolism (Hsu et al., 2025; Watanabe et al., 2017). Uremic toxins disrupt the delicate equilibrium of bone formation and resorption, effectively suppressing osteoblast function and the formation of mineralised bone nodules. This is mediated by the downregulation of essential osteogenic transcription factors and phenotypic markers such as osterix, osteocalcin, and BMP2 (Watanabe et al., 2017). Moreover, IS has been found to adversely affect the activity and function of adipose-derived mesenchymal stem cells (Thi Do et al., 2016). Despite this growing body of evidence, the direct effects of IS on mesenchymal stromal cells are yet to be thoroughly investigated.

Cumulatively, the multitude of factors associated with CKD may create a bone marrow microenvironment that skews the differentiation of mesenchymal stromal cells toward adipogenesis at the expense of osteoblastogenesis. Such multifaceted interactions may lead to impaired bone formation and an increase in marrow adiposity, thereby exacerbating skeletal fragility. To effectively unravel the complexities of CKD-MBD and to foster the development of targeted therapeutic strategies, a comprehensive understanding of the individual effects of these diverse factors on BMSC differentiation is paramount.

Osteocytes play a pivotal role as central regulators of bone modelling and remodelling, orchestrating the intricate activities of osteoblasts and osteoclasts through the secretion of various signalling molecules, notably sclerostin, RANKL, and OPG (Bellido, 2014). Among these signalling molecules, sclerostin has garnered particular

attention due to its inhibitory effect on Wnt/β-catenin signalling, which is critical for osteoblastogenesis. The association of CKD with elevated levels of sclerostin represents another layer of complexity in the landscape of bone metabolism and poses significant implications for bone health, particularly in terms of low bone turnover and compromised bone formation (Moysés & Schiavi, 2015).

In addition to its inhibitory influence on bone formation via impairment of osteoblast Wnt-signalling pathways (Fairfield et al., 2017) it can also promote adipogenic differentiation from mesenchymal stem cells, fostering the accumulation of adipose tissue within the bone marrow (Fairfield et al., 2018). Conversely, treatment with sclerostin-neutralising antibodies can enhance osteogenic potential and restore mesenchymal stem cell function even in detrimental skeletal conditions such as skeletal unloading (Shahnazari et al., 2012).

Recent investigations have identified hyperphosphatemia and IS, as key contributors to the upregulation of osteocytic sclerostin production. In rodent models of CKD, dietary Pi intake has been shown to elevate osteocytic sclerostin levels, leading to diminished bone formation and impaired mineralisation (Ferreira et al., 2013). Moreover, extracellular Pi has been demonstrated to function as a signalling entity within bone cells, whereby osteoblasts respond to increased Pi levels by downregulating the expression of *Sost* and *Dkk1* (Rendenbach et al., 2014).The accumulation of IS in CKD patients has been associated with enhanced expression of sclerostin in osteocytes (Liu et al., 2018). Previous studies have also found that IS increased the expression of *Sost* and *Dkk1*, in osteocytes (Chen et al., 2024). The direct influence of elevated Pi and IS on Sost expression by osteocytes, however, remains underexplored, and such knowledge may help elucidate the individual impact of these CKD-related factors on disease progression.

Collectively, the systemic factors raised in CKD-MBD may have the potential to enhance osteocytic sclerostin production and suppress osteoblastogenesis and promote adipogenesis from their precursor BMSCs. This would ultimately result in impaired bone formation, increased marrow fat accumulation, and heightened skeletal fragility. Animal models and *in vitro* studies have consistently corroborated these mechanisms, establishing a robust framework for further mechanistic investigation. A comprehensive understanding

of the individual contributions of these factors on BMSC differentiation may be helpful for the development of targeted therapeutic strategies aimed at restoring bone health in patients with CKD.

4.2. Hypothesis and aims

Several systemic factors are increased during CKD progression and are recognised to be critical for CKD-MBD manifestation *i.e.* FGF23, PTH, Pi, IS and sclerostin. These factors may contribute to altered BMSC differentiation. This hypothesis was tested by completing the following aims:

I. Evaluate the ability of CKD associated systemic factors (*i.e.* Pi, PTH, FGF23, sclerostin and IS) to directly affect the differentiation of BMSCs to the adipocytes or osteoblast phenotype.
II. Evaluate the effect of high Pi and IS on sclerostin secretion by MLO-Y4 osteocyte-like cells.

4.3. Materials and methods

4.3.1. Primary BMSCs

Primary BMSCs were isolated from long bones of wild-type 8-9 weeks old male mice as described in section 2.10.1. For the individual study, 250,000 cells/well were plated into 6-well plates and cultured in BMSC basal medium until confluency. Culture media was changed every other day (described in section 2.10.1).

4.3.2. Differentiation media for BMSC culture during treatment with Pi, FGF23, PTH, sclerostin or IS.

On confluency (day 0), the BMSC basal medium was replaced with either osteogenic or adipogenic differentiation media, depending on the targeted lineage, as detailed in section 2.10.1.1.

4.3.2.1. BMSCs differentiation: influence of PTH treatment

Recombinant human PTH fragment 1-34 was utilised in this study. A stock solution (stock 1) was prepared by reconstituting PTH in PBS at a concentration of 1

mg/mL. For further dilution, 1 µL of stock 1 was added to 999 µL of distilled water to produce stock 2, yielding a concentration of 1 µg/mL. Stock 2 or distilled water was freshly diluted in culture medium to generate final PTH working concentrations of 0, 0.5, 1, and 5 ng/ml, informed by relevant preclinical studies with primary osteoblasts (Hsu et al., 2022). Upon reaching confluency, BMSCs were cultured in either osteogenic or adipogenic media, each supplemented with the designated concentration of PTH. For osteogenic differentiation, the media was replaced every other day for 21 days as described in section 2.10.1.1. For adipogenic differentiation, media changes were performed as described in Section 2.10.1.1 over a 7-day period.

4.3.2.2. BMSCs differentiation: influence of Pi treatment

Culture medium contains ~ 1mM Pi and 10% FBS contains ~ 0.33 mM Pi (Lee et al., 2023). To achieve the desired experimental concentrations of Pi, sodium dihydrogen phosphate (NaH_2PO_4 was resuspended in sterile distilled water to prepare a 20 mM stock solution. At confluency, either 20 mM stock solution or PBS was freshly combined with osteogenic or adipogenic culture medium to achieve final supplementary Pi concentrations of 0, 1, 3, and 5 mM and maintained as outlined in Section 2.10.1.1., All mentions in the text and figures to the amount of Pi present in individual cultures refer to the amount of additional Pi added and do not include the ~1.33 mM present in the FBS-supplemented basal medium.

4.3.2.3. BMSCs differentiation: influence of FGF23 treatment

Recombinant human FGF23 was employed in this study. The growth factor was first reconstituted in PBS containing 0.1% FBS to generate a primary stock solution at a concentration of 100 µg/ml. A secondary stock solution (1 µg/mL) was prepared by diluting 10 µL of the primary stock with 990 µL of PBS. For each experimental condition, either the secondary stock or PBS was freshly combined with osteogenic or adipogenic culture medium to achieve final FGF23 concentrations of 0, 1, 10 and 50 ng/ml. The treated cells were maintained according to the procedures outlined in Section 2.10.1.1. The chosen concentration range was informed by previous studies (Hsu et al., 2022).

4.3.2.4. BMSCs differentiation: influence of sclerostin treatment

Recombinant human sclerostin was utilised in this study. The protein was initially reconstituted in sterile PBS to prepare a primary stock solution with a concentration of 200 µg/ml. Subsequently, 5 µL of this primary stock was diluted with 995 µL of PBS to generate a secondary stock solution at 1 µg/mL. At confluency, BMSC cultured in either osteogenic or adipogenic media were supplemented with PBS or with 1 ug/mL sclerostin to achieve final concentrations of 0, 0.5, 1, and 5 ng/mL. The cells were maintained as described in Section 2.10.1.1. The selected concentration range was informed by prior preclinical studies (Fairfield et al., 2018; Ferreira et al., 2013).

4.3.2.5. BMSCs differentiation: influence of IS treatment

IS was tested at concentrations of 0, 0.25, 0.5, and 1 mM in this study. This concentration range was informed by prior publications and was not found to be toxic to osteoblasts (Hsu et al., 2025). Due to the protein-bound nature of IS, it was initially resuspended in bovine serum albumin (BSA; 1 mg/ml) and dimethyl sulfoxide (DMSO) before being further diluted in culture media formulated for either osteogenic or adipogenic differentiation. Control cultures received an equivalent final concentration of DMSO (1:4000 dilution) as the experimental groups. Confluent BMSCs were exposed to the conditioned osteogenic or adipogenic media containing IS and maintained as described in Section 2.10.1.1.

4.3.3. Osteocyte cell line: *Sost* expression in response of high Pi and IS treatment

MLO-Y4 osteocyte-like cells were used in this experiment. Cells were cultured and maintained as described in section 2.10.2. 250,000 cells/well were plated in 6-well plates for Pi and IS treatment. The amount of supplementary Pi and IS used to treat MLO-Y4 cells was as described in sections 4.3.2.2 and 4.3.3.5, respectively. Cells were maintained in their respective media for 2 weeks, and fresh media were changed every other day.

4.3.4. RNA extraction and quantitative polymerase chain reaction

At the end of each study, RNA was extracted from cultured primary BMSCs as described in section 2.11.1. RNA was reverse transcribed and gene expression was

quantified using the SYBR green detection as described in Section 2.11.3 and 2.11.4, respectively.

4.3.5. Statistical analysis

All quantitative results are presented as mean ± S.E.M., with a minimum of three independent biological replicates included in each experimental group. Statistical comparisons were carried out using one-way ANOVA, followed by Tukey's post hoc test where appropriate. Analyses were conducted using GraphPad Prism software. Statistical significance was defined as $p < 0.05$ and denoted by *. More stringent significance levels were indicated as follows: ** for $p < 0.01$, *** for $p < 0.001$, and **** for $p < 0.0001$.

4.4. Results

4.4.1. Effect of PTH on adipogenic and osteogenic gene expression of BMSCs

Under adipogenic differentiation conditions, PTH treatment did not alter the expression levels of key adipogenic marker genes, including *Pparg2, Cebpa, Adipoq,* and *Pnpla2*, compared with the control group (no PTH). Although a reduction in *Fabp4* expression was observed at the lowest PTH concentration tested, the expression of other adipogenic genes remained unchanged. These data indicate that PTH at the concentrations tested does not significantly influence adipocyte differentiation of BMSCs (Figure. 4.1A).

In contrast, under osteogenic conditions, PTH treatment resulted in a significant upregulation of osteogenic marker genes. The expression levels of *Sp7, Runx2, Alpl,* and *Tnfrsf11b* gradually increased up to 1 ng/ml PTH, whereas gene expression when challenged with 5 ng/ml PTH was comparable to control levels. Additionally, *Tnfsf11* expression was elevated only at the lowest PTH concentration, with no changes observed at higher concentrations (Figure 4.1B). These findings suggest that low concentrations of PTH can promote osteogenic differentiation of BMSCs.

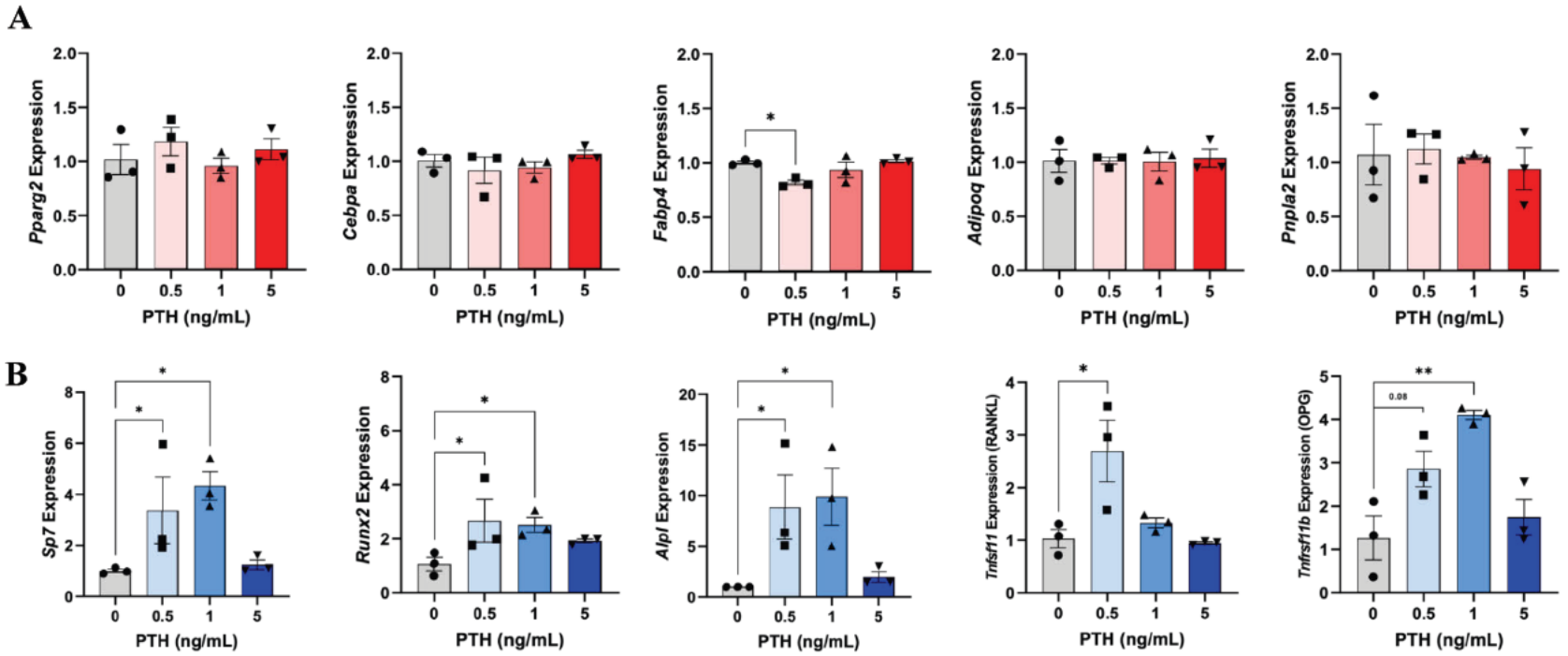

Figure 4.1 Effect of PTH on adipogenic and osteogenic gene expression of primary BMSCs cultured in adipogenic or osteogenic media. (A) Expression of adipogenic genes, *Pparg2, Cebpa, Fabp4, Adipoq* and *Pnpla2* of BMSCs cultured in adipogenic medium treated with or with PTH. (B) Expression of osteogenic gene including *Sp7, Runx2, Alpl, Tnfsf11* and *Tnfrsf11b* of BMSCs cultured in osteogenic medium treated with or without PTH. The data are represented as the mean ± SEM (n = 3); * $p < 0.05$; ** $p < 0.01$in comparison with 0 ng/ml PTH.

4.4.2. Effect of supplemented Pi on adipogenic and osteogenic gene expression of BMSCs

Under adipogenic differentiation conditions, increasing concentrations of Pi resulted in a progressive, dose-dependent decrease in the expression of key adipogenic marker genes, including the transcription factor, *Pparg2* and the adipokine gene, *Adipoq*, compared to the control group (no additional Pi). *Fabp4* gene expression also demonstrated a similar downward trend, reaching statistical significance only at the highest Pi concentration tested. In contrast, the expression levels of *Cebpa* and *Pnpla2* were not affected by supplementary Pi (Figure 4.2A). These results suggest that high extracellular Pi may impair adipogenic differentiation of BMSCs, potentially through the downregulation of critical components of the adipogenic transcriptional network.

Conversely, when BMSCs were cultured under osteogenic conditions, increased Pi concentrations did not significantly alter the expression of osteogenic marker genes, including *Sp7, Runx2,* and *Alpl.* Furthermore, high Pi treatment did not affect the expression of *Tnfsf11* (RANKL), a gene involved in osteoblast-mediated osteoclast differentiation, but led to an upregulation of *Tnfrsf11b* (OPG), which acts to neutralise RANKL activity (Figure 4.2B). These findings indicate that while elevated Pi concentrations suppress adipogenic differentiation, they do not directly enhance osteogenic gene expression in BMSCs.

4.4.3. Effect of FGF23 on adipogenic and osteogenic gene expression in BMSCs

When BMSCs were cultured in adipogenic differentiation medium, treatment with FGF23 had no significant impact on the expression of early adipogenic transcription factors *Pparg2* and *Cebpa*. Expression levels of the downstream adipocyte-associated genes, *Fabp4* and *Adipoq*, also remained stable across all FGF23 concentrations tested, although a modest increase in Adipoq was observed at the highest dose. *Pnpla2* exhibited a comparable pattern (Figure 4.3A). Similarly, the expression of osteogenic marker genes remained unchanged in response to FGF23 treatment (Figure 4.3B). Collectively, these findings indicate that FGF23 has little or no direct ability to alter adipogenic and osteogenic gene expression during BMSC differentiation.

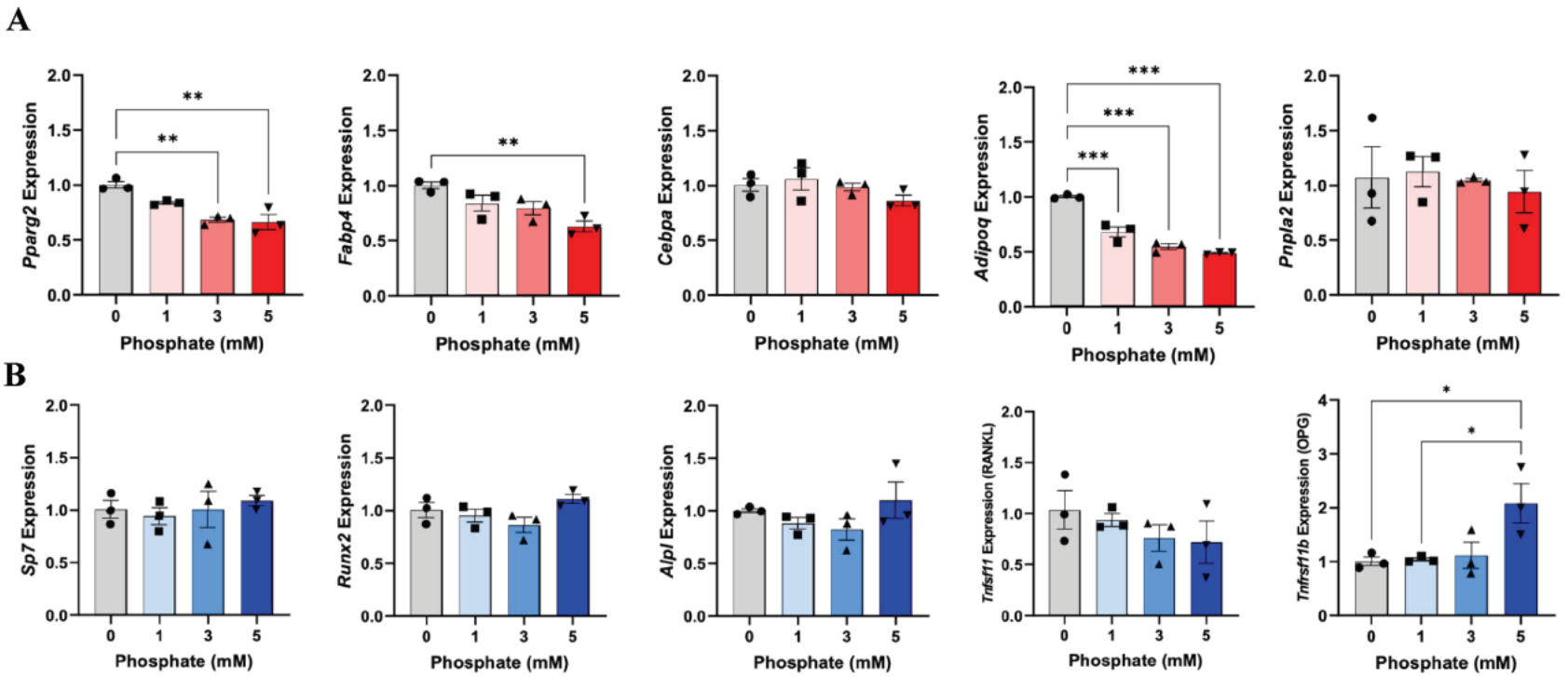

Figure 4.2 Effect of Pi on adipogenic and osteogenic gene expression of primary BMSCs cultured in adipogenic or osteogenic media. (A) Expression of adipogenic genes, *Pparg2, Cebpa, Fabp4, Adipoq* and *Pnpla2* of BMSCs cultured in adipogenic medium treated with or with Pi. (B) Expression of osteogenic genes including *Sp7, Runx2, Alpl, Tnfsf11* and *Tnfrsf11b* of BMSCs cultured in osteogenic medium treated with or without Pi. The data are represented as the mean ± SEM (n = 3); * $p < 0.05$; ** $p < 0.01$ and *** $p < 0.001$in comparison with no Pi

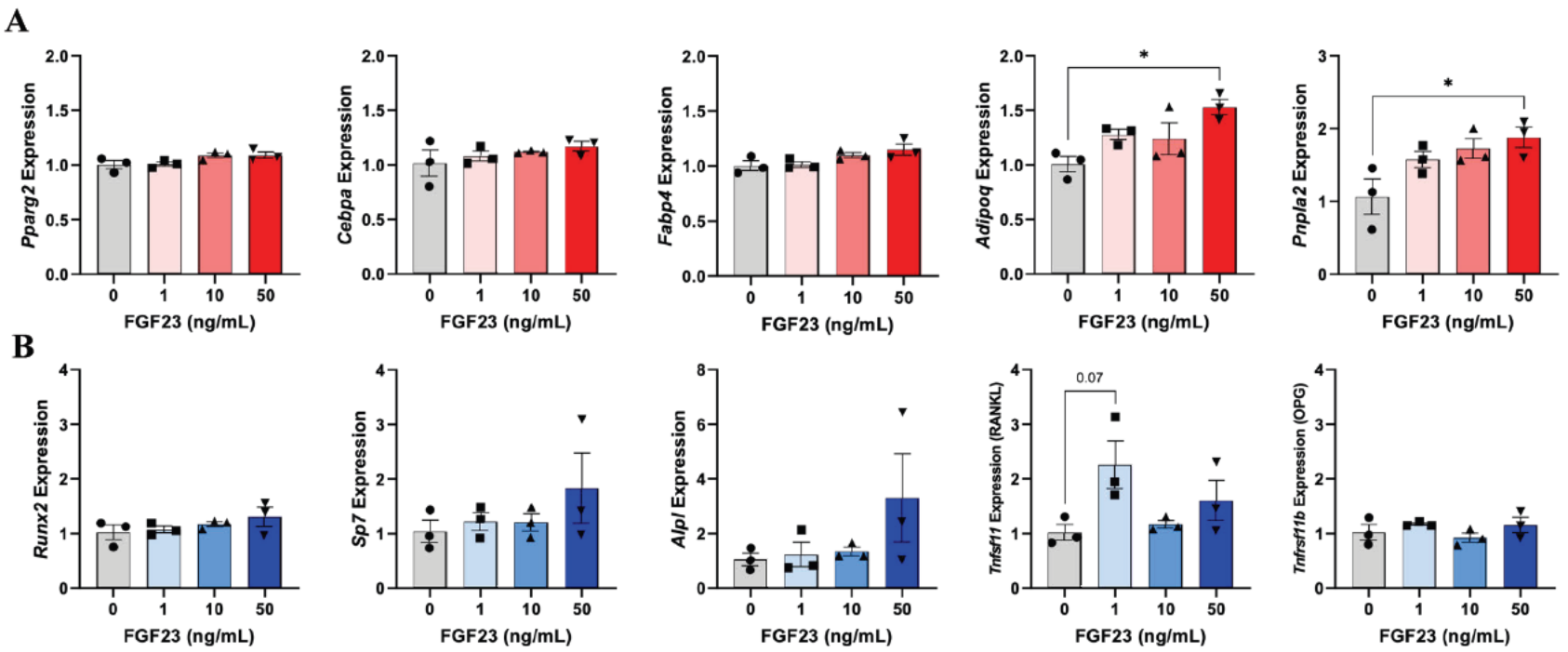

Figure 4.3 Effect of FGF23 on adipogenic and osteogenic gene expression of primary BMSCs cultured in adipogenic or osteogenic media. (A) Adipogenic gene Expression of *Pparg2, Cebpa, Fabp4, Adipoq* and *Pnpla2* of BMSCs cultured in adipogenic medium treated with or without FGF23. (B) Expression of osteogenic genes *Sp7, Runx2, Alpl, Tnfsf11* and *Tnfrsf11b* of BMSCs cultured in osteogenic medium treated with or without FGF23. The data are represented as the mean ± SEM (n = 3) in comparison with 0 ng/ml FGF23.

4.4.4. Effect of sclerostin on adipogenic and osteogenic gene expression of BMSCs

When BMSCs were cultured under adipogenic conditions, the mRNA levels of key adipocyte transcription factors, *Pparg2* and *Cebpa*, as well as the adipocyte-associated genes *Fabp4* and *Pnpla2*, remained similar between sclerostin-treated and control (0 ng/ml) groups. A significant increase in *Adipoq* expression was observed at the lowest sclerostin concentration tested, but no changes were detected at higher concentrations (Figure 4.4A). These findings indicate that sclerostin does not substantially influence the adipogenic differentiation potential of BMSCs.

During osteogenic differentiation, a significant upregulation of *Tnfsf11* mRNA was detected only at the highest concentration of sclerostin tested. Expression levels of other osteogenic markers, including *Sp7, Runx2, Alpl,* and *Tnfrsf11b*, did not differ between sclerostin-treated and control (0 ng/ml) groups (Figure 4.4B). Overall, these results suggest that sclerostin does not significantly affect the osteogenic differentiation of BMSCs.

4.4.5. Effect of IS on adipogenic and osteogenic gene expression in BMSCs

When BMSCs were cultured in adipogenic differentiation medium containing IS, a dose-dependent inhibition of adipogenesis was observed. This was evidenced by the downregulation of key adipogenic marker genes, including *Pparg2, Cebpa, Fabp4, Adipoq,* and *Pnpla2*. Although statistically significant decreases in *Cebpa* and *Pnpla2* expression were only detected at the highest IS concentration tested, all markers showed a consistent trend towards reduced expression, indicating a direct inhibitory effect of IS on adipogenic differentiation (Figure 4.5A).

Under osteogenic differentiation conditions, IS treatment suppressed osteoblastogenesis, as demonstrated by reduced mRNA expression levels of *Sp7, Runx2,* and *Alpl* across all IS concentrations compared to control (0 ng/ml) treated cells. Notably, IS exposure led to an upregulation of *Tnfsf11* (RANKL) but did not affect the expression of *Tnfrsf11b* (OPG) (Figure 4.5B). These findings suggest that IS not only impairs osteogenic differentiation of BMSCs but also promotes the expression of genes involved in osteoclastogenesis, potentially enhancing bone resorption.

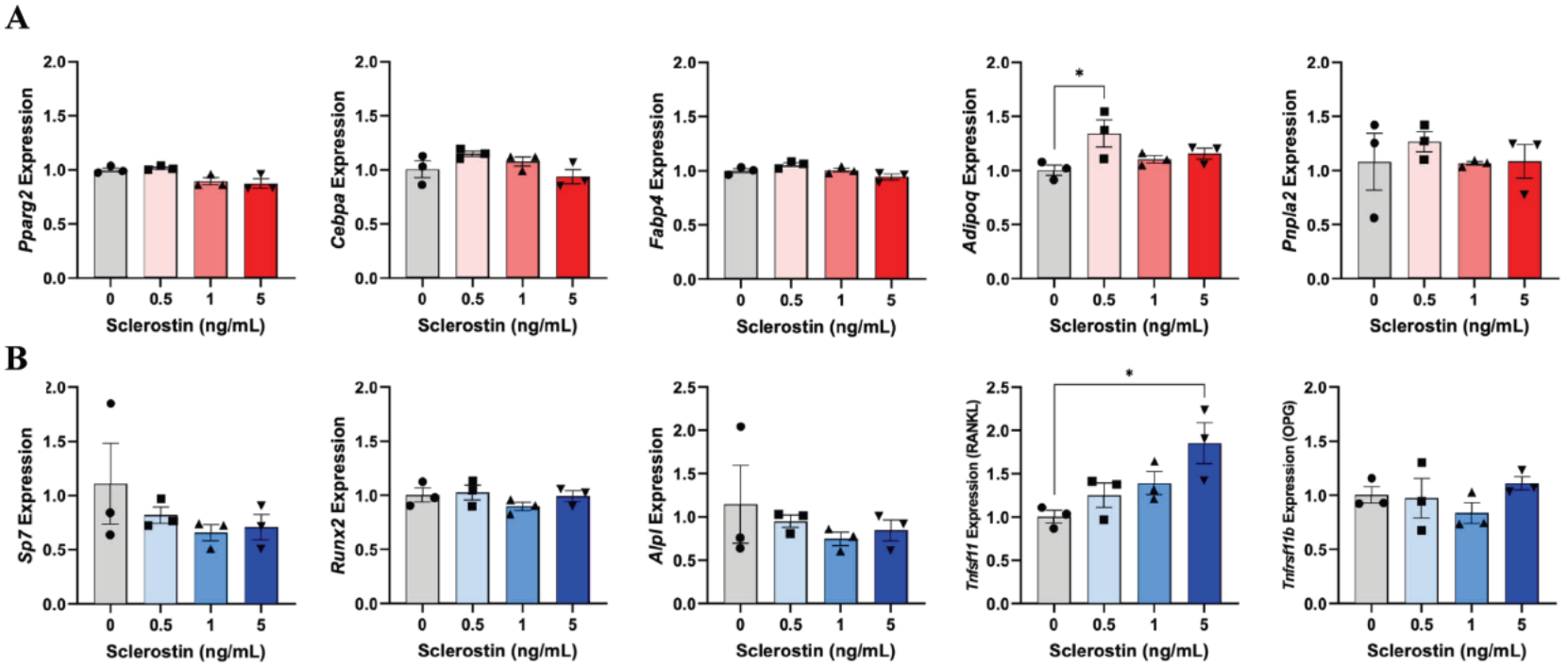

Figure 4.4 Effect of sclerostin on adipogenic and osteogenic gene expression of primary BMSCs cultured in adipogenic or osteogenic media. (A) Adipogenic gene Expression of *Pparg2, Cebpa, Fabp4, Adipoq* and *Pnpla2* of BMSCs cultured in adipogenic medium treated with or with sclerostin. (B) Osteogenic gene Expression of osteogenic genes, *Sp7, Runx2, Alpl, Tnfsf11* and *Tnfrsf11b* of BMSCs cultured in osteogenic medium treated with or without sclerostin. The data are represented as the mean ± SEM (n = 3); * $p < 0.05$ in comparison with 0 ng/ml sclerostin.

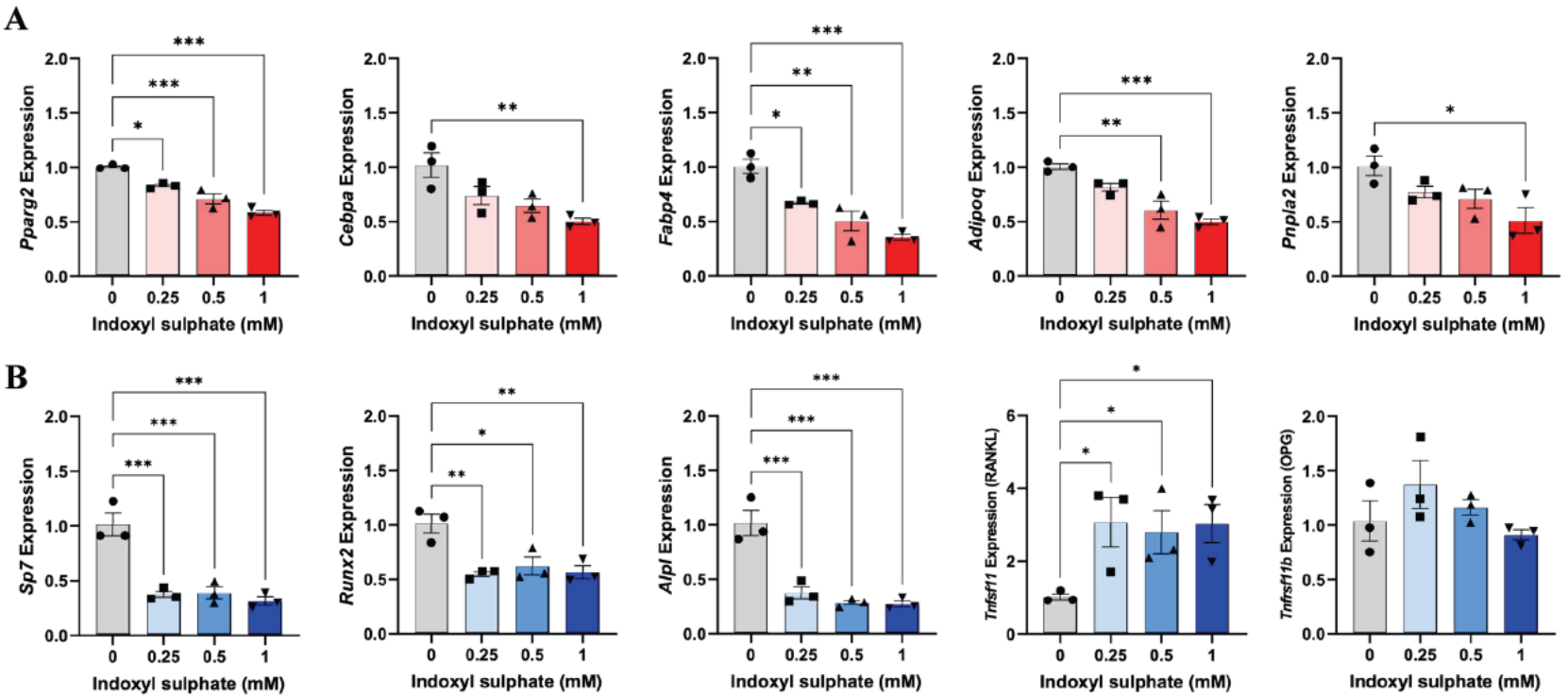

Figure 4.5 Effect of IS on adipogenic and osteogenic gene expression of primary BMSCs cultured in adipogenic or osteogenic media. (A) Adipogenic gene Expression of *Pparg2, Cebpa, Fabp4, Adipoq* and *Pnpla2* of BMSCs cultured in adipogenic medium treated with or without IS. (B) Expression of osteogenic genes, *Sp7, Runx2, Alpl, Tnfsf11* and *Tnfrsf11b* of BMSCs cultured in osteogenic medium treated with or without IS. The data are represented as the mean ± SEM (n = 3); * $p < 0.05$; ** $p < 0.01$ and *** $p < 0.001$in comparison with 0 mM IS

4.4.6. *Sost* gene expression in MLO-Y4 in response to high Pi or IS treatment

Treatment of MLO-Y4 cells with either supplementary Pi or IS had no significant effects on *Sost* expression. This was observed at all Pi and IS concentrations tested (Figure 4.6A and B). This results suggest that 2-weeks treatment with supplementary Pi and IS has no direct effect on *Sost* gene expression by this osteocyte cell line.

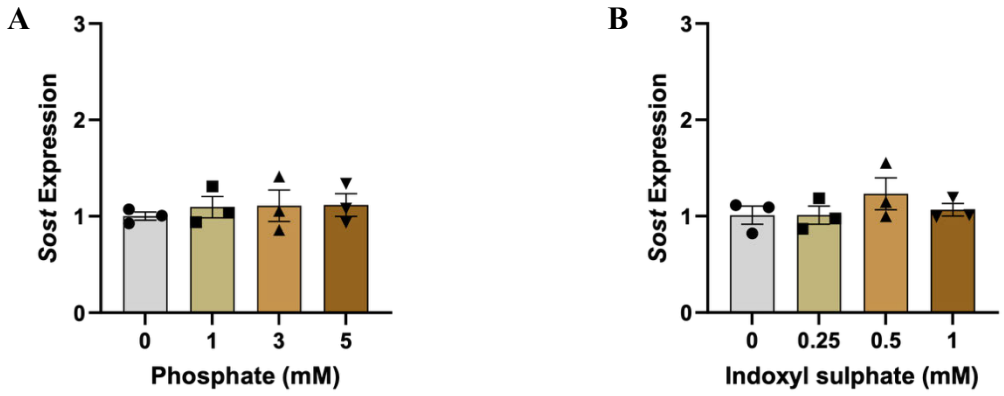

Figure 4.6 Effect of high Pi or IS on *Sost* gene expression in MLO-Y4 osteocyte-like cells. *Sost* gene expression by MLO-Y4 cells cultured in medium supplemented with different concentration of (A) Pi or (B) IS. The data are represented as the mean ± SEM (n = 3).

4.5. Discussion

This study examined if key CKD associated systemic factors such as PTH, Pi, FGF23, sclerostin, and IS could influence the lineage commitment of BMSCs towards adipogenic and osteogenic fates. These regulatory factors are critical indicators of CKD progression that are tightly linked to mineral metabolism and skeletal homeostasis in this disease (Hsu et al., 2020). Understanding how these systemic factors directly affect BMSC differentiation provides insight into the mechanisms driving the imbalance between osteogenesis and marrow adiposity commonly observed in CKD-associated bone disorders.

Exposure of BMSCs to PTH under adipogenic differentiation conditions did not substantially alter adipogenic commitment or maturation. The expression of canonical adipocyte-associated transcription factors and structural genes such as *Pparg2, Cebpa,*

Adipoq and *Pnpla2*, remained stable. This observation suggests that, at least under the present *in vitro* conditions, PTH exerts minimal influence on adipogenic lineage specification. These findings differ from reports demonstrating an anti-adipogenic role of PTH when administered intermittently. Specifically, intermittent PTH (1-34) exposure (1 hour per day) has been shown to decrease adipocyte number and downregulate the expression of *PPARγ* and *LPL* (lipoprotein lipase) in human mesenchymal stem cells (Fan et al., 2017; Rickard et al., 2006). Similar inhibitory effects on adipogenesis have been reported in rodent models, in which more frequent intermittent dosing of PTH reduced adipogenic markers in $LepR^{+}$ mesenchymal progenitors (Yang et al., 2019), and daily PTH administration diminished marrow adipocyte number and size in caloric restricted mice (Maridas et al., 2018). The discrepancies between the results of my studies and those of others may be attributed to differences in dosing frequency, exposure duration, or cell maturity stage. The modest reduction of *Fabp4* expression observed at the lowest PTH concentration in the present study may represent a minor effect on terminal adipocyte maturation rather than on the early transcriptional activation of adipogenic genes.

Interestingly, previous studies have also shown that PTH can influence lipid metabolism in mature adipocytes rather than in undifferentiated progenitors. In co-culture systems of mature adipocytes and osteoblast progenitors, PTH promotes lipid transfer from adipocytes to osteoblasts, thereby facilitating osteogenic energy metabolism (Maridas et al., 2018). Taken together, these findings suggest that PTH may act more prominently on mature adipocyte function and intercellular metabolic coupling, rather than directly altering BMSC differentiation toward the adipogenic lineage.

In contrast to the lack of effect of PTH on adipogenesis, PTH exerted a marked stimulatory effect on osteogenic differentiation of BMSCs. Under osteogenic conditions, expression of *Sp7, Runx2, Alpl,* and *Tnfrsf11b* increased significantly in a dose-dependent manner up to 1 ng/ml PTH. This observation is consistent with the well-established anabolic actions of PTH, which has been reported to enhance osteoblast differentiation and function through activation of cAMP/PKA–PKCδ signalling cascades (Kuo et al., 2017) and engagement of the Wnt co-receptor LRP6 (Yu et al., 2012). The diminished response observed at 5 ng/ml PTH may reflect a dose threshold beyond which the anabolic

effect plateaus or transitions toward a catabolic response, a phenomenon consistent with the biphasic nature of PTH signalling (Locklin et al., 2003). Moreover, the transient upregulation of *Tnfsf11* (RANKL) at the lowest PTH concentration likely represents an early remodelling cue associated with osteoblast-osteoclast coupling. Previous studies have reported that PTH-induced anabolic remodelling involves increased osteoblast-derived RANKL expression to transiently activate osteoclastogenesis, which facilitates subsequent bone formation (Walker et al., 2012).

The osteo-anabolic effects of PTH in this study was a little surprising as the nature of the PTH administration described in this study *e.g.* continual exposure for 21 days, most closely represents a continuous exposure to PTH. Such prolonged and continuous exposure to PTH (as commonly experienced in CKD) has been reported to model the catabolic effects of PTH (Ishizuya et al., 1997; Liu et al., 2012) and alter the expression of *Alpl, Phospho1* and *Smpd3*; osteoblast genes critical for matrix mineralisation (Houston et al., 2016). Due to the 10 -12h half-life of bovine PTH, however, it is possible that a lack of PTH biological activity after 1 – 2 days of culture may represent a pseudo-intermittent PTH dosing regimen. Indeed, it may mimic *in vitro* studies which set out to model the effects of intermittent PTH, whereby cell culture media is supplemented with PTH for 1–6 h per 24-h or 48-h incubation cycle (Ishizuya et al., 1997; Lotinun et al., 2002). Systemically, the study in CR mice receiving intermittent PTH have demonstrated increased bone mass by shifting the lineage allocation toward osteoblast differentiation. This effect was accompanied by enhanced lipolysis in mature marrow adipocytes rather than a suppression of adipocyte differentiation. The resulting reduction in bone marrow adiposity may augment the anabolic actions of PTH by increasing osteoprogenitor availability and providing energy substrates that support osteoblast function during bone formation (Maridas et al., 2018).

Collectively, these results indicate that PTH preferentially promotes osteogenic differentiation of BMSCs at low physiological concentrations without significantly altering adipogenic gene expression. This selective responsiveness underscores the capacity of PTH to bias mesenchymal lineage allocation toward osteoblastogenesis, thereby contributing to bone anabolic remodelling. The findings further suggest that the

context of PTH exposure, particularly dose, timing, and differentiation stage, is critical in determining its regulatory outcome on mesenchymal lineage balance within the bone marrow microenvironment.

It was found that increasing extracellular Pi progressively suppressed the expression of *Pparg2, Adipoq,* and, at the highest concentration, *Fabp4,* indicating that of the many cellular functions attributed to Pi including physiological and pathological mineralisation (Qin et al., 2025), there is also a role for Pi acting as a signalling molecule capable of reprogramming BMSC transcriptional networks. Although direct investigations of Pi effects on BMSC adipogenesis are limited, the findings of this study are indirectly supported by *in vivo* evidence showing that Pi restriction in mice significantly increases (BMAT compared to controls (Ko et al., 2016). Mechanistically, Pi deprivation induces adipogenic differentiation of CXCL12-abundant reticular (CAR) cells by upregulating key adipogenic transcription factors *Pparg* and *Cebpa* (Ko et al., 2021). This process has been linked to impaired mTORC1 signalling, which diverts bone marrow stromal cells from the osteogenic to the adipogenic lineage, as confirmed by lineage tracing studies (Ko et al., 2021). Taken together, these observations suggest a reciprocal relationship between Pi availability and adipogenic potential. Low Pi impairs osteogenic signalling and promotes adipogenic differentiation, whereas high Pi exerts the opposite effect by suppressing adipogenic gene expression. In the present study, high Pi did not significantly affect osteogenic marker expression, although there was a modest non-significant trend towards upregulation at the highest Pi concentration tested (5 mM). This is consistent with previous findings that reported the ability of Pi to promote osteoblast differentiation and mineralization of human BMSCs within a range of 4–10 mM during short-term culture (up to 10 days) (Lin et al., 2021). The lack of strong osteogenic induction in the long-term (21- days) cultures of the present study suggests that Pi is unable to trigger osteoblast differentiation at low concentrations Mechanistically, the observation of increased *Tnfrsf11b* (OPG) expression is consistent with classical findings showing that elevated extracellular Pi upregulates OPG in bone cells, thereby inhibiting osteoclast differentiation and shifting the RANKL/OPG balance towards reduced bone resorption (Kanatani et al., 2003). Given the central role of the RANKL/OPG axis in bone (re)modelling, a Pi -induced increase in OPG provides a

plausible mechanism for altered bone coupling without a primary increase in early osteogenic markers. Collectively, these data suggest that while high extracellular Pi suppresses adipogenesis, its influence on osteogenesis may depend on culture duration and concentration thresholds, with long-term or low-dose exposure exerting minimal stimulatory effects on BMSC differentiation towards the osteoblast lineage.

The results of this study indicated that FGF23 treatment does not significantly alter the adipogenic or osteogenic differentiation potential of BMSCs under *in vitro* conditions. Despite its well-characterised role as a Pi-regulating hormone primarily secreted by osteocytes and osteoblasts (Shimada et al., 2004; Shimada et al., 2001), FGF23 did not influence the expression of early adipogenic transcription factors *Pparg2* and *Cebpa*, nor did it have a major effect on downstream adipocyte markers *Fabp4, Adipoq,* or *Pnpla2* during adipogenic induction. The small significant increase in *Adipoq* and *Pnpla2* expression at the highest FGF23 concentration tested (50 ng/ml) suggests a limited or indirect influence on mature adipocyte function rather than on adipogenic commitment itself. Similarly, the expression of osteogenic marker genes remained unchanged in FGF23 treated BMSC, suggesting that FGF23 does not directly modulate osteoblastic differentiation pathways in BMSCs.

These findings are consistent with prior studies reporting that FGF23 primarily acts in an endocrine manner on target organs such as the kidney and parathyroid gland, where it regulates Pi and vitamin D metabolism (Bär et al., 2019; Shimada et al., 2004). Although FGF23 receptors (FGFR1–4) are expressed in mesenchymal and bone-lineage cells, effective FGF23 signalling requires the co-receptor Klotho (Urakawa et al., 2006), which is minimally expressed in BMSC (Li et al., 2013). This likely explains the absence of a significant direct effect of FGF23 on BMSC lineage commitment observed in the present study. In the absence of Klotho, FGF23 may have only weak paracrine or autocrine actions through noncanonical signalling, which appear insufficient to modify transcriptional programs governing adipogenic or osteogenic differentiation (Richter & Faul, 2018). Future experiments should study the effects of FGF23 on the differentiation of BMSC in the presence of Klotho.

Interestingly, emerging evidence suggests that elevated circulating FGF23 levels, as seen in CKD, may indirectly affect bone and marrow homeostasis through systemic mechanisms such as altered Pi handling, secondary hyperparathyroidism, and suppression of vitamin C synthesis (Aguilar et al., 2023; Wolf, 2012). These systemic disturbances could contribute to the imbalance between osteogenesis and adipogenesis observed in CKD bone, even if FGF23 itself does not exert direct effects on BMSCs. Therefore, while the present *in vitro* data indicate that FGF23 alone is not a potent regulator of BMSC differentiation, it may act in concert with other CKD-associated factors such as PTH, Pi, or inflammatory cytokines, to influence bone marrow niche dynamics *in vivo*. Collectively, these results suggest that FGF23 influence on bone marrow adiposity and osteogenesis is likely mediated through indirect or systemic pathways rather than direct modulation of BMSC differentiation *per se*.

Sclerostin and its effects on BMSC differentiation were examined under both adipogenic and osteogenic conditions. The lack of change in *Pparg2* and *Cebpa* expression, key transcriptional regulators of adipogenesis, implies that sclerostin does not markedly influence lineage commitment toward adipocytes. The slight increase in *Adipoq* expression at the lowest sclerostin concentration tested may represent a subtle enhancement of adipokine production during terminal differentiation rather than a genuine shift in adipogenic programming. This mild, non-linear response suggests that physiological levels of sclerostin may fine-tune differentiation signalling, whereas higher doses exert minimal or no effect. Previous studies have reported inconsistent outcomes: recombinant sclerostin promoted adipogenesis in 3T3-L1 preadipocytes and mouse BMSCs through Wnt inhibition (Fairfield et al., 2018; Kim et al., 2017). Such discrepancies likely reflect variations in species, cell source, differentiation potency, and experimental context. However, the strong adipogenic induction by AIM in the present study may have saturated the transcriptional response, limiting any observable effects of exogenous sclerostin. Moreover, sclerostin may exert its regulatory influence primarily through paracrine or post-transcriptional mechanisms, affecting lipid metabolism or protein-level signalling, rather than transcriptional control of adipogenic genes.

Under osteogenic differentiation, sclerostin similarly showed little impact on the transcription of canonical osteogenic markers (*Runx2, Sp7, Alpl,* and *Tnfrsf11b*), suggesting limited direct inhibition of osteogenic differentiation in isolated BMSCs. Only *Tnfsf11* (RANKL) expression was elevated by the highest concentration of sclerostin tested (5 ng/ml), indicating a possible role in promoting osteoclastogenic signalling rather than suppressing osteoblastogenesis. This observation aligns with sclerostin's established function as an osteocyte-derived Wnt antagonist that regulates RANKL and OPG balance to control bone (re)modelling (Wijenayaka et al., 2011). Sclerostin's inhibitory actions on bone formation are well documented *in vivo*, where it binds LRP5/6 to suppress Wnt/β-catenin signalling in osteoblasts (Iwamoto et al., 2022; Wijenayaka et al., 2011). However, these effects depend on the mechanical and paracrine context of the bone microenvironment. In the simplified culture conditions used in this study, where potent osteogenic stimuli such as ascorbic acid and βGP drive differentiation, sclerostin alone is unlikely to override such induction. Thus, while sclerostin may fine-tune osteoblast–osteoclast coupling via RANKL upregulation, it does not appear to directly alter osteogenic commitment of BMSCs *in vitro.* Collectively, these findings indicate that sclerostin has limited direct effects on BMSC differentiation but may act indirectly through modulation of bone (re)modelling signals *in vivo*.

Under adipogenic conditions, IS reduced the expression of early transcriptional regulators *Pparg2* and *Cebpa*, as well as downstream adipocyte-associated markers *Fabp4, Adipoq* and *Pnpla2*. Although statistically significant suppression was most evident at the highest concentrations tested, the consistent downward trend across all genes suggests a direct inhibitory influence of IS on adipogenic commitment and maturation. This finding was the first study (to the best of my knowledge) to evaluate the effect of IS on BMSCs differentiation toward adipocytes. Nevertheless, it has been reported that IS exerts anti-proliferation and anti-migration effects of adipose-derived mesenchymal stem cells, resulting in decreased cell function (Thi Do et al., 2016) and also increased cellular senescence in human umbilical cord MSCs (Wang et al., 2016). The present data extend these findings by showing that IS also perturbs the adipogenic potential of BMSCs, suggesting that its deleterious actions on the bone marrow microenvironment may involve broad suppression of mesenchymal lineage

differentiation. This inhibition of adipogenesis contrasts with the *in vivo* phenotype of CKD, where marrow adiposity is often increased in humans and preclinical models and as also reported in the data of Chapter 3 (Sirimongkolchaiyakul et al., 2021; Woods et al., 2018). The discrepancy may be due to secondary systemic alterations in CKD, such as increased Pi, PTH, and altered Wnt signalling, rather than a direct pro-adipogenic effect of uremic toxins themselves.

The IS induced reduced expression of osteogenic transcription factors *Runx2* and *Sp7*, as well as the mature osteoblast protein *Alpl*, indicates impaired osteoblastogenesis. This aligns with previous studies showing that IS impairs osteoblast differentiation and mineralisation (Hsieh et al., 2024; Kamprom et al., 2021; Kim et al., 2013). A particularly intriguing finding in the present study is that IS upregulated *Tnfsf11* (RANKL) expression while leaving *Tnfrsf11b* (OPG) levels unchanged, suggesting an enhanced RANKL/OPG ratio that favours osteoclastogenesis. This observation aligns with earlier reports that IS promotes osteoclast differentiation and bone resorption (Liu et al., 2020). Increased RANKL expression from osteoblast-lineage cells could amplify osteoclast activation in the bone microenvironment, contributing to the increased bone turnover and increased cortical porosity characteristic of CKD-related bone disease (Metzger et al., 2024; Metzger et al., 2021; Moe et al., 2014). Thus, IS may exacerbate skeletal fragility not only by inhibiting bone formation but also by indirectly promoting bone resorption through altered paracrine signalling.

The effects of IS on BMSC differentiation as reported in this study could also be a result of cellular toxicity and while not examined in this study, previous work has shown that concentrations of IS of $\leq$ 2 mM were not found to be toxic to murine primary osteoblasts cultured for up to 7 days (Hsu et al., 2025). Also, IS and other uremic toxins are known to have many adverse effects on cells which could influence the differentiation potential of BMSC. Specifically, uremic toxins can induce oxidative stress via mitochondrial oxygen free radical production (Popkov et al., 2019; Watanabe et al., 2017). In a recent study on cultured murine osteoblasts, both IS and PCS increased mitolysosome (degraded mitochondrial components within lysosomes which is an index of mitophagy (McWilliams et al., 2016). number and mitochondria with distorted morphology (Hsu et

al., 2025). These unfavourable effects on osteoblasts and osteoclasts are likely to disrupt bone quantity and quality.

In the present study, treatment of MLO-Y4 osteocyte-like cells with either high Pi or IS at various concentrations did not result in significantly altered expression of *Sost* compared with the untreated control. This finding suggests that neither elevated extracellular Pi nor IS exerts a direct regulatory effect on *Sost* gene expression in this osteocyte cell line. One possible explanation for the absence of change in Sost expression is the inherently low or undetectable basal expression of this gene in the MLO-Y4 cell line. Several studies have highlighted that MLO-Y4 cells, although exhibiting osteocyte-like morphology and expressing certain osteocytic markers such as *E11/gp38* and *Dmp1*, do not consistently express *Sost* or *Fgf23* under conventional two-dimensional culture conditions (Brady et al., 2022; Zhang et al., 2019). Consequently, the dynamic range for transcriptional modulation of *Sost* expression in these cells may be very limited. Recent reports demonstrate that *Sost* expression becomes evident only when MLO-Y4 cells are cultured within a three-dimensional mineralised matrix or hydroxyapatite-containing scaffold that mimics the osteocytic lacuno-canalicular environment (Brady et al., 2022). Therefore, the control levels of *Sost* expression in Pi or IS challenged BMSC observed in this study are likely attributable to the intrinsic characteristics of the model rather than a true absence of responsiveness to the tested stimuli. Another possibility is that the magnitude or nature of the Pi and IS exposures was insufficient to elicit transcriptional regulation of *Sost*. The concentration and duration of treatment may not have achieved thresholds necessary to activate intracellular signalling pathways that influence *Sost* expression. Moreover, both Pi and IS might exert their effects on osteocytes indirectly through systemic or paracrine mechanisms rather than by directly modulating gene transcription within osteocytes. For example, high Pi levels can alter osteoblast–osteocyte differentiation or induce oxidative stress, whereas IS is a known ligand of the aryl hydrocarbon receptor (AhR), affects bone (re)modelling through downstream inflammatory and Wnt-inhibitory pathways (Chen et al., 2024; Shyu et al., 2021). Such pathways may require interactions among multiple cell types or the presence of hormonal cofactors absent in this simplified culture system. Using other osteocyte models may be an alternative way to see their effects. Chen et al. (2024) demonstrated that IS challenged

differentiated IDG-SW3 osteocytes significantly increased the expression of *Sost* and *Dkk1* in a dose-dependent manner, suggesting that IS can enhance Wnt inhibition and suppress bone formation in more mature osteocytes (Chen et al., 2024). The discrepancy between their findings and the present results likely reflects differences in osteocyte maturity, as IDG-SW3 cells progress through a mineralising stage and express high basal levels of *Sost*. In contrast, MLO-Y4 cells represent an early, less mature osteocytic phenotype. Similarly, with respect to Pi treatment, Miyagawa et al. (2014) reported that while high Pi concentrations induced *Dmp1* expression, it did not alter *Sost* expression in primary osteocytic cultures, aligning with the current observation that Pi alone may not directly regulate *Sost* transcription *in vitro* (Miyagawa et al., 2014). These results provide useful insight into the molecular responsiveness of osteocytes to uremic and Pi -related stimuli and underscore the importance of selecting an appropriate *in vitro* model when investigating osteocytic gene regulation.

However, this study has several limitations. As this was my first *in vitro* experiment, there may have been some minor deviations from standard procedures. In addition, protein expression analyses and staining assays (Oil Red O and Alizarin Red) and ALP activity should have been performed to further validate the observed changes. Unfortunately, these experiments could not be conducted due to an insufficient number of BMSC obtained, which may have resulted from the challenges inherent to primary BMSC isolation or cell death during culture. In this study, I followed BMSC isolation and differentiation protocols described for both adipogenic and osteogenic media (Maridas et al., 2018). However, the same group recently updated their protocol (Liu et al., 2024), refining the concentrations of several media supplements that could be harmful to BMSCs. Therefore, applying this updated method in future experiments may help achieve more consistent and reliable results. Overall, despite these limitations, this experience provided me with valuable practical insight and has strengthened my confidence to repeat and improve this experiment in the future as I continue my research career.

In summary, this study reveals that CKD-associated systemic factors differentially regulate BMSC fate and bone-related signalling pathways: PTH and Pi favour osteogenesis or suppress adipogenesis, whereas IS broadly impairs both processes. FGF23

and sclerostin act mainly through indirect or contextual mechanisms. These findings provide new insight into how CKD disturbs the balance between bone formation and marrow adiposity. However, it is important to consider that, in biological systems, these factors rarely act independently. Instead, they often interact or work together in complex ways. Such interactions can lead to synergistic or additive effects, meaning that the combined influence of two or more factors may be greater or different from what would be expected from their individual actions alone. Recognising these potential interactions is crucial for fully understanding the overall impact of CKD on BMSC differentiation and offers a foundation for future work aimed at identifying therapeutic strategies to preserve skeletal integrity in CKD.

Chapter 5

Bispecific antibody against sclerostin and DKK1 improves bone health and reduces bone marrow adipose tissue accumulation in experimental chronic kidney disease

---

Under review at *Bone Research*

6 October 2025

Introduction

The progressive decline in kidney function characteristic of CKD leads to profound disturbances in mineral and hormonal homeostasis, including hyperphosphatemia, hypercalcemia, SHPT, and elevated circulating FGF23 levels (Moe et al., 2006). These systemic alterations emerge early in CKD progression and lead to CKD-MBD complications which has prevalence of osteoporosis up to 32% in CKD patients (Abdalbary et al., 2022). These complications associated with bone disorders, characterised by abnormalities in bone turnover, mineralisation, and volume, are known as ROD (Fang et al., 2014; Graciolli et al., 2017). There are two subtypes of bone pathology in ROD: high-turnover lesions, such as osteitis fibrosa and mixed uremic osteodystrophy, and low-turnover lesions, including adynamic bone disease and osteomalacia (Salera et al., 2025). Enhanced osteoclastic activity, often driven by persistently elevated PTH, leads to excessive bone resorption and the formation of immature and poorly mineralised bone tissue (Graciolli et al., 2017; Hou et al., 2018; Jadoul et al., 2006; Nickolas et al., 2013). While SHPT is commonly associated with high-turnover bone disease in advanced CKD, low-turnover lesions have become increasingly recognised, especially in the early stages of CKD, where suppressed PTH levels correlate with reduced bone remodelling and an increased risk of fragility fractures (Coco & Rush, 2000; Massy & Drueke, 2017). This observation has significant clinical implications, as low bone turnover disease is now considered the predominant form of ROD in early CKD, representing a critical window for intervention before irreversible skeletal damage occurs (Massy & Drueke, 2017).

The mechanisms underlying the transition toward low bone turnover remain incompletely understood but may involve elevated serum Pi, increased FGF23, and the accumulation of protein-bound uremic toxins (Campos-Obando et al., 2017; Dhayat et al., 2016; Jayash et al., 2025). A previous study using nephrectomy and parathyroidectomy in CKD rat models on a high- Pi diet revealed reduced bone formation rates and impaired osteoblast activity (Ferreira et al., 2013). These results suggest a Pi-driven pathway that causes bone loss, acting independently of PTH (Batista et al., 2010). Uremic toxins have been shown to impair osteoblast function by inducing skeletal resistance to PTH,

oxidative stress, and mitochondrial dysfunction in osteoblasts and osteocytes (Bover et al., 1999; Hsu et al., 2025; Lee et al., 2015; Nii-Kono et al., 2007; Watanabe et al., 2017). In addition, CKD is associated with elevated circulating concentrations of sclerostin, an osteocyte-derived inhibitor of Wnt/β-catenin signalling. Numerous clinical and experimental studies have demonstrated that serum sclerostin levels rise progressively as kidney function declines and are inversely correlated with eGFR (Behets et al., 2017; Cejka et al., 2014; Evenepoel et al., 2015; Fang, Ginsberg, Sugatani, et al., 2014; Kanbay et al., 2014; Laster et al., 2023; Moe et al., 2015; Neto et al., 2021; Pelletier et al., 2013; Sabbagh et al., 2012). Importantly, this increase often precedes elevations in PTH and FGF23, suggesting that disrupted Wnt/β-catenin signalling may represent an early molecular event in CKD-MBD pathogenesis. Consistent with these reports, Chapter 3 of this thesis also demonstrated an increase in circulating sclerostin levels in adenine-induced CKD mice, coinciding with bone loss and BMAT expansion.

The role of another Wnt/β-catenin pathway antagonist, DKK1, in CKD remains less well defined, with conflicting reports of unchanged (Behets et al., 2017; Cejka et al., 2011), decreased (Forster et al., 2020; Neto et al., 2021), or increased (Fang, Ginsberg, Sugatani, et al., 2014 et al., 2014; Moe et al., 2015) serum levels. Nevertheless, both sclerostin and DKK1 act to suppress canonical Wnt/β-catenin signalling, thereby impairing osteoblast differentiation and bone formation. Disruption of this pathway contributes to the low bone mass and poor skeletal quality characteristic of ROD. Although *Sost*-deficient ($Sost^{-/-}$) mice display high bone mass, they are only partially protected from nephrectomy-induced cortical and trabecular bone loss (Cejka et al., 2016; Kaesler et al., 2018), suggesting that compensatory mechanisms, potentially involving DKK1, may limit the skeletal benefits of sclerostin deficiency.

Therapeutically, neutralisation of sclerostin using monoclonal antibodies such as romosozumab has been shown to increase bone mineral density and reduce fracture risk in postmenopausal women and men with osteoporosis (Cosman et al., 2014; Lewiecki et al., 2018; McClung et al., 2014; Saag et al., 2017). Limited clinical evidence in CKD patients supports similar trends: romosozumab improved BMD at multiple skeletal sites and reduced new vertebral fractures in postmenopausal women with mild-to-moderate

CKD (Miller et al., 2022; Miyauchi et al., 2022). However, in preclinical models of progressive CKD, administration of sclerostin-neutralising antibodies provided only modest protection of bone architecture and failed to improve biomechanical properties (Moe et al., 2015). These findings suggest that compensatory upregulation of DKK1 following sclerostin inhibition (Adami et al., 2025; Florio et al., 2016; Holdsworth et al., 2018; Moe et al., 2015; van Lierop et al., 2014) may attenuate the anabolic efficacy of sclerostin antibody (Scl-Ab) therapy. Indeed, elevated DKK1 levels have been observed in patients with sclerosteosis, van Buchem disease, and after prolonged romosozumab treatment, underscoring a potential feedback mechanism that limits Wnt/ β-catenin pathway activation (Adami et al., 2025; van Lierop et al., 2014).

In addition to bone deterioration, CKD is also associated with abnormal accumulation of BMAT in both animal models (Ni et al., 2019; Promruk et al., 2025; Wang et al., 2017) and patients (Moorthi et al., 2015; Woods et al., 2018). Chapter 3 of this thesis demonstrated that BMAT expansion occurs early in the progression of CKD, preceding bone loss, and that this process is independent of BMSCs' commitment in the onset of CKD but is rather driven by intrinsic alterations in the BMSC lineage commitment, which are affected by CKD severity. Chapter 4 further revealed that CKD-associated systemic factors, such as PTH, Pi, FGF23, sclerostin, and the uremic toxin indoxyl sulfate, differentially regulate osteogenic and adipogenic signalling of BMSCs, even though the results were difficult to interpret and further *in vitro* studies using combination of two and more CKD-associated systemic factors are required. Notably, sclerostin and DKK1, through their suppression of Wnt/β-catenin signalling, may represent key molecular mediators that shift BMSC differentiation toward adipogenesis at the expense of osteogenesis.

Consistent with this hypothesis, inhibition of sclerostin using Scl-Ab has been shown to reduce BMAT accumulation in various experimental contexts, including ovariectomy (Li et al., 2019), irradiation (Costa et al., 2021), diabetes (Yee et al., 2016), and rosiglitazone-induced adipogenesis (Farrell et al., 2021). However, these effects were modest, again suggesting compensatory DKK1 upregulation may blunt the therapeutic benefit of sclerostin inhibition alone.

Given these findings, it is plausible that simultaneous blockade of both sclerostin and DKK1 function would more effectively restore Wnt/β-catenin signalling, thereby enhancing osteogenesis, reducing BMAT accumulation, and improving overall skeletal health in CKD. Therefore, in this chapter, it was hypothesised that treatment with a rodent bispecific antibody (rbsAb) targeting both sclerostin and DKK1 would confer superior protection against bone loss and BMAT expansion in an experimental model of CKD.

All experiments were conducted by myself, except the vertebral phenotype μCT data analysis, performed by Soher N Jayash, and the proteomics analysis, carried out by Chartinun Chutoe and his supervisor Alexander von Kriegsheim. I had no prior experience in either of these two types of analysis but I worked closely with my colleagues during the data analysis to learn both techniques. The first draft of the manuscript was written by myself.

Bispecific antibody against sclerostin and DKK1 improves bone health and reduces bone marrow adipose tissue accumulation in experimental chronic kidney disease

Worachet Promruk[1,2*], Soher N Jayash[1], Chartinun Chutoe[3], Hua Zhu Ke[4], Xiaofeng Liu[4], Alexander von Kriegsheim[3], William P Cawthorn[5], Katherine A Staines[6], Louise A Stephen[1], Colin Farquharson[1*]

[1] Functional Genetics Division, The Roslin Institute and Royal (Sadick et al.) School of Veterinary Studies, University of Edinburgh, UK.

[2] Chulabhorn Royal Academy, Bangkok, Thailand

[3] Edinburgh Cancer Research UK Centre, Institute of Genetics and Cancer, University of Edinburgh, UK

[4] Angitia Biopharmaceuticals (Angitia Incorporated Limited), Guangzhou, China and Westlake Village, California, USA

[5]Institute for Neuroscience and Cardiovascular Research, Edinburgh Bioquarter, University of Edinburgh, UK.

[6] Centre for Lifelong Health, School of Applied Sciences, University of Brighton, UK

Running Title: SOST and DDK1 inhibition in renal osteodystrophy

Worachet Promruk –

Soher N Jayash -

Chartinun Chutoe -

Hua Zhu Ke-

Xiaofeng Liu -

Alexander von Kriegsheim -

William P Cawthorn -

Katherine A Staines -

Louise Stephen -

Colin Farquharson –

*Corresponding Authors:

Worachet Promruk - Functional Genetics Division, The Roslin Institute and Royal (Sadick et al.) School of Veterinary Studies, University of Edinburgh, EH25 9RG, UK.

Colin Farquharson – Functional Genetics Division, The Roslin Institute and Royal (Sadick et al.) School of Veterinary Studies, University of Edinburgh, EH25 9RG, UK.

(0) +44 131 651 9176

Abstract

Chronic kidney disease (CKD) leads to bone loss and bone marrow adipose tissue (BMAT) accumulation. Sclerostin and dickkopf-1 (DKK1) are two inhibitors of Wnt signalling, which suppress bone formation, promote bone marrow adipogenesis, and are elevated in CKD. However, therapies targeting sclerostin have shown limited efficacy in improving bone health in CKD animal models. Herein, we explored whether dual inhibition of sclerostin and DKK1 via a rodent bispecific antibody (rbsAb) could prevent bone loss and suppress BMAT accumulation in a CKD mouse model. CKD was induced using an adenine-supplemented diet in male mice, with CKD and control mice treated weekly for 6-weeks with vehicle or 30 mg/kg body weight of rbsAb. Circulating sclerostin and DKK1 were ~2- and ~3-fold higher, respectively, in CKD mice compared to controls. Proteomic profiling by LC-MS/MS and functional enrichment analysis suggested that in CKD mice, adipogenesis, osteoclast differentiation and bone resorption

were increased whereas osteoblast differentiation was inhibited. These changes were prevented by antibody treatment. MicroCT revealed that long bones of CKD mice were characterised by lower bone mineral density, trabecular and cortical bone, and impaired biomechanical properties, but their vertebrae were unaffected. RbsAb treatment prevented cortical and trabecular bone loss and restored biomechanical properties. BMAT, as visualised by microCT imaging of osmium-stained bones, was elevated in CKD but reduced to control levels by rbsAb treatment. In conclusion, dual inhibition of sclerostin and DKK1 improved bone integrity and suppressed BMAT in experimental CKD, suggesting a promising therapeutic avenue for renal osteodystrophy.

Introduction

The progressive loss of kidney function that occurs in chronic kidney disease (CKD) leads to disturbed mineral metabolism, with CKD patients commonly presenting with hyperphosphatemia, hypercalcemia, hyperparathyroidism and increased fibroblastic growth factor-23 (FGF23) levels [1]. These systemic changes are the primary indicators for the diagnosis of CKD–mineral bone disorder (CKD–MBD), which develops in the early stages of CKD. Disease progression results in a myriad of complications including vascular calcification and a wide spectrum of bone disorders characterised by abnormalities in bone quantity and quality, and generally referred to as renal osteodystrophy (ROD) [2, 3]. The prevalence of osteoporosis in CKD patients ranges from 18 – 32% and fracture incidence of patients with end-stage kidney disease is 8-fold higher than that of the general population [4].

A histopathological classification system based on abnormalities in bone turnover, volume and mineralisation is used to diagnose ROD and categorise it into various diseases states. These include high turnover with either fibrosis (osteitis fibrosa) or abnormal mineralisation (mixed disease), and low turnover with either normal (adynamic bone disease) or abnormal mineralisation (osteomalacia) [5]. The stimuli for increased bone remodelling are unclear, but enhanced osteoclastic bone resorption in response to elevated parathyroid hormone (PTH) is associated with a net loss of bone mass despite an accelerating bone turnover [6-8]. Rapid remodelling also results in bone that is both

immature and poorly mineralised [3]. Nevertheless, while high-turnover bone lesions induced by secondary hyperparathyroidism are common in late-stage CKD, alternative causative mechanisms are likely as very low serum PTH levels correlate with adynamic bone disease and an increased fracture rate [9, 10]. This is clinically important, as accumulating evidence suggests that low bone turnover disease is the dominant form of ROD in the early stages of CKD, making it an ideal period to develop targeted therapeutic interventions [10].

The factors contributing to the development of low bone turnover disease are unclear but may include elevated levels of phosphate, FGF23 and/or protein-bound uremic toxins [11-14]. Uremic toxins can induce skeletal resistance to PTH and oxidative stress and mitochondrial dysfunction in osteoblasts/osteocytes [15-19]. Circulating concentrations of sclerostin, a Wnt/β-catenin antagonist, are also increased in CKD patients and animal models, and these changes, which are inversely correlated to estimated glomerular filtration rate in CKD patients, are increased during adynamic bone disease and prior to rises in circulating PTH and FGF-23 [20-29]. The relationship between CKD and another Wnt/β-catenin inhibitor, dickkopf-related protein 1 (DKK1), is less clear, with studies reporting unchanged [28, 30] decreased [29, 31] or increased [26, 27] serum levels.

Disturbed Wnt/β-catenin signalling may contribute to the low bone mass characteristic of ROD. Although Sost-deficient ($Sost^{-/-}$) mice have increased bone mass, they have limited protection against nephrectomy-induced cortical and trabecular bone loss [32, 33]; however, the high bone mass of $Sost^{-/-}$ mice at baseline may confound the interpretation of these data. Therefore, approaches using a sclerostin-neutralising antibody (Scl-Ab) such as romosozumab, which is widely recognised to increase bone mineral density (BMD) and reduce fractures in healthy men and postmenopausal women, may be more informative and offer potential therapeutic options to prevent bone loss in CKD [34-37].

Studies on CKD patients are limited. Two studies reported that romosozumab improved BMD at the lumbar spine, total hip, and femoral neck and reduced the relative risk of new vertebral fractures in postmenopausal women with osteoporosis and mild-moderate

CKD [38, 39]. However, in a preclinical rat model of progressive ROD, administration of a Scl-Ab provided limited protection to the architecture of the long bones and no improvement in their biomechanical properties [26]. Interestingly, DKK1 serum levels are raised with prolonged romosozumab treatment and also in patients with sclerosteosis and van Buchem disease [40, 41]. Similarly, *Sost*$^{-/-}$ mice and mice administered sclerostin antibody also present with a compensatory increase in the expression of DKK1 [26, 42, 43] raising the possibility that elevated DKK1 may attenuate the anabolic effects of sclerostin inhibition and negate major improvement in skeletal health in Scl-Ab-treated mice [26].

In addition to bone loss, CKD can also lead to bone marrow adipose tissue (BMAT) accumulation in animal models [44-46] and humans [47, 48]. The mechanism(s) responsible are unclear but may also involve Wnt/β-catenin signalling, which can inhibit adipogenesis and adipocyte-specific gene expression in white adipose tissue [49-51]. Congruently, Scl-Ab treatment reduced BMAT accumulation in ovariectomised rabbits [52] and irradiated [53], diabetic [54] and rosiglitazonetreated [55] mice; however, the changes were modest, suggesting that additional mechanisms may be involved and/or a compensatory increase in DKK1 may blunt the neutralising effects of the Scl-Ab.

The increased DKK1 expression in response to Scl-Ab treatment may limit the ability of the antibody to protect bone health in CKD mice and decrease BMAT accumulation. Therefore, in this study we tested whether a rodent bispecific antibody (rbsAb) against sclerostin and DKK1 can improve bone health and decrease BMAT accumulation in an experimental model of CKD.

Results

Disease profile is similar in vehicle- and rbsAb-treated CKD mice

We first confirmed the development of the CKD-MBD phenotype in the experimental mice. Dietary adenine-supplementation led to a loss of bodyweight within the first week

and by end of the study the CKD mice were ~40% lighter than control (CTRL) mice. This was reflected in a decreased mass of the inguinal and gonadal white adipose tissue depots (iWAT and gWAT, respectively) of the vehicletreated CKD mice (Figs. 1A - C). The CKD mice also presented with hyperphosphatemia and increased BUN, creatinine and calcium (Figs 1D - F). Similar effects were observed between CTRL and CKD mice administered the rbsAb. The rbsAb treatment also modestly decreased iWAT and gWAT masses and increased serum phosphate in CTRL mice (Figs 1B, C, G). Plasma PTH levels were similar in vehicletreated CTRL and CKD mice but were raised in both CTRL and CKD mice with the rbsAb administration (Fig. 1H).

Plasma DKK1 and sclerostin levels are elevated in CKD mice

The ability of the rbsAb to reduce circulating levels of sclerostin and DKK1 was next investigated. In vehicle-treated mice, plasma levels of sclerostin were higher in CKD compared to CTRL mice (Figs. 1I). Sclerostin concentrations in rbsAb-treated mice were extremely high, reaching supraphysiological concentrations and with no evidence of antibody-mediated neutralisation (Fig. 1I). This is likely due to the antibody-sclerostin complex having cross-reactivity with the sclerostin ELISA, as reported previously [26, 41]. In vehicle-treated mice, CKD increased median DKK1 concentrations by almost 3fold. However, the unadjusted P value for this relatively large effect (*P =0.0297)* was no longer below the significance threshold after adjusting for multiple comparisons (Fig. 1J). Moreover, treatment with the rbsAb strongly and significantly decreased DKK1 concentrations in both CTRL and CKD mice to levels that were indistinguishable from each other (Fig. 1J). This demonstrates effective DKK1 neutralisation by the rbsAb. Plasma sclerostin and DKK1 levels of vehicle treated CTRL and CKD mice were not correlated to plasma PTH levels (Suppl Figs. 1A, B).

RbsAb treatment prevents tibial bone loss in CKD mice

Given that CKD causes bone loss [17, 56], we next tested if rbsAb treatment was able to prevent bone loss in the tibia and vertebrae of CKD mice. Trabecular structure and BMD of the tibia were compromised in vehicle- but not rbsAb-treated CKD mice (Figs 2A – F). Moreover, while rbsAb administration increased trabecular BMD, bone volume

fraction, thickness and number in the tibia of CTRL mice, these rbsAb effects were even greater in the CKD mice. This resulted in higher values for these skeletal properties in rbsAb-treated CKD mice compared to similarly treated CTRL mice (Figs 2B - E). The decrease in trabecular separation in rbsAb-treated CTRL and CKD mice showed a similar effect (Fig 2F). In cortical bone of vehicle-treated CKD mice, bone area, thickness, periosteal perimeter and polar moment of inertia were reduced whereas medullary area, endosteal perimeter and porosity were increased when compared to the tibia of vehicle-treated CTRL mice (Figs 2G - N). RbsAb treatment increased bone area, thickness, periosteal perimeter, porosity and polar moment of inertia but reduced medullary area and endosteal perimeter along the tibial length in both CTRL and CKD mice. The cortical bone changes in response to rbsAb treatment were similar in CTRL and CKD mice and accordingly the magnitude of differences noted between vehicle-treated CTRL and CKD mice were maintained in the rbsAb-treated mice (Figs 2G - N). This suggests that, within long bones, CKD alters the skeletal effects of sclerostin and DKK1 in a bone-type-specific manner. Furthermore, the influence of CKD and/or rbsAb treatment on cortical architecture appeared to be site dependent. For example, differences in cortical porosity were greater in the proximal tibia (Fig. 2N) whereas more marked differences in cortical thickness were noted in the distal tibia (Fig 2I). Neither plasma sclerostin or plasma DKK1 had any correlation with trabecular BV/TV (Suppl Figs. 1C, D).

In L4 vertebrae, CKD also had significant effects on trabecular and cortical BMD and bone architecture (Figs. 3A-H). In vehicle-treated mice, only cortical thickness was decreased by CKD, whereas the effects of CKD were more pronounced in rbsAb-treated mice (Figs. 3A-H). RbsAb administration increased trabecular BMD, bone volume fraction, thickness and number whereas trabecular separation was unaffected (Figs. 3A – E). Similarly, cortical BMD, volume and thickness were also increased in response to the rbsAb (Figs. 3F – H). However, the anabolic effects of the rbsAb on vertebral trabecular and cortical bone differed between CTRL and CKD mice: for trabecular bone, the rbsAb had a stronger anabolic effect in CKD than in CTRL mice (Figs. 3A, B, D, E), while the rbsAb effects on cortical bone were stronger in CTRL than in CKD mice (Figs.

3F - H). This bone-type specific response, within the vertebrae, to rbsAb treatment is similar to that observed in the tibia (Fig. 2).

RbsAb treatment improves tibiae and vertebrae biomechanical properties of CKD mice

As bone structure and geometry influence biomechanical properties, we next examined the response of the femur and L4 vertebrae to mechanical loading. Femur stiffness, maximum load and work to fracture were all lower in vehicle-treated CKD mice when compared to their respective CTRLs (Figs. 3I, J, L). All biomechanical properties apart from post-yield displacement were increased in rbsAbtreated CTRL and CKD mice and, in all cases, the values from the rbsAb-treated CKD mice remained lower than similarly treated CTRL mice (Figs 3I - M) and reflect the structural changes observed in the cortical bone of the tibia (Figs. 2G – M). In contrast, compression loading of L4 vertebrae revealed that stiffness, maximum load, yield load and work to fracture were similar in vertebrae from vehicletreated CTRL and CKD mice (Figs. 3N - Q) and reflect their similar trabecular and cortical architecture (Figs. 3A – H). Similarity in biomechanical properties was also observed in vertebrae from rbsAbadministered CTRL and CKD mice, albeit all were increased when compared to their respective vehicletreated mice (Figs 3N - Q).

Gene and proteomic profiling of cortical bone reveals rbsAb-mediated prevention of CKD-induced dysregulation of osteoblast differentiation

To further understand the cellular events responsible for bone loss in CKD mice and its prevention by rbsAb administration, we performed gene expression and proteomic analyses of cortical bone. The expression of osteoblast/osteocyte genes was similar in tibial cortical bone of vehicle-treated CTRL and CKD mice (Figs. 4A - J), while the effects of rbsAb treatment were variable: it increased the expression of *Sost* in both CTRL and CKD mice (Fig. 4I); increased *Sp7, Bglap, Alpl, Col1a1* and *Dkk1* in tibiae of

CTRL mice but not CKD mice (Figs. 4B – E, J); and increased *Tnfrsf11b* expression in CKD mice only (Fig. 4H).

The proteomic analysis by LC-MS/MS revealed that 199 proteins were down regulated and 189 proteins were upregulated in bone from vehicle-treated CKD mice compared to vehicle-treated CTRL mice (Fig. 5A, C). Moreover, in CKD mice, the expression of 123 proteins was downregulated and 336 proteins were upregulated in bone by the administration of rbsAb compared with vehicle (Fig. 5B, D). To identify the osteoblast/osteocyte-related pathways implicated in the aetiology of ROD, we performed functional enrichment analysis. From the top 8 ontology terms, the osteoblast differentiation pathway was depleted, whereas both bone resorption and bone remodelling pathways were enriched in vehicle-treated CKD mice (Fig. 5E). The enrichment analysis of CKD mice further indicated that the rbsAb was able to prevent the defective osteoblast differentiation and excessive bone resorption and bone remodelling which is consistent with the increased cortical bone mass observed in the rbsAb-treated mice (Figs. 2G – L). Given that the osteoblast differentiation pathway was notably affected by CKD and rbsAb treatment, we further assessed the expression patterns of some of the significantly altered proteins associated with this pathway (Figs 5F – M). The expression of COL1A1 and TNAP, were both down regulated in vehicle-treated CKD mice but the osteoblast transcription factor, SP7 was unchanged (Figs 5F – H). With regard to Wnt signalling, the expression of LRP5, LRP6 and sclerostin, but not CTNNB1 and DKK1, was decreased in vehicle-treated CKD mice (Figs 5I – M). The rbsAb increased TNAP, SOST and DKK1 expression which is in accord with the gene expression results (Figs 4 D, I, J).

RbsAb treatment prevents BMAT accumulation in CKD mice

We next quantified BMAT along the tibial length as visualised by microCT imaging of osmium-stained bones to determine if the accumulation of BMAT that occurs in CKD animal models and patients was prevented by rbsAb treatment [44, 46, 48]. Total BMAT area, or BMAT area normalised to bone marrow area, of vehicle-treated CKD mice was increased compared to vehicle-treated CTRL mice (Figs. 6A - C). RbsAb treatment reduced BMAT accumulation along the entire length of both CTRL and CKD tibiae

(Figs. 6A - C). Moreover, rbsAb treatment of CKD mice decreased the relative BMAT volume to levels similar to those observed in vehicle-treated CTRL mice (Fig. 6C). Correlation analysis revealed an inverse relationship between rBMAT and trabecular BV/TV, which is in agreement with previous studies [46] (Fig. 6D). Bone marrow adiposity can be decreased by PTH [57, 58], but no correlation was found between plasma PTH and rBMAT (Suppl Fig. 1E); this is in broad agreement with prior observations [47, 59]. Similarly, neither plasma sclerostin nor plasma DKK1 had any correlation with rBMAT (Suppl Figs. 1F, G).

Bone marrow adipocyte and osteoclast gene and protein expression are dysregulated in CKD but normalised by rbsAb treatment

We next investigated the cellular and molecular mechanisms responsible for the accumulation of BMAT in CKD and its prevention by the rbsAb. To do so, we assessed the expression of key adipocyte transcription factors and phenotype-specific genes and proteins in bone marrow from CTRL and CKD mice, both with and without rbsAb treatment. In comparison to vehicle-treated CTRL mice, the expression of *Pparg2* and *Adipoq*, but not *Cebpa*, *Fabp4* or the lipase-encoding genes, *Pnpla2* and *Lipe*, was increased in vehicle-treated CKD mice (Figs. 6E - J). RbsAb treatment down regulated *Pparg2* and *Adipoq* expression in CKD mice, resulting in similar levels to those in rbsAb -treated CTRL mice; this is consistent with the effects on relative marrow adiposity (Fig. 6C). *Fabp4* expression was also down regulated by antibody treatment of both CTRL and CKD mice (Fig. 6H). Sclerostin can promote the differentiation of bone marrow stem cells into osteoclasts; thus, we also quantified the expression of osteoclast transcription factors and mature osteoclast genes. The expression of the master transcription regulator of osteoclast differentiation, *Nfatc1*, was similar in CTRL and CKD samples and was not affected by rbsAb treatment (Fig. 6L). In contrast, the expression of *Ctsk, Mmp9, Acp5* and *Tnfsf11* was increased by CKD in vehicle-treated mice and rbsAb treatment reduced Tnfsf11 and Ctsk expression in CKD samples resulting in similar expression levels between CTRL and CKD mice (Figs. 6K - O).

We further interrogated these bone marrow effects using proteomics. The volcano plots (Figs. 7A, B) and Venn diagrams (Figs. 7C, D) illustrate the global proteomic alterations observed under CKD conditions and the modulatory effects of rbsAb treatment in CKD mice. Functional enrichment analysis of the top 6 ontology terms disclosed that, under vehicle treatment, adipogenesis, osteoclast differentiation and signalling, and bone resorption pathways were enriched in CKD vs CTRL mice (Fig. 7E). These enriched pathways were depleted by rbsAb treatment of CKD mice (Fig. 7E) and together these data are in accord with the ability of the rbsAb to protect CKD mice from bone loss and BMAT accumulation (Figs. 2 and 6), respectively. Adipocyte proteins were then analysed, which illustrated upregulation of FABP4, PLIN1, LEPR, ADIPOQ, LPL, LIPE and PNPLA2 in CKD mice. These increases were significantly prevented by rbsAb treatment, thereby cancelling or minimising the difference in their expression levels between CTRL and CKD mice (Figs. 7F-L). In addition, proteins associated with osteoclast differentiation and bone resorption were upregulated in vehicle-treated CKD vs CTRL mice (Figs. 7O – R). This CKD effect was generally prevented by rbsAb administration, resulting in expression levels of NFKB, NFATC and CTSK that were similar between rbsAb -treated CTRL and CKD mice (Figs. 7O – R). SOST and DKK1 expression were similar in vehicle-treated CTRL and CKD mice but, in agreement with the bone gene expression data (Figs. 5J, K), the expression of both β-catenin inhibitors was increased by rbsAb treatment (Fig. 7M, N).

Discussion

Therapies for the treatment of ROD are currently focussed on the use of calcitriol and calcimimetics to lower circulating levels of PTH and reduce the adverse skeletal effects of secondary hyperparathyroidism [60, 61]. This approach is recommended prior to consideration of other more targeted interventions but as elevated PTH levels are a poor indicator of low bone turnover disease there is a requirement for alternative treatments that can improve bone health regardless of PTH status [9]. Furthermore, CKD often coexists with osteoporosis in the ageing population, resulting in an increased fracture risk in patients with these combined comorbidities [62]. While there are some recognised limitations and caveats, many established therapeutic approaches to

osteoporosis can improve bone health in CKD patients [63]. In patients with mild to-moderate CKD, bisphosphonates raise BMD and reduce fractures but their administration to patients with pre-existing very low bone turnover is a concern, as is their accumulation in CKD patients with impaired renal clearance [64, 65]. Other anti-osteoporosis drugs such as denosumab, teriparatide and abaloparatide increase BMD and reduce fracture risk in patients with mild to moderate CKD. However, PTH analogues may aggravate existing hyperparathyroidism and denosumab, like bisphosphonates, can induce hypocalcemia [63, 66-68].

An attractive alternative approach may involve the neutralisation of sclerostin; an inhibitor of bone formation and recognised to be elevated in bone [3, 20] and serum [20, 22, 25] of CKD patients. Romosozumab is a humanised antibody that targets sclerostin resulting in the transient activation of bone formation and inhibition of bone resorption [34, 69]. Romosozumab can reduce fracture risk in CKD but evidence is limited to a recent post hoc analysis of patients from the phase 3 clinical trials,
FRAME and ARCH [38]. Preclinical studies have also reported that romosozumab can improve bone health in murine models of diabetes and CKD [70, 71]. A limitation of targeting sclerostin alone to promote bone formation is the up-regulation of DKK1 expression, which may dampen the bone formation response to sclerostin neutralisation [26, 41-43]. Therefore, one of the aims of this present study was to examine the ability of a bispecific antibody to sclerostin and DKK1 to improve bone health in a mouse model of CKD.

It has been widely reported that the structure and biomechanical properties of long bones are compromised in CKD rodents [17, 72-74]. A role for secondary hyperparathyroidism is often implicated in the progression of ROD but structural and mechanical integrity defects are also found in the tibia of this study despite normal levels of circulating PTH. However, in contrast to previous animal studies in which PTH levels were elevated we do not observe structural or biomechanical abnormalities in the vertebrae of the CKD mice [75-77]. The gene expression and functional pathway analysis suggest that rbsAb treatment promotes osteoblast differentiation and inhibits bone resorption and this consistent with the rbsAb profound effects on both cortical geometry and trabecular

architecture of the vertebrae and long bones of CTRL and CKD mice. The efficacy, of the rbsAb to improve biomechanical and structural properties of the tibia of CKD mice is in stark contrast to that observed in a rat model of CKD where the effects of a Scl-Ab on the structure and biomechanical properties of vertebrae and long bones were limited and only observed in low PTH conditions [26, 75]. This superior skeletal response in CKD mice to the neutralisation of sclerostin and DKK1 rather than sclerostin alone is consistent with previous studies where a bispecific antibody targeting sclerostin and DKK1 was more effective than monotherapy treatment in increasing BMD, biomechanical properties and bone repair activity in rats and nonhuman primates [42, 78-80]. Also, a 3:1 mixture of Scl-Ab and DKK1-Ab promotes the formation of 2-3 times more trabecular bone than an equivalent dose of Scl-Ab alone despite DKK1-Ab having no consistent osteoanabolic effects [42, 81-83]. The increased cortical porosity in the rbsAb treated mice was however unexpected as previous studies have indicated that when corrected for bone volume, cortical porosity in $Sost^{-/-}$ mice was similar to wild-type mice [84].

In this study we also aimed to verify if the rbsAb was able to reduce the amount of BMAT that is known to accumulate in CKD patients and animal models [44, 45, 47, 48]. Though Wnt/β-catenin signalling is known to block expression of C/EBPα and PPARγ in white adipocytes and the loss of Wnt/β-catenin signalling causes a cell fate shift of pre-osteoblasts from osteoblasts to adipocytes, less is known about the regulatory effects of this pathway on bone marrow adipocytes (BMad) [85, 86]. Sclerostin levels positively associate with higher vertebral marrow fat in men and in cell culture studies, adipogenesis is promoted in sclerostin challenged bone marrow mesenchymal stromal cells [87, 88]. Decreased

BMAT accumulation in $Sost^{-/-}$ mice provides further evidence that BMad accumulation in CKD could be a consequence of increased sclerostin levels [87]. Nevertheless, romosozumab has no effect on bone marrow adiposity of the iliac crest in postmenopausal osteoporotic women and the ability of SclAb to decrease BMAT in irradiated or rosiglitazone treated mice was modest and limited to specific regions of the long bones [53, 55, 89]. These subtle, depot specific effects of Scl-Ab on BMad contrast with the results of this present study. Gene and protein expression data suggest an inhibition of

bone marrow adipogenesis with rbsAb treatment and this is consistent with the reduced BMAT accumulation along the entire tibia of rbsAb -treated CTRL and CKD mice. The decrease in total BMAT in rbsAb -treated mice is similar to that reported in Scl-Ab-treated normal adult rats [90] but this reduction may in part be a consequence of an increase in trabecular bone volume and a corresponding reduction in marrow space in which adipocytes can inhabit. However, when normalised to marrow area, BMAT is still decreased in rbsAb -treated mice and suggests that an increase in Wnt/β-catenin signalling has a direct negative effect on BMad, independent of bone changes. When normalised to marrow area a reduction in BMAT was not observed in Scl-Ab-treated rats [90] and suggests that the ability of the Scl-Ab alone to restore normal amounts of BMAT is impeded by a compensatory increase in the expression of DKK1.

Wnt pathway inhibition increases gradually as kidney function declines and is considered an early event in the pathogenesis of CKD [24]. Nevertheless, the relationship between blood sclerostin and PTH levels in CKD patients and animal models is unclear. A positive, negative or, as found in this present study, no correlation between circulating levels of sclerostin and PTH have been reported [26, 30]. Although PTH is known to supress *Sost* and *Dkk1* expression by bone cells [91, 92], a regulatory role for PTH in this study is unclear as circulating PTH levels in the CKD mice is normal. Possibly, the chronic elevation of circulating sclerostin and DKK1 in CKD overwhelms the ability of PTH to regulate their circulating levels leading to PTH resistance and the promotion/aggravation of adynamic bone disease as well as an inability to decrease marrow adipogenesis [57, 58, 93].

Nevertheless, an explanation for the higher circulating levels of sclerostin and DKK1 in CKD remains unclear [20-29]. Reduced renal excretion is unlikely [25], and others have reported immunohistochemistry data indicating increased osteocyte expression of sclerostin in CKD [3, 20, 25]. Alternatively, the increased expression of sclerostin and DKK1 may involve TGF-β, which is elevated in serum and bone in CKD and promotes osteocyte sclerostin expression [94, 95]. Furthermore, sclerostin levels are positively correlated with inflammation markers, phosphate and uremic toxins whereas FGF23 can induce DKK1 and inhibit osteoblast Wnt/β-catenin signalling via a soluble

Klotho/MAPK–mediated process [96-98]. The upregulation of *Sost* and *Dkk1* expression and their encoded proteins in bone of rbsAb -treated mice may be a consequence of lowered circulating levels of the proteins although for sclerostin we were unable to confirm this due to possible ELISA crossreactivity with the bispecific antibody [26, 41]. A similar increase in osteocyte *Sost* expression has been observed previously in Scl-Ab-treated CKD rats [26].

While the rbsAb improves bone health and decreases BMad accumulation in an experimental model of CKD, it is important to recognise that there may be limitations to this possible therapeutic approach. Cardiovascular adverse events have been reported with romosozumab in some (ARCH and BRIDGE) but not all (FRAME) clinical trials [35-37, 99]. The presence of sclerostin [100, 101] and DKK1 [102] in cardiovascular tissue may protect against vascular calcification and while theoretically romosozumab inhibition may aggravate the progression of vascular calcification in CKD there is no evidence of aortic mineralisation in rats or cynomolgus monkeys treated long-term with romosozumab [103-105]. Furthermore, neutralisation of DKK1 prevents vascular calcification in mice with renal insufficiency [27] and to the best of our knowledge, cardiovascular events have not been reported in *Sost* deficient mice or individuals with sclerosteosis or van Buchem disease [106-108]. Nevertheless, further animal and clinical studies focused on potential vascular effects in the setting of sclerostin and/or DKK1 blockade are required to evaluate the effect of prolonged treatment on cardiovascular health.

In conclusion, mice fed an adenine enriched diet present with BMAT accumulation, trabecular and cortical bone loss and impaired biomechanical properties. A bispecific antibody to sclerostin and DKK1 was able to improve bone structure and biomechanical properties of bone and suppress BMAT accumulation. These results highlight a novel therapeutic strategy to enhance bone health in patients with CKD and pave the way for future translational applications in ROD management.

Materials and Methods Mice

To induce CKD, eight-week-old male C57BL/6JCrl mice (Charles River Laboratories, Margate, UK) were fed a diet supplemented with 0.2% adenine for 6-weeks (Envigo, Bicester, UK). Each week the adenine diet was offered for 5-days and replaced by a normal diet for 2 days. This modification of our previous protocol was based on the studies of Lair and colleagues and introduced to induce CKD but avoid pathological weight loss [109, 110]. The CTRL mice received the same diet without adenine (Envigo). The bispecific antibody against sclerostin and DKK1 (Angitia Biopharmaceuticals, Guangzhou, China) or vehicle (PBS) was administered (30 mg/kg body weight) by subcutaneous injection to CTRL and CKD mice once a week for 6 weeks (n = 10/group). Body weights were obtained from mice twice weekly until sacrifice at 14-weeks of age. All mouse studies were approved by the University of Edinburgh Animal Welfare and Ethical Review Board and were conducted under a project license granted by the
UK Home Office. Animal studies were conducted and are reported in line with the ARRIVE guidelines.

Plasma biochemistry

All mice were sacrificed after 6-weeks treatment and blood was collected by cardiac puncture under terminal anaesthesia. Plasma creatinine, blood urea nitrogen (Zuccarini et al.), phosphate and calcium were quantified using a biochemistry analyser (Beckman Coulter AU480). Intact PTH (QuidelOrtho, San Diego, USA), sclerostin and DKK1 (R&D Systems, Abbington, UK) were measured by ELISA according to the manufacturers' instructions.

Micro computed tomography (microCT)

The changes in trabecular and cortical bone structure and BMD of L4 vertebrae (unfixed) and left tibia (fixed in 10% formaldehyde for 24 hours) were assessed by microCT (NeoScan N80, Mechelen, Belgium). Briefly, the bones were scanned with an isotropic voxel size of 5 μm (60 kV, 167 μA and 0.5 mm aluminium filter, 0.6° rotation angle) and

the scans were reconstructed using the NRecon 1.7.3.0 program (Bruker, Kontich, Belgium) to remove artefacts, including beam-hardening and ring artefacts. CTAn software 1.15.4.0 (Skyscan, Kontich, Belgium) was used to evaluate bone histomorphometric parameters. To generate three-dimensional (3D) images, the scans were reconstructed and 3D images were created using the Neoscan80 software package (NeoScan).

For L4 vertebrae, a 300-slice subset through the middle of the vertebrae's body was analysed and the following trabecular [bone mineral density (BMD; g/cm^2), bone volume/tissue volume (BV/TV; %), thickness (Tb. Th; mm), number (Tb. N; 1/mm) and separation (Tb. Sp; mm)] and cortical [BMD; g/cm^2, bone volume (BV; mm^3) and Th (mm)] parameters were calculated [56]. Each tibia was aligned along its longitudinal axis and the trabecular volume of interest (Bellorin-Font et al.) in the proximal metaphysis was a 1000µm section of the metaphysis, 250 µm subjacent to the growth plate. The same trabecular parameters measured in the L4 vertebrae were quantified in the tibial reconstructions. For cortical analysis of the tibia, the proximal and distal portions were digitally cropped to exclude the epiphysis, growth plates and trabecular bone from the analysis [57]. Bone area (B.Ar; mm^2), thickness (Th; mm), polar moment of inertia (*J*; mm^4), medullary area (Med.Ar; mm^2), periosteal perimeter (P.Pm; mm), endosteal perimeter (E.Pm; mm) and porosity (%) were determined. Hydroxyapatite phantoms of known densities (0.25 and 0.75 g/cm^3) were scanned and reconstructed under identical conditions as the experimental samples to allow the calculation of BMD. R studio was used to create the line graph of the cortical bone parameters along the tibia length [55, 58].

Quantification of BMAT

After initial microCT scanning, the bone marrow adipocytes within the left tibiae were stained with osmium tetroxide as previously described [46]. In brief, the decalcified bones were incubated with 1% osmium tetroxide for 48h, washed and stored in Sorensens' buffer at 4°C. The osmium-stained bones were re-scanned by microCT and total BMAT area was calculated as well as being normalised to the size of the bone marrow cavity with trabecular bone was excluded. BMAT volume was quantified in two

distinct anatomical regions: the growth plate to tibia/fibula junction (GP-T/F J), which contains regulated BMAT (rBMAT); and the tibia/fibula junction to the end of distal bone (T/F J-End), which contains constitutive BMAT (cBMAT) [111]. R studio was used to create the line graph of BMAT accumulation along the tibia length.

Biomechanical testing of tibia and vertebrae

The L4 vertebrae and right femora were stored, unfixed, at −20 °C in water and their biomechanical properties were evaluated by a LS5 Lloyds materials testing machine with NEXYGEN Plus software (Ametek, Leicester, UK). For the 3-point bending, the femora were positioned horizontally on custom supports and a 100N load cell was applied perpendicular to the mid-diaphysis at a speed of 10 mm/min. For compression loading, the vertebral body was isolated from the spinal processes and prepared with flat and parallel ends using a polishing wheel and finally bonded to a fixed bottom plate with cyanoacrylate glue. A 500N load cell at a speed of 10 mm/min, compressed the vertebra. Each femur and vertebra were tested to fracture and data recorded after every 0.2 N change in load. The load–displacement curve for each bone was analysed, and stiffness, maximum load, yield load, work to fracture and post-yield displacement were calculated [112].

RT-qPCR

The proximal and distal ends of the right tibiae were removed and the bone marrow was flushed out by centrifugation. Both the tibial shaft and the bone marrow were snap frozen in liquid nitrogen and stored at -80^{0}C. The tissue was homogenised by a Rotor-Stator Homogenizer and RNA was extracted using a Qiagen RNeasy Mini kit (Qiagen, Manchester, UK) and quantified by nanodrop spectrophotometry (Thermo Fisher Scientific, Loughborough, UK). RNA quality was evaluated by the 260/280 nm ratio. After reverse transcription, gene expression was quantified using the SYBER green method and an Agilent Aria 2.1 real-time qPCR system (Agilent Technologies, Cheadle, UK). Target gene expression was normalised to a housekeeping gene (*Ppia*) and analysed using the ΔΔCt method. Oligonucleotide primers (Supp. table 1) were obtained from Sigma-Aldrich (Gillingham, UK) and Thermo Fisher Scientific.

Proteomics

Both proximal and distal ends of the right tibia were removed and bone morrow isolated by centrifugation. Cortical bone and bone marrow tissue were homogenised by a Rotor-Stator Homogenizer in a 100 µl of lysis buffer containing 5% sodium deoxycholate, 100 mM Tris-HCl (pH 8.5), 1 mg/mL chloroacetamide, and 1.5 mg/mL tris(2-carboxyethyl)phosphine. The lysates were subsequently heated at 95°C for 15 minutes. Protein capture and digestion from bone and bone marrow lysates were performed using an automated KingFisher Flex system (Thermo Fisher Scientific) [113]. Briefly, proteins were captured using MagReSyn HILIC magnetic microspheres (ReSyn Biosciences, Pretoria, South Africa). Protein-bound beads were then digested with 0.5 µg of MS-grade trypsin (Thermo Fisher Scientific) in 50 mM triethylammonium bicarbonate buffer (Sigma-Aldrich) at 37°C. The tryptic peptides were sequentially washed with 95% (v/v) acetonitrile (ACN) and 70% ethanol (EtOH). Digestion was terminated by acidification with 2% formic acid. Peptides were subsequently desalted using a C18-based desalting procedure, eluted with 0.1% trifluoroacetic acid (TFA) in 50% ACN, and dried by speed vacuum. Thereafter, dried peptides were reconstituted in 0.1% TFA for subsequent mass spectrometry analysis.

One microgram of desalted peptides was loaded onto 25 cm Aurora columns (IonOptiks, Australia) using an RSLC nano μHPLC system coupled to a Fusion Lumos mass spectrometer. Peptide separation was achieved with a 70-min linear gradient ranging from 5% to 30% acetonitrile in 0.5% acetic acid. The mass spectrometer was operated in data-independent acquisition (DIA) mode, collecting MS scans from 350–1650 Da at 120k resolution, followed by MS/MS acquisition across 45 windows with 0.5 Da overlap (200–2000 Da range) at 30k resolution and a normalized collision energy (NCE) of 28. The raw data were processed using DIA-NN 2.0 software with spectral matching performed against the Mus musculus UniProt protein database [114]. Normalization was conducted based on the total peptide abundance across LC-MS runs. GSEA was done using GSEA software (version 4.4.3, Broad institute, USA).

Statistical analysis

Data are presented as mean ± SEM or as violin plots, as indicated in the figure legends, with individual data points representing each biological replicate. Statistical analysis was performed using a two-way analysis of variance (ANOVA) to determine the effect of the rbsAb treatment and CKD status on bone and BMAT alterations. Correlations between individual parameters were performed using Spearman correlation. As the plasma DKK1 levels were not normally distributed the data were analysed using the Mann–Whitney test with Bonferroni correction for multiple comparisons. Statistical analysis was implemented using GraphPad Prism software (GraphPad Software, Inc., USA) and R studio (for cortical bone and BMAT analysis) and statistical significance was shown as; * $p<0.05$; ** $p<0.01$ and *** $p<0.001$. For differential expression of proteomic profile, the data were processed using Perseus software [115]. Log_2 transformation was applied to the data, and missing values were imputed based on a normal distribution. Pairwise comparisons between groups were conducted using a two-sample t-test. Proteins exhibiting a p-value of less than 0.05 and a fold-change greater than 1.5 were considered significantly altered between the compared groups.

Data Availability

The proteomics data including raw files and search results have been deposited to the ProteomeXchange Consortium via the PRIDE partner repository with the dataset identifier PXD069117.

Acknowledgements

We thank Heather Warnock and the staff of the Biological Research Facility (BRF) at the University of Edinburgh for providing invaluable animal support, Colin Wood and the staff at Easter Bush Pathology, Royal (Sadick et al.) School of Veterinary Studies, University of Edinburgh for conducting mouse serum biochemistries. We acknowledge financial support from Chulabhorn Royal Academy to WP and the Biotechnology and Biological Sciences Research Council (BBSRC) for supporting LAS via a Discovery Fellowship (BB/X009904/1) and for Institute Strategic Programme Grant Funding (BBS/E/RL/230001C) to CF and SNJ. We also acknowledge the Medical Research

Council for funding to KAS (MR/V033506/1 and MR/R022240/2) and WPC (MR/M021394/1 and MR/S010505/1). For the purpose of open access, the authors have applied a CC-BY public copyright license to any Author Accepted Manuscript version arising from this submission.

Author contributions

Conceptualisation: WP, CF, WPC, KAS, LAS, HZK, XL Methodology: WP, SNJ, CC, AVK, HZK, XL. Formal analysis: WP, CF, CC, AVK, WPC, KS, LAS. Writing—original draft: WP and CF. Writing—review and editing: all authors. Visualisation: WP, CC. Supervision: KAS, LAS, WPC and CF. Funding acquisition: WP and CF. All authors read and approved the final manuscript.

Conflict of Interest

HZK and XL are employees of Angitia Biopharmaceuticals (Angitia Incorporated Limited). All other authors declare that the research was conducted in the absence of any commercial or financial relationships that could be construed as a potential conflict of interest.

References

1. Moe, S., et al., *Definition, evaluation, and classification of renal osteodystrophy: a position statement from Kidney Disease: Improving Global Outcomes (KDIGO).* Kidney Int, 2006. **69**(11): p. 1945-53.
2. Fang, Y., et al., *Early chronic kidney disease-mineral bone disorder stimulates vascular calcification.* Kidney Int, 2014. **85**(1): p. 142-50.
3. Graciolli, F.G., et al., *The complexity of chronic kidney disease-mineral and bone disorder across stages of chronic kidney disease.* Kidney Int, 2017. **91**(6): p. 1436-1446.
4. Abdalbary, M., et al., *Management of osteoporosis in patients with chronic kidney disease.* Osteoporos Int, 2022. **33**(11): p. 2259-2274.
5. Ott, S.M., *Histomorphometric measurements of bone turnover, mineralization, and volume.* Clin J Am Soc Nephrol, 2008. **3 Suppl 3**(Suppl 3): p. S151-6.

6. Jadoul, M., et al., *Incidence and risk factors for hip or other bone fractures among hemodialysis patients in the Dialysis Outcomes and Practice Patterns Study.* Kidney International, 2006. **70**(7): p. 1358-1366.
7. Nickolas, T.L., et al., *Rapid cortical bone loss in patients with chronic kidney disease.* Journal of Bone and Mineral Research, 2013. **28**(8): p. 1811-1820.
8. Hou, Y.C., C.L. Lu, and K.C. Lu, *Mineral bone disorders in chronic kidney disease.* Nephrology (Carlton), 2018. **23 Suppl 4**: p. 88-94.
9. Coco, M. and H. Rush, *Increased incidence of hip fractures in dialysis patients with low serum parathyroid hormone.* Am J Kidney Dis, 2000. **36**(6): p. 1115-21.
10. Massy, Z. and T. Drueke, *Adynamic bone disease is a predominant bone pattern in early stages of chronic kidney disease.* J Nephrol, 2017. **30**(5): p. 629-634.
11. Campos-Obando, N., et al., *Serum Phosphate Is Associated With Fracture Risk: The Rotterdam Study and MrOS.* J Bone Miner Res, 2017. **32**(6): p. 1182-1193.
12. Dhayat, N.A., et al., *Fibroblast growth factor 23 and markers of mineral metabolism in individuals with preserved renal function.* Kidney Int, 2016. **90**(3): p. 648-57.
13. Chen, N.X., et al., *The uremic toxin indoxyl sulfate decreases osteocyte RANKL/OPG and increases Wnt inhibitor RNA expression that is reversed by PTH.* JBMR Plus, 2025. **9**(1): p. ziae136.
14. Jayash, S.N., et al., *Osteoblasts sense extracellular levels of phosphate to control the local expression of phosphatases for matrix mineralisation.* Bone Rep, 2025. **26**: p. 101863.
15. Lee, W.C., et al., *Indoxyl sulfate-induced oxidative stress, mitochondrial dysfunction, and impaired biogenesis are partly protected by vitamin C and N-acetylcysteine.* ScientificWorldJournal, 2015. **2015**: p. 620826.
16. Watanabe, K., et al., *Indoxyl sulfate, a uremic toxin in chronic kidney disease, suppresses both bone formation and bone resorption.* FEBS Open Bio, 2017. **7**(8): p. 1178-1185.
17. Hsu, S.N., et al., *Mitochondrial dysfunction and mitophagy blockade contribute to renal osteodystrophy in chronic kidney disease-mineral bone disorder.* Kidney Int, 2025.

18. Nii-Kono, T., et al., *Indoxyl sulfate induces skeletal resistance to parathyroid hormone in cultured osteoblastic cells.* Kidney Int, 2007. **71**(8): p. 738-43.
19. Bover, J., et al., *Dynamics of skeletal resistance to parathyroid hormone in the rat: effect of renal failure and dietary phosphorus.* Bone, 1999. **25**(3): p. 279-85.
20. Sabbagh, Y., et al., *Repression of osteocyte Wnt/β-catenin signaling is an early event in the progression of renal osteodystrophy.* J Bone Miner Res, 2012. **27**(8): p. 1757-72.
21. Laster, M., et al., *Sclerostin, Osteocytes, and Wnt Signaling in Pediatric Renal Osteodystrophy.* Nutrients, 2023. **15**(19).
22. Kanbay, M., et al., *Serum sclerostin and adverse outcomes in nondialyzed chronic kidney disease patients.* J Clin Endocrinol Metab, 2014. **99**(10): p. E1854-61.
23. Evenepoel, P., P. D'Haese, and V. Brandenburg, *Sclerostin and DKK1: new players in renal bone and vascular disease.* Kidney Int, 2015. **88**(Moe et al.): p. 235-40.
24. Pelletier, S., et al., *The relation between renal function and serum sclerostin in adult patients with CKD.* Clin J Am Soc Nephrol, 2013. **8**(5): p. 819-23.
25. Cejka, D., et al., *Renal elimination of sclerostin increases with declining kidney function.* J Clin Endocrinol Metab, 2014. **99**(1): p. 248-55.
26. Moe, S.M., et al., *Anti-sclerostin antibody treatment in a rat model of progressive renal osteodystrophy.* J Bone Miner Res, 2015. **30**(3): p. 499-509.
27. Fang, Y., et al., *CKD-induced wingless/integration1 inhibitors and phosphorus cause the CKDmineral and bone disorder.* J Am Soc Nephrol, 2014. **25**(8): p. 1760-73.
28. Behets, G.J., et al., *Circulating levels of sclerostin but not DKK1 associate with laboratory parameters of CKD-MBD.* PLoS One, 2017. **12**(5): p. e0176411.
29. Neto, R., et al., *Sclerostin and DKK1 circulating levels associate with low bone turnover in patients with chronic kidney disease Stages 3 and 4.* Clin Kidney J, 2021. **14**(11): p. 24012408.
30. Cejka, D., et al., *Sclerostin and Dickkopf-1 in renal osteodystrophy.* Clin J Am Soc Nephrol, 2011. **6**(4): p. 877-82.

31. Forster, C.M., et al., *Circulating Levels of Dickkopf-Related Protein 1 Decrease as Measured GFR Declines and Are Associated with PTH Levels.* Am J Nephrol, 2020. **51**(11): p. 871-880.
32. Cejka, D., et al., *Only minor differences in renal osteodystrophy features between wild-type and sclerostin knockout mice with chronic kidney disease.* Kidney Int, 2016. **90**(4): p. 828-34.
33. Kaesler, N., et al., *Sclerostin deficiency modifies the development of CKD-MBD in mice.* Bone, 2018. **107**: p. 115-123.
34. McClung, M.R., et al., *Romosozumab in postmenopausal women with low bone mineral density.* N Engl J Med, 2014. **370**(5): p. 412-20.
35. Saag, K.G., et al., *Romosozumab or Alendronate for Fracture Prevention in Women with Osteoporosis.* N Engl J Med, 2017. **377**(15): p. 1417-1427.
36. Lewiecki, E.M., et al., *A Phase III Randomized Placebo-Controlled Trial to Evaluate Efficacy and Safety of Romosozumab in Men With Osteoporosis.* J Clin Endocrinol Metab, 2018. **103**(9): p. 3183-3193.
37. Cosman, F., et al., *Romosozumab Treatment in Postmenopausal Women with Osteoporosis.* N Engl J Med, 2016. **375**(16): p. 1532-1543.
38. Miller, P.D., et al., *Efficacy and Safety of Romosozumab Among Postmenopausal Women With Osteoporosis and Mild-to-Moderate Chronic Kidney Disease.* J Bone Miner Res, 2022. **37**(8): p. 1437-1445.
39. Miyauchi, A., et al., *Efficacy and safety of romosozumab among Japanese postmenopausal women with osteoporosis and mild-to-moderate chronic kidney disease.* J Bone Miner Metab, 2022. **40**(4): p. 677-687.
40. van Lierop, A.H., et al., *Serum Dickkopf 1 levels in sclerostin deficiency.* J Clin Endocrinol Metab, 2014. **99(Moe et al.)**: p. E252-6.
41. Adami, G., et al., *Increase in Serum DKK1 Levels Attenuates the Anabolic Response to Romosozumab in Postmenopausal Osteoporosis.* J Bone Miner Res, 2025.
42. Florio, M., et al., *A bispecific antibody targeting sclerostin and DKK-1 promotes bone mass accrual and fracture repair.* Nat Commun, 2016. **7**: p. 11505.

43. Holdsworth, G., et al., *Dampening of the bone formation response following repeat dosing with sclerostin antibody in mice is associated with up-regulation of Wnt antagonists.* Bone, 2018. **107**: p. 93-103.
44. Wang, C.Y., et al., *Knee subchondral bone perfusion and its relationship to marrow fat and trabeculation on multi-parametric MRI and micro-CT in experimental CKD.* Sci Rep, 2017. **7**(1): p. 3073.
45. Ni, L.H., et al., *Cinacalcet attenuated bone loss via inhibiting parathyroid hormone-induced endothelial-to-adipocyte transition in chronic kidney disease rats.* Ann Transl Med, 2019. **7**(14): p. 312.
46. Promruk, W., et al., *Bone marrow adipose tissue expansion and bone loss in experimental chronic kidney disease is independent of altered bone marrow stromal cell lineage determination.* Frontiers in Endocrinology, 2025. **16**: p. 1-15.
47. Moorthi, R.N., et al., *Bone marrow fat is increased in chronic kidney disease by magnetic resonance spectroscopy.* Osteoporos Int, 2015. **26**(6): p. 1801-7.
48. Woods, G.N., et al., *Chronic Kidney Disease Is Associated With Greater Bone Marrow Adiposity.* J Bone Miner Res, 2018. **33**(12): p. 2158-2164.
49. Kurgan, N., et al., *Sclerostin Influences Exercise-Induced Adaptations in Body Composition and White Adipose Tissue Morphology in Male Mice.* J Bone Miner Res, 2023. **38**(4): p. 541555.
50. Kim, S.P., et al., *Sclerostin influences body composition by regulating catabolic and anabolic metabolism in adipocytes.* Proc Natl Acad Sci U S A, 2017. **114**(52): p. E11238-e11247.
51. Kennell, J.A. and O.A. MacDougald, *Wnt signaling inhibits adipogenesis through betacatenin-dependent and -independent mechanisms.* J Biol Chem, 2005. **280**(25): p. 24004-10.
52. Li, S., et al., *Sclerostin Antibody Mitigates Estrogen Deficiency-Inducted Marrow Lipid Accumulation Assessed by Proton MR Spectroscopy.* Front Endocrinol (Lausanne), 2019. **10**: p. 159.

53. Costa, S., et al., *Sclerostin antibody increases trabecular bone and bone mechanical properties by increasing osteoblast activity damaged by whole-body irradiation in mice.* Bone, 2021. **147**: p. 115918.
54. Yee, C.S., et al., *Sclerostin antibody treatment improves fracture outcomes in a Type I diabetic mouse model.* Bone, 2016. **82**: p. 122-34.
55. Farrell, M., et al., *Sclerostin-Neutralizing Antibody Treatment Rescues Negative Effects of Rosiglitazone on Mouse Bone Parameters.* J Bone Miner Res, 2021. **36**(1): p. 158-169.
56. Hsu, S.N., et al., *Increased PHOSPHO1 expression mediates cortical bone mineral density in renal osteodystrophy.* J Endocrinol, 2022. **254**(3): p. 153-167.
57. Fan, Y., et al., *Parathyroid Hormone Directs Bone Marrow Mesenchymal Cell Fate.* Cell Metab, 2017. **25**(3): p. 661-672.
58. Yang, Y., et al., *Influences of teriparatide administration on marrow fat content in postmenopausal osteopenic women using MR spectroscopy.* Climacteric, 2016. **19**(3): p. 28591.
59. Borelli, C., et al., *Assessment of bone marrow fat by 3-Tesla magnetic resonance spectroscopy in patients with chronic kidney disease.* Quant Imaging Med Surg, 2023. **13**(11): p. 7432-7443.
60. Slatopolsky, E., et al., *Marked suppression of secondary hyperparathyroidism by intravenous administration of 1,25-dihydroxy-cholecalciferol in uremic patients.* J Clin Invest, 1984. **74**(6): p. 2136-43.
61. Block, G.A., et al., *Cinacalcet for secondary hyperparathyroidism in patients receiving hemodialysis.* N Engl J Med, 2004. **350**(15): p. 1516-25.
62. Khairallah, P. and T.L. Nickolas, *Management of Osteoporosis in CKD.* Clin J Am Soc Nephrol, 2018. **13**(6): p. 962-969.
63. Haarhaus, M., et al., *Management of fracture risk in CKD-traditional and novel approaches.*
Clin Kidney J, 2023. **16**(3): p. 456-472.
64. Miller, P.D., et al., *Safety and efficacy of risedronate in patients with age-related reduced renal function as estimated by the Cockcroft and Gault method: a*

pooled analysis of nine clinical trials. J Bone Miner Res, 2005. **20**(12): p. 2105-15.

65. Jamal, S.A., et al., *Alendronate treatment in women with normal to severely impaired renal function: an analysis of the fracture intervention trial.* J Bone Miner Res, 2007. **22**(4): p. 5038.
66. Nitta, K., A. Yajima, and K. Tsuchiya, *Management of Osteoporosis in Chronic Kidney Disease.* Intern Med, 2017. **56**(24): p. 3271-3276.
67. Hara, T., et al., *Pharmacological interventions versus placebo, no treatment or usual care for osteoporosis in people with chronic kidney disease stages 3-5D.* Cochrane Database Syst Rev, 2021. **7**(7): p. Cd013424.
68. Whitlock, R., et al., *The Efficacy and Safety of Bisphosphonate Therapy for Osteopenia/Osteoporosis in Patients With Chronic Kidney Disease: A Systematic Review and Individual Patient-Level Meta-Analysis of Placebo-Controlled Randomized Trials.* Can J Kidney Health Dis, 2024. **11**: p. 20543581241283523.
69. Appelman-Dijkstra, N.M. and S.E. Papapoulos, *Sclerostin Inhibition in the Management of Osteoporosis.* Calcif Tissue Int, 2016. **98**(4): p. 370-80.
70. Marino, S., et al., *Reversal of the diabetic bone signature with anabolic therapies in mice.* Bone Res, 2023. **11**(1): p. 19.
71. Kohler, R., et al., *Romosozumab rescues impaired bone mass and strength in a murine model of diabetic kidney disease.* Bone Rep, 2024. **21**: p. 101774.
72. Miller, M.A., et al., *Disparate effects of mild, moderate, and severe secondary hyperparathyroidism on cancellous and cortical bone in rats with chronic renal insufficiency.* Bone, 1998. **23**(3): p. 257-66.
73. Metzger, C.E., et al., *Adenine-induced chronic kidney disease induces a similar skeletal phenotype in male and female C57BL/6 mice with more severe deficits in cortical bone properties of male mice.* PLoS One, 2021. **16**(4): p. e0250438.
74. Iwasaki, Y., et al., *Changes in chemical composition of cortical bone associated with bone fragility in rat model with chronic kidney disease.* Bone, 2011. **48**(6): p. 1260-7.

75. Newman, C.L., et al., *Compromised vertebral structural and mechanical properties associated with progressive kidney disease and the effects of traditional pharmacological interventions.* Bone, 2015. **77**: p. 50-6.
76. Ni, L.H., et al., *A rat model of SHPT with bone abnormalities in CKD induced by adenine and a high phosphorus diet.* Biochem Biophys Res Commun, 2018. **498**(3): p. 654-659.
77. Matsumoto, T., et al., *Relationship between aortic mineral elements and osteodystrophy in mice with chronic kidney disease.* Biol Trace Elem Res, 2012. **150**(1-3): p. 278-84.
78. Florio, M., et al., *Dual Inhibition of the Wnt Inhibitors DKK1 and Sclerostin Promotes Fracture Healing and Increases the Density and Strength of Uninjured Bone: An Experimental Study in Nonhuman Primates.* J Bone Joint Surg Am, 2023. **105**(15): p. 1145-1155.
79. Bienvenu, J.G., et al., *Inhibition of both sclerostin and DKK1 results in novel skull findings in the rat and non-human primate that is not observed with inhibition of sclerostin alone.* Bone, 2024. **179**: p. 116985.
80. Liu, M., et al., *Sclerostin and DKK1 Inhibition Preserves and Augments Alveolar Bone Volume and Architecture in Rats with Alveolar Bone Loss.* J Dent Res, 2018. **97**(9): p. 1031-1038.
81. Choi, R.B., et al., *Improving Bone Health by Optimizing the Anabolic Action of Wnt Inhibitor Multitargeting.* JBMR Plus, 2021. **5**(5): p. e10462.
82. Li, X., et al., *Dickkopf-1 regulates bone formation in young growing rodents and upon traumatic injury.* J Bone Miner Res, 2011. **26**(11): p. 2610-21.
83. Witcher, P.C., et al., *Sclerostin neutralisation unleashes the osteoanabolic effects of Dkk1 inhibition.* JCI Insight, 2018. **3**(11).
84. Mosey, H., et al., *Sost Deficiency does not Alter Bone's Lacunar or Vascular Porosity in Mice.* Front Mater, 2017. **4**: p. 27.
85. Ross, S.E., et al., *Inhibition of adipogenesis by Wnt signaling.* Science, 2000. **289**(5481): p. 950-3.

86. Song, L., et al., *Loss of wnt/β-catenin signaling causes cell fate shift of preosteoblasts from osteoblasts to adipocytes.* J Bone Miner Res, 2012. **27**(11): p. 2344-58.
87. Fairfield, H., et al., *The skeletal cell-derived molecule sclerostin drives bone marrow adipogenesis.* J Cell Physiol, 2018. **233**(Moe et al.): p. 1156-1167.
88. Ma, Y.H., et al., *Circulating sclerostin associated with vertebral bone marrow fat in older men but not women.* J Clin Endocrinol Metab, 2014. **99**(12): p. E2584-90.
89. Chavassieux, P., et al., *Evaluation of romosozumab's effects on bone marrow adiposity in postmenopausal osteoporotic women: results from the FRAME bone biopsy sub-study.* J Bone Miner Res, 2024. **39**(9): p. 1278-1283.
90. Costa, S., H. Fairfield, and M.R. Reagan, *Inverse correlation between trabecular bone volume and bone marrow adipose tissue in rats treated with osteoanabolic agents.* Bone, 2019. **123**: p. 211-223.
91. Bellido, T., et al., *Chronic elevation of parathyroid hormone in mice reduces expression of sclerostin by osteocytes: a novel mechanism for hormonal control of osteoblastogenesis.* Endocrinology, 2005. **146**(11): p. 4577-83.
92. Carrillo-López, N., et al., *Direct inhibition of osteoblastic Wnt pathway by fibroblast growth factor 23 contributes to bone loss in chronic kidney disease.* Kidney Int, 2016. **90**(1): p. 77-89.
93. Kramer, I., et al., *Parathyroid hormone (PTH)-induced bone gain is blunted in SOST overexpressing and deficient mice.* J Bone Miner Res, 2010. **25**(Moe et al.): p. 178-89.
94. Liu, S., et al., *Role of TGF-β in a mouse model of high turnover renal osteodystrophy.* J Bone Miner Res, 2014. **29**(5): p. 1141-57.
95. Moysés, R.M. and S.C. Schiavi, *Sclerostin, Osteocytes, and Chronic Kidney Disease - Mineral Bone Disorder.* Semin Dial, 2015. **28**(6): p. 578-86.
96. Carrillo-López, N., et al., *Direct inhibition of osteoblastic Wnt pathway by fibroblast growth factor 23 contributes to bone loss in chronic kidney disease.* Kidney International, 2016. **90**(1): p. 77-89.

97. Desjardins, L., et al., *Uremic toxicity and sclerostin in chronic kidney disease patients.* Nephrol Ther, 2014. **10**(6): p. 463-70.
98. Ferreira, J.C., et al., *Effects of dietary phosphate on adynamic bone disease in rats with chronic kidney disease--role of sclerostin?* PLoS One, 2013. **8**(11): p. e79721.
99. Bovijn, J., et al., *Evaluating the cardiovascular safety of sclerostin inhibition using evidence from meta-analysis of clinical trials and human genetics.* Sci Transl Med, 2020. **12**(549).
100. Didangelos, A., et al., *Proteomics characterization of extracellular space components in the human aorta.* Mol Cell Proteomics, 2010. **9**(9): p. 2048-62.
101. Zhu, D., et al., *The appearance and modulation of osteocyte marker expression during calcification of vascular smooth muscle cells.* PLoS One, 2011. **6**(5): p. e19595.
102. Shao, J.S., et al., *Msx2 promotes cardiovascular calcification by activating paracrine Wnt signals.* J Clin Invest, 2005. **115**(5): p. 1210-20.
103. Claes, K.J., et al., *Sclerostin: Another vascular calcification inhibitor?* J Clin Endocrinol Metab, 2013. **98**(8): p. 3221-8.
104. Chouinard, L., et al., *Carcinogenicity risk assessment of romosozumab: A review of scientific weight-of-evidence and findings in a rat lifetime pharmacology study.* Regul Toxicol Pharmacol, 2016. **81**: p. 212-222.
105. Ominsky, M.S., et al., *Romosozumab Improves Bone Mass and Strength While Maintaining Bone Quality in Ovariectomized Cynomolgus Monkeys.* J Bone Miner Res, 2017. **32**(4): p. 788801.
106. Li, X., et al., *Targeted deletion of the sclerostin gene in mice results in increased bone formation and bone strength.* J Bone Miner Res, 2008. **23**(6): p. 860-9.
107. Vanhoenacker, F.M., et al., *Van Buchem disease: lifetime evolution of radioclinical features.* Skeletal Radiol, 2003. **32**(12): p. 708-18.
108. Balemans, W., et al., *Identification of a 52 kb deletion downstream of the SOST gene in patients with van Buchem disease.* J Med Genet, 2002. **39**(Moe et al.): p. 91-7.

109. Lair, B., et al., *Common mouse models of chronic kidney disease are not associated with cachexia.* Commun Biol, 2024. **7**(1): p. 346.
110. Hsu, S.-N., et al., *Increased PHOSPHO1 expression mediates cortical bone mineral density in renal osteodystrophy.* 2022. **254**: p. 153-167.
111. Scheller, E.L., et al., *Region-specific variation in the properties of skeletal adipocytes reveals regulated and constitutive marrow adipose tissues.* Nat Commun, 2015. **6**: p. 7808.
112. Jayash, S.N., et al., *Anti-RANKL Therapy Prevents Glucocorticoid-Induced Bone Loss and Promotes Muscle Function in a Mouse Model of Duchenne Muscular Dystrophy.* Calcif Tissue Int, 2023. **113**(4): p. 449-468.
113. Batth, T.S., et al., *Protein Aggregation Capture on Microparticles Enables Multipurpose Proteomics Sample Preparation.* Mol Cell Proteomics, 2019. **18**(5): p. 1027-1035.
114. Demichev, V., et al., *DIA-NN: neural networks and interference correction enable deep proteome coverage in high throughput.* Nat Methods, 2020. **17**(1): p. 41-44.
115. Tyanova, S., et al., *The Perseus computational platform for comprehensive analysis of (prote)omics data.* Nat Methods, 2016. **13**(9): p. 731-40.

Figures

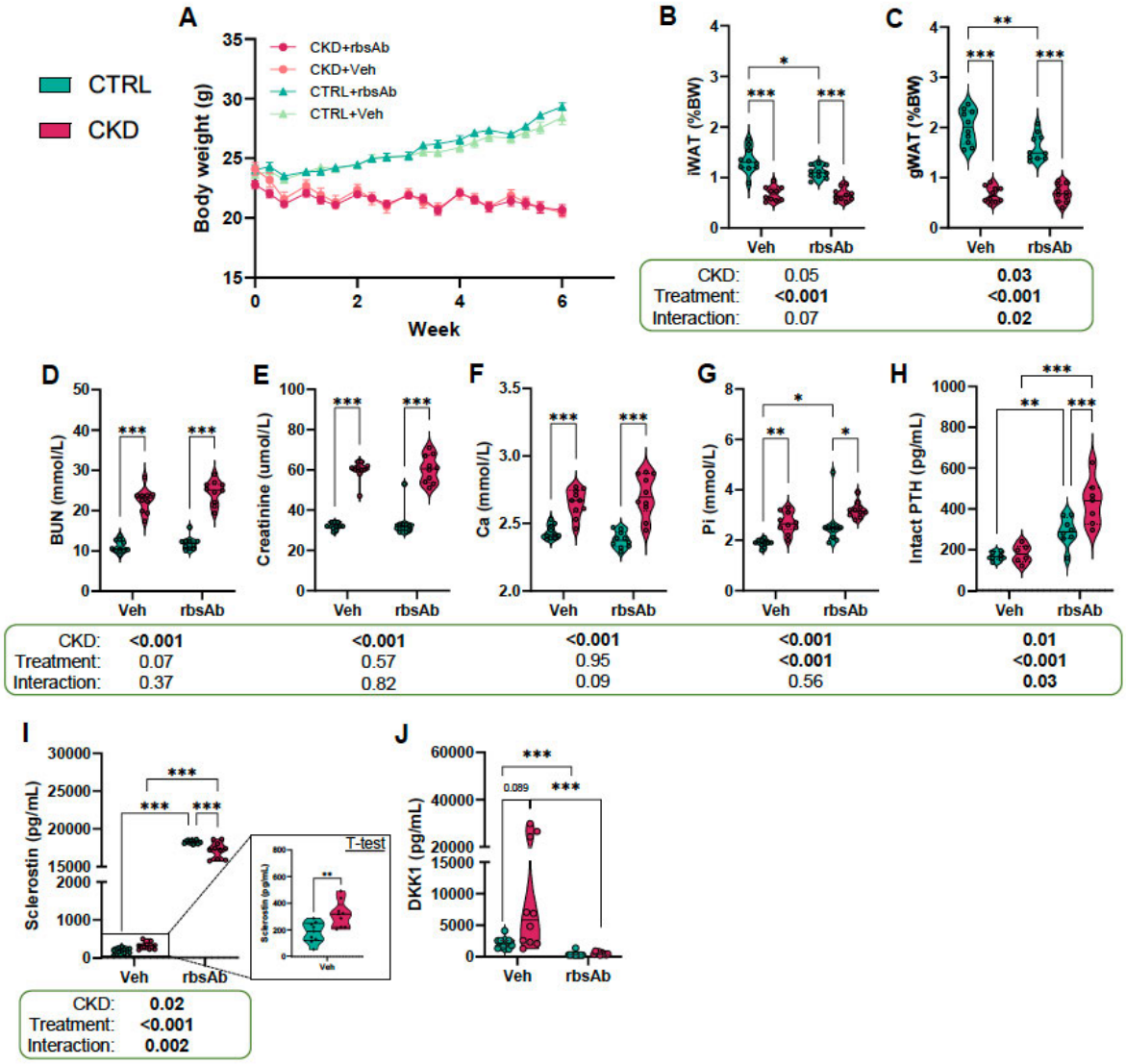

Figure 1. Validation of CKD development in adenine-treated mice and effect of rbsAb on plasma concentrations of sclerostin and DKK1. (A) Body weight of CKD mice was decreased over the 6weeks of the study. The administration of antibody to either CTRL or CKD mice had no additional effect on body weight. (B, C) Inguinal (iWAT) and gonadal (gWAT) white adipose depots were decreased in vehicle and antibody-treated CKD mice. (D – G) Plasma concentrations of blood urea nitrogen (BUN), creatinine, calcium (Ca) and phosphate (Pi) were increased in vehicle and antibodytreated CKD mice. Pi levels were increased in antibody-treated control, but not CKD, mice. (H) Plasma concentrations of PTH were similar in vehicle-treated control

and CKD mice but increased following antibody administration. (I, J) Plasma levels of sclerostin and DKK1 were both higher in vehicle-treated CKD compared to vehicle-treated control mice. The antibody lowered DKK1 levels in CTRL and CKD mice to levels that were indistinguishable from each other however sclerostin levels in antibodytreated mice were erronously high possibly due to cross-reactivity with the antigen-antibody complex and the sclerostin ELISA. For the data shown in the violin plots (C – I), significant effects of CKD, antibody treatment, and CKD - antibody treatment interaction were assessed using two-way ANOVA and overall p values for each variable, and their interactions, are shown beneath each graph. For plasma DKK1 data (J), the Mann–Whitney test with Bonferroni correction was used to test nonnormally distributed data. Significant differences between comparable groups were assessed using Tukey's multiple comparison test and are indicated by * $P < 0.05$, **$P < 0.01$ or ***$P < 0.001$.

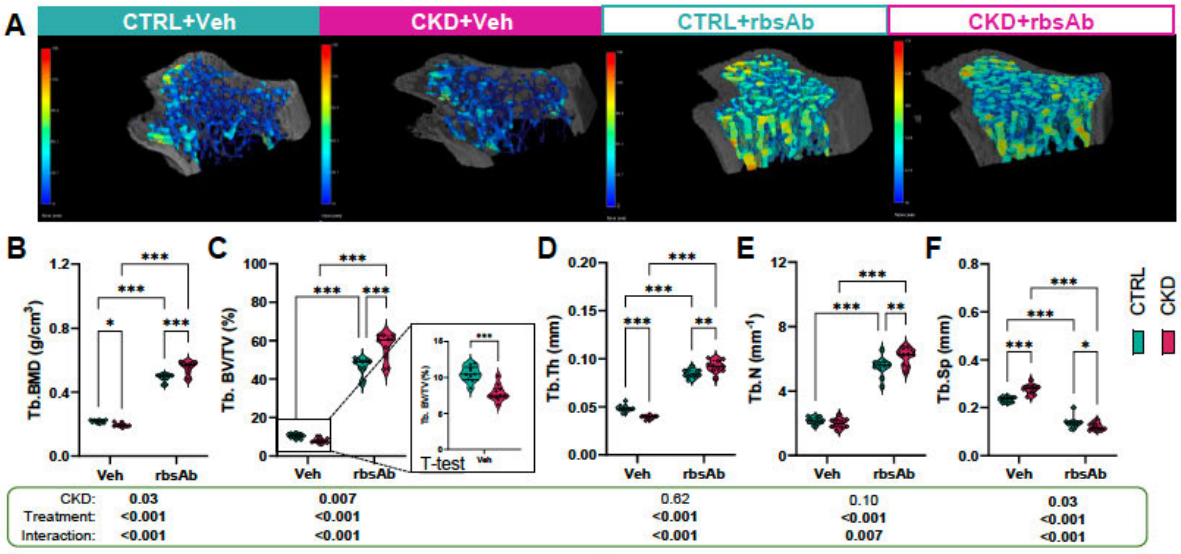

Figure 2. MicroCT analysis of tibial trabecular and cortical bone.

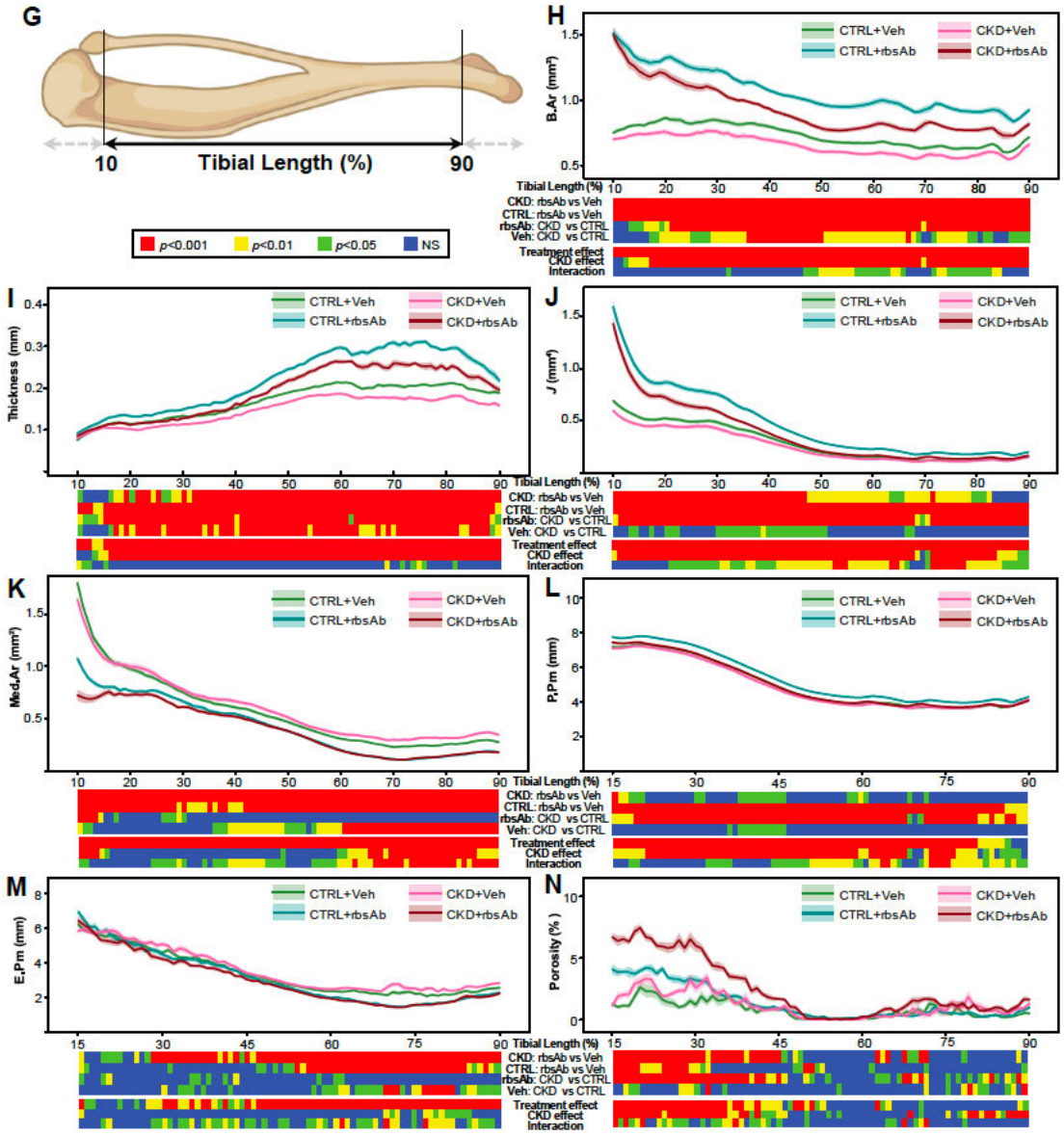

(Continued) Figure 2. MicroCT analysis of tibial trabecular and cortical bone. (A) Representative microCT images of trabecular bone from mice of the four experimental groups. The colour range represent the size of trabecular bone from big (red) to small (blue). Trabecular (Tb) (B) bone mineral density (BMD), (C) bone volume fraction (BV/TV), (D) thickness (Th) were decreased in vehicle-treated CKD mice whereas (F) Tb separation (Sp) was increased in vehicle-treated CKD mice. No effect on (E) Tb number (N) was observed. Although antibody treated increased Tb. BMD, BV/TV, Th, and N and decreased Tb.Sp in control and CKD mice the effect was greater in the CKD mice. (G – N) Quantification of whole cortical bone analysis excluding proximal and

distal metaphyseal bone (G). Cortical (H) bone area (B.Ar), (I) thickness, (J) polar moment of inertia (J) and (L) periosteal perimeter (P.Pm) of vehicletreated CKD mice were all reduced in various regions whereas (K) medullary area (Med.Ar), (M) endosteal perimeter (E.Pm) and (M) porosity were increased when compared to bones of vehicletreated CTRL mice. Antibody treatment increased B.Ar, thickness, P.Pm, porosity and J but reduced Med.Ar and E.Pm along the tibial length in both CTRL and CKD mice. For the data shown in the violin plots (B - F), significant effects of CKD, antibody treatment, and CKD – antibody treatment interaction were assessed using two-way ANOVA and overall p values for each variable, and their interactions, are shown beneath each graph. Significant differences between comparable groups were assess using Tukey's multiple comparison test and are indicated by * P < 0.05, **P < 0.01 or

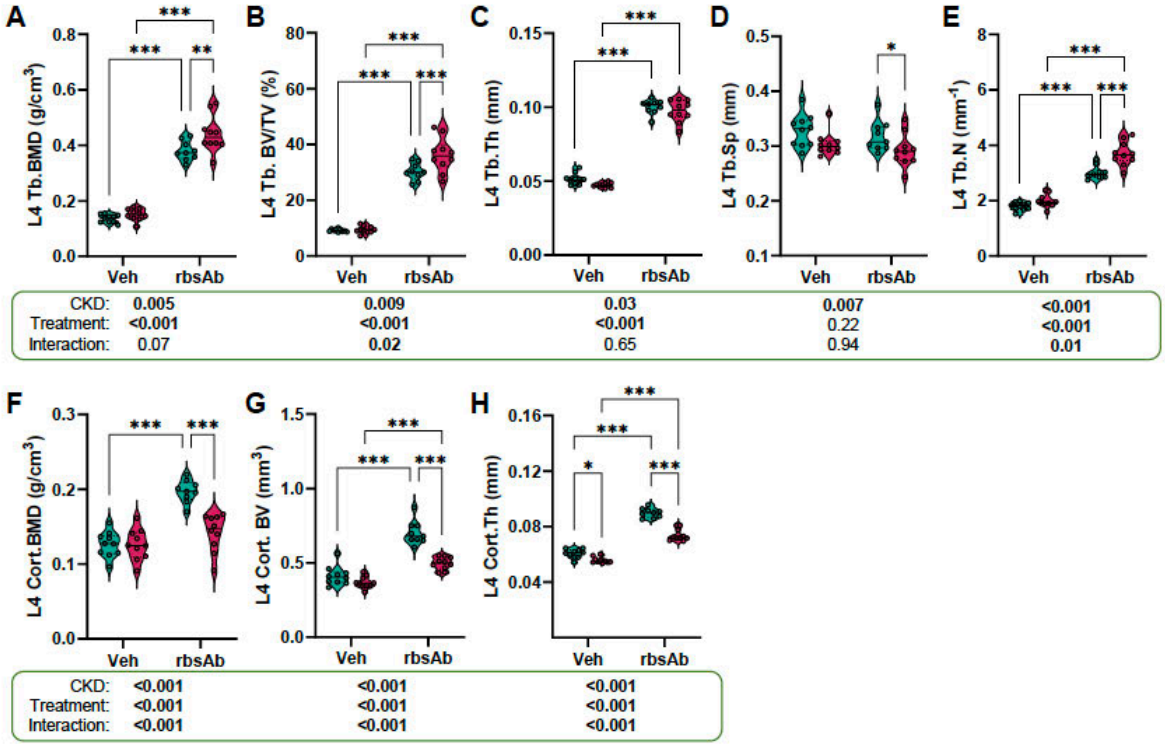

***P < 0.001.

Figure 3. MicroCT analysis of vertebrae trabecular and cortical bone and biomechanical properties of tibia and vertebrae.

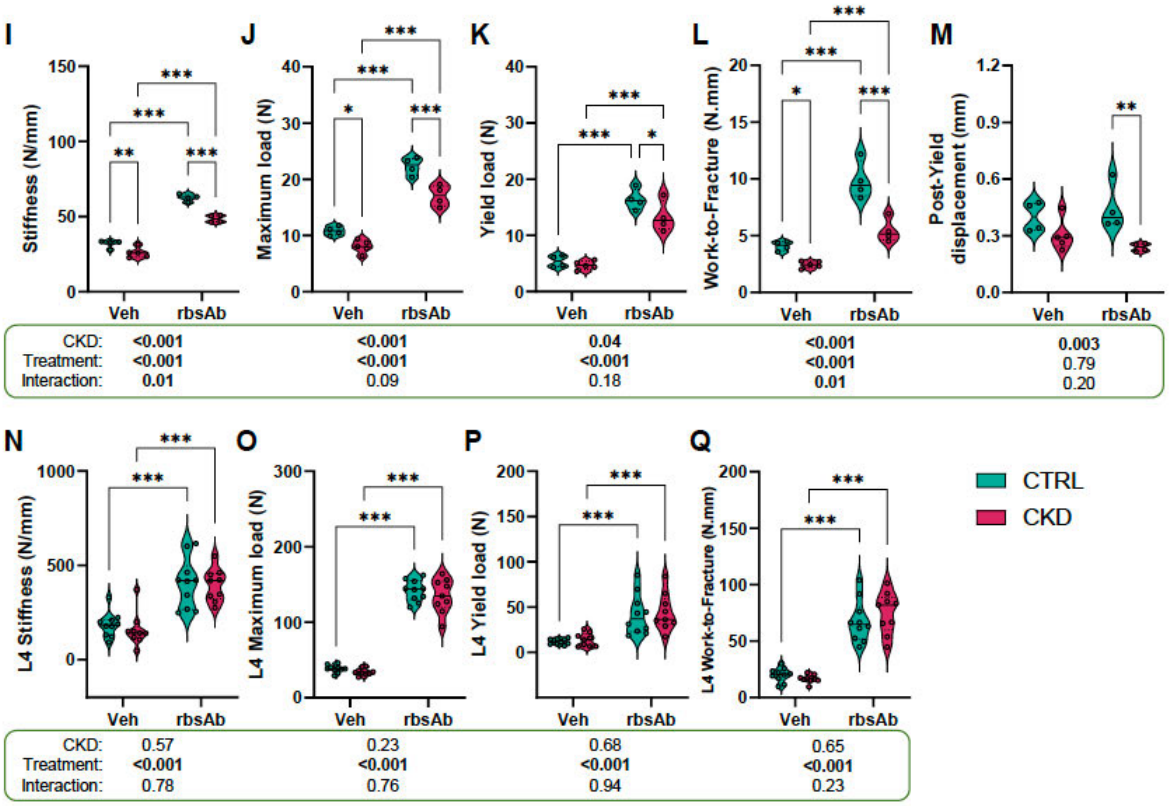

(Continued) Figure 3. MicroCT analysis of vertebrae trabecular and cortical bone and biomechanical properties of tibia and vertebrae. Analysis of (A – E) trabecular and (F – H) cortical bone indicated that only (H) cortical thickness of L4 vertebrae was affected in vehicle-treated CKD mice compared to similarly treated CTRL mice. Antibody administration increased trabecular (Tb) (A) bone mineral density (BMD), (B) bone volume fraction (BV/TV), (C) thickness (Th), (E) number (N) and cortical (Badr et al.) (F) BMD, (G) BV and (H) Th in CTRL and CKD mice whereas (D) Tb separation (sp) was unaffected. Biomechanical analysis indicated that femur (I) stiffness, (J) maximum load, (L) work to fracture but not (K) yield load were lower in vehicle-treated CKD mice when compared to their respective CTRLs and all biomechanical properties apart from (M) post-yield displacement were increased in CTRL and CKD mice treated with antibody. L4 vertebrae (N) stiffness, (O) maximum load, (P) yield load and (Q) work to fracture of vehicle-treated CTRL and CKD mice were similar and all biomechanical properties were increased in all mice treated with antibody. All data are shown as violin plots and significant effects of CKD, antibody treatment, and CKD – antibody treatment interaction were assessed using two-way ANOVA and overall p

values for each variable, and their interactions, are shown beneath each graph. Significant differences between comparable groups were assess using Tukey's multiple comparison test and are indicated by * P < 0.05, **P < 0.01 or ***P < 0.001.

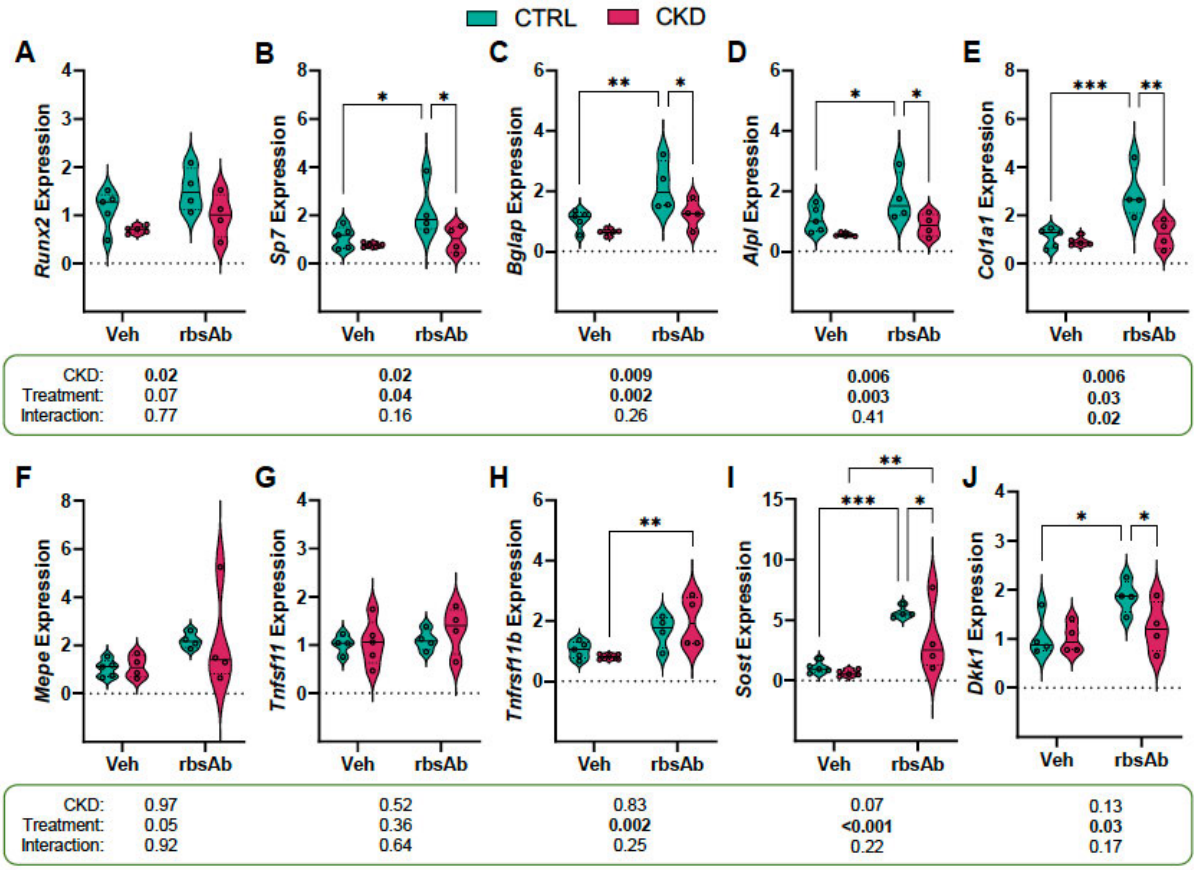

Figure 4. Osteogenic gene expression in cortical bone of the tibia. The expression of the osteoblast/osteocyte genes (A) *Runx2*, (B) *Sp7*, (C) *Bglap* (D) *Alpl* (E) *Col1a1* (F) *Mepe* (G) *Tnfsf11* (H) *Tnfrsf11b* (I) *Sost* and (J) *Dkk1* were similar in vehicle-treated CTRL and CKD mice. Antibody treatment increased the expression of *Sp7, Bglap, Alpl, Col1a1* and *Dkk1* in CTRL mice, *Tnfrsf11b* expression in CKD mice and *Sost* expression CTRL and CKD mice. *Runx2, Mepe* and *Tnfsf11* expression by CTRL and CKD mice were altered by antibody treatment. All data are shown as violin plots and significant effects of CKD, antibody treatment, and CKD – antibody treatment interaction were assessed using two-way ANOVA and overall p values for each variable, and their interactions, are shown beneath each graph. Significant differences between comparable

groups were assess using Tukey's multiple comparison test and are indicated by * P < 0.05, **P < 0.01 or ***P < 0.001.

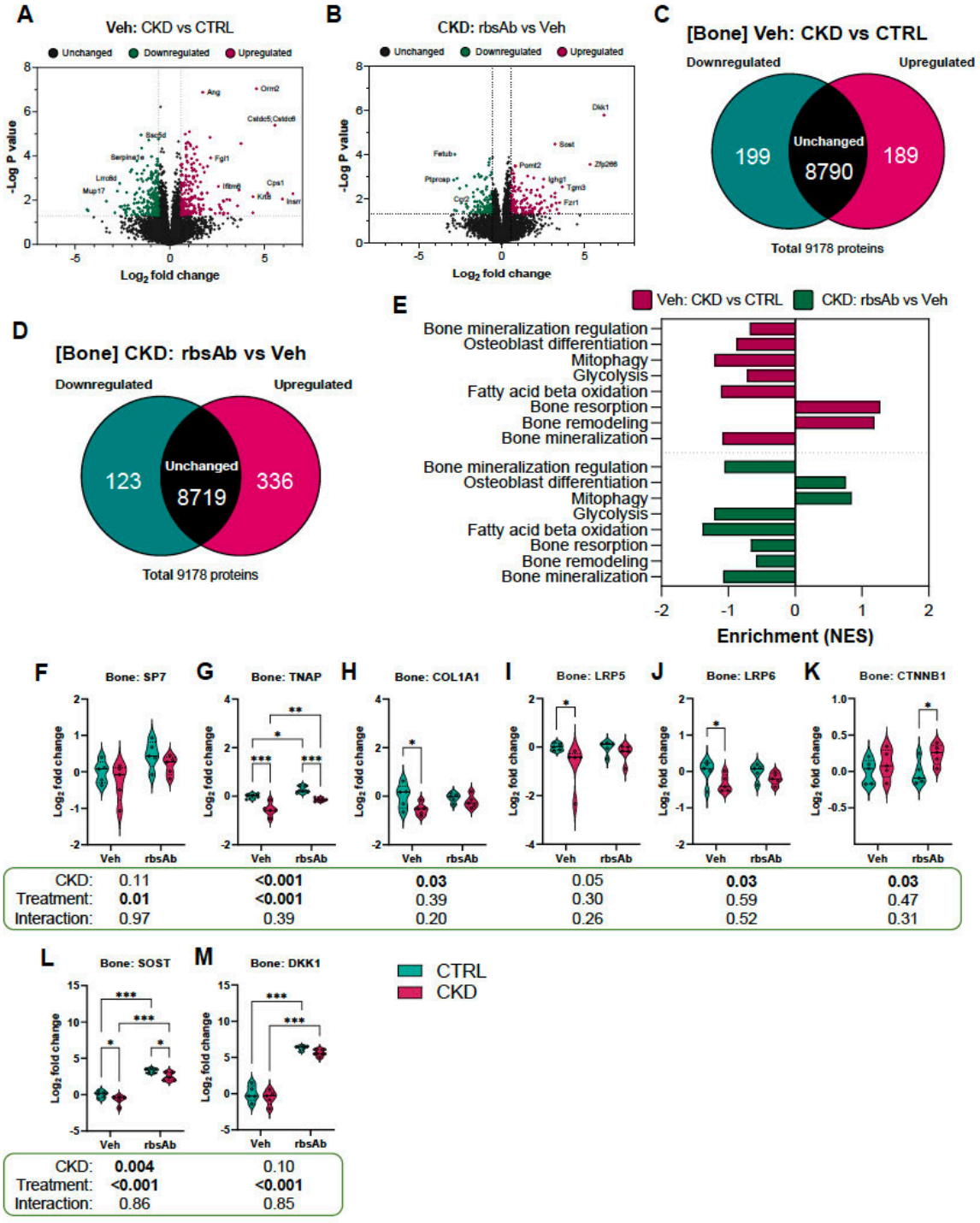

Figure 5. Proteomic profiling of cortical bone. (A, B) Volcano plots and (C, D) Venn diagrams illustrate global differential protein expression in the tibia of CKD mice and mice treated with antibody. (E) Gene set enrichment analysis identified the

osteoblast/osteocyte-related pathways implicated in the aetiology of ROD and those affected by antibody-treatment. From the proteomics analysis the expression of some of the significantly altered proteins associated with osteoblast differentiation such as (G) TNAP and (H) COL1A1, but not (F) SP7 were reduced in vehicle-treated CKD mice. The expression of proteins involved in Wnt-signalling, (I) LRP5, (J) LRP6, and (L) SOST were reduced in vehicle-treated CKD mice whereas (K) CTNNB1 and (M) DKK1 were unchanged. Antibody treatment increased (G) TNAP, (L) SOST and (M) DKK1 expression in both control and CKD bones. Comparison of the expression of individual protein are shown as violin plots and significant effects of CKD, antibody treatment, and CKD – antibody treatment interaction were assessed using two-way ANOVA and overall p values for each variable, and their interactions, are shown beneath each graph. Significant differences between comparable groups were assessed using Tukey's multiple comparison test and are indicated by * $P < 0.05$, ** $P < 0.01$ or *** $P < 0.001$.

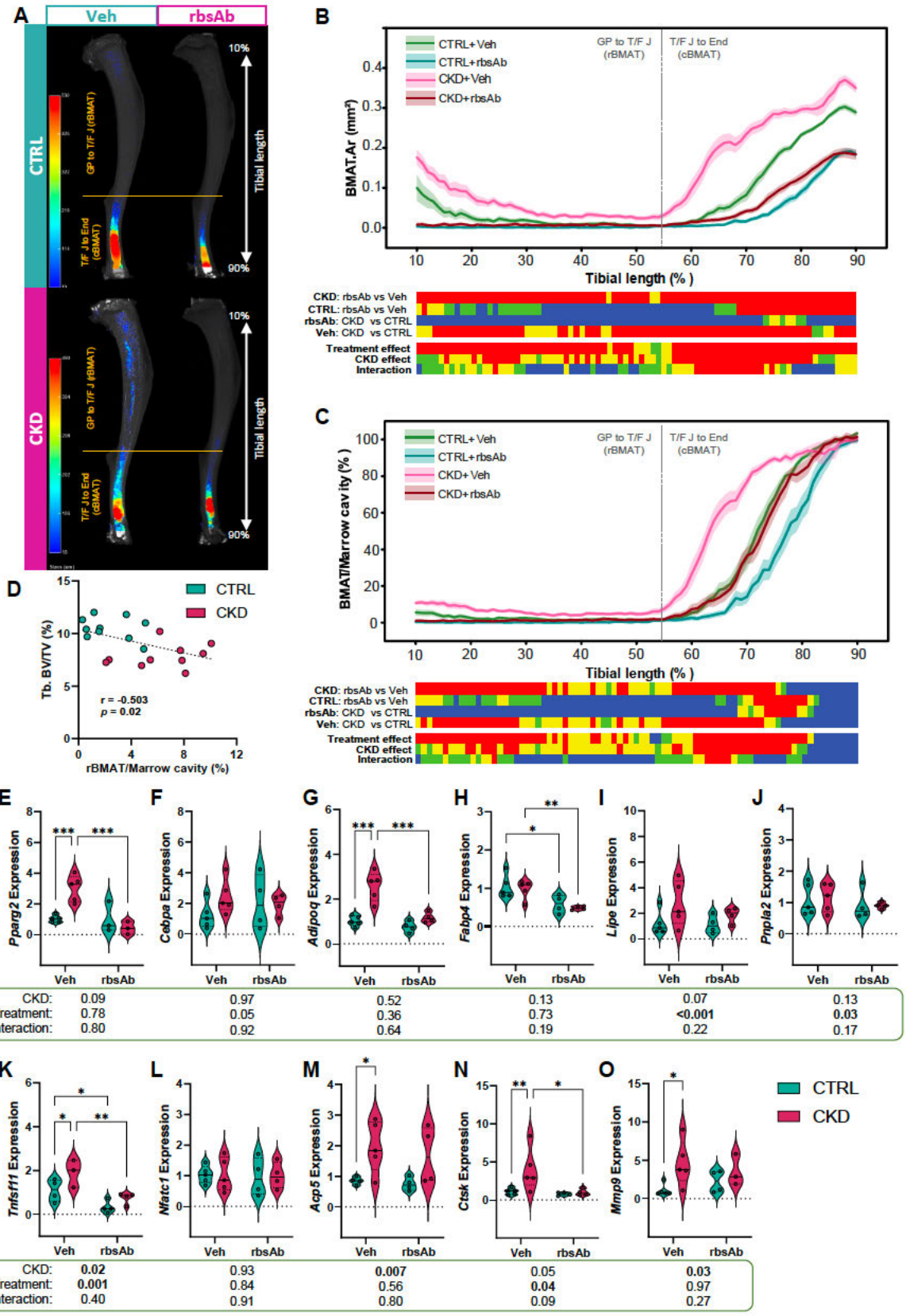

Figure 6. BMAT distribution along the tibial bone shaft and adipogenic and

osteoclastogenic gene expression in bone marrow tissue. (A) Visualisation of osmium-stained bone marrow adipose tissue (BMAT) present between the growth plate to tibia/fibula junction (GP-T/F J), which contains regulated BMAT (rBMAT) and the tibia/fibula junction to the end of distal bone (T/F J-End), which contains constitutive BMAT (cBMAT) of vehicle and antibody treated CTRL and CKD mice. (B) Total BMAT and (C) BMAT normalised to bone marrow area (with trabecular bone excluded) was increased in vehicletreated CKD mice compared to similarly treated CTRL mice. Antibody treatment reduced BMAT accumulation along the entire length of the tibia of CTRL and CKD mice. (D) Spearman correlations between trabecular bone volume fraction (Tb.BV/TV) and rBMAT indicated a negative correlation. The expression of the adipogenic genes (E) *Pparg2* and (G) *Adipoq* but not (F) *Cebpa*, (H) *Fabp4*, (I) *Lipe* or (J) *Pnpla2* was increased in vehicle-treated CKD mice. Antibody treatment had no effect on the expression of *Cebpa, Lipe* or *Pnpla2* but the difference in expression of *Pparg2* and *Adipoq* seen in the vehicle-treated mice was abolished by antibody treatment. The expression of osteoclast genes (K) *Tnfsf11,* (M) *Acp5,* (N) *Ctsk,* and (O) *Mmp9* was increased in vehicle-treated CKD mice and this difference in expression was nullified by antibody treatment. (L) *Nfatc1*, was similar in CTRL and CKD samples and was not affected by antibody treatment. For the data shown in the violin plots (E - O) the significant effects of CKD, antibody treatment, and CKD – antibody treatment interaction were assessed using two-way ANOVA and overall p values for each variable, and their interactions, are shown beneath each graph. Significant differences between comparable groups were assess using Tukey's multiple comparison test and are indicated by * $P < 0.05$, ** $P < 0.01$ or *** $P < 0.001$.

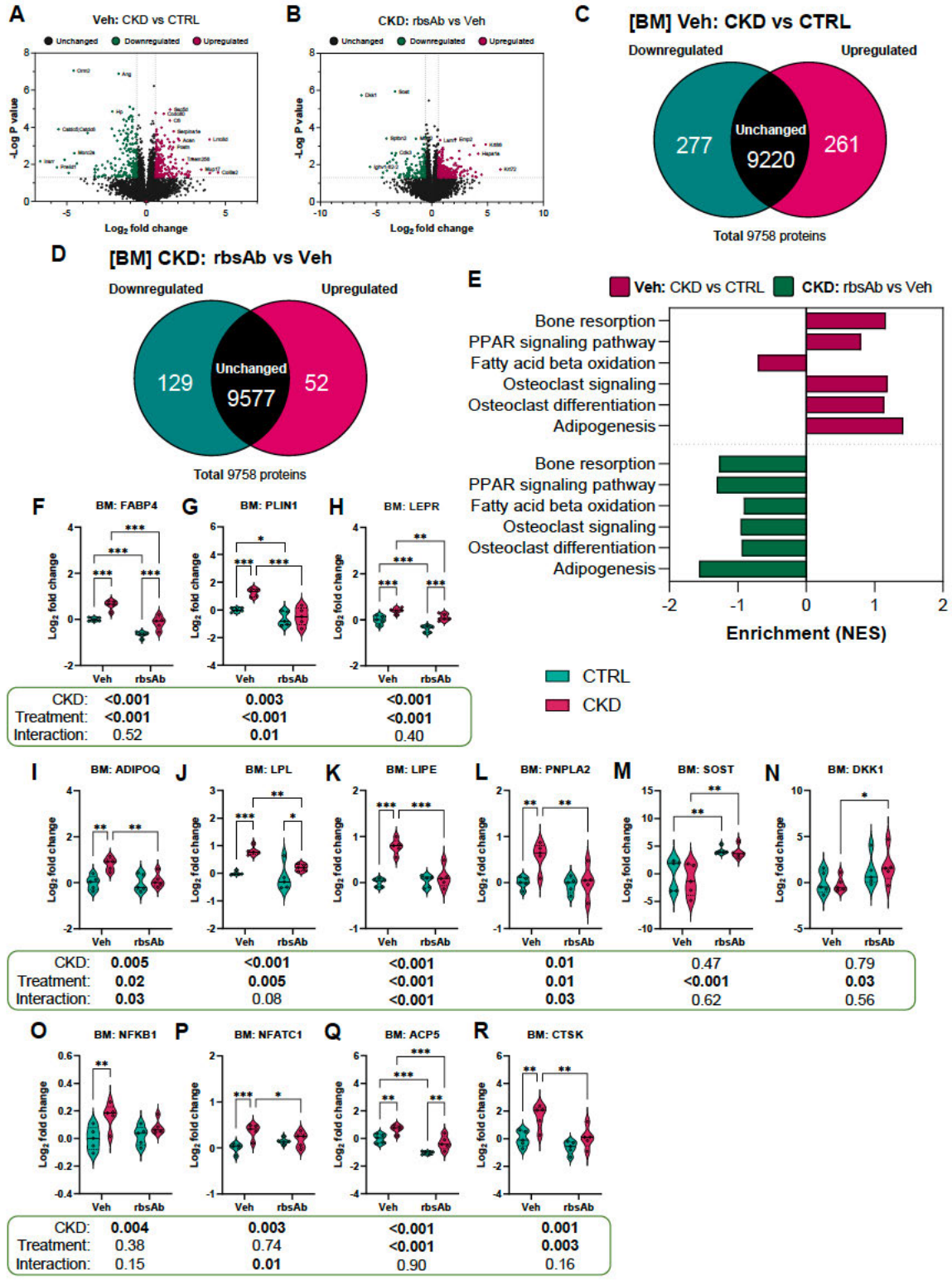

Figure 7. Proteomic profiling of bone marrow. (A, B) Volcano plots and (C, D) Venn diagrams illustrate global differential protein expression in the bone marrow of CKD mice and mice treated with antibody. (E) Gene set enrichment analysis revealed that

gene sets associated with adipogenesis, osteoclast differentiation and signalling, and bone resorption pathways were enriched in vehicle-treated CKD mice as compared to similarly treated CTRL mice. Antibody treatment reversed these pathway changes in CKD mice. The expression of proteins associated with adipocyte differentiation including (F) FABP4, (G) PLIN1, (H) LEPR, (I) ADIPOQ and (J) LPL and lipolytic protein, (K) LIPE and (L) PNPLA2 were increased in vehicle-treated CKD mice compared to vehicle-treated control mice. This increased expression was decreased by antibody treatment. In addition, CKD increased the expression of (O) NFKB1, (P) NFATC1, (Q) ACP5 and (R) CTSK which are critical for osteoclast differentiation and bone resorption, while antibody treatment normalized (O) NFKB, (P) NFATC and (R) CTSK but not (Q) ACP5. (M and N) SOST and DKK1 expression was similar in vehicle-treated CTRL and CKD mice and increased with antibody treatment. Comparison of the expression of individual protein are shown as violin plots and significant effects of CKD, antibody treatment, and CKD – antibody treatment interaction were assessed using two-way ANOVA and overall p values for each variable, and their interactions, are shown beneath each graph. Significant differences between comparable groups were assessed using Tukey's multiple comparison test and are indicated by * P < 0.05, **P < 0.01 or ***P < 0.001.

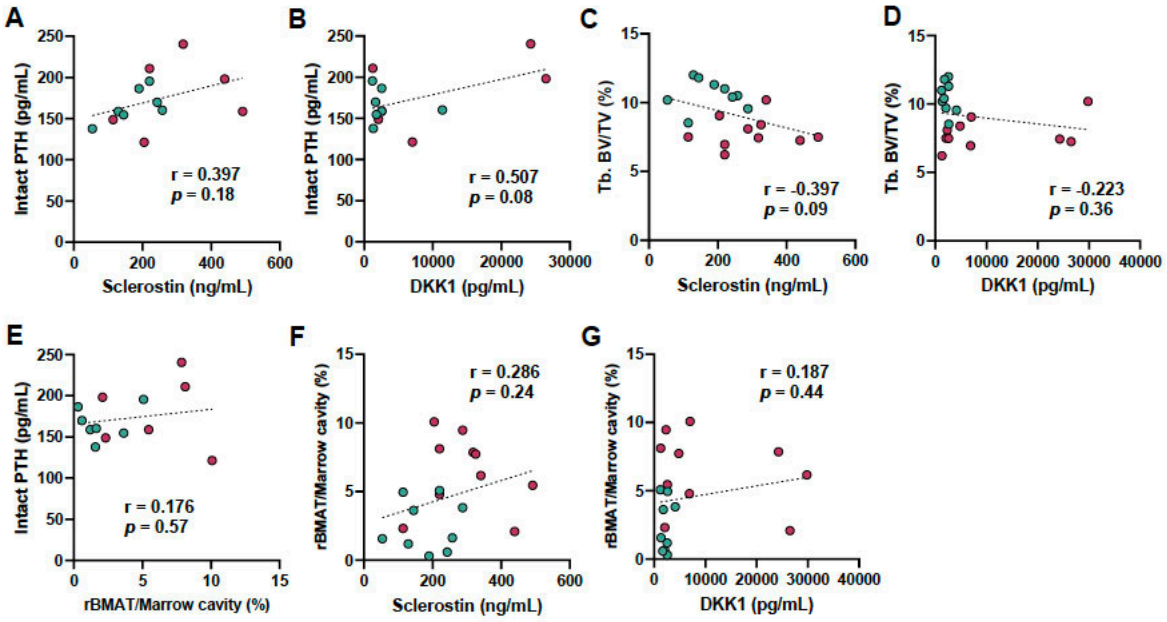

Suppl Figure 1. Correlation analysis. No correlation was found between plasma sclerostin and (C) trabecular bone volume fraction (Tb.BV/TV) and (F) rBMAT or

between plasma DKK1 and (D) trabecular bone volume fraction (Tb.BV/TV) and (G) rBMAT. No correlation was found between (E) rBMAT and plasma PTH. Correlations between individual parameters were performed using Spearman correlation.

Supplementary Table 1 Primers for qPCR

Gene	Forward (5`-3`)	Reverse (5`-3`)
Adipoq	AAGAAGGACAAGGCCGTTCTCTT	GCTATGGGTAGTTGCAGTCAGTT
Cebpa	TGGACAAGAACAGCAACGAG	TCACTGGTCAACTCCAGCAC
Fabp4	TGGAAGCTTGTCTCCAGTGA	AATCCCCATTTACGCTGATG
Lipe	CCTTGTGGCTTGCGCTCTGGA	CCGCGCGAACATGACCGAGT
Pparg2	CCAGAGCATGGTGCCTTCGC	TTCCGAAGTTGGTGGGCCAGA
Pnpla2	CGGCTTCCTCGGGGTCTAC	CGCGCTCATGGCAATCAG
Runx2	ACCATAACAGTCTTCACAAATCCT	CAGGCGATCAGAGAACAAACTA
Sp7	ATGGCGTCCTCTCTGCTTG	TGAAAGGTCAGCGTATGGCTT
Col1a1	ACATGTTCAGCTTTGTGGACC	TAGGCCATTGTGTATGCAGC
Alpl	GGGACGAATCTCAGGGTACA	AGTAACTGGGGTCTCTCTC
Mepe	AGAAATATCACGCAGCCTGTAA	GGAGACTTAGCATCATTGACATC
Bglap	CCGGGAGCAGTGTGAGCTTA	TAGATGCGTTTGTAGGCGGTC
Tnfrsf11b	CCTTGCCCTGACCACTCTTA	CACACACTCGGTTGTGGGT
Tnfsf11	CAGCATCGCTCTGTTCCTGTA	CTGCGTTTTCATGGAGTCTCA
sost	TGAGAACAACCAGACCATGAAC	TCAGGAAGCGGGTGTAGTG
Dkk1	CCGGGAACTACTGCAAAAAT	CCAAGGTTTTCAATGATGCTT
Ctsk	GAAGAAGACTCACCAGAAGCAG	TCCAGGTTATGGGCAGAGATT
Mmp9	CAAAGACCTGAAAACCTCCAAC	GACTGCTTCTCTCCCATCATC
Acp5	AGCAGCCAAGGAGGACTACG	TGGCTAACAATGGTCGCAAG
Nfatc1	GGCTGGTCTTCCGAGTTCACATC	GCTGTCTGTGCTCTGCTTCTCC
Ppia	CACCGTGTTCTTCGACATCA	CAGTGCTCAGAGCTCGAAAGT

Conclusion

This chapter examined whether a bispecific antibody targeting both sclerostin and DKK1 could prevent bone loss and BMAT accumulation in a CKD mouse model. Young adult male mice were fed an adenine diet to induce CKD and received a subcutaneous antibody injection for six weeks. The antibody, provided generously by Angitia Biopharmaceuticals (via Hua Zhu Ke and Xiaofeng Liu), was administered alongside body weight monitoring throughout the study. At the end, CKD was characterised, and plasma levels of sclerostin and DKK1 were measured. Bone architecture and BMAT accumulation, stained with osmium, were quantified through microCT. The study also evaluated the mechanical properties of femurs and vertebrae, as well as gene expression and proteomics profiles of osteogenic and adipogenic markers to understand the molecular changes. Based on the results in this chapter, the conclusion can be summarised as follows:

1. CKD progression was similar in the vehicle and rbsAb treatment.
2. Plasma levels of sclerostin and DKK1 were elevated in CKD mice, and DKK1 levels were reduced by rbsAb treatment.
3. The rbsAb prevented bone loss in tibia of CKD mice with a predominantly anabolic effect on the trabecular compartment.
4. Vertebral bone loss was not observed in the CKD mice, but the rbsAb improved vertebral bone health in both CKD and control mice indicating that the influence of CKD on bone appeared to be site dependent.
5. The rbsAb improved the mechanical properties in both the vertebrae and the femur of CKD mice.
6. Gene and proteomics profiles revealed the mechanism by which rbsAb prevents CKD-induced osteoblast dysdifferentiation.
7. The rbsAb prevented BMAT accumulation in CKD mice.
8. The rbsAb treatment normalised CKD-induced adipogenic and osteoclastic gene and protein expressions.

This study introduced a novel therapeutic strategy for preventing CKD-MBD. However, the impact of this antibody treatment on reversing bone pathogenesis of ROD

in the advance stages of CKD should be considered. Additionally, experiments involving BMSC lineage tracing should be undertaken to determine whether sclerostin and DKK1 are key mediators of BMSC differentiation towards adipocytes during CKD progression. Moreover, the longitudinal study should be performed to more the underlying mechanism of BMAT expansion together with bone loss during the CKD progression. Furthermore, potential adverse effects of this antibody treatment on the cardiovascular system in CKD conditions should also be acknowledged. These gaps in our knowledge will form the focus of my future research.

Chapter 6

Discussion and future work

General discussion

It is well established that CKD is accompanied by skeletal deterioration that increases the risks of osteoporosis and fragility fractures (Tariq & Sulaiman, 2020). In experimental CKD-MBD models, bone loss and high circulating bone-turnover markers are common, and chronically elevated PTH is often considered central to the development of ROD (Hsu et al., 2022; Jadoul et al., 2006; Nickolas et al., 2013). However, fracture risk is also higher in patients with low or normal PTH (Coco & Rush, 2000; Massy & Drueke, 2017), indicating that additional mechanisms, beyond SHPT, such as uremic toxin-induced mitochondrial injury and broader changes in the bone marrow niche, contribute to ROD. Furthermore, a consistent feature emerging from both animal and human studies is the expansion of BMAT as shown in this thesis and by others (Moorthi et al., 2015; Ni et al., 2019; Wang et al., 2017; Woods et al., 2018). Since BMSCs can develop into both osteoblasts and adipocytes, shifts in lineage that favour adipogenesis are likely to reduce osteoblastogenesis and impair bone formation; such "see-saw" dynamics have been seen in osteopenia/osteoporosis (Morris et al., 2024; Yeung et al., 2005), ageing (Shen et al., 2007; Xu et al., 2025), obesity (Ambrosi et al., 2017), and CR (L. Liu et al., 2024). This thesis investigates three interconnected aspects of CKD bone pathology: (i) the timing and implications of BMAT expansion during disease progression (Chapter 3); (ii) the direct effects of systemic CKD-associated factors (PTH, Pi, FGF23, sclerostin, and IS) on BMSC fate decisions (Chapter 4); and (iii) the therapeutic potential of jointly neutralising the osteocytic Wnt antagonists sclerostin and DKK1 with a bispecific antibody, rbsAb, to enhance bone structure and biomechanics and prevent BMAT accumulation (Chapter 5). Collectively, these chapters support a model where CKD-related systemic cues and marrow-intrinsic changes drive early BMAT expansion, disrupt bone remodelling signals, and escalate skeletal fragility. Finally, the results also demonstrate that the neutralisation of both sclerostin and DKK1 more effectively restores bone mass and reduces BMAT than inhibiting sclerostin alone.

In the longitudinal adenine-induced CKD model, BMAT expansion increased with CKD severity and was inversely associated with trabecular bone mass, aligning with previous clinical and preclinical findings (Borelli et al., 2023; Moorthi et al., 2015;

Sirimongkolchaiyakul et al., 2021; Woods et al., 2018). Notably, BMAT accumulation occurred before detectable trabecular bone loss. By week 3, when body weight loss and biochemical CKD markers appeared, total BMAT and marrow expression of *Fabp4* and *Adipoq* were already elevated, while trabecular BMD, BV/TV, trabecular number/thickness, and connectivity remained unchanged. This sequence of events suggests that BMAT expansion is not merely a consequence of bone loss; it may serve as an initiating or priming event in CKD-related skeletal deterioration. An inverse relationship between bone mass and BMAT was also observed in the CKD mice studied here and reflects clinical patterns in both adult and pediatric CKD (Borelli et al., 2023; Sirimongkolchaiyakul et al., 2021).

Several mechanisms could explain this coupling. A shift in lineage allocation from osteoblastogenesis to adipogenesis remains a compelling explanation for BMAT expansion in CKD. The CKD mice also exhibited higher serum adiponectin levels, mirroring human CKD, where adiponectin correlates with renal dysfunction (Song et al., 2020), and marrow *Adipoq* up-regulation, supporting BMAT as a plausible source. The link between adiponectin and BMAT volume mirrors CR models, where marrow adipocytes contribute to circulating adiponectin (Cawthorn et al., 2016), although contributions from WAT cannot be entirely ruled out. However, the reduction in subcutaneous and visceral fat depots, along with the known behaviour of WAT in CR, suggests that BMAT probably plays a primary role (Cawthorn et al., 2016; Perry et al., 2018). Conversely, circulating leptin, mainly WAT-derived, was decreased, likely reflecting reduced fat mass and food intake (Perry et al., 2018). In contrast, low leptin has been associated with increased BMAT and decreased BMD in ob/ob mice (Hamrick et al., 2004), and CR studies suggest hypoleptinemia alone is neither necessary nor sufficient for BMAT expansion (Cawthorn et al., 2016). These patterns point to BMAT-intrinsic (and possibly feed-forward) mechanisms, with adipokines modulating marrow microenvironments that promote adipogenesis and/or resorption (Fu et al., 2005).

BMAT may also affect bone remodelling more directly. Increased *Tnfsf11* (RANKL) expression in CKD marrow was observed without a corresponding rise in *Tnfrsf11b* (OPG), which aligns with BMAT-derived RANKL playing a role in

osteoclastogenesis and bone resorption (Li et al., 2018). Clinical data linking marrow fat to vertebral fracture risk, independent of BMD in ageing adults (Rinotas et al., 2024; Schwartz et al., 2013), and *TNFSF11* expression with marrow adiposity (Xu et al., 2025) support a functional link between BMAT and bone fragility. Whether BMAT is independently related to fractures in CKD remains to be determined.

Importantly, these longitudinal observations also reveal that BMAT expansion can happen without immediate bone loss, and bone loss can occur without simultaneous BMAT increases, as observed in CR models (Cawthorn et al., 2016; Ziru Li et al., 2022; Rosen et al., 2009). Recent identification of separate BMSC subpopulations (Deng et al., 2021) also questions the idea of strictly reciprocal osteogenic–adipogenic commitment. Definitive lineage-tracing experiments employing inducible Cre lines that label pre-commitment stromal populations (e.g., Cxcl12-CreE) (Zhong et al., 2020) will be essential to determine whether BMAT expansion results from lineage skewing, progenitor depletion, survival or proliferation defects, or paracrine re-programming of the niche.

In CKD progression, several factors are elevated and thought to be linked with ROD phenotypes, such as PTH, Pi, FGF23, sclerostin, and IS. Examining their effects on BMSC commitment and differentiation could help clarify the molecular mechanisms behind this complication. An *in vitro* study (chapter 4) showed that PTH did not significantly influence adipogenic differentiation; expression of *Pparg2*, *Cebpa*, *Adipoq*, and *Pnpla2* remained stable, contrasting with reports that intermittent PTH reduces adipogenesis in human and rodent systems (Fan et al., 2017; Maridas et al., 2018; Rickard et al., 2006; Yang et al., 2019). Conversely, PTH promoted osteogenesis, up-regulating *Sp7*, *Runx2*, *Alpl*, and *Tnfrsf11b* (OPG) expression at doses up to approximately 1 ng/mL, consistent with cAMP/PKA–PKCδ signalling and LRP6 engagement (Kuo et al., 2017; Yu et al., 2012). The diminished response at 5 ng/mL aligns with its biphasic behaviour (Locklin et al., 2003), and the transient rise in *Tnfsf11* at the lowest PTH levels supports the idea that early, controlled osteoclastogenesis facilitates anabolic remodelling (Walker et al., 2012). Notably, although PTH exposure was nominally continuous, the approximately 10–12-hour half-life of bovine PTH likely created a pseudo-intermittent profile, resembling traditional intermittent protocols and explaining the net anabolic effect

despite catabolic associations in CKD (Houston et al., 2016; Ishizuya et al., 1997; Lotinun et al., 2002).

High extracellular Pi suppressed adipogenic transcription (*Pparg2*, *Adipoq*, and, at the highest dose, *Fabp4*), supporting a role for Pi as a signalling cue that reprograms BMSC gene networks (Qin et al., 2025). These observations align with *in vivo* findings that Pi restriction increases BMAT (Ko et al., 2016) and with mechanistic studies showing that phosphate deprivation promotes adipogenesis of CXCL12-abundant reticular cells via Pparg/Cebpa upregulation and impaired mTORC1 signalling (Ko et al., 2021). Higher *Tnfrsf11b* (OPG) expression with Pi was also observed, consistent with classical phosphate-induced OPG upregulation, thereby shifting the RANKL/OPG balance towards reduced resorption (Kanatani et al., 2003). While early osteogenic markers were not strongly induced over 21 days, short-term exposure to 4–10 mM Pi can promote osteoblast differentiation and mineralisation (Lin et al., 2021), suggesting dose–time thresholds are critical. In contrast, FGF23, despite its endocrine role in phosphate/vitamin D homeostasis, did not alter adipogenic or osteogenic commitment across the tested range, which is expected given low Klotho levels in BMSCs and the Klotho dependency of effective FGF23 signalling (Bär et al., 2019; Li et al., 2013; Shimada et al., 2004; Shimada et al., 2001; Urakawa et al., 2006). Systemically, however, elevated FGF23 may still influence bone via phosphate handling, SHPT, and broader metabolic disturbances (Aguilar et al., 2023; Wolf, 2012).

Sclerostin exerted little direct influence on lineage commitment under these conditions: *Pparg2* and *Cebpa* remained unchanged, and only a small, non-linear increase in *Adipoq* was observed at a low dose, indicating a subtle terminal differentiation effect rather than a switch in cell fate. Under osteogenic conditions, canonical markers did not change, whereas Tnfsf11 increased at 5 ng/mL, consistent with sclerostin's modulation of RANKL/OPG and bone remodelling (Iwamoto et al., 2022; Wijenayaka et al., 2011). Reports of sclerostin-enhanced adipogenesis in 3T3-L1 and murine BMSCs (Fairfield et al., 2018; Kim et al., 2017) likely reflect differences in species, cell source, and experimental context; in strongly pro-osteogenic media, sclerostin alone was insufficient to override differentiation cues. Conversely, IS broadly suppresses both adipogenic

(*Pparg2*, *Cebpa*, *Fabp4*, *Adipoq*, *Pnpla2*) and osteogenic (*Runx2*, *Sp7*, *Alpl*) programmes while increasing Tnfsf11 without affecting Tnfrsf11b, suggesting a higher RANKL/OPG ratio that favours resorption. These findings align with reports of IS impairing osteoblastogenesis and mineralisation (Hsieh et al., 2024; Kamprom et al., 2021; Kim et al., 2013) and augmenting osteoclastogenesis (Liu et al., 2020), reflecting CKD-associated high turnover, cortical porosity, and fragility (Metzger et al., 2024; Metzger et al., 2021; Moe et al., 2015). Although toxicity remains a concern, IS ≤ 2 mM is not overtly toxic to murine osteoblasts over seven days (Hsu et al., 2025). Mechanistically, IS and related uremic toxins induce oxidative stress, mitophagy, and mitochondrial damage—likely drivers of broad differentiation impairments (Hsu et al., 2025; McWilliams et al., 2016; Popkov et al., 2019; Watanabe et al., 2017).

Osteocytes, the primary source of sclerostin expression, were studied to determine whether high Pi and IS affect sclerostin expression using MLO-Y4 cells. These readouts appeared dependent on the osteocyte model studied. In MLO-Y4 cells, as used in this thesis, neither high Pi nor IS altered *Sost* expression, likely reflecting the low or absent baseline *Sost/Fgf23* in 2D culture and the requirement for bone-mimetic 3D scaffolds to restore osteocytic transcription (Brady et al., 2022; Zhang et al., 2019). In a more mature model (IDG-SW3), IS increased *Sost* and *Dkk1* expression (Chen et al., 2024), whereas high Pi had no effect on *Sost* expression by primary osteocytes (Miyagawa et al., 2014). These comparisons highlight that conclusions about Pi and uremic toxin effects on osteocyte Wnt antagonists depend critically on cellular maturity and culture context, emphasising the importance of using bone-mimetic systems to infer *in vivo* osteocytic regulation.

Clinically, ROD management focuses on controlling SHPT with calcitriol and calcimimetics (Block et al., 2004; Slatopolsky et al., 1984), but PTH alone is a poor predictor of bone turnover status (Coco & Rush, 2000). Traditional osteoporosis treatments can improve BMD and reduce fractures in mild-to-moderate CKD, though each has potential limitations—bisphosphonates may accumulate with low clearance and pose risks in very-low-turnover bone (Jamal et al., 2007; Miller et al., 2005); denosumab (anti-RANKL) can cause hypocalcemia, and PTH analogues (teriparatide) may worsen

hyperparathyroidism (Haarhaus et al., 2023; Hara et al., 2021; Nitta et al., 2017; Whitlock et al., 2024). Since sclerostin and DKK1 are elevated in CKD bone and/or serum (Cejka et al., 2014; Graciolli et al., 2017; Kanbay et al., 2014; Sabbagh et al., 2012), Wnt disinhibition emerges as an appealing anabolic strategy. Romosozumab (anti-sclerostin) reduces fracture risk (post-hoc CKD evidence from FRAME/ARCH) (Appelman-Dijkstra & Papapoulos, 2016; Cosman et al., 2016; McClung et al., 2014) and improves bone in models of diabetes and CKD (Kohler et al., 2024; Marino et al., 2023). However, blockade of sclerostin alone can lead to compensatory up-regulation of DKK1, which diminishes the anabolic response (Adami et al., 2025; Florio et al., 2016; Holdsworth et al., 2018; Moe et al., 2015).

In this thesis (chapter 5), the bispecific antibody targeting sclerostin and DKK1, rbsAb, produced significant improvements in cortical geometry and trabecular architecture in the vertebrae and long bones of both control and CKD mice. These effects were accompanied by gene-set signatures indicating increased osteoblast differentiation and decreased resorption. These results exceeded those reported for sclerostin-only treatment in CKD rats, where benefits were extremely limited and PTH-dependent (Moe et al., 2015; Newman et al., 2015). This aligns with previous studies showing that dual targeting outperforms monotherapy in rodents and primates (Bienvenu et al., 2024; Florio et al., 2016; Florio et al., 2023; M. Liu et al., 2018), and that a 3:1 Scl-Ab: DKK1-Ab mixture yields considerably more trabecular bone than Scl-Ab alone (R. B. Choi et al., 2021; Florio et al., 2016; Li et al., 2011; Witcher et al., 2018). An increase in cortical porosity with rbsAb was unexpected, especially given the similar cortical porosity in *Sost*$^{-/-}$ versus WT mice (Mosey et al., 2017). This warrants mechanistic follow-up, such as modelling the remodelling balance, cortical drift, and microdamage repair dynamics under potent Wnt activation.

Notably, rbsAb reduced BMAT along the tibial length in both control and CKD mice. While Wnt/β-catenin signalling is recognised to suppress adipogenic programmes via C/EBPα and PPARγ in white adipocytes and to redirect pre-osteoblast fate away from adipocytes (Ross et al., 2000; Song et al., 2012), its regulation of BMAT has been less clear. Circulating sclerostin levels positively correlate with vertebral marrow fat in

men and *in vitro* studies, sclerostin promotes adipogenesis (Fairfield et al., 2018; Ma et al., 2014). In contrast, sclerostin deficiency reduces BMAT accumulation in mice (Fairfield et al., 2018). Clinical data in postmenopausal women reported no change in iliac crest BMAT with romosozumab treatment, and Scl-Ab modestly reduced BMAT accumulation, and is specific regions only in irradiated or rosiglitazone-treated mice (Chavassieux et al., 2024; Costa et al., 2021; Farrell et al., 2021). In this thesis, the rbsAb decreasedBMAT accumulation even after normalisation to marrow area, implying a direct anti-adipogenic effect of dual Wnt disinhibition in marrow adipocytes, not solely a geometric consequence of decreased bone marrow volume. In contrast, Scl-Ab alone did not reduce area-normalised BMAT in rats (Costa et al., 2019), suggesting that compensatory DKK1 blunts the BMAT response to sclerostin-only therapy.

Interpreting the data on circulating Wnt antagonists in CKD remains complex. Reports variably describe positive, negative, or absent correlations between systemic sclerostin and PTH (Cejka et al., 2011; Moe et al., 2015). Although PTH suppresses *Sost* and *Dkk1* expression in bone (Bellido et al., 2005; Carrillo-López et al., 2016), the CKD mice described in chapter 5 had elevated levels of sclerostin and DKK1 but normal PTH levels and therefore the regulatory role of PTH is uncertain. Chronic elevations of sclerostin and DKK1 in CKD could reflect osteocytic overproduction (Cejka et al., 2014; Graciolli et al., 2017; Sabbagh et al., 2012), TGF-β–driven induction (Liu et al., 2014; Moysés & Schiavi, 2015), links to inflammation, phosphate, and uremic toxins, or FGF23-induced DKK1 via a soluble Klotho/MAPK pathway (Carrillo-López et al., 2016; Desjardins et al., 2014; Ferreira et al., 2013), rather than impaired renal clearance alone (Cejka et al., 2014). Notably, rbsAb treatment increased bone Sost/Dkk1 transcripts and proteins, potentially a homeostatic response to Wnt activation, paralleling Scl-Ab–treated CKD rats (Moe et al., 2015). A word of caution however; sclerostin and DKK1 are present in vascular tissues to inhibit soft tissue mineralisation and therefore cardiovascular safety remains a key consideration in the use of romosozumab (ARCH, BRIDGE trials) where adverse cardiovascular events were reported (Bovijn et al., 2020; Cosman et al., 2016; Didangelos et al., 2010; Lewiecki et al., 2018; Saag et al., 2017; Shao et al., 2005; Zhu et al., 2011). Nevertheless, preclinical studies have reported no aortic mineralisation in rats and monkeys with long-term romosozumab treatment (Chouinard et al., 2016; Claes et

al., 2013; Ominsky et al., 2017). Furthermore, DKK1 inhibition prevents vascular calcification in renal insufficiency (Fang et al., 2014), and no cardiovascular events have been reported in Sost-deficient mice or sclerosteosis/van Buchem disease (Balemans et al., 2002; Li et al., 2008; Vanhoenacker et al., 2003). Therefore, dedicated renal–cardiovascular outcome studies such as aortic microCT scanning are essential before the dual inhibition of sclerostin and DKK1 can be considered a safe therapeutic option for ROD in CKD patients.

However, there are several limitations to the studies described in this thesis and therefore I would focus my future research to address these issues and strengthen the conclusions made. In Chapter 3, while a longitudinal design clarifies the order of events in CKD-MBD pathogenesis, it does not establish causality between BMAT expansion and subsequent bone loss. Advanced lineage tracing (*i.e*. Cxcl12-CreE) (Zhong et al., 2020), *in vivo* live imaging, and single-cell multi-omics would help determine whether BMAT expansion reflects fate switching, progenitor attrition, or microenvironmental reprogramming. The *in vitro* work in Chapter 4, by design, isolates direct effects of systemic CKD-associated factors but cannot capture complex factor interactions (e.g., PTH × Pi × IS × FGF23), mechanotransduction, or the crosstalk between osteocytes, osteoblasts, and osteoclasts. Follow-up studies should: (i) vary PTH exposure kinetics to compare continuous versus intermittent regimens; (ii) map Pi dose–time windows aligned with pro-mineralisation ranges; (iii) test FGF23 with Klotho supplementation; (iv) evaluate IS under redox-modulated conditions with mitochondrial readouts; and (v) extend analyses to protein levels, osteoblast function (ALP activity, mineralisation), and co-culture remodelling assays. The MLO-Y4 osteocyte data highlight the importance of mature 3D systems (Brady et al., 2022); repeating Pi/IS challenges in IDG-SW3/Ocy454 or primary osteocytes with mechanical loading would better approximate *in vivo* osteocytic regulation (Chen et al., 2024). While rbsAb efficacy in protecting the skeleton and reducing BMAT accumulation in a CKD mouse model is apparent, the increase in cortical porosity warrants mechanistic investigation. Additionally, it is important to replicate this rbsAb study in a different animal model of CKD, *i.e.* nephrectomy model and consider how rbsAb might reverse bone pathology of ROD in the advanced stages of CKD. Further experiments using BMSC lineage tracing are necessary to determine

whether sclerostin and DKK1 are vital in guiding BMSC differentiation into adipocytes during CKD progression.

In addition, an important consideration not directly addressed in this thesis is sexual dimorphism in bone and BMAT biology. Only male mice were used to minimize variability associated with hormonal fluctuations during the oestrous cycle; however, sex differences significantly influence bone remodelling, marrow adiposity, and ROD progression. Oestrogen deficiency is known to accelerate bone loss and promotes adipogenic lineage allocation (Ali et al., 2022; Bouxsein et al., 2005; Cenci et al., 2000; Dang et al., 2002; Yao et al., 2025), while androgens exert partially protective skeletal effects (Frenkel et al., 2010; Ucer et al., 2015). Both clinical and experimental studies show sex-specific differences in BMAT distribution and metabolism (Beekman et al., 2022; Bukowska et al., 2018; Suchacki et al., 2023). Moreover, sex-specific responses to PTH, and metabolic stressors have been reported (Bouxsein et al., 2005; Wang et al., 2006). Therefore, extrapolation of these findings to females should be cautious, and future studies incorporating female CKD models are warranted.

Moreover, the findings of this thesis also raise broader questions regarding systemic metabolism in CKD. BMAT is increasingly recognized as a metabolically active and endocrine tissue rather than a passive fat depot. CKD is characterized by profound metabolic alterations, including disrupted lipid metabolism, insulin resistance, and altered adipokine profiles (Noels et al., 2021; Slee, 2012). The observed expansion of BMAT alongside reductions in peripheral fat depots suggests depot-specific adaptations rather than uniform fat responses which can be seen in caloric restriction (Cawthorn et al., 2016; Devlin, 2011). Whether BMAT expansion contributes directly to systemic metabolic imbalance, reflects compensatory energy storage, or influences whole-body substrate utilization remains unresolved. Future studies combining body composition analysis, metabolic phenotyping (energy expenditure, glucose tolerance), and adipose depot-specific gene expression profiling would clarify the systemic metabolic consequences of CKD and Wnt-targeted therapies on bone metabolism.

Furthermore, the emerging evidence also indicates that CKD-associated metabolic disturbances and uremic toxins may exert long-lasting effects on skeletal cells through

epigenetic mechanisms. DNA methylation, histone modifications, and non-coding RNA expression have been reported to regulate osteogenic–adipogenic lineage commitment (Dashti et al., 2024; Meyer et al., 2016; Teven et al., 2011). Uremic toxins such as indoxyl sulfate have been shown to induce oxidative stress and mitochondrial dysfunction (Hsu et al., 2025). Such modifications could influence BMSC lineage commitment, potentially stabilizing adipogenic bias or suppressing osteoblast differentiation even after removal of the initiating stimulus. Similarly, Wnt signaling — strongly modulated by sclerostin and DKK1 — interacts with chromatin regulatory machinery, suggesting that therapeutic Wnt activation may partially reverse maladaptive epigenetic states (Dees et al., 2014; Foltz et al., 2010). Although epigenetic regulation was beyond the scope of this thesis, integrating chromatin accessibility analysis, methylation profiling, or microRNA studies into future work would provide deeper mechanistic insight into how CKD reshapes BMSC plasticity and marrow niche function.

References

Abdalbary, M., Sobh, M., Elnagar, S., Elhadedy, M. A., Elshabrawy, N., Abdelsalam, M., Asadipooya, K., Sabry, A., Halawa, A., & El-Husseini, A. (2022). Management of osteoporosis in patients with chronic kidney disease. *Osteoporos Int*, *33*(11), 2259–2274. https://doi.org/10.1007/s00198-022-06462-3

Abdelrahman, R. M., Abdallah, A. M. A., Ahmed, A. A., Musa, T. H., Arbab, I. A., Abuelgasim, E. O., Jalal, M., Ahmed, K. O., Hassan, Y. A., Altrefe, Z., & Ahmed, H. B. (2025). Real-world evaluation of cinacalcet on hard outcomes in hemodialysis patients in Saudi Arabia. *BMC Nephrol*, *26*(1), 528. https://doi.org/10.1186/s12882-025-04455-y

Adami, G., Montanari, F., Fassio, A., Pollastri, F., Piccinelli, A., Benini, C., Pasetto, E., Tugnolli, M., Gatti, D., Rossini, M., & Viapiana, O. (2025). Increase in Serum DKK1 Levels Attenuates the Anabolic Response to Romosozumab in Postmenopausal Osteoporosis. *J Bone Miner Res*. https://doi.org/10.1093/jbmr/zjaf110

Agoro, R., Ni, P., Noonan, M. L., & White, K. E. (2020). Osteocytic FGF23 and Its Kidney Function. *Front Endocrinol (Lausanne)*, *11*, 592. https://doi.org/10.3389/fendo.2020.00592

Aguilar, A., Gifre, L., Urena-Torres, P., Carrillo-Lopez, N., Rodriguez-Garcia, M., Masso, E., da Silva, I., Lopez-Baez, V., Sanchez-Baya, M., Prior-Espanol, A., Urrutia, M., Paul, J., Bustos, M. C., Vila, A., Garnica-Leon, I., Navarro-Gonzalez, J. F., Mateo, L., & Bover, J. (2023). Pathophysiology of bone disease in chronic kidney disease: from basics to renal osteodystrophy and osteoporosis. *Front Physiol*, *14*, 1177829. https://doi.org/10.3389/fphys.2023.1177829

Akizawa, T., Kurita, N., Mizobuchi, M., Fukagawa, M., Onishi, Y., Yamaguchi, T., Ellis, A. R., Fukuma, S., Alan Brookhart, M., Hasegawa, T., Kurokawa, K., & Fukuhara, S. (2016). PTH-dependence of the effectiveness of cinacalcet in hemodialysis patients with secondary hyperparathyroidism. *Sci Rep*, *6*, 19612. https://doi.org/10.1038/srep19612

Akune, T., Ohba, S., Kamekura, S., Yamaguchi, M., Chung, U.-I., Kubota, N., Terauchi, Y., Harada, Y., Azuma, Y., Nakamura, K., Kadowaki, T., & Kawaguchi, H. (2004). PPAR γ insufficiency enhances osteogenesis through osteoblast formation from bone marrow progenitors. *Journal of Clinical Investigation*, *113*(6), 846–855. https://doi.org/10.1172/jci19900

Al-Dujaili, S. A., Lau, E., Al-Dujaili, H., Tsang, K., Guenther, A., & You, L. (2011). Apoptotic osteocytes regulate osteoclast precursor recruitment and differentiation in vitro. *J Cell Biochem*, *112*(9), 2412–2423. https://doi.org/10.1002/jcb.23164

Ali, D., Figeac, F., Caci, A., Ditzel, N., Schmal, C., Kerckhofs, G., Havelund, J., Faergeman, N., Rauch, A., Tencerova, M., & Kassem, M. (2022). High-fat diet-induced obesity augments the deleterious effects of estrogen deficiency on bone: Evidence from ovariectomized mice. *Aging Cell*, *21*(12), e13726. https://doi.org/10.1111/acel.13726

Ali, D., Tencerova, M., Figeac, F., Kassem, M., & Jafari, A. (2022). The pathophysiology of osteoporosis in obesity and type 2 diabetes in aging women and men: The

mechanisms and roles of increased bone marrow adiposity. *Front Endocrinol (Lausanne)*, *13*, 981487. https://doi.org/10.3389/fendo.2022.981487

Alicic, R. Z., Rooney, M. T., & Tuttle, K. R. (2017). Diabetic Kidney Disease: Challenges, Progress, and Possibilities. *Clin J Am Soc Nephrol*, *12*(12), 2032–2045. https://doi.org/10.2215/cjn.11491116

Ambati, S., Li, Q., Rayalam, S., Hartzell, D. L., Della-Fera, M. A., Hamrick, M. W., & Baile, C. A. (2010). Central leptin versus ghrelin: effects on bone marrow adiposity and gene expression. *Endocrine*, *37*(1), 115–123. https://doi.org/10.1007/s12020-009-9274-z

Ambrosi, T. H., & Schulz, T. J. (2017). The emerging role of bone marrow adipose tissue in bone health and dysfunction. *J Mol Med (Berl)*, *95*(12), 1291–1301. https://doi.org/10.1007/s00109-017-1604-7

Ambrosi, T. H., Scialdone, A., Graja, A., Gohlke, S., Jank, A. M., Bocian, C., Woelk, L., Fan, H., Logan, D. W., Schurmann, A., Saraiva, L. R., & Schulz, T. J. (2017). Adipocyte Accumulation in the Bone Marrow during Obesity and Aging Impairs Stem Cell-Based Hematopoietic and Bone Regeneration. *Cell Stem Cell*, *20*(6), 771–784 e776. https://doi.org/10.1016/j.stem.2017.02.009

Ambrosi, T. H., Sinha, R., Steininger, H. M., Hoover, M. Y., Murphy, M. P., Koepke, L. S., Wang, Y., Lu, W. J., Morri, M., Neff, N. F., Weissman, I. L., Longaker, M. T., & Chan, C. K. (2021). Distinct skeletal stem cell types orchestrate long bone skeletogenesis. *Elife*, *10*. https://doi.org/10.7554/eLife.66063

Andersen, T. L., Sondergaard, T. E., Skorzynska, K. E., Dagnaes-Hansen, F., Plesner, T. L., Hauge, E. M., Plesner, T., & Delaisse, J. M. (2009). A physical mechanism for coupling bone resorption and formation in adult human bone. *Am J Pathol*, *174*(1), 239–247. https://doi.org/10.2353/ajpath.2009.080627

Ansari, N., & Sims, N. A. (2020). The Cells of Bone and Their Interactions. *Handb Exp Pharmacol*, *262*, 1–25. https://doi.org/10.1007/164_2019_343

Appelman-Dijkstra, N. M., & Papapoulos, S. E. (2016). Sclerostin Inhibition in the Management of Osteoporosis. *Calcif Tissue Int*, *98*(4), 370–380. https://doi.org/10.1007/s00223-016-0126-6

Arendshorst, W. J., Vendrov, A. E., Kumar, N., Ganesh, S. K., & Madamanchi, N. R. (2024). Oxidative Stress in Kidney Injury and Hypertension. *Antioxidants (Basel)*, *13*(12). https://doi.org/10.3390/antiox13121454

Arif, E., Solanki, A. K., & Nihalani, D. (2016). Adriamycin susceptibility among C57BL/6 substrains. *Kidney Int*, *89*(3), 721–723. https://doi.org/10.1016/j.kint.2015.10.019

Arnsdorf, E. J., Tummala, P., Kwon, R. Y., & Jacobs, C. R. (2009). Mechanically induced osteogenic differentiation--the role of RhoA, ROCKII and cytoskeletal dynamics. *J Cell Sci*, *122*(Pt 4), 546–553. https://doi.org/10.1242/jcs.036293

Atashi, F., Modarressi, A., & Pepper, M. S. (2015). The role of reactive oxygen species in mesenchymal stem cell adipogenic and osteogenic differentiation: a review. *Stem Cells Dev*, *24*(10), 1150–1163. https://doi.org/10.1089/scd.2014.0484

Babij, P., Roudier, M., Graves, T., Han, C. Y., Chhoa, M., Li, C. M., Juan, T., Morony, S., Grisanti, M., Li, X., Yu, L., Dwyer, D., Lloyd, D. J., Bass, M. B., Richards, W. G., Ebeling, C., Amato, J., & Carlson, G. (2009). New variants in the Enpp1 and Ptpn6 genes cause low BMD, crystal-related arthropathy, and vascular

calcification. *J Bone Miner Res*, *24*(9), 1552–1564. https://doi.org/10.1359/jbmr.090417

Bacchetta, J., Boutroy, S. V., Nicolas, Juillard, L., Guebre-Egziabher, F., Rognant, N., Sornay-Rendu, E., Szulc, P., Laville, M., Delmas, P. D., Fouque, D., & Chapurlat, R. (2010). Early impairment of trabecular microarchitecture assessed with HR-pQCT in patients with stage II-IV chronic kidney disease. *25*, 849–857. https://doi.org/10.1359/JBMR.090831

Baccin, C., Al-Sabah, J., Velten, L., Helbling, P. M., Grunschlager, F., Hernandez-Malmierca, P., Nombela-Arrieta, C., Steinmetz, L. M., Trumpp, A., & Haas, S. (2020). Combined single-cell and spatial transcriptomics reveal the molecular, cellular and spatial bone marrow niche organization. *Nat Cell Biol*, *22*(1), 38–48. https://doi.org/10.1038/s41556-019-0439-6

Badr, S., Cotten, A., Mentaverri, R., Lombardo, D., Labreuche, J., Martin, C., Henaut, L., Cortet, B., & Paccou, J. (2023). Relationship between bone marrow adipose tissue and kidney function in postmenopausal women. *Bone Rep*, *19*, 101713. https://doi.org/10.1016/j.bonr.2023.101713

Baek, J. E., Choi, J. Y., & Kim, J. E. (2014). Skeletal analysis and differential gene expression in Runx2/Osterix double heterozygous embryos. *Biochem Biophys Res Commun*, *451*(3), 442–448. https://doi.org/10.1016/j.bbrc.2014.08.010

Bairey Merz, C. N., Dember, L. M., Ingelfinger, J. R., Vinson, A., Neugarten, J., Sandberg, K. L., Sullivan, J. C., Maric-Bilkan, C., Rankin, T. L., Kimmel, P. L., Star, R. A., participants of the National Institute of, D., Digestive, Kidney Diseases Workshop on, S., & the, K. (2019). Sex and the kidneys: current understanding and research opportunities. *Nat Rev Nephrol*, *15*(12), 776–783. https://doi.org/10.1038/s41581-019-0208-6

Bala, Y., Farlay, D., & Boivin, G. (2013). Bone mineralization: from tissue to crystal in normal and pathological contexts. *Osteoporos Int*, *24*(8), 2153–2166. https://doi.org/10.1007/s00198-012-2228-y

Balemans, W., Patel, N., Ebeling, M., Van Hul, E., Wuyts, W., Lacza, C., Dioszegi, M., Dikkers, F. G., Hildering, P., Willems, P. J., Verheij, J. B., Lindpaintner, K., Vickery, B., Foernzler, D., & Van Hul, W. (2002). Identification of a 52 kb deletion downstream of the SOST gene in patients with van Buchem disease. *J Med Genet*, *39*(2), 91–97. https://doi.org/10.1136/jmg.39.2.91

Bao, J., Yang, Y., Xia, M., Sun, W., & Chen, L. (2021). Wnt signaling: An attractive target for periodontitis treatment. *Biomed Pharmacother*, *133*, 110935. https://doi.org/10.1016/j.biopha.2020.110935

Bao, Y. W., Yuan, Y., Chen, J. H., & Lin, W. Q. (2018). Kidney disease models: tools to identify mechanisms and potential therapeutic targets. *Zool Res*, *39*(2), 72–86. https://doi.org/10.24272/j.issn.2095-8137.2017.055

Bär, L., Stournaras, C., Lang, F., & Föller, M. (2019). Regulation of fibroblast growth factor 23 (FGF23) in health and disease. In (Vol. 593, pp. 1879–1900): John Wiley & Sons, Ltd.

Barak, M. M. (2024). Cortical and Trabecular Bone Modeling and Implications for Bone Functional Adaptation in the Mammalian Tibia. *Bioengineering (Basel)*, *11*(5). https://doi.org/10.3390/bioengineering11050514

Baryawno, N., Przybylski, D., Kowalczyk, M. S., Kfoury, Y., Severe, N., Gustafsson, K., Kokkaliaris, K. D., Mercier, F., Tabaka, M., Hofree, M., Dionne, D., Papazian, A., Lee, D., Ashenberg, O., Subramanian, A., Vaishnav, E. D., Rozenblatt-Rosen, O., Regev, A., & Scadden, D. T. (2019). A Cellular Taxonomy of the Bone Marrow Stroma in Homeostasis and Leukemia. *Cell*, *177*(7), 1915–1932 e1916. https://doi.org/10.1016/j.cell.2019.04.040

Batista, D. G., Neves, K. R., Graciolli, F. G., dos Reis, L. M., Graciolli, R. G., Dominguez, W. V., Neves, C. L., Magalhaes, A. O., Custodio, M. R., Moyses, R. M., & Jorgetti, V. (2010). The bone histology spectrum in experimental renal failure: adverse effects of phosphate and parathyroid hormone disturbances. *Calcif Tissue Int*, *87*(1), 60–67. https://doi.org/10.1007/s00223-010-9367-y

Batth, T. S., Tollenaere, M. X., Ruther, P., Gonzalez-Franquesa, A., Prabhakar, B. S., Bekker-Jensen, S., Deshmukh, A. S., & Olsen, J. V. (2019). Protein Aggregation Capture on Microparticles Enables Multipurpose Proteomics Sample Preparation. *Mol Cell Proteomics*, *18*(5), 1027–1035. https://doi.org/10.1074/mcp.TIR118.001270

Beekman, K. M., Regenboog, M., Nederveen, A. J., Bravenboer, N., den Heijer, M., Bisschop, P. H., Hollak, C. E., Akkerman, E. M., & Maas, M. (2022). Gender- and Age-Associated Differences in Bone Marrow Adipose Tissue and Bone Marrow Fat Unsaturation Throughout the Skeleton, Quantified Using Chemical Shift Encoding-Based Water-Fat MRI. *Front Endocrinol (Lausanne)*, *13*, 815835. https://doi.org/10.3389/fendo.2022.815835

Beekman, K. M., Veldhuis-Vlug, A. G., den Heijer, M., Maas, M., Oleksik, A. M., Tanck, M. W., Ott, S. M., van 't Hof, R. J., Lips, P., Bisschop, P. H., & Bravenboer, N. (2019). The effect of raloxifene on bone marrow adipose tissue and bone turnover in postmenopausal women with osteoporosis. In (Vol. 118, pp. 62–68): Bone.

Behera, J., Ison, J., Tyagi, A., Mbalaviele, G., & Tyagi, N. (2022). Mechanisms of autophagy and mitophagy in skeletal development, diseases and therapeutics. *Life Sci*, *301*, 120595. https://doi.org/10.1016/j.lfs.2022.120595

Behets, G. J., Viaene, L., Meijers, B., Blocki, F., Brandenburg, V. M., Verhulst, A., D'Haese, P. C., & Evenepoel, P. (2017). Circulating levels of sclerostin but not DKK1 associate with laboratory parameters of CKD-MBD. *PLoS One*, *12*(5), e0176411. https://doi.org/10.1371/journal.pone.0176411

Bellido, T. (2014). Osteocyte-driven bone remodeling. *Calcif Tissue Int*, *94*(1), 25–34. https://doi.org/10.1007/s00223-013-9774-y

Bellido, T., Ali, A. A., Gubrij, I., Plotkin, L. I., Fu, Q., O'Brien, C. A., Manolagas, S. C., & Jilka, R. L. (2005). Chronic elevation of parathyroid hormone in mice reduces expression of sclerostin by osteocytes: a novel mechanism for hormonal control of osteoblastogenesis. *Endocrinology*, *146*(11), 4577–4583. https://doi.org/10.1210/en.2005-0239

Bello, A. K., Alrukhaimi, M., Ashuntantang, G. E., Basnet, S., Rotter, R. C., Douthat, W. G., Kazancioglu, R., Kottgen, A., Nangaku, M., Powe, N. R., White, S. L., Wheeler, D. C., & Moe, O. (2017). Complications of chronic kidney disease: current state, knowledge gaps, and strategy for action. *Kidney Int Suppl (2011)*, *7*(2), 122–129. https://doi.org/10.1016/j.kisu.2017.07.007

Bellorin-Font, E., Voinescu, A., & Martin, K. J. (2022). Chapter 23 - Calcium, phosphate, PTH, vitamin D, and FGF-23 in CKD-mineral and bone disorder. In J. D. Kopple, S. G. Massry, K. Kalantar-Zadeh, & D. Fouque (Eds.), *Nutritional Management of Renal Disease (Fourth Edition)* (pp. 353–381). Academic Press. https://doi.org/https://doi.org/10.1016/B978-0-12-818540-7.00013-6

Bertani, T., Rocchi, G., Sacchi, G., Mecca, G., & Remuzzi, G. (1986). Adriamycin-induced glomerulosclerosis in the rat. *Am J Kidney Dis*, *7*(1), 12–19. https://doi.org/10.1016/s0272-6386(86)80051-8

Beto, J., Bhatt, N., Gerbeling, T., Patel, C., & Drayer, D. (2019). Overview of the 2017 KDIGO CKD-MBD Update: Practice Implications for Adult Hemodialysis Patients. *J Ren Nutr*, *29*(1), 2–15. https://doi.org/10.1053/j.jrn.2018.05.006

Bianco, P., & Robey, P. G. (2015). Skeletal stem cells. *Development*, *142*(6), 1023–1027. https://doi.org/10.1242/dev.102210

Bienvenu, J. G., Chouinard, L., Felx, M., Boyce, R. W., & Monticello, T. M. (2024). Inhibition of both sclerostin and DKK1 results in novel skull findings in the rat and non-human primate that is not observed with inhibition of sclerostin alone. *Bone*, *179*, 116985. https://doi.org/10.1016/j.bone.2023.116985

Bird, S. T., Smith, E. R., Gelperin, K., Jung, T. H., Thompson, A., Kambhampati, R., Lyu, H., Zhao, H., Zhao, Y., Zhu, Y., Easley, O., Niak, A., Wernecke, M., Chillarige, Y., Zemskova, M., Kelman, J. A., & Graham, D. J. (2024). Severe Hypocalcemia With Denosumab Among Older Female Dialysis-Dependent Patients. *JAMA*, *331*(6), 491–499. https://doi.org/10.1001/jama.2023.28239

Block, G. A., Bushinsky, D. A., Cheng, S., Cunningham, J., Dehmel, B., Drueke, T. B., Ketteler, M., Kewalramani, R., Martin, K. J., Moe, S. M., Patel, U. D., Silver, J., Sun, Y., Wang, H., & Chertow, G. M. (2017). Effect of Etelcalcetide vs Cinacalcet on Serum Parathyroid Hormone in Patients Receiving Hemodialysis With Secondary Hyperparathyroidism: A Randomized Clinical Trial. *JAMA*, *317*(2), 156–164. https://doi.org/10.1001/jama.2016.19468

Block, G. A., Klassen, P. S., Lazarus, J. M., Ofsthun, N., Lowrie, E. G., & Chertow, G. M. (2004). Mineral Metabolism, Mortality, and Morbidity in Maintenance Hemodialysis. *Journal of the American Society of Nephrology.*, *15*(8), 2208–2218. https://doi.org/10.1097/01.ASN.0000133041.27682.A2

Block, G. A., Martin, K. J., de Francisco, A. L., Turner, S. A., Avram, M. M., Suranyi, M. G., Hercz, G., Cunningham, J., Abu-Alfa, A. K., Messa, P., Coyne, D. W., Locatelli, F., Cohen, R. M., Evenepoel, P., Moe, S. M., Fournier, A., Braun, J., McCary, L. C., Zani, V. J.,…Goodman, W. G. (2004). Cinacalcet for secondary hyperparathyroidism in patients receiving hemodialysis. *N Engl J Med*, *350*(15), 1516–1525. https://doi.org/10.1056/NEJMoa031633

Block, G. A., Raggi, P., Bellasi, A., Kooienga, L., & Spiegel, D. M. (2007). Mortality effect of coronary calcification and phosphate binder choice in incident hemodialysis patients. *Kidney Int*, *71*(5), 438–441. https://doi.org/10.1038/sj.ki.5002059

Bolamperti, S., Villa, I., & Rubinacci, A. (2022). Bone remodeling: an operational process ensuring survival and bone mechanical competence. *Bone Res*, *10*(1), 48. https://doi.org/10.1038/s41413-022-00219-8

Borelli, C., Vergara, D., Guglielmi, R., Aucella, F., Testini, V., & Guglielmi, G. (2023). Assessment of bone marrow fat by 3-Tesla magnetic resonance spectroscopy in patients with chronic kidney disease. *Quant Imaging Med Surg*, *13*(11), 7432–7443. https://doi.org/10.21037/qims-23-530

Bourne, L. E., Jayash, S. N., Michels, L. V., Hopkinson, M., Guppy, F. M., Clarkin, C. E., Gard, P., Brissett, N., & Staines, K. A. (2024). Sexually dimorphic effects of prenatal alcohol exposure on the murine skeleton. *Biol Sex Differ*, *15*(1), 51. https://doi.org/10.1186/s13293-024-00626-y

Bourne, L. E., Wheeler-Jones, C. P., & Orriss, I. R. (2021). Regulation of mineralisation in bone and vascular tissue: a comparative review. *The Journal of endocrinology*, *248*(2), R51–R65. https://doi.org/10.1530/JOE-20-0428

Bouxsein, M. L., Myers, K. S., Shultz, K. L., Donahue, L. R., Rosen, C. J., & Beamer, W. G. (2005). Ovariectomy-induced bone loss varies among inbred strains of mice. *J Bone Miner Res*, *20*(7), 1085–1092. https://doi.org/10.1359/JBMR.050307

Bouxsein, M. L., Pierroz, D. D., Glatt, V., Goddard, D. S., Cavat, F., Rizzoli, R., & Ferrari, S. L. (2005). beta-Arrestin2 regulates the differential response of cortical and trabecular bone to intermittent PTH in female mice. *J Bone Miner Res*, *20*(4), 635–643. https://doi.org/10.1359/JBMR.041204

Bover, J., Jara, A., Trinidad, P., Rodriguez, M., & Felsenfeld, A. J. (1999). Dynamics of skeletal resistance to parathyroid hormone in the rat: effect of renal failure and dietary phosphorus. *Bone*, *25*(3), 279–285. https://doi.org/10.1016/s8756-3282(99)00169-6

Bover, J., Urena, P., Brandenburg, V., Goldsmith, D., Ruiz, C., DaSilva, I., & Bosch, R. J. (2014). Adynamic bone disease: from bone to vessels in chronic kidney disease. *Semin Nephrol*, *34*(6), 626–640. https://doi.org/10.1016/j.semnephrol.2014.09.008

Bovijn, J., Krebs, K., Chen, C. Y., Boxall, R., Censin, J. C., Ferreira, T., Pulit, S. L., Glastonbury, C. A., Laber, S., Millwood, I. Y., Lin, K., Li, L., Chen, Z., Milani, L., Smith, G. D., Walters, R. G., Magi, R., Neale, B. M., Lindgren, C. M., & Holmes, M. V. (2020). Evaluating the cardiovascular safety of sclerostin inhibition using evidence from meta-analysis of clinical trials and human genetics. *Sci Transl Med*, *12*(549). https://doi.org/10.1126/scitranslmed.aay6570

Boyce, B. F. (2013). Advances in the regulation of osteoclasts and osteoclast functions. *J Dent Res*, *92*(10), 860–867. https://doi.org/10.1177/0022034513500306

Boyle, W. J., Simonet, W. S., & Lacey, D. L. (2003). Osteoclast differentiation and activation. *Nature*, *423*(6937), 337–342. https://doi.org/10.1038/nature01658

Brady, R. T., O'Brien, F. J., & Hoey, D. A. (2022). The Impact of the Extracellular Matrix Environment on Sost Expression by the MLO-Y4 Osteocyte Cell Line. *Bioengineering (Basel)*, *9*(1). https://doi.org/10.3390/bioengineering9010035

Brandenburg, V. M., Verhulst, A., Babler, A., D'Haese, P. C., Evenepoel, P., & Kaesler, N. (2019). Sclerostin in chronic kidney disease-mineral bone disorder think first before you block it! In (Vol. 34, pp. 408–414): Nephrol Dial Transplant.

Bredella, M. A., Fazeli, P. K., Miller, K. K., Misra, M., Torriani, M., Thomas, B. J., Ghomi, R. H., Rosen, C. J., & Klibanski, A. (2009). Increased bone marrow fat

in anorexia nervosa. *J Clin Endocrinol Metab*, *94*(6), 2129–2136. https://doi.org/10.1210/jc.2008-2532

Brown, C., McKee, C., Bakshi, S., Walker, K., Hakman, E., Halassy, S., Svinarich, D., Dodds, R., Govind, C. K., & Chaudhry, G. R. (2019). Mesenchymal stem cells: Cell therapy and regeneration potential. *J Tissue Eng Regen Med*, *13*(9), 1738–1755. https://doi.org/10.1002/term.2914

Bukowska, J., Frazier, T., Smith, S., Brown, T., Bender, R., McCarthy, M., Wu, X., Bunnell, B. A., & Gimble, J. M. (2018). Bone Marrow Adipocyte Developmental Origin and Biology. *Curr Osteoporos Rep*, *16*(3), 312–319. https://doi.org/10.1007/s11914-018-0442-z

Calvi, L. M., Sims, N. A., Hunzelman, J. L., Knight, M. C., Giovannetti, A., Saxton, J. M., Kronenberg, H. M., Baron, R., & Schipani, E. (2001). Activated parathyroid hormone/parathyroid hormone-related protein receptor in osteoblastic cells differentially affects cortical and trabecular bone. *107*, 277–286. https://doi.org/10.1172/JCI11296

Campos-Obando, N., Koek, W. N. H., Hooker, E. R., Van Der Eerden, B. C., Pols, H. A., Hofman, A., Van Leeuwen, J. P., Uitterlinden, A. G., Nielson, C. M., & Zillikens, M. C. (2017). Serum Phosphate Is Associated With Fracture Risk: The Rotterdam Study and MrOS. *Journal of bone and mineral research*, *32*(6), 1182–1193. https://doi.org/10.1002/jbmr.3094

Cao, W., Helder, M. N., Bravenboer, N., Wu, G., Jin, J., Ten Bruggenkate, C. M., Klein-Nulend, J., & Schulten, E. (2020). Is There a Governing Role of Osteocytes in Bone Tissue Regeneration? *Curr Osteoporos Rep*, *18*(5), 541–550. https://doi.org/10.1007/s11914-020-00610-6

Carrillo-López, N., Panizo, S., Alonso-Montes, C., Román-García, P., Rodríguez, I., Martínez-Salgado, C., Dusso, A. S., Naves, M., & Cannata-Andía, J. B. (2016). Direct inhibition of osteoblastic Wnt pathway by fibroblast growth factor 23 contributes to bone loss in chronic kidney disease. *Kidney International*, *90*(1), 77–89. https://doi.org/10.1016/j.kint.2016.01.024

Cawthorn, P., William, Scheller, L., Erica, Learman, S., Brian, Parlee, D., Sebastian, Simon, R., Becky, Mori, H., Ning, X., Bree, J., Adam, Schell, B., Broome, T., David, Soliman, S., Sandra, Delproposto, L., Jenifer, Lumeng, N., Carey, Mitra, A., Pandit, V., Sandeep, Gallagher, A., Katherine, Miller, D., Joshua, Krishnan, V., Hui, K., Susanta,…Macdougald, A., Ormond. (2014). Bone Marrow Adipose Tissue Is an Endocrine Organ that Contributes to Increased Circulating Adiponectin during Caloric Restriction. *Cell Metab*, *20*(2), 368–375. https://doi.org/10.1016/j.cmet.2014.06.003

Cawthorn, W. P., Scheller, E. L., Parlee, S. D., Pham, H. A., Learman, B. S., Redshaw, C. M. H., Sulston, R. J., Burr, A. A., Das, A. K., Simon, B. R., Mori, H., Bree, A. J., Schell, B., Krishnan, V., & Macdougald, O. A. (2016). Expansion of Bone Marrow Adipose Tissue During Caloric Restriction Is Associated With Increased Circulating Glucocorticoids and Not With Hypoleptinemia. *48109*. https://doi.org/10.1210/en.2015-1477

Cejka, D. (2021). Cardiovascular Safety of Anti-Sclerostin Therapy in Chronic Kidney Disease. *Metabolites*, *11*(11). https://doi.org/10.3390/metabo11110770

Cejka, D., Herberth, J., Branscum, A. J., Fardo, D. W., Monier-Faugere, M. C., Diarra, D., Haas, M., & Malluche, H. H. (2011). Sclerostin and Dickkopf-1 in renal osteodystrophy. *Clin J Am Soc Nephrol*, *6*(4), 877–882. https://doi.org/10.2215/CJN.06550810

Cejka, D., Marculescu, R., Kozakowski, N., Plischke, M., Reiter, T., Gessl, A., & Haas, M. (2014). Renal elimination of sclerostin increases with declining kidney function. *J Clin Endocrinol Metab*, *99*(1), 248–255. https://doi.org/10.1210/jc.2013-2786

Cejka, D., Parada-Rodriguez, D., Pichler, S., Marculescu, R., Kramer, I., Kneissel, M., Gross, T., Reisinger, A., Pahr, D., Monier-Faugere, M.-C., Haas, M., & Malluche, H. H. (2016). Only minor differences in renal osteodystrophy features between wild-type and sclerostin knockout mice with chronic kidney disease. *Kidney International*, *90*(4), 828–834. https://doi.org/10.1016/j.kint.2016.06.019

Cenci, S., Weitzmann, M. N., Roggia, C., Namba, N., Novack, D., Woodring, J., & Pacifici, R. (2000). Estrogen deficiency induces bone loss by enhancing T-cell production of TNF-alpha. *J Clin Invest*, *106*(10), 1229–1237. https://doi.org/10.1172/JCI11066

Chagnac, A., Zingerman, B., Rozen-Zvi, B., & Herman-Edelstein, M. (2019). Consequences of Glomerular Hyperfiltration: The Role of Physical Forces in the Pathogenesis of Chronic Kidney Disease in Diabetes and Obesity. *Nephron*, *143*(1), 38–42. https://doi.org/10.1159/000499486

Chan, C. K., Seo, E. Y., Chen, J. Y., Lo, D., McArdle, A., Sinha, R., Tevlin, R., Seita, J., Vincent-Tompkins, J., Wearda, T., Lu, W. J., Senarath-Yapa, K., Chung, M. T., Marecic, O., Tran, M., Yan, K. S., Upton, R., Walmsley, G. G., Lee, A. S.,…Longaker, M. T. (2015). Identification and specification of the mouse skeletal stem cell. *Cell*, *160*(1-2), 285–298. https://doi.org/10.1016/j.cell.2014.12.002

Charles, C., & Ferris, A. H. (2013). Chronic Kidney Disease. In.

Chavassieux, P., Roux, J. P., Libanati, C., Shi, Y., & Chapurlat, R. (2024). Evaluation of romosozumab's effects on bone marrow adiposity in postmenopausal osteoporotic women: results from the FRAME bone biopsy sub-study. *J Bone Miner Res*, *39*(9), 1278–1283. https://doi.org/10.1093/jbmr/zjae118

Chen, G., Deng, C., & Li, Y. P. (2012). TGF-beta and BMP signaling in osteoblast differentiation and bone formation. *Int J Biol Sci*, *8*(2), 272–288. https://doi.org/10.7150/ijbs.2929

Chen, N. X., O'Neill, K. D., Wilson, H. E., Srinivasan, S., Bonewald, L., & Moe, S. M. (2024). The uremic toxin indoxyl sulfate decreases osteocyte RANKL/OPG and increases Wnt inhibitor RNA expression that is reversed by PTH. *JBMR Plus*, *9*(1). https://doi.org/10.1093/jbmrpl/ziae136

Chen, X., Wang, Z., Duan, N., Zhu, G., Schwarz, E. M., & Xie, C. (2018). Osteoblast-osteoclast interactions. *Connect Tissue Res*, *59*(2), 99–107. https://doi.org/10.1080/03008207.2017.1290085

Cheung, J. O., Hillarby, M. C., Ayad, S., Hoyland, J. A., Jones, C. J., Denton, J., Thomas, J. T., Wallis, G. A., & Grant, M. E. (2001). A novel cell culture model of chondrocyte differentiation during mammalian endochondral ossification. *J Bone Miner Res*, *16*(2), 309–318. https://doi.org/10.1359/jbmr.2001.16.2.309

Choi, J. U. A., Kijas, A. W., Lauko, J., & Rowan, A. E. (2021). The Mechanosensory Role of Osteocytes and Implications for Bone Health and Disease States. *Front Cell Dev Biol*, *9*, 770143. https://doi.org/10.3389/fcell.2021.770143

Choi, R. B., Bullock, W. A., Hoggatt, A. M., Loots, G. G., Genetos, D. C., & Robling, A. G. (2021). Improving Bone Health by Optimizing the Anabolic Action of <scp>Wnt</scp> Inhibitor Multitargeting. *JBMR Plus*, *5*(5). https://doi.org/10.1002/jbm4.10462

Chouinard, L., Felx, M., Mellal, N., Varela, A., Mann, P., Jolette, J., Samadfam, R., Smith, S. Y., Locher, K., Buntich, S., Ominsky, M. S., Pyrah, I., & Boyce, R. W. (2016). Carcinogenicity risk assessment of romosozumab: A review of scientific weight-of-evidence and findings in a rat lifetime pharmacology study. *Regul Toxicol Pharmacol*, *81*, 212–222. https://doi.org/10.1016/j.yrtph.2016.08.010

Christodoulides, C., Laudes, M., Cawthorn, W. P., Schinner, S., Soos, M., O'Rahilly, S., Sethi, J. K., & Vidal-Puig, A. (2006). The Wnt antagonist Dickkopf-1 and its receptors are coordinately regulated during early human adipogenesis. *J Cell Sci*, *119*(Pt 12), 2613–2620. https://doi.org/10.1242/jcs.02975

Claes, K. J., Viaene, L., Heye, S., Meijers, B., d'Haese, P., & Evenepoel, P. (2013). Sclerostin: Another vascular calcification inhibitor? *J Clin Endocrinol Metab*, *98*(8), 3221–3228. https://doi.org/10.1210/jc.2013-1521

Clews, C., Dillon, S., Nudelman, F., Farquharson, C., & Stephen, L. A. (2025). Taking a closer look at matrix vesicle biogenesis. *J Bone Miner Res*, *40*(8), 931–945. https://doi.org/10.1093/jbmr/zjaf076

Coco, M., & Rush, H. (2000). Increased incidence of hip fractures in dialysis patients with low serum parathyroid hormone. *Am J Kidney Dis*, *36*(6), 1115–1121. https://doi.org/10.1053/ajkd.2000.19812

Cohen, A., Stein, E. M., Recker, R. R., Lappe, J. M., Dempster, D. W., Zhou, H., Cremers, S., McMahon, D. J., Nickolas, T. L., Müller, R., Zwahlen, A., Young, P., Stubby, J., & Shane, E. (2013). Teriparatide for idiopathic osteoporosis in premenopausal women: a pilot study. *98*, 1971–1981. https://doi.org/10.1210/JC.2013-1172

Collaboration, G. B. D. C. K. D. (2020). Global, regional, and national burden of chronic kidney disease, 1990-2017: a systematic analysis for the Global Burden of Disease Study 2017. *Lancet*, *395*(10225), 709–733. https://doi.org/10.1016/S0140-6736(20)30045-3

Coppola, A., Marfella, R., Coppola, L., Tagliamonte, E., Fontana, D., Liguori, E., Cirillo, T., Cafiero, M., Natale, S., & Astarita, C. (2009). Effect of weight loss on coronary circulation and adiponectin levels in obese women. *Int J Cardiol*, *134*(3), 414–416. https://doi.org/10.1016/j.ijcard.2007.12.087

Cosman, F., Crittenden, D. B., Adachi, J. D., Binkley, N., Czerwinski, E., Ferrari, S., Hofbauer, L. C., Lau, E., Lewiecki, E. M., Miyauchi, A., Zerbini, C. A., Milmont, C. E., Chen, L., Maddox, J., Meisner, P. D., Libanati, C., & Grauer, A. (2016). Romosozumab Treatment in Postmenopausal Women with Osteoporosis. *N Engl J Med*, *375*(16), 1532–1543. https://doi.org/10.1056/NEJMoa1607948

Cosman, F., de Beur, S. J., LeBoff, M., Lewiecki, E., Tanner, B., Randall, S., & Lindsay, R. (2014). Clinician's guide to prevention and treatment of osteoporosis. *Osteoporosis International*, *25*(10), 2359–2381.

Costa, A. G., Cremers, S., Rubin, M. R., McMahon, D. J., Sliney, J., Jr., Lazaretti-Castro, M., Silverberg, S. J., & Bilezikian, J. P. (2011). Circulating sclerostin in disorders of parathyroid gland function. *J Clin Endocrinol Metab*, *96*(12), 3804–3810. https://doi.org/10.1210/jc.2011-0566

Costa, S., Fairfield, H., Farrell, M., Murphy, C. S., Soucy, A., Vary, C., Holdsworth, G., & Reagan, M. R. (2021). Sclerostin antibody increases trabecular bone and bone mechanical properties by increasing osteoblast activity damaged by whole-body irradiation in mice. *Bone*, *147*, 115918. https://doi.org/10.1016/j.bone.2021.115918

Costa, S., Fairfield, H., & Reagan, M. R. (2019). Inverse correlation between trabecular bone volume and bone marrow adipose tissue in rats treated with osteoanabolic agents. *Bone*, *123*, 211–223. https://doi.org/10.1016/j.bone.2019.03.038

Costantino, V. V., Gil Lorenzo, A. F., Bocanegra, V., & Valles, P. G. (2021). Molecular Mechanisms of Hypertensive Nephropathy: Renoprotective Effect of Losartan through Hsp70. *Cells*, *10*(11). https://doi.org/10.3390/cells10113146

Courbebaisse, M., & Lanske, B. (2018). Biology of Fibroblast Growth Factor 23: From Physiology to Pathology. *Cold Spring Harb Perspect Med*, *8*(5). https://doi.org/10.1101/cshperspect.a031260

Cowan, A., Jeyakumar, N., McArthur, E., Fleet, J. L., Kanagalingam, T., Karp, I., Khan, T., Muanda, F. T., Nash, D. M., Silver, S. A., Thain, J., Weir, M. A., Garg, A. X., & Clemens, K. K. (2023). Hypocalcemia Risk of Denosumab Across the Spectrum of Kidney Disease: A Population-Based Cohort Study. *J Bone Miner Res*, *38*(5), 650–658. https://doi.org/10.1002/jbmr.4804

Coyne, D. W., Andress, D. L., Amdahl, M. J., Ritz, E., & de Zeeuw, D. (2013). Effects of paricalcitol on calcium and phosphate metabolism and markers of bone health in patients with diabetic nephropathy: results of the VITAL study. *Nephrol Dial Transplant*, *28*(9), 2260–2268. https://doi.org/10.1093/ndt/gft227

Craft, C. S., Li, Z., MacDougald, O. A., & Scheller, E. L. (2018). Molecular differences between subtypes of bone marrow adipocytes. In (Vol. 4, pp. 16): NIH Public Access.

Craft, C. S., & Scheller, E. L. (2017). Evolution of the Marrow Adipose Tissue Microenvironment. In (Vol. 100, pp. 461–475): Calcif Tissue Int.

Dacic, S., Kalajzic, I., Visnjic, D., Lichtler, A. C., & Rowe, D. W. (2001). Col1a1-driven transgenic markers of osteoblast lineage progression. *J Bone Miner Res*, *16*(7), 1228–1236. https://doi.org/10.1359/jbmr.2001.16.7.1228

Dallas, S. L., Prideaux, M., & Bonewald, L. F. (2013). The osteocyte: an endocrine cell ... and more. *Endocrine reviews*, *34*(5), 658–690. https://doi.org/10.1210/er.2012-1026

Dang, Z. C., van Bezooijen, R. L., Karperien, M., Papapoulos, S. E., & Lowik, C. W. (2002). Exposure of KS483 cells to estrogen enhances osteogenesis and inhibits adipogenesis. *J Bone Miner Res*, *17*(3), 394–405. https://doi.org/10.1359/jbmr.2002.17.3.394

Dashti, P., Lewallen, E. A., Gordon, J. A. R., Montecino, M. A., Davie, J. R., Stein, G. S., van Leeuwen, J., van der Eerden, B. C. J., & van Wijnen, A. J. (2024). Epigenetic regulators controlling osteogenic lineage commitment and bone formation. *Bone*, *181*, 117043. https://doi.org/10.1016/j.bone.2024.117043

de Winter, T. J. J., & Nusse, R. (2021). Running Against the Wnt: How Wnt/beta-Catenin Suppresses Adipogenesis. *Front Cell Dev Biol*, *9*, 627429. https://doi.org/10.3389/fcell.2021.627429

Dees, C., Schlottmann, I., Funke, R., Distler, A., Palumbo-Zerr, K., Zerr, P., Lin, N. Y., Beyer, C., Distler, O., Schett, G., & Distler, J. H. (2014). The Wnt antagonists DKK1 and SFRP1 are downregulated by promoter hypermethylation in systemic sclerosis. *Ann Rheum Dis*, *73*(6), 1232–1239. https://doi.org/10.1136/annrheumdis-2012-203194

Delaisse, J. M., Andersen, T. L., Kristensen, H. B., Jensen, P. R., Andreasen, C. M., & Soe, K. (2020). Re-thinking the bone remodeling cycle mechanism and the origin of bone loss. *Bone*, *141*, 115628. https://doi.org/10.1016/j.bone.2020.115628

Delgado-Calle, J., & Bellido, T. (2022). The osteocyte as a signaling cell. *Physiological reviews*, *102*(1), 379–410. https://doi.org/10.1152/physrev.00043.2020

Delporte, M. L., Brichard, S. M., Hermans, M. P., Beguin, C., & Lambert, M. (2003). Hyperadiponectinaemia in anorexia nervosa. *Clin Endocrinol (Oxf)*, *58*(1), 22–29. https://doi.org/10.1046/j.1365-2265.2003.01702.x

Demichev, V., Messner, C. B., Vernardis, S. I., Lilley, K. S., & Ralser, M. (2020). DIA-NN: neural networks and interference correction enable deep proteome coverage in high throughput. *Nat Methods*, *17*(1), 41–44. https://doi.org/10.1038/s41592-019-0638-x

Deng, P., Yuan, Q., Cheng, Y., Li, J., Liu, Z., Liu, Y., Li, Y., Su, T., Wang, J., Salvo, M. E., Wang, W., Fan, G., Lyons, K., Yu, B., & Wang, C. Y. (2021). Loss of KDM4B exacerbates bone-fat imbalance and mesenchymal stromal cell exhaustion in skeletal aging. *Cell Stem Cell*, *28*(6), 1057–1073 e1057. https://doi.org/10.1016/j.stem.2021.01.010

Desjardins, L., Liabeuf, S., Oliveira, R. B., Louvet, L., Kamel, S., Lemke, H. D., Vanholder, R., Choukroun, G., Massy, Z. A., & European Uremic Toxin Work, G. (2014). Uremic toxicity and sclerostin in chronic kidney disease patients. *Nephrol Ther*, *10*(6), 463–470. https://doi.org/10.1016/j.nephro.2014.04.002

Devlin, M. J. (2011). Why does starvation make bones fat? , *23*, 577–585. https://doi.org/10.1002/AJHB.21202

Devlin, M. J., Cloutier, A. M., Thomas, N. A., Panus, D. A., Lotinun, S., Pinz, I., Baron, R., Rosen, C. J., & Bouxsein, M. L. (2010). Caloric restriction leads to high marrow adiposity and low bone mass in growing mice. *J Bone Miner Res*, *25*(9), 2078–2088. https://doi.org/10.1002/jbmr.82

Dhayat, N. A., Ackermann, D., Pruijm, M., Ponte, B., Ehret, G., Guessous, I., Leichtle, A. B., Paccaud, F., Mohaupt, M., Fiedler, G.-M., Devuyst, O., Pechère-Bertschi, A., Burnier, M., Martin, P.-Y., Bochud, M., Vogt, B., & Fuster, D. G. (2016). Fibroblast growth factor 23 and markers of mineral metabolism in individuals with preserved renal function. *Kidney International*, *90*(3), 648–657. https://doi.org/10.1016/j.kint.2016.04.024

Didangelos, A., Yin, X., Mandal, K., Baumert, M., Jahangiri, M., & Mayr, M. (2010). Proteomics characterization of extracellular space components in the human aorta. *Mol Cell Proteomics*, *9*(9), 2048–2062. https://doi.org/10.1074/mcp.M110.001693

Dillon, S., Staines, K. A., Millan, J. L., & Farquharson, C. (2019). How To Build a Bone: PHOSPHO1, Biomineralization, and Beyond. *JBMR Plus*, *3*(7), e10202. https://doi.org/10.1002/jbm4.10202

Ding, M., Odgaard, A., Danielsen, C. C., & Hvid, I. (2002). Mutual associations among microstructural, physical and mechanical properties of human cancellous bone. *J Bone Joint Surg Br*, *84*(6), 900–907. https://doi.org/10.1302/0301-620x.84b6.11994

Diwan, V., Brown, L., & Gobe, G. C. (2018). Adenine-induced chronic kidney disease in rats. *Nephrology (Carlton)*, *23*(1), 5–11. https://doi.org/10.1111/nep.13180

Diwan, V., Mistry, A., Gobe, G., & Brown, L. (2013). Adenine-induced chronic kidney and cardiovascular damage in rats. *J Pharmacol Toxicol Methods*, *68*(2), 197–207. https://doi.org/10.1016/j.vascn.2013.05.006

Diwan, V., Small, D., Kauter, K., Gobe, G. C., & Brown, L. (2014). Gender differences in adenine-induced chronic kidney disease and cardiovascular complications in rats. *Am J Physiol Renal Physiol*, *307*(11), F1169–1178. https://doi.org/10.1152/ajprenal.00676.2013

Duan, X., Murata, Y., Liu, Y., Nicolae, C., Olsen, B. R., & Berendsen, A. D. (2015). Vegfa regulates perichondrial vascularity and osteoblast differentiation in bone development. *Development*, *142*(11), 1984–1991. https://doi.org/10.1242/dev.117952

Ducy, P., Amling, M., Takeda, S., Priemel, M., Schilling, A. F., Beil, F. T., Shen, J., Vinson, C., Rueger, J. M., & Karsenty, G. (2000). Leptin inhibits bone formation through a hypothalamic relay: a central control of bone mass. *Cell*, *100*(2), 197–207. https://doi.org/10.1016/s0092-8674(00)81558-5

Duque, G., Li, W., Vidal, C., Bermeo, S., Rivas, D., & Henderson, J. (2013). Pharmacological inhibition of PPARgamma increases osteoblastogenesis and bone mass in male C57BL/6 mice. *J Bone Miner Res*, *28*(3), 639–648. https://doi.org/10.1002/jbmr.1782

Evenepoel, P., D'Haese, P., & Brandenburg, V. (2015). Sclerostin and DKK1: new players in renal bone and vascular disease. *Kidney Int*, *88*(2), 235–240. https://doi.org/10.1038/ki.2015.156

Fairfield, H., Falank, C., Harris, E., Demambro, V., Mcdonald, M., Pettitt, J. A., Mohanty, S. T., Croucher, P., Kramer, I., Kneissel, M., Rosen, C. J., & Reagan, M. R. (2018). The skeletal cell-derived molecule sclerostin drives bone marrow adipogenesis. *Journal of Cellular Physiology*, *233*(2), 1156–1167. https://doi.org/10.1002/jcp.25976

Fairfield, H., Rosen, C. J., & Reagan, M. R. (2017). Connecting Bone and Fat: The Potential Role for Sclerostin. *Curr Mol Biol Rep*, *3*(2), 114–121. https://doi.org/10.1007/s40610-017-0057-7

Fan, Y., Hanai, J. I., Le, P. T., Bi, R., Maridas, D., DeMambro, V., Figueroa, C. A., Kir, S., Zhou, X., Mannstadt, M., Baron, R., Bronson, R. T., Horowitz, M. C., Wu, J. Y., Bilezikian, J. P., Dempster, D. W., Rosen, C. J., & Lanske, B. (2017). Parathyroid Hormone Directs Bone Marrow Mesenchymal Cell Fate. *Cell Metab*, *25*(3), 661–672. https://doi.org/10.1016/j.cmet.2017.01.001

Fang, Y., Ginsberg, C., Seifert, M., Agapova, O., Sugatani, T., Register, T. C., Freedman, B. I., Monier-Faugere, M. C., Malluche, H., & Hruska, K. A. (2014). CKD-

induced wingless/integration1 inhibitors and phosphorus cause the CKD-mineral and bone disorder. *J Am Soc Nephrol*, *25*(8), 1760–1773. https://doi.org/10.1681/ASN.2013080818

Fang, Y., Ginsberg, C., Sugatani, T., Monier-Faugere, M. C., Malluche, H., & Hruska, K. A. (2014). Early chronic kidney disease-mineral bone disorder stimulates vascular calcification. *Kidney Int*, *85*(1), 142–150. https://doi.org/10.1038/ki.2013.271

Farrell, M., Fairfield, H., Costa, S., D'Amico, A., Falank, C., Brooks, D. J., & Reagan, M. R. (2021). Sclerostin-Neutralizing Antibody Treatment Rescues Negative Effects of Rosiglitazone on Mouse Bone Parameters. *J Bone Miner Res*, *36*(1), 158–169. https://doi.org/10.1002/jbmr.4170

Feng, X., & McDonald, J. M. (2011). Disorders of bone remodeling. *Annu Rev Pathol*, *6*, 121–145. https://doi.org/10.1146/annurev-pathol-011110-130203

Ferreira, J. C., Ferrari, G. O., Neves, K. R., Cavallari, R. T., Dominguez, W. V., Dos Reis, L. M., Graciolli, F. G., Oliveira, E. C., Liu, S., Sabbagh, Y., Jorgetti, V., Schiavi, S., & Moysés, R. M. (2013). Effects of dietary phosphate on adynamic bone disease in rats with chronic kidney disease--role of sclerostin? *PLoS One*, *8*(11), e79721. https://doi.org/10.1371/journal.pone.0079721

Florio, M., Gunasekaran, K., Stolina, M., Li, X., Liu, L., Tipton, B., Salimi-Moosavi, H., Asuncion, F. J., Li, C., Sun, B., Tan, H. L., Zhang, L., Han, C. Y., Case, R., Duguay, A. N., Grisanti, M., Stevens, J., Pretorius, J. K., Pacheco, E.,…Ominsky, M. S. (2016). A bispecific antibody targeting sclerostin and DKK-1 promotes bone mass accrual and fracture repair. *Nat Commun*, *7*, 11505. https://doi.org/10.1038/ncomms11505

Florio, M., Kostenuik, P. J., Stolina, M., Asuncion, F. J., Grisanti, M., Ke, H. Z., & Ominsky, M. S. (2023). Dual Inhibition of the Wnt Inhibitors DKK1 and Sclerostin Promotes Fracture Healing and Increases the Density and Strength of Uninjured Bone: An Experimental Study in Nonhuman Primates. *J Bone Joint Surg Am*, *105*(15), 1145–1155. https://doi.org/10.2106/JBJS.22.01092

Foltz, G., Yoon, J. G., Lee, H., Ma, L., Tian, Q., Hood, L., & Madan, A. (2010). Epigenetic regulation of wnt pathway antagonists in human glioblastoma multiforme. *Genes Cancer*, *1*(1), 81–90. https://doi.org/10.1177/1947601909356103

Forster, C. M., White, C. A., Turner, M. E., Norman, P. A., Ward, E. C., Hopman, W. M., Adams, M. A., & Holden, R. M. (2020). Circulating Levels of Dickkopf-Related Protein 1 Decrease as Measured GFR Declines and Are Associated with PTH Levels. *Am J Nephrol*, *51*(11), 871–880. https://doi.org/10.1159/000511658

Frenkel, B., Hong, A., Baniwal, S. K., Coetzee, G. A., Ohlsson, C., Khalid, O., & Gabet, Y. (2010). Regulation of adult bone turnover by sex steroids. *J Cell Physiol*, *224*(2), 305–310. https://doi.org/10.1002/jcp.22159

Fu, Y., Luo, N., Klein, R. L., & Garvey, W. T. (2005). Adiponectin promotes adipocyte differentiation, insulin sensitivity, and lipid accumulation. *J Lipid Res*, *46*(7), 1369–1379. https://doi.org/10.1194/jlr.M400373-JLR200

Gal-Moscovici, A., & Sprague, S. M. (2007). Role of vitamin D deficiency in chronic kidney disease. *J Bone Miner Res*, *22 Suppl 2*, V91–94. https://doi.org/10.1359/jbmr.07s203

Gattineni, J., Bates, C., Twombley, K., Dwarakanath, V., Robinson, M. L., Goetz, R., Mohammadi, M., & Baum, M. (2009). FGF23 decreases renal NaPi-2a and NaPi-2c expression and induces hypophosphatemia in vivo predominantly via FGF receptor 1. *Am J Physiol Renal Physiol*, *297*(2), F282–291. https://doi.org/10.1152/ajprenal.90742.2008

Genge, B. R., Wu, L. N., & Wuthier, R. E. (1990). Differential fractionation of matrix vesicle proteins. Further characterization of the acidic phospholipid-dependent Ca2(+)-binding proteins. *Journal of Biological Chemistry*, *265*(8), 4703–4710. https://doi.org/https://doi.org/10.1016/S0021-9258(19)39619-X

Gimble, J. M., Robinson, C. E., Wu, X., Kelly, K. A., Rodriguez, B. R., Kliewer, S. A., Lehmann, J. M., & Morris, D. C. (1996). Peroxisome proliferator-activated receptor-gamma activation by thiazolidinediones induces adipogenesis in bone marrow stromal cells. *Mol Pharmacol*, *50*(5), 1087–1094.

Graciolli, F. G., Neves, K. R., Barreto, F., Barreto, D. V., Dos Reis, L. M., Canziani, M. E., Sabbagh, Y., Carvalho, A. B., Jorgetti, V., Elias, R. M., Schiavi, S., & Moysés, R. M. A. (2017). The complexity of chronic kidney disease-mineral and bone disorder across stages of chronic kidney disease. In.

Griffith, J. F., Yeung, D. K. W., Leung, J. C. S., Kwok, T. C. Y., & Leung, P. C. (2011). Prediction of bone loss in elderly female subjects by MR perfusion imaging and spectroscopy. In (Vol. 21, pp. 1160–1169): Eur Radiol.

Guimaraes, G. C., Coelho, J. B. C., Silva, J. G. O., de Sant'Ana, A. C. C., de Sa, C. A. C., Moreno, J. M., Reis, L. M., & de Oliveira Guimaraes, C. S. (2024). Obesity, diabetes and risk of bone fragility: How BMAT behavior is affected by metabolic disturbances and its influence on bone health. *Osteoporos Int*, *35*(4), 575–588. https://doi.org/10.1007/s00198-023-06991-5

Haarhaus, M., Aaltonen, L., Cejka, D., Cozzolino, M., de Jong, R. T., D'Haese, P., Evenepoel, P., Lafage-Proust, M. H., Mazzaferro, S., McCloskey, E., Salam, S., Skou Jorgensen, H., & Vervloet, M. (2023). Management of fracture risk in CKD-traditional and novel approaches. *Clin Kidney J*, *16*(3), 456–472. https://doi.org/10.1093/ckj/sfac230

Hajjawi, M. O., MacRae, V. E., Huesa, C., Boyde, A., Millan, J. L., Arnett, T. R., & Orriss, I. R. (2014). Mineralisation of collagen rich soft tissues and osteocyte lacunae in Enpp1(-/-) mice. *Bone*, *69*, 139–147. https://doi.org/10.1016/j.bone.2014.09.016

Hamrick, M. W., Pennington, C., Newton, D., Xie, D., & Isales, C. (2004). Leptin deficiency produces contrasting phenotypes in bones of the limb and spine. *Bone*, *34*(3), 376–383. https://doi.org/10.1016/j.bone.2003.11.020

Han, T., Rong, G., Quan, D., Shu, Y., Liang, Z., She, N., Liu, M., Yang, B., Cheng, G., Lv, Y., & Stern, L. (2013). Meta-analysis: the efficacy and safety of paricalcitol for the treatment of secondary hyperparathyroidism and proteinuria in chronic kidney disease. *BioMed research international*, *2013*, 320560. https://doi.org/10.1155/2013/320560

Hara, T., Hijikata, Y., Matsubara, Y., & Watanabe, N. (2021). Pharmacological interventions versus placebo, no treatment or usual care for osteoporosis in people with chronic kidney disease stages 3-5D. *Cochrane Database Syst Rev*, *7*(7), CD013424. https://doi.org/10.1002/14651858.CD013424.pub2

Hardouin, P., Rharass, T., & Lucas, S. (2016). Bone Marrow Adipose Tissue: To Be or Not To Be a Typical Adipose Tissue? *Front Endocrinol (Lausanne)*, *7*, 85. https://doi.org/10.3389/fendo.2016.00085

Harris, R. B. (2014). Direct and indirect effects of leptin on adipocyte metabolism. *Biochim Biophys Acta*, *1842*(3), 414–423. https://doi.org/10.1016/j.bbadis.2013.05.009

Hart, N. H., Nimphius, S., Rantalainen, T., Ireland, A., Siafarikas, A., & Newton, R. (2017). Mechanical basis of bone strength: influence of bone material, bone structure and muscle action. *Journal of musculoskeletal & neuronal interactions*, *17*(3), 114.

Hata, K., Nishimura, R., Ueda, M., Ikeda, F., Matsubara, T., Ichida, F., Hisada, K., Nokubi, T., Yamaguchi, A., & Yoneda, T. (2005). A CCAAT/enhancer binding protein beta isoform, liver-enriched inhibitory protein, regulates commitment of osteoblasts and adipocytes. *Mol Cell Biol*, *25*(5), 1971–1979. https://doi.org/10.1128/MCB.25.5.1971-1979.2005

Henriksen, K., Neutzsky-Wulff, A. V., Bonewald, L. F., & Karsdal, M. A. (2009). Local communication on and within bone controls bone remodeling. *Bone*, *44*(6), 1026–1033. https://doi.org/10.1016/j.bone.2009.03.671

Henriquez, B., Hepp, M., Merino, P., Sepulveda, H., van Wijnen, A. J., Lian, J. B., Stein, G. S., Stein, J. L., & Montecino, M. (2011). C/EBPbeta binds the P1 promoter of the Runx2 gene and up-regulates Runx2 transcription in osteoblastic cells. *J Cell Physiol*, *226*(11), 3043–3052. https://doi.org/10.1002/jcp.22652

Hernandez, M. J., Dos Reis, L. M., Marques, I. D., Araujo, M. J., Truyts, C. A. M., Oliveira, I. B., Barreto, F. C., David-Neto, E., Custodio, M. R., Moyses, R. M., Bellorin-Font, E., & Jorgetti, V. (2018). The effect of vitamin D and zoledronic acid in bone marrow adiposity in kidney transplant patients: A post hoc analysis. *PLoS One*, *13*(5), e0197994. https://doi.org/10.1371/journal.pone.0197994

Hessle, L., Johnson, K. A., Anderson, H. C., Narisawa, S., Sali, A., Goding, J. W., Terkeltaub, R., & Millan, J. L. (2002). Tissue-nonspecific alkaline phosphatase and plasma cell membrane glycoprotein-1 are central antagonistic regulators of bone mineralization. *Proc Natl Acad Sci U S A*, *99*(14), 9445–9449. https://doi.org/10.1073/pnas.142063399

Hill, T. P., Spater, D., Taketo, M. M., Birchmeier, W., & Hartmann, C. (2005). Canonical Wnt/beta-catenin signaling prevents osteoblasts from differentiating into chondrocytes. *Dev Cell*, *8*(5), 727–738. https://doi.org/10.1016/j.devcel.2005.02.013

Ho, A. M., Johnson, M. D., & Kingsley, D. M. (2000). Role of the mouse ank gene in control of tissue calcification and arthritis. *Science*, *289*(5477), 265–270. https://doi.org/10.1126/science.289.5477.265

Hochmann, S., Ou, K., Poupardin, R., Mittermeir, M., Textor, M., Ali, S., Wolf, M., Ellinghaus, A., Jacobi, D., Elmiger, J. A. J., Donsante, S., Riminucci, M., Schafer, R., Kornak, U., Klein, O., Schallmoser, K., Schmidt-Bleek, K., Duda, G. N., Polansky, J. K.,…Strunk, D. (2023). The enhancer landscape predetermines the skeletal regeneration capacity of stromal cells. *Sci Transl Med*, *15*(688), eabm7477. https://doi.org/10.1126/scitranslmed.abm7477

Hohling, H. J., Steffens, H., & Stamm, G. (1976). Transmission microscopy of freeze dried, unstained epiphyseal cartilage of the guinea pig. *Cell Tissue Res*, *167*(2), 243–263. https://doi.org/10.1007/BF00224331

Holdsworth, G., Greenslade, K., Jose, J., Stencel, Z., Kirby, H., Moore, A., Ke, H. Z., & Robinson, M. K. (2018). Dampening of the bone formation response following repeat dosing with sclerostin antibody in mice is associated with up-regulation of Wnt antagonists. *Bone*, *107*, 93–103. https://doi.org/10.1016/j.bone.2017.11.003

Horner, A., Bishop, N. J., Bord, S., Beeton, C., Kelsall, A. W., Coleman, N., & Compston, J. E. (1999). Immunolocalisation of vascular endothelial growth factor (VEGF) in human neonatal growth plate cartilage. *J Anat*, *194 (Pt 4)*(Pt 4), 519–524. https://doi.org/10.1046/j.1469-7580.1999.19440519.x

Hosain, O., & Clinkenbeard, E. L. (2024). Adiposity and Mineral Balance in Chronic Kidney Disease. *Curr Osteoporos Rep*, *22*(6), 561–575. https://doi.org/10.1007/s11914-024-00884-0

Hou, Y. C., Lu, C. L., & Lu, K. C. (2018). Mineral bone disorders in chronic kidney disease. *Nephrology (Carlton)*, *23 Suppl 4*, 88–94. https://doi.org/10.1111/nep.13457

Houston, D. A., Myers, K., MacRae, V. E., Staines, K. A., & Farquharson, C. (2016). The Expression of PHOSPHO1, nSMase2 and TNAP is Coordinately Regulated by Continuous PTH Exposure in Mineralising Osteoblast Cultures. *Calcif Tissue Int*, *99*(5), 510–524. https://doi.org/10.1007/s00223-016-0176-9

Hruska, K. A., Sugatani, T., Agapova, O., & Fang, Y. (2017). The chronic kidney disease — Mineral bone disorder (CKD-MBD): Advances in pathophysiology. *Bone*, *100*, 80–86. https://doi.org/10.1016/j.bone.2017.01.023

Hsieh, C. W., Chang, L. H., Wang, Y. H., Li, W. T., Chang, J. K., Chen, C. H., & Ho, M. L. (2024). Indoxyl Sulfate Inhibits Osteogenesis in Bone Marrow Mesenchymal Stem Cells through the AhR/Hes1 Pathway. *Int J Mol Sci*, *25*(16). https://doi.org/10.3390/ijms25168770

Hsu, C. Y., Chen, L. R., & Chen, K. H. (2020). Osteoporosis in patients with chronic kidney diseases: A systemic review. *21*, 1–24. https://doi.org/10.3390/ijms21186846

Hsu, S.-N., Stephen, L. A., Dillon, S., Milne, E., Javaheri, B., Pitsillides, A. A., Novak, A., Millán, J. L., MacRae, V. E., Staines, K. A., & Farquharson, C. (2022). Increased PHOSPHO1 expression mediates cortical bone mineral density in renal osteodystrophy. *254*, 153–167. https://doi.org/10.1530/JOE-22-0097

Hsu, S. N., Stephen, L. A., Phadwal, K., Dillon, S., Carter, R., Morton, N. M., Luijten, I., Emelianova, K., Amin, A. K., Macrae, V. E., Freeman, T. C., Hsu, Y. J., Staines, K. A., & Farquharson, C. (2025). Mitochondrial dysfunction and mitophagy blockade contribute to renal osteodystrophy in chronic kidney disease-mineral bone disorder. *Kidney Int*, *107*(6), 1017–1036. https://doi.org/10.1016/j.kint.2025.01.022

Hu, L., Napoletano, A., Provenzano, M., Garofalo, C., Bini, C., Comai, G., & La Manna, G. (2022). Mineral Bone Disorders in Kidney Disease Patients: The Ever-Current Topic. *Int J Mol Sci*, *23*(20). https://doi.org/10.3390/ijms232012223

Huang, K., Cai, S., Fu, T., Zhu, Q., Liu, L., Yao, Z., Rao, P., Lan, X., Li, Q., & Xiao, J. (2024). Wnt10b regulates osteogenesis of adipose-derived stem cells through

Wnt/beta-catenin signalling pathway in osteoporosis. *Cell Prolif*, *57*(1), e13522. https://doi.org/10.1111/cpr.13522

Iantomasi, T., Romagnoli, C., Palmini, G., Donati, S., Falsetti, I., Miglietta, F., Aurilia, C., Marini, F., Giusti, F., & Brandi, M. L. (2023). Oxidative Stress and Inflammation in Osteoporosis: Molecular Mechanisms Involved and the Relationship with microRNAs. *Int J Mol Sci*, *24*(4). https://doi.org/10.3390/ijms24043772

Ikeda, K., & Takeshita, S. (2016). The role of osteoclast differentiation and function in skeletal homeostasis. *J Biochem*, *159*(1), 1–8. https://doi.org/10.1093/jb/mvv112

Infante, A., & Rodriguez, C. I. (2018). Osteogenesis and aging: lessons from mesenchymal stem cells. *Stem Cell Res Ther*, *9*(1), 244. https://doi.org/10.1186/s13287-018-0995-x

Investigators, E. T., Chertow, G. M., Block, G. A., Correa-Rotter, R., Drueke, T. B., Floege, J., Goodman, W. G., Herzog, C. A., Kubo, Y., London, G. M., Mahaffey, K. W., Mix, T. C., Moe, S. M., Trotman, M. L., Wheeler, D. C., & Parfrey, P. S. (2012). Effect of cinacalcet on cardiovascular disease in patients undergoing dialysis. *N Engl J Med*, *367*(26), 2482–2494. https://doi.org/10.1056/NEJMoa1205624

Ionescu, A. M., Drissi, M. H., & O'Keefe, R. J. (2004). Regulation of Chondrocyte Differentiation. In E. J. Massaro & J. M. Rogers (Eds.), *The Skeleton: Biochemical, Genetic, and Molecular Interactions in Development and Homeostasis* (pp. 43–53). Humana Press. https://doi.org/10.1007/978-1-59259-736-9_3

Ishizuya, T., Yokose, S., Hori, M., Noda, T., Suda, T., Yoshiki, S., & Yamaguchi, A. (1997). Parathyroid hormone exerts disparate effects on osteoblast differentiation depending on exposure time in rat osteoblastic cells. *J Clin Invest*, *99*(12), 2961–2970. https://doi.org/10.1172/JCI119491

Iwamoto, R., Koide, M., Udagawa, N., & Kobayashi, Y. (2022). Positive and Negative Regulators of Sclerostin Expression. *Int J Mol Sci*, *23*(9). https://doi.org/10.3390/ijms23094895

Jabalee, J., & Franz-Odendaal, T. A. (2015). Vascular endothelial growth factor signaling affects both angiogenesis and osteogenesis during the development of scleral ossicles. *Dev Biol*, *406*(1), 52–62. https://doi.org/10.1016/j.ydbio.2015.07.014

Jadoul, M., Albert, J. M., Akiba, T., Akizawa, T., Arab, L., Bragg-Gresham, J. L., Mason, N., Prutz, K.-G., Young, E. W., & Pisoni, R. L. (2006). Incidence and risk factors for hip or other bone fractures among hemodialysis patients in the Dialysis Outcomes and Practice Patterns Study. *Kidney International*, *70*(7), 1358–1366. https://doi.org/10.1038/sj.ki.5001754

Jamal, S. A., Bauer, D. C., Ensrud, K. E., Cauley, J. A., Hochberg, M., Ishani, A., & Cummings, S. R. (2007). Alendronate treatment in women with normal to severely impaired renal function: an analysis of the fracture intervention trial. *J Bone Miner Res*, *22*(4), 503–508. https://doi.org/10.1359/jbmr.070112

Jamal, S. A., Vandermeer, B., Raggi, P., Mendelssohn, D. C., Chatterley, T., Dorgan, M., Lok, C. E., Fitchett, D., & Tsuyuki, R. T. (2013). Effect of calcium-based versus non-calcium-based phosphate binders on mortality in patients with chronic

kidney disease: an updated systematic review and meta-analysis. *Lancet*, *382*(9900), 1268–1277. https://doi.org/10.1016/S0140-6736(13)60897-1

James, A. W. (2013). Review of Signaling Pathways Governing MSC Osteogenic and Adipogenic Differentiation. *2013*, 1–17. https://doi.org/10.1155/2013/684736

Javaheri, B., Razi, H., Gohin, S., Wylie, S., Chang, Y. M., Salmon, P., Lee, P. D., & Pitsillides, A. A. (2020). Lasting organ-level bone mechanoadaptation is unrelated to local strain. *Sci Adv*, *6*(10), eaax8301. https://doi.org/10.1126/sciadv.aax8301

Jayash, S. N., Duff, T., Tanveer, Q., Promruk, W., & Farquharson, C. (2025). Osteoblasts sense extracellular levels of phosphate to control the local expression of phosphatases for matrix mineralisation. *Bone Rep*, *26*, 101863. https://doi.org/10.1016/j.bonr.2025.101863

Jia, T., Olauson, H., Lindberg, K., Amin, R., Edvardsson, K., Lindholm, B., Andersson, G., Wernerson, A., Sabbagh, Y., Schiavi, S., & Larsson, T. E. (2013). A novel model of adenine-induced tubulointerstitial nephropathy in mice. *BMC Nephrol*, *14*, 116. https://doi.org/10.1186/1471-2369-14-116

Jilka, R. L., Noble, B., & Weinstein, R. S. (2013). Osteocyte apoptosis. *Bone*, *54*(2), 264–271. https://doi.org/10.1016/j.bone.2012.11.038

Jones, J. R., Barrick, C., Kim, K. A., Lindner, J., Blondeau, B., Fujimoto, Y., Shiota, M., Kesterson, R. A., Kahn, B. B., & Magnuson, M. A. (2005). Deletion of PPARgamma in adipose tissues of mice protects against high fat diet-induced obesity and insulin resistance. *Proc Natl Acad Sci U S A*, *102*(17), 6207–6212. https://doi.org/10.1073/pnas.0306743102

Justesen, J., Stenderup, K., Ebbesen, E. N., Mosekilde, L., Steiniche, T., & Kassem, M. (2001). Adipocyte tissue volume in bone marrow is increased with aging and in patients with osteoporosis. *Biogerontology*, *2*(3), 165–171. https://doi.org/10.1023/a:1011513223894

Kaesler, N., Verhulst, A., De Mare, A., Deck, A., Behets, G. J., Hyusein, A., Evenepoel, P., Floege, J., Marx, N., Babler, A., Kramer, I., Kneissel, M., Kramann, R., Weis, D., D'Haese, P. C., & Brandenburg, V. M. (2018). Sclerostin deficiency modifies the development of CKD-MBD in mice. *Bone*, *107*, 115–123. https://doi.org/10.1016/j.bone.2017.11.015

Kajimura, D., Lee, H. W., Riley, K. J., Arteaga-Solis, E., Ferron, M., Zhou, B., Clarke, C. J., Hannun, Y. A., DePinho, R. A., Guo, X. E., Mann, J. J., & Karsenty, G. (2013). Adiponectin regulates bone mass via opposite central and peripheral mechanisms through FoxO1. *Cell Metab*, *17*(6), 901–915. https://doi.org/10.1016/j.cmet.2013.04.009

Kamprom, W., Tawonsawatruk, T., Mas-Oodi, S., Anansilp, K., Rattanasompattikul, M., & Supokawej, A. (2021). P-cresol and Indoxyl Sulfate Impair Osteogenic Differentiation by Triggering Mesenchymal Stem Cell Senescence. *Int J Med Sci*, *18*(3), 744–755. https://doi.org/10.7150/ijms.48492

Kanatani, M., Sugimoto, T., Kano, J., Kanzawa, M., & Chihara, K. (2003). Effect of high phosphate concentration on osteoclast differentiation as well as bone-resorbing activity. *J Cell Physiol*, *196*(1), 180–189. https://doi.org/10.1002/jcp.10270

Kanbay, M., Siriopol, D., Saglam, M., Kurt, Y. G., Gok, M., Cetinkaya, H., Karaman, M., Unal, H. U., Oguz, Y., Sari, S., Eyileten, T., Goldsmith, D., Vural, A., Veisa,

G., Covic, A., & Yilmaz, M. I. (2014). Serum sclerostin and adverse outcomes in nondialyzed chronic kidney disease patients. *J Clin Endocrinol Metab*, *99*(10), E1854–1861. https://doi.org/10.1210/jc.2014-2042

Kang, S., Bennett, C. N., Gerin, I., Rapp, L. A., Hankenson, K. D., & Macdougald, O. A. (2007). Wnt signaling stimulates osteoblastogenesis of mesenchymal precursors by suppressing CCAAT/enhancer-binding protein alpha and peroxisome proliferator-activated receptor gamma. *J Biol Chem*, *282*(19), 14515–14524. https://doi.org/10.1074/jbc.M700030200

Katagiri, T., & Takahashi, N. (2002). Regulatory mechanisms of osteoblast and osteoclast differentiation. *Oral Dis*, *8*(3), 147–159. https://doi.org/10.1034/j.1601-0825.2002.01829.x

Kawashima, Y., Kodera, Y., Singh, A., Matsumoto, M., & Matsumoto, H. (2014). Efficient extraction of proteins from formalin-fixed paraffin-embedded tissues requires higher concentration of tris(hydroxymethyl)aminomethane. *Clin Proteomics*, *11*(1), 4. https://doi.org/10.1186/1559-0275-11-4

Kemmak, A. R., Rezapour, A., Jahangiri, R., Nikjoo, S., Farabi, H., & Soleimanpour, S. (2020). Economic burden of osteoporosis in the world: A systematic review. In (Vol. 34, pp. 154): Iran University of Medical Sciences.

Ketteler, M., Evenepoel, P., Holden, R. M., Isakova, T., Jorgensen, H. S., Komaba, H., Nickolas, T. L., Sinha, S., Vervloet, M. G., Cheung, M., King, J. M., Grams, M. E., Jadoul, M., Moyses, R. M. A., & Conference, P. (2025). Chronic kidney disease-mineral and bone disorder: conclusions from a Kidney Disease: Improving Global Outcomes (KDIGO) Controversies Conference. *Kidney Int*, *107*(3), 405–423. https://doi.org/10.1016/j.kint.2024.11.013

Khairallah, P., & Nickolas, T. L. (2018). Management of Osteoporosis in CKD. *Clin J Am Soc Nephrol*, *13*(6), 962–969. https://doi.org/10.2215/CJN.11031017

Khosla, S., Westendorf, J. J., & Modder, U. I. (2010). Concise review: Insights from normal bone remodeling and stem cell-based therapies for bone repair. *Stem Cells*, *28*(12), 2124–2128. https://doi.org/10.1002/stem.546

Kim, H. J., Minashima, T., McCarthy, E. F., Winkles, J. A., & Kirsch, T. (2010). Progressive ankylosis protein (ANK) in osteoblasts and osteoclasts controls bone formation and bone remodeling. *J Bone Miner Res*, *25*(8), 1771–1783. https://doi.org/10.1002/jbmr.60

Kim, J. H., & Kim, N. (2020). Bone Cell Communication Factors Provide a New Therapeutic Strategy for Osteoporosis. *Chonnam Med J*, *56*(2), 94–98. https://doi.org/10.4068/cmj.2020.56.2.94

Kim, J. M., Lin, C., Stavre, Z., Greenblatt, M. B., & Shim, J. H. (2020). Osteoblast-Osteoclast Communication and Bone Homeostasis. *Cells*, *9*(9). https://doi.org/10.3390/cells9092073

Kim, S. P., Frey, J. L., Li, Z., Kushwaha, P., Zoch, M. L., Tomlinson, R. E., Da, H., Aja, S., Noh, H. L., Kim, J. K., Hussain, M. A., Thorek, D. L. J., Wolfgang, M. J., & Riddle, R. C. (2017). Sclerostin influences body composition by regulating catabolic and anabolic metabolism in adipocytes. *Proc Natl Acad Sci U S A*, *114*(52), E11238–E11247. https://doi.org/10.1073/pnas.1707876115

Kim, Y. H., Kwak, K. A., Gil, H. W., Song, H. Y., & Hong, S. Y. (2013). Indoxyl sulfate promotes apoptosis in cultured osteoblast cells. *BMC Pharmacol Toxicol*, *14*, 60. https://doi.org/10.1186/2050-6511-14-60

Ko, F. C., Kobelski, M. M., Zhang, W., Grenga, G. M., Martins, J. S., & Demay, M. B. (2021). Phosphate restriction impairs mTORC1 signaling leading to increased bone marrow adipose tissue and decreased bone in growing mice. *J Bone Miner Res*, *36*(8), 1510–1520. https://doi.org/10.1002/jbmr.4312

Ko, F. C., Martins, J. S., Reddy, P., Bragdon, B., Hussein, A. I., Gerstenfeld, L. C., & Demay, M. B. (2016). Acute Phosphate Restriction Impairs Bone Formation and Increases Marrow Adipose Tissue in Growing Mice. *J Bone Miner Res*, *31*(12), 2204–2214. https://doi.org/10.1002/jbmr.2891

Kohler, R., Segvich, D. M., Reul, O., Metzger, C. E., Allen, M. R., & Wallace, J. M. (2024). Romosozumab rescues impaired bone mass and strength in a murine model of diabetic kidney disease. *Bone Rep*, *21*, 101774. https://doi.org/10.1016/j.bonr.2024.101774

Kollmannsberger, P., Kerschnitzki, M., Repp, F., Wagermaier, W., Weinkamer, R., & Fratzl, P. (2017). The small world of osteocytes: connectomics of the lacuno-canalicular network in bone. *New Journal of Physics*, *19*(7), 073019. https://doi.org/10.1088/1367-2630/aa764b

Komori, T. (2010). Regulation of osteoblast differentiation by Runx2. *Adv Exp Med Biol*, *658*, 43–49. https://doi.org/10.1007/978-1-4419-1050-9_5

Komori, T. (2017). Roles of Runx2 in Skeletal Development. *Adv Exp Med Biol*, *962*, 83–93. https://doi.org/10.1007/978-981-10-3233-2_6

Komori, T. (2019). Regulation of Proliferation, Differentiation and Functions of Osteoblasts by Runx2. *Int J Mol Sci*, *20*(7). https://doi.org/10.3390/ijms20071694

Kong, Y. Y., Yoshida, H., Sarosi, I., Tan, H. L., Timms, E., Capparelli, C., Morony, S., Oliveira-dos-Santos, A. J., Van, G., Itie, A., Khoo, W., Wakeham, A., Dunstan, C. R., Lacey, D. L., Mak, T. W., Boyle, W. J., & Penninger, J. M. (1999). OPGL is a key regulator of osteoclastogenesis, lymphocyte development and lymph-node organogenesis. *Nature*, *397*(6717), 315–323. https://doi.org/10.1038/16852

Kovesdy, C. P. (2022). Epidemiology of chronic kidney disease: an update 2022. *Kidney Int Suppl (2011)*, *12*(1), 7–11. https://doi.org/10.1016/j.kisu.2021.11.003

Ku, E., Lee, B. J., Wei, J., & Weir, M. R. (2019). Hypertension in CKD: Core Curriculum 2019. *Am J Kidney Dis*, *74*(1), 120–131. https://doi.org/10.1053/j.ajkd.2018.12.044

Kular, J., Tickner, J., Chim, S. M., & Xu, J. (2012). An overview of the regulation of bone remodelling at the cellular level. *Clin Biochem*, *45*(12), 863–873. https://doi.org/10.1016/j.clinbiochem.2012.03.021

Kumar Pasupulati, A., Chitra, P. S., & Reddy, G. B. (2016). Advanced glycation end products mediated cellular and molecular events in the pathology of diabetic nephropathy. *Biomol Concepts*, *7*(5-6), 293–309. https://doi.org/10.1515/bmc-2016-0021

Kuo, S. W., Rimando, M. G., Liu, Y. S., & Lee, O. K. (2017). Intermittent Administration of Parathyroid Hormone 1-34 Enhances Osteogenesis of Human Mesenchymal Stem Cells by Regulating Protein Kinase Cdelta. *Int J Mol Sci*, *18*(10). https://doi.org/10.3390/ijms18102221

Kuriwaka-Kido, R., Kido, S., Miyatani, Y., Ito, Y., Kondo, T., Omatsu, T., Dong, B., Endo, I., Miyamoto, K., & Matsumoto, T. (2013). Parathyroid hormone (1-34) counteracts the suppression of interleukin-11 expression by glucocorticoid in murine osteoblasts: a possible mechanism for stimulating osteoblast differentiation against glucocorticoid excess. *Endocrinology*, *154*(3), 1156–1167. https://doi.org/10.1210/en.2013-1915

Lad, S. E. (2023). Absence of secondary osteons in femora of aged rats: Implications of lifespan on Haversian remodeling in mammals. *J Morphol*, *284*(7), e21600. https://doi.org/10.1002/jmor.21600

Lair, B., Lac, M., Frassin, L., Brunet, M., Buleon, M., Feuillet, G., Maslo, C., Marques, M., Monbrun, L., Bourlier, V., Montastier, E., Viguerie, N., Tavernier, G., Laurens, C., & Moro, C. (2024). Common mouse models of chronic kidney disease are not associated with cachexia. *Commun Biol*, *7*(1), 346. https://doi.org/10.1038/s42003-024-06021-y

Laster, M., Pereira, R. C., Noche, K., Gales, B., Salusky, I. B., & Albrecht, L. V. (2023). Sclerostin, Osteocytes, and Wnt Signaling in Pediatric Renal Osteodystrophy. *Nutrients*, *15*(19). https://doi.org/10.3390/nu15194127

Lee, D. Y., Yun, S. H., Lee, S. Y., Lee, J., Jr Mariano, E., Joo, S. T., Choi, I., Choi, J. S., Kim, G. D., Lee, J., Choi, S. H., & Hur, S. J. (2023). Analysis of commercial fetal bovine serum (FBS) and its substitutes in the development of cultured meat. *Food Res Int*, *174*(Pt 1), 113617. https://doi.org/10.1016/j.foodres.2023.113617

Lee, H. W., Kim, S. Y., Kim, A. Y., Lee, E. J., Choi, J. Y., & Kim, J. B. (2009). Adiponectin stimulates osteoblast differentiation through induction of COX2 in mesenchymal progenitor cells. *Stem Cells*, *27*(9), 2254–2262. https://doi.org/10.1002/stem.144

Lee, W. C., Li, L. C., Chen, J. B., & Chang, H. W. (2015). Indoxyl sulfate-induced oxidative stress, mitochondrial dysfunction, and impaired biogenesis are partly protected by vitamin C and N-acetylcysteine. *ScientificWorldJournal*, *2015*, 620826. https://doi.org/10.1155/2015/620826

Lee, Z. H., & Kim, H. H. (2003). Signal transduction by receptor activator of nuclear factor kappa B in osteoclasts. *Biochem Biophys Res Commun*, *305*(2), 211–214. https://doi.org/10.1016/s0006-291x(03)00695-8

Lewiecki, E. M., Blicharski, T., Goemaere, S., Lippuner, K., Meisner, P. D., Miller, P. D., Miyauchi, A., Maddox, J., Chen, L., & Horlait, S. (2018). A Phase III Randomized Placebo-Controlled Trial to Evaluate Efficacy and Safety of Romosozumab in Men With Osteoporosis. *J Clin Endocrinol Metab*, *103*(9), 3183–3193. https://doi.org/10.1210/jc.2017-02163

Lewis, K. J., Yi, X., Wright, C. S., Pemberton, E. Z., Bullock, W. A., Thompson, W. R., & Robling, A. G. (2020). The mTORC2 Component Rictor Is Required for Load-Induced Bone Formation in Late-Stage Skeletal Cells. *JBMR Plus*, *4*(7), e10366. https://doi.org/10.1002/jbm4.10366

Li, H. X., Luo, X., Liu, R. X., Yang, Y. J., & Yang, G. S. (2008). Roles of Wnt/beta-catenin signaling in adipogenic differentiation potential of adipose-derived mesenchymal stem cells. *Mol Cell Endocrinol*, *291*(1-2), 116–124. https://doi.org/10.1016/j.mce.2008.05.005

Li, J., Bao, Q., Chen, S., Liu, H., Feng, J., Qin, H., Li, A., Liu, D., Shen, Y., Zhao, Y., & Zong, Z. (2017). Different bone remodeling levels of trabecular and cortical bone in response to changes in Wnt/beta-catenin signaling in mice. *J Orthop Res*, *35*(4), 812–819. https://doi.org/10.1002/jor.23339

Li, S., Liu, G., & Hu, S. (2024). Osteoporosis: interferon-gamma-mediated bone remodeling in osteoimmunology. *Front Immunol*, *15*, 1396122. https://doi.org/10.3389/fimmu.2024.1396122

Li, W. Q., Tan, S. L., Li, X. H., Sun, T. L., Li, D., Du, J., Wei, S. S., Li, Y. J., & Zhang, B. K. (2019). Calcitonin gene-related peptide inhibits the cardiac fibroblasts senescence in cardiac fibrosis via up-regulating klotho expression. *Eur J Pharmacol*, *843*, 96–103. https://doi.org/10.1016/j.ejphar.2018.10.023

Li, X., Grisanti, M., Fan, W., Asuncion, F. J., Tan, H. L., Dwyer, D., Han, C. Y., Yu, L., Lee, J., Lee, E., Barrero, M., Kurimoto, P., Niu, Q. T., Geng, Z., Winters, A., Horan, T., Steavenson, S., Jacobsen, F., Chen, Q.,…Richards, W. G. (2011). Dickkopf-1 regulates bone formation in young growing rodents and upon traumatic injury. *J Bone Miner Res*, *26*(11), 2610–2621. https://doi.org/10.1002/jbmr.472

Li, X., Ominsky, M. S., Niu, Q. T., Sun, N., Daugherty, B., D'Agostin, D., Kurahara, C., Gao, Y., Cao, J., Gong, J., Asuncion, F., Barrero, M., Warmington, K., Dwyer, D., Stolina, M., Morony, S., Sarosi, I., Kostenuik, P. J., Lacey, D. L.,…Paszty, C. (2008). Targeted deletion of the sclerostin gene in mice results in increased bone formation and bone strength. *J Bone Miner Res*, *23*(6), 860–869. https://doi.org/10.1359/jbmr.080216

Li, Y., He, X., Olauson, H., Larsson, T. E., & Lindgren, U. (2013). FGF23 Affects the Lineage Fate Determination of Mesenchymal Stem Cells. *Calcified Tissue International*, *93*(6), 556–564. https://doi.org/10.1007/s00223-013-9795-6

Li, Z., Bagchi, D. P., Zhu, J., Bowers, E., Yu, H., Hardij, J., Mori, H., Granger, K., Skjaerlund, J., Mandair, G., Abrishami, S., Singer, K., Hankenson, K. D., Rosen, C. J., & MacDougald, O. A. (2022). Constitutive bone marrow adipocytes suppress local bone formation. *JCI Insight*, *7*(21). https://doi.org/10.1172/jci.insight.160915

Li, Z., Bowers, E., Zhu, J., Yu, H., Hardij, J., Bagchi, D. P., Mori, H., Lewis, K. T., Granger, K., Schill, R. L., Romanelli, S. M., Abrishami, S., Hankenson, K. D., Singer, K., Rosen, C. J., & MacDougald, O. A. (2022). Lipolysis of bone marrow adipocytes is required to fuel bone and the marrow niche during energy deficits. *ELife.*, *11*. https://doi.org/10.7554/eLife.78496

Li, Z., Hardij, J., Bagchi, D. P., Scheller, E. L., & MacDougald, O. A. (2018). Development, regulation, metabolism and function of bone marrow adipose tissues. *110*, 134–140. https://doi.org/10.1016/J.BONE.2018.01.008

Li, Z., & Rosen, C. J. (2023). The Multifaceted Roles of Bone Marrow Adipocytes in Bone and Hematopoietic Homeostasis. *J Clin Endocrinol Metab*, *108*(12), e1465–e1472. https://doi.org/10.1210/clinem/dgad355

Liang, J., & Liu, Y. (2023). Animal Models of Kidney Disease: Challenges and Perspectives. *Kidney360*, *4*(10), 1479–1493. https://doi.org/10.34067/KID.0000000000000227

Lin, H., Zhou, Y., Lei, Q., Lin, D., Chen, J., & Wu, C. (2021). Effect of inorganic phosphate on migration and osteogenic differentiation of bone marrow mesenchymal stem cells. *BMC Dev Biol*, *21*(1), 1. https://doi.org/10.1186/s12861-020-00229-x

Linhart, H. G., Ishimura-Oka, K., DeMayo, F., Kibe, T., Repka, D., Poindexter, B., Bick, R. J., & Darlington, G. J. (2001). C/EBPalpha is required for differentiation of white, but not brown, adipose tissue. *Proc Natl Acad Sci U S A*, *98*(22), 12532–12537. https://doi.org/10.1073/pnas.211416898

Liu, H., Wada, A., Le, I., Le, P. T., Lee, A. W. F., Zhou, J., Gori, F., Baron, R., & Rosen, C. J. (2023). PTH regulates osteogenesis and suppresses adipogenesis through Zfp467 in a feed-forward, PTH1R-cyclic AMP-dependent manner. *Elife*, *12*. https://doi.org/10.7554/eLife.83345

Liu, L., Le, P. T., Stohn, J. P., Liu, H., Ying, W., Baron, R., & Rosen, C. J. (2024). Calorie restriction in mice impairs cortical but not trabecular peak bone mass by suppressing bone remodeling. *J Bone Miner Res*, *39*(8), 1188–1199. https://doi.org/10.1093/jbmr/zjae104

Liu, L., Le, P. T., Stohn, J. P., Liu, H., Ying, W., Baron, R., & Rosen, C. J. (2024). Calorie restriction in mice impairs cortical but not trabecular peak bone mass by suppressing bone remodeling. *Journal of bone and mineral research*. https://doi.org/10.1093/jbmr/zjae104

Liu, M., Kurimoto, P., Zhang, J., Niu, Q. T., Stolina, M., Dechow, P. C., Feng, J. Q., Hesterman, J., Silva, M. D., Ominsky, M. S., Richards, W. G., Ke, H., & Kostenuik, P. J. (2018). Sclerostin and DKK1 Inhibition Preserves and Augments Alveolar Bone Volume and Architecture in Rats with Alveolar Bone Loss. *J Dent Res*, *97*(9), 1031–1038. https://doi.org/10.1177/0022034518766874

Liu, Q., Wan, Q., Yang, R., Zhou, H., & Li, Z. (2012). Effects of intermittent versus continuous parathyroid hormone administration on condylar chondrocyte proliferation and differentiation. *Biochem Biophys Res Commun*, *424*(1), 182–188. https://doi.org/10.1016/j.bbrc.2012.06.106

Liu, S., Song, W., Boulanger, J. H., Tang, W., Sabbagh, Y., Kelley, B., Gotschall, R., Ryan, S., Phillips, L., Malley, K., Cao, X., Xia, T. H., Zhen, G., Cao, X., Ling, H., Dechow, P. C., Bellido, T. M., Ledbetter, S. R., & Schiavi, S. C. (2014). Role of TGF-beta in a mouse model of high turnover renal osteodystrophy. *J Bone Miner Res*, *29*(5), 1141–1157. https://doi.org/10.1002/jbmr.2120

Liu, W. C., Shyu, J. F., Lim, P. S., Fang, T. C., Lu, C. L., Zheng, C. M., Hou, Y. C., Wu, C. C., Lin, Y. F., & Lu, K. C. (2020). Concentration and Duration of Indoxyl Sulfate Exposure Affects Osteoclastogenesis by Regulating NFATc1 via Aryl Hydrocarbon Receptor. *Int J Mol Sci*, *21*(10). https://doi.org/10.3390/ijms21103486

Liu, W. C., Wu, C. C., Lim, P. S., Chien, S. W., Hou, Y. C., Zheng, C. M., Shyu, J. F., Lin, Y. F., & Lu, K. C. (2018). Effect of uremic toxin-indoxyl sulfate on the skeletal system. *Clin Chim Acta*, *484*, 197–206. https://doi.org/10.1016/j.cca.2018.05.057

Liu, W. C., Yen, J. F., Lang, C. L., Yan, M. T., & Lu, K. C. (2013). Bisphophonates in CKD patients with low bone mineral density. *ScientificWorldJournal*, *2013*, 837573. https://doi.org/10.1155/2013/837573

Liu, Y., Strecker, S., Wang, L., Kronenberg, M. S., Wang, W., Rowe, D. W., & Maye, P. (2013). Osterix-cre labeled progenitor cells contribute to the formation and maintenance of the bone marrow stroma. *PLoS One*, *8*(8), e71318. https://doi.org/10.1371/journal.pone.0071318

Livak, K. J., & Schmittgen, T. D. (2001). Analysis of relative gene expression data using real-time quantitative PCR and the 2(-Delta Delta C(T)) Method. *25*, 402–408. https://doi.org/10.1006/METH.2001.1262

Locklin, R. M., Khosla, S., Turner, R. T., & Riggs, B. L. (2003). Mediators of the biphasic responses of bone to intermittent and continuously administered parathyroid hormone. *J Cell Biochem*, *89*(1), 180–190. https://doi.org/10.1002/jcb.10490

Lotinun, S., Sibonga, J. D., & Turner, R. T. (2002). Differential effects of intermittent and continuous administration of parathyroid hormone on bone histomorphometry and gene expression. *Endocrine*, *17*(1), 29–36. https://doi.org/10.1385/ENDO:17:1:29

Lovdel, A., Suchacki, K. J., Roberts, F., Sulston, R. J., Wallace, R. J., Thomas, B. J., Bell, R. M. B., Pruñonosa Cervera, I., Macpherson, G. J., Morton, N. M., Homer, N. Z. M., Chapman, K. E., & Cawthorn, W. P. (2024). Deletion of Hsd11b1 suppresses caloric restriction-induced bone marrow adiposity in male but not female mice. *Journal of Endocrinology*, *262*(2). https://doi.org/10.1530/joe-24-0072

Luxenburg, C., Geblinger, D., Klein, E., Anderson, K., Hanein, D., Geiger, B., & Addadi, L. (2007). The architecture of the adhesive apparatus of cultured osteoclasts: from podosome formation to sealing zone assembly. *PLoS One*, *2*(1), e179. https://doi.org/10.1371/journal.pone.0000179

Ma, Y. H., Schwartz, A. V., Sigurdsson, S., Hue, T. F., Lang, T. F., Harris, T. B., Rosen, C. J., Vittinghoff, E., Eiriksdottir, G., Hauksdottir, A. M., Siggeirsdottir, K., Sigurdsson, G., Oskarsdottir, D., Napoli, N., Palermo, L., Gudnason, V., & Li, X. (2014). Circulating sclerostin associated with vertebral bone marrow fat in older men but not women. *J Clin Endocrinol Metab*, *99*(12), E2584–2590. https://doi.org/10.1210/jc.2013-4493

Mac Way, F., Lessard, M., & Lafage-Proust, M. H. (2012). Pathophysiology of chronic kidney disease-mineral and bone disorder. In (Vol. 79, pp. 544–549).

MacDonald, B. T., & He, X. (2012). Frizzled and LRP5/6 receptors for Wnt/beta-catenin signaling. *Cold Spring Harb Perspect Biol*, *4*(12). https://doi.org/10.1101/cshperspect.a007880

Mace, M. L., Olgaard, K., & Lewin, E. (2020). New Aspects of the Kidney in the Regulation of Fibroblast Growth Factor 23 (FGF23) and Mineral Homeostasis. *Int J Mol Sci*, *21*(22). https://doi.org/10.3390/ijms21228810

Madsen, M. S., Siersbaek, R., Boergesen, M., Nielsen, R., & Mandrup, S. (2014). Peroxisome proliferator-activated receptor gamma and C/EBPalpha synergistically activate key metabolic adipocyte genes by assisted loading. *Mol Cell Biol*, *34*(6), 939–954. https://doi.org/10.1128/MCB.01344-13

Maggiano, I. S., Maggiano, C. M., Clement, J. G., Thomas, C. D., Carter, Y., & Cooper, D. M. (2016). Three-dimensional reconstruction of Haversian systems in human cortical bone using synchrotron radiation-based micro-CT: morphology and

quantification of branching and transverse connections across age. *J Anat*, *228*(5), 719–732. https://doi.org/10.1111/joa.12430

Maridas, D. E., , Rendina-Ruedy, E., , Helderman, R. C., , DeMambro, V. E., , Brooks, D., , Guntur, A. R., , Lanske, B., , Bouxsein, M. L., , Rosen, C. J., & (2018). Progenitor recruitment and adipogenic lipolysis contribute to the anabolic actions of parathyroid hormone on the skeleton. *33*, 2885–2898. https://doi.org/10.1096/fj.201800948RR

Maridas, D. E., Rendina-Ruedy, E., Helderman, R. C., DeMambro, V. E., Brooks, D., Guntur, A. R., Lanske, B., Bouxsein, M. L., & Rosen, C. J. (2018). Progenitor recruitment and adipogenic lipolysis contribute to the anabolic actions of parathyroid hormone on the skeleton. *33*, 2885–2898. https://doi.org/10.1096/fj.201800948RR

Maridas, D. E., Rendina-Ruedy, E., Le, P. T., & Rosen, C. J. (2018). Isolation, Culture, and Differentiation of Bone Marrow Stromal Cells and Osteoclast Progenitors from Mice. *J Vis Exp*(131). https://doi.org/10.3791/56750

Marino, S., Akel, N., Li, S., Cregor, M., Jones, M., Perez, B., Troncoso, G., Meeks, J., Stewart, S., Sato, A. Y., Nookaew, I., & Bellido, T. (2023). Reversal of the diabetic bone signature with anabolic therapies in mice. *Bone Res*, *11*(1), 19. https://doi.org/10.1038/s41413-023-00261-0

Marques, I. D. B., Araújo, M. J. C. L. N., Graciolli, F. G., Reis, L. M. D., Pereira, R. M., Custódio, M. R., Jorgetti, V., Elias, R. M., David-Neto, E., & Moysés, R. M. A. (2017). Biopsy vs. peripheral computed tomography to assess bone disease in CKD patients on dialysis: differences and similarities. *Osteoporosis International*, *28*(5), 1675–1683. https://doi.org/10.1007/s00198-017-3956-9

Martin, T. J. (2004). Paracrine regulation of osteoclast formation and activity: milestones in discovery. *J Musculoskelet Neuronal Interact*, *4*(3), 243–253.

Massy, Z., & Drueke, T. (2017). Adynamic bone disease is a predominant bone pattern in early stages of chronic kidney disease. *J Nephrol*, *30*(5), 629–634. https://doi.org/10.1007/s40620-017-0397-7

Matsuoka, K., Park, K. A., Ito, M., Ikeda, K., & Takeshita, S. (2014). Osteoclast-derived complement component 3a stimulates osteoblast differentiation. *J Bone Miner Res*, *29*(7), 1522–1530. https://doi.org/10.1002/jbmr.2187

Maurice, F., Dutour, A., Vincentelli, C., Abdesselam, I., Bernard, M., Dufour, H., Lefur, Y., Graillon, T., Kober, F., Cristofari, P., Jouve, E., Pini, L., Fernandez, R., Chagnaud, C., Brue, T., Castinetti, F., & Gaborit, B. (2018). Active Cushing syndrome patients have increased ectopic fat deposition and bone marrow fat content compared to cured patients and healthy subjects: a pilot 1H-MRS study. *European Journal of Endocrinology*, *179*(5), 307–317. https://doi.org/10.1530/eje-18-0318

McCarthy, T. L., & Centrella, M. (2010). Novel links among Wnt and TGF-beta signaling and Runx2. *Mol Endocrinol*, *24*(3), 587–597. https://doi.org/10.1210/me.2009-0379

McClung, M. R., Grauer, A., Boonen, S., Bolognese, M. A., Brown, J. P., Diez-Perez, A., Langdahl, B. L., Reginster, J. Y., Zanchetta, J. R., Wasserman, S. M., Katz, L., Maddox, J., Yang, Y. C., Libanati, C., & Bone, H. G. (2014). Romosozumab in

postmenopausal women with low bone mineral density. *N Engl J Med*, *370*(5), 412–420. https://doi.org/10.1056/NEJMoa1305224

McWilliams, T. G., Prescott, A. R., Allen, G. F., Tamjar, J., Munson, M. J., Thomson, C., Muqit, M. M., & Ganley, I. G. (2016). mito-QC illuminates mitophagy and mitochondrial architecture in vivo. *J Cell Biol*, *214*(3), 333–345. https://doi.org/10.1083/jcb.201603039

Melsom, T., Norvik, J. V., Enoksen, I. T., Stefansson, V., Mathisen, U. D., Fuskevag, O. M., Jenssen, T. G., Solbu, M. D., & Eriksen, B. O. (2022). Sex Differences in Age-Related Loss of Kidney Function. *J Am Soc Nephrol*, *33*(10), 1891–1902. https://doi.org/10.1681/ASN.2022030323

Mendez-Ferrer, S., Michurina, T. V., Ferraro, F., Mazloom, A. R., Macarthur, B. D., Lira, S. A., Scadden, D. T., Ma'ayan, A., Enikolopov, G. N., & Frenette, P. S. (2010). Mesenchymal and haematopoietic stem cells form a unique bone marrow niche. *Nature*, *466*(7308), 829–834. https://doi.org/10.1038/nature09262

Metzger, C. E., Kittaka, M., LaPlant, A. N., Ueki, Y., & Allen, M. R. (2024). Inhibition of RANKL improves the skeletal phenotype of adenine-induced chronic kidney disease in mice. *JBMR Plus*, *8*(2), ziae004. https://doi.org/10.1093/jbmrpl/ziae004

Metzger, C. E., Swallow, E. A., & Allen, M. R. (2020). Elevations in Cortical Porosity Occur Prior to Significant Rise in Serum Parathyroid Hormone in Young Female Mice with Adenine-Induced CKD. *Calcif Tissue Int*, *106*(4), 392–400. https://doi.org/10.1007/s00223-019-00642-w

Metzger, C. E., Swallow, E. A., Stacy, A. J., Tippen, S. P., Hammond, M. A., Chen, N. X., Moe, S. M., & Allen, M. R. (2021). Reversing cortical porosity: Cortical pore infilling in preclinical models of chronic kidney disease. In (Vol. 143, pp. 115632).

Metzger, C. E., Tak, L. Y., Scholz, S., & Allen, M. R. (2025). Prolonged secondary hyperparathyroidism in adenine-induced CKD leads to skeletal changes consistent with skeletal hyporesponsiveness to PTH. *PLoS One*, *20*(5), e0324628. https://doi.org/10.1371/journal.pone.0324628

Meyer, M. B., Benkusky, N. A., Sen, B., Rubin, J., & Pike, J. W. (2016). Epigenetic Plasticity Drives Adipogenic and Osteogenic Differentiation of Marrow-derived Mesenchymal Stem Cells. *J Biol Chem*, *291*(34), 17829–17847. https://doi.org/10.1074/jbc.M116.736538

Millan, J. L., & Whyte, M. P. (2016). Alkaline Phosphatase and Hypophosphatasia. *Calcif Tissue Int*, *98*(4), 398–416. https://doi.org/10.1007/s00223-015-0079-1

Miller, P. D., Adachi, J. D., Albergaria, B. H., Cheung, A. M., Chines, A. A., Gielen, E., Langdahl, B. L., Miyauchi, A., Oates, M., Reid, I. R., Santiago, N. R., Vanderkelen, M., Wang, Z., & Yu, Z. (2022). Efficacy and Safety of Romosozumab Among Postmenopausal Women With Osteoporosis and Mild-to-Moderate Chronic Kidney Disease. *J Bone Miner Res*, *37*(8), 1437–1445. https://doi.org/10.1002/jbmr.4563

Miller, P. D., Roux, C., Boonen, S., Barton, I. P., Dunlap, L. E., & Burgio, D. E. (2005). Safety and efficacy of risedronate in patients with age-related reduced renal function as estimated by the Cockcroft and Gault method: a pooled analysis of nine clinical trials. *J Bone Miner Res*, *20*(12), 2105–2115. https://doi.org/10.1359/JBMR.050817

Miyagawa, K., Yamazaki, M., Kawai, M., Nishino, J., Koshimizu, T., Ohata, Y., Tachikawa, K., Mikuni-Takagaki, Y., Kogo, M., Ozono, K., & Michigami, T. (2014). Dysregulated gene expression in the primary osteoblasts and osteocytes isolated from hypophosphatemic Hyp mice. *PLoS One*, *9*(4), e93840. https://doi.org/10.1371/journal.pone.0093840

Miyauchi, A., Hamaya, E., Nishi, K., Tolman, C., & Shimauchi, J. (2022). Efficacy and safety of romosozumab among Japanese postmenopausal women with osteoporosis and mild-to-moderate chronic kidney disease. *J Bone Miner Metab*, *40*(4), 677–687. https://doi.org/10.1007/s00774-022-01332-8

Mizoguchi, T., Pinho, S., Ahmed, J., Kunisaki, Y., Hanoun, M., Mendelson, A., Ono, N., Kronenberg, H. M., & Frenette, P. S. (2014). Osterix marks distinct waves of primitive and definitive stromal progenitors during bone marrow development. *Dev Cell*, *29*(3), 340–349. https://doi.org/10.1016/j.devcel.2014.03.013

Moe, S., Drueke, T., Cunningham, J., Goodman, W., Martin, K., Olgaard, K., Ott, S., Sprague, S., Lameire, N., Eknoyan, G., & Kidney Disease: Improving Global, O. (2006). Definition, evaluation, and classification of renal osteodystrophy: a position statement from Kidney Disease: Improving Global Outcomes (KDIGO). *Kidney Int*, *69*(11), 1945–1953. https://doi.org/10.1038/sj.ki.5000414

Moe, S. M., Chen, N. X., Newman, C. L., Gattone, V. H., 2nd, Organ, J. M., Chen, X., & Allen, M. R. (2014). A comparison of calcium to zoledronic acid for improvement of cortical bone in an animal model of CKD. *J Bone Miner Res*, *29*(4), 902–910. https://doi.org/10.1002/jbmr.2089

Moe, S. M., Chen, N. X., Newman, C. L., Organ, J. M., Kneissel, M., Kramer, I., Gattone, V. H., & Allen, M. R. (2015). Anti-sclerostin antibody treatment in a rat model of progressive renal osteodystrophy. In (Vol. 30, pp. 539–549): J Bone Miner Res.

Moochhala, S. H., Sayer, J. A., Carr, G., & Simmons, N. L. (2008). Renal calcium stones: insights from the control of bone mineralization. *Exp Physiol*, *93*(1), 43–49. https://doi.org/10.1113/expphysiol.2007.040790

Moon, J. B., Kim, J. H., Kim, K., Youn, B. U., Ko, A., Lee, S. Y., & Kim, N. (2012). Akt induces osteoclast differentiation through regulating the GSK3beta/NFATc1 signaling cascade. *J Immunol*, *188*(1), 163–169. https://doi.org/10.4049/jimmunol.1101254

Moorthi, R. N., Fadel, W., Eckert, G. J., Ponsler-Sipes, K., Moe, S. M., & Lin, C. (2015). Bone marrow fat is increased in chronic kidney disease by magnetic resonance spectroscopy. *Osteoporos Int*, *26*(6), 1801–1807. https://doi.org/10.1007/s00198-015-3064-7

Morris, D. M., Wang, C., Papanastasiou, G., Gray, C. D., Xu, W., Sjostrom, S., Badr, S., Paccou, J., Semple, S. I., MacGillivray, T., & Cawthorn, W. P. (2024). A novel deep learning method for large-scale analysis of bone marrow adiposity using UK Biobank Dixon MRI data. *Comput Struct Biotechnol J*, *24*, 89–104. https://doi.org/10.1016/j.csbj.2023.12.029

Mosey, H., Nunez, J. A., Goring, A., Clarkin, C. E., Staines, K. A., Lee, P. D., Pitsillides, A. A., & Javaheri, B. (2017). Sost Deficiency does not Alter Bone's Lacunar or Vascular Porosity in Mice. *Front Mater*, *4*, 27. https://doi.org/10.3389/fmats.2017.00027

Moysés, R. M. A., & Schiavi, S. C. (2015). Sclerostin, Osteocytes, and Chronic Kidney Disease - Mineral Bone Disorder. In (Vol. 28, pp. 578–586): Semin Dial.

Mushtaq, T., Farquharson, C., Seawright, E., & Ahmed, S. F. (2002). Glucocorticoid effects on chondrogenesis, differentiation and apoptosis in the murine ATDC5 chondrocyte cell line. *The Journal of endocrinology*, *175*(3), 705–713. https://doi.org/10.1677/joe.0.1750705

Mwale, F., Tchetina, E., Wu, C. W., & Poole, A. R. (2002). The assembly and remodeling of the extracellular matrix in the growth plate in relationship to mineral deposition and cellular hypertrophy: an in situ study of collagens II and IX and proteoglycan. *J Bone Miner Res*, *17*(2), 275–283. https://doi.org/10.1359/jbmr.2002.17.2.275

Nakamura, S., Shigeyama, S., Minami, S., Shima, T., Akayama, S., Matsuda, T., Esposito, A., Napolitano, G., Kuma, A., Namba-Hamano, T., Nakamura, J., Yamamoto, K., Sasai, M., Tokumura, A., Miyamoto, M., Oe, Y., Fujita, T., Terawaki, S., Takahashi, A.,…Yoshimori, T. (2020). LC3 lipidation is essential for TFEB activation during the lysosomal damage response to kidney injury. *Nat Cell Biol*, *22*(10), 1252–1263. https://doi.org/10.1038/s41556-020-00583-9

Nakashima, K., Zhou, X., Kunkel, G., Zhang, Z., Deng, J. M., Behringer, R. R., & de Crombrugghe, B. (2002). The novel zinc finger-containing transcription factor osterix is required for osteoblast differentiation and bone formation. *Cell*, *108*(1), 17–29. https://doi.org/10.1016/s0092-8674(01)00622-5

Naylor, K. L., Garg, A. X., Zou, G., Langsetmo, L., Leslie, W. D., Fraser, L. A., Adachi, J. D., Morin, S., Goltzman, D., Lentle, B., Jackson, S. A., Josse, R. G., & Jamal, S. A. (2015). Comparison of fracture risk prediction among individuals with reduced and normal kidney function. *Clin J Am Soc Nephrol*, *10*(4), 646–653. https://doi.org/10.2215/CJN.06040614

Neto, R., Pereira, L., Magalhaes, J., Quelhas-Santos, J., Martins, S., Carvalho, C., & Frazao, J. M. (2021). Sclerostin and DKK1 circulating levels associate with low bone turnover in patients with chronic kidney disease Stages 3 and 4. *Clin Kidney J*, *14*(11), 2401–2408. https://doi.org/10.1093/ckj/sfab081

Newman, C. L., Chen, N. X., Smith, E., Smith, M., Brown, D., Moe, S. M., & Allen, M. R. (2015). Compromised vertebral structural and mechanical properties associated with progressive kidney disease and the effects of traditional pharmacological interventions. *Bone*, *77*, 50–56. https://doi.org/10.1016/j.bone.2015.04.021

Ni, L. H., Tang, R. N., Yuan, C., Song, K. Y., Wang, L. T., Zhang, X. L., Lv, L. L., Wang, B., Wu, M., Tang, T. T., Li, Z. L., Yin, D., Cao, J. Y., Wang, X. C., Liu, H., Chen, Q., & Liu, B. C. (2019). Cinacalcet attenuated bone loss via inhibiting parathyroid hormone-induced endothelial-to-adipocyte transition in chronic kidney disease rats. *Ann Transl Med*, *7*(14), 312. https://doi.org/10.21037/atm.2019.06.44

Nickolas, T. L., Stein, E. M., Dworakowski, E., Nishiyama, K. K., Komandah-Kosseh, M., Zhang, C. A., Mcmahon, D. J., Liu, X. S., Boutroy, S., Cremers, S., & Shane, E. (2013). Rapid cortical bone loss in patients with chronic kidney disease. *Journal of bone and mineral research*, *28*(8), 1811–1820. https://doi.org/10.1002/jbmr.1916

Nii-Kono, T., Iwasaki, Y., Uchida, M., Fujieda, A., Hosokawa, A., Motojima, M., Yamato, H., Kurokawa, K., & Fukagawa, M. (2007). Indoxyl sulfate induces skeletal resistance to parathyroid hormone in cultured osteoblastic cells. *Kidney Int*, *71*(8), 738–743. https://doi.org/10.1038/sj.ki.5002097

Nishimura, R., Kato, Y., Chen, D., Harris, S. E., Mundy, G. R., & Yoneda, T. (1998). Smad5 and DPC4 are key molecules in mediating BMP-2-induced osteoblastic differentiation of the pluripotent mesenchymal precursor cell line C2C12. *J Biol Chem*, *273*(4), 1872–1879. https://doi.org/10.1074/jbc.273.4.1872

Nitta, K., Yajima, A., & Tsuchiya, K. (2017). Management of osteoporosis in chronic kidney disease. *56*, 3271–3276. https://doi.org/10.2169/internalmedicine.8618-16

Noels, H., Lehrke, M., Vanholder, R., & Jankowski, J. (2021). Lipoproteins and fatty acids in chronic kidney disease: molecular and metabolic alterations. *Nat Rev Nephrol*, *17*(8), 528–542. https://doi.org/10.1038/s41581-021-00423-5

Obi, Y., & Kalantar-Zadeh, K. (2016). Yet Another Vitamin D Analogue for the Management of Secondary Hyperparathyroidism: A Triton among the Minnows? *Am J Nephrol*, *43*(3), 221–224. https://doi.org/10.1159/000445762

Okamura, M., Kudo, H., Wakabayashi, K., Tanaka, T., Nonaka, A., Uchida, A., Tsutsumi, S., Sakakibara, I., Naito, M., Osborne, T. F., Hamakubo, T., Ito, S., Aburatani, H., Yanagisawa, M., Kodama, T., & Sakai, J. (2009). COUP-TFII acts downstream of Wnt/beta-catenin signal to silence PPARgamma gene expression and repress adipogenesis. *Proc Natl Acad Sci U S A*, *106*(14), 5819–5824. https://doi.org/10.1073/pnas.0901676106

Ominsky, M. S., Boyd, S. K., Varela, A., Jolette, J., Felx, M., Doyle, N., Mellal, N., Smith, S. Y., Locher, K., Buntich, S., Pyrah, I., & Boyce, R. W. (2017). Romosozumab Improves Bone Mass and Strength While Maintaining Bone Quality in Ovariectomized Cynomolgus Monkeys. *J Bone Miner Res*, *32*(4), 788–801. https://doi.org/10.1002/jbmr.3036

Oshima, K., Nampei, A., Matsuda, M., Iwaki, M., Fukuhara, A., Hashimoto, J., Yoshikawa, H., & Shimomura, I. (2005). Adiponectin increases bone mass by suppressing osteoclast and activating osteoblast. *Biochem Biophys Res Commun*, *331*(2), 520–526. https://doi.org/10.1016/j.bbrc.2005.03.210

Ott, S. M. (2008). Histomorphometric measurements of bone turnover, mineralization, and volume. *Clin J Am Soc Nephrol*, *3 Suppl 3*(Suppl 3), S151–156. https://doi.org/10.2215/CJN.04301206

Ott, S. M. (2017). Chapter 2 - Bone Biology and Effects of Pharmaceutical Intervention on Bone Quality. In S. Bose & A. Bandyopadhyay (Eds.), *Materials for Bone Disorders* (pp. 29–82). Academic Press. https://doi.org/https://doi.org/10.1016/B978-0-12-802792-9.00002-1

Park, J. H., Lee, N. K., & Lee, S. Y. (2017). Current Understanding of RANK Signaling in Osteoclast Differentiation and Maturation. *Mol Cells*, *40*(10), 706–713. https://doi.org/10.14348/molcells.2017.0225

Park, S. Y., Choi, K. H., Jun, J. E., & Chung, H. Y. (2021). Effects of Advanced Glycation End Products on Differentiation and Function of Osteoblasts and Osteoclasts. *J Korean Med Sci*, *36*(37), e239. https://doi.org/10.3346/jkms.2021.36.e239

Pawlak, D., Oksztulska-Kolanek, E., Znorko, B., Domaniewski, T., Rogalska, J., Roszczenko, A., Brzoska, M. M., Pryczynicz, A., Kemona, A., & Pawlak, K. (2016). The Association between Elevated Levels of Peripheral Serotonin and Its Metabolite - 5-Hydroxyindoleacetic Acid and Bone Strength and Metabolism in Growing Rats with Mild Experimental Chronic Kidney Disease. *PLoS One*, *11*(10), e0163526. https://doi.org/10.1371/journal.pone.0163526

Pazzaglia, U. E., Congiu, T., Sibilia, V., & Quacci, D. (2014). Osteoblast-osteocyte transformation. A SEM densitometric analysis of endosteal apposition in rabbit femur. *J Anat*, *224*(2), 132–141. https://doi.org/10.1111/joa.12138

Pei, T., Su, G., Yang, J., Gao, W., Yang, X., Zhang, Y., Ren, J., Shen, Y., & Liu, X. (2022). Fluid Shear Stress Regulates Osteogenic Differentiation via AnnexinA6-Mediated Autophagy in MC3T3-E1 Cells. *Int J Mol Sci*, *23*(24). https://doi.org/10.3390/ijms232415702

Pelletier, S., Dubourg, L., Carlier, M. C., Hadj-Aissa, A., & Fouque, D. (2013). The relation between renal function and serum sclerostin in adult patients with CKD. *Clin J Am Soc Nephrol*, *8*(5), 819–823. https://doi.org/10.2215/CJN.07670712

Percival, C. J., & Richtsmeier, J. T. (2013). Angiogenesis and intramembranous osteogenesis. *Dev Dyn*, *242*(8), 909–922. https://doi.org/10.1002/dvdy.23992

Pereira, L., Meng, C., Marques, D., & Frazao, J. M. (2018). Old and new calcimimetics for treatment of secondary hyperparathyroidism: impact on biochemical and relevant clinical outcomes. *Clin Kidney J*, *11*(1), 80–88. https://doi.org/10.1093/ckj/sfx125

Peretti, G. M., & Domenicucci, M. (2022). Bone Structure and Function in the Distance Runner. In G. L. Canata, P. D'Hooghe, K. J. Hunt, G. M. M. J. Kerkhoffs, & U. G. Longo (Eds.), *Management of Track and Field Injuries* (pp. 55–60). Springer International Publishing. https://doi.org/10.1007/978-3-030-60216-1_6

Perry, R. J., Wang, Y., Cline, G. W., Rabin-Court, A., Song, J. D., Dufour, S., Zhang, X. M., Petersen, K. F., & Shulman, G. I. (2018). Leptin Mediates a Glucose-Fatty Acid Cycle to Maintain Glucose Homeostasis in Starvation. *Cell*, *172*(1-2), 234–248 e217. https://doi.org/10.1016/j.cell.2017.12.001

Perry, R. J., Zhang, X. M., Zhang, D., Kumashiro, N., Camporez, J. P., Cline, G. W., Rothman, D. L., & Shulman, G. I. (2014). Leptin reverses diabetes by suppression of the hypothalamic-pituitary-adrenal axis. *Nat Med*, *20*(7), 759–763. https://doi.org/10.1038/nm.3579

Peterson, M. C., & Riggs, M. M. (2010). A physiologically based mathematical model of integrated calcium homeostasis and bone remodeling. *Bone*, *46*(1), 49–63. https://doi.org/10.1016/j.bone.2009.08.053

Pierce, J. L., Begun, D. L., Westendorf, J. J., & McGee-Lawrence, M. E. (2019). Defining osteoblast and adipocyte lineages in the bone marrow. *118*, 2–7. https://doi.org/10.1016/j.bone.2018.05.019

Pimentel, A., Ureña-Torres, P., Bover, J., Luis Fernandez-Martín, J., & Cohen-Solal, M. (2021). Bone Fragility Fractures in CKD Patients. In (Vol. 108, pp. 539–550): Springer.

Pittenger, M. F., Discher, D. E., Peault, B. M., Phinney, D. G., Hare, J. M., & Caplan, A. I. (2019). Mesenchymal stem cell perspective: cell biology to clinical progress. *NPJ Regen Med*, *4*, 22. https://doi.org/10.1038/s41536-019-0083-6

Popkov, V. A., Silachev, D. N., Zalevsky, A. O., Zorov, D. B., & Plotnikov, E. Y. (2019). Mitochondria as a Source and a Target for Uremic Toxins. *Int J Mol Sci*, *20*(12). https://doi.org/10.3390/ijms20123094

Prié, D., Torres, P. U., & Friedlander, G. (2009). Latest findings in phosphate homeostasis. *Kidney International*, *75*(9), 882–889. https://doi.org/10.1038/ki.2008.643

Qian, S. W., Li, X., Zhang, Y. Y., Huang, H. Y., Liu, Y., Sun, X., & Tang, Q. Q. (2010). Characterization of adipocyte differentiation from human mesenchymal stem cells in bone marrow. *BMC Dev Biol*, *10*, 47. https://doi.org/10.1186/1471-213X-10-47

Qin, W., Yu, S. Y., Gao, J. L., Yan, J. F., Wan, Q. Q., Jia, S. L., Tay, F., Jiao, K., & Niu, L. (2025). Phosphate in Physiological and Pathological Mineralization: Important yet Often Unheeded. *MedComm (2020)*, *6*(7), e70298. https://doi.org/10.1002/mco2.70298

Raggatt, L. J., & Partridge, N. C. (2010). Cellular and molecular mechanisms of bone remodeling. *J Biol Chem*, *285*(33), 25103–25108. https://doi.org/10.1074/jbc.R109.041087

Rahman, A., Yamazaki, D., Sufiun, A., Kitada, K., Hitomi, H., Nakano, D., & Nishiyama, A. (2018). A novel approach to adenine-induced chronic kidney disease associated anemia in rodents. *PLoS One*, *13*(2), e0192531. https://doi.org/10.1371/journal.pone.0192531

Reidy, K., Kang, H. M., Hostetter, T., & Susztak, K. (2014). Molecular mechanisms of diabetic kidney disease. *J Clin Invest*, *124*(6), 2333–2340. https://doi.org/10.1172/JCI72271

Ren, X., Wang, J., Wei, H., Li, X., Tian, Y., Wang, Z., Yin, Y., Guo, Z., Qin, Z., Wu, M., & Zeng, X. (2024). Impaired TFEB-mediated autophagy-lysosome fusion promotes tubular cell cycle G2/M arrest and renal fibrosis by suppressing ATP6V0C expression and interacting with SNAREs. *Int J Biol Sci*, *20*(5), 1905–1926. https://doi.org/10.7150/ijbs.91480

Rendenbach, C., Yorgan, T. A., Heckt, T., Otto, B., Baldauf, C., Jeschke, A., Streichert, T., David, J. P., Amling, M., & Schinke, T. (2014). Effects of extracellular phosphate on gene expression in murine osteoblasts. *Calcif Tissue Int*, *94*(5), 474–483. https://doi.org/10.1007/s00223-013-9831-6

Richter, B., & Faul, C. (2018). FGF23 Actions on Target Tissues-With and Without Klotho. *Front Endocrinol (Lausanne)*, *9*, 189. https://doi.org/10.3389/fendo.2018.00189

Rickard, D. J., Wang, F. L., Rodriguez-Rojas, A. M., Wu, Z., Trice, W. J., Hoffman, S. J., Votta, B., Stroup, G. B., Kumar, S., & Nuttall, M. E. (2006). Intermittent treatment with parathyroid hormone (PTH) as well as a non-peptide small molecule agonist of the PTH1 receptor inhibits adipocyte differentiation in human bone marrow stromal cells. *Bone*, *39*(6), 1361–1372. https://doi.org/10.1016/j.bone.2006.06.010

Rinotas, V., Gkikopoulou, E., Tzortzis, E., Kritikos, K., Siatra, P., Papadopoulos, A., Perivolidi, V. I., & Douni, E. (2024). Interplay between bone marrow adiposity and bone resorption in RANKL-mediated modelled osteoporosis. *J Cell Physiol*, e31434. https://doi.org/10.1002/jcp.31434

Roberts, F., Zhu, D., Farquharson, C., & Macrae, V. E. (2019). ENPP1 in the Regulation of Mineralization and Beyond. *Trends Biochem Sci*, *44*(7), 616–628. https://doi.org/10.1016/j.tibs.2019.01.010

Roberts, W. E., Huja, S., & Roberts, J. A. (2004). Bone modeling: biomechanics, molecular mechanisms, and clinical perspectives. *Seminars in Orthodontics*, *10*(2), 123–161. https://doi.org/https://doi.org/10.1053/j.sodo.2004.01.003

Robinson, D. E., Ali, M. S., Pallares, N., Tebe, C., Elhussein, L., Abrahamsen, B., Arden, N. K., Ben-Shlomo, Y., Caskey, F. J., Cooper, C., Dedman, D., Delmestri, A., Judge, A., Perez-Saez, M. J., Pascual, J., Nogues, X., Diez-Perez, A., Strauss, V. Y., Javaid, M. K., & Prieto-Alhambra, D. (2021). Safety of Oral Bisphosphonates in Moderate-to-Severe Chronic Kidney Disease: A Binational Cohort Analysis. *J Bone Miner Res*, *36*(5), 820–832. https://doi.org/10.1002/jbmr.4235

Robles, H., Park, S. J., Joens, M. S., Fitzpatrick, J. A. J., Craft, C. S., & Scheller, E. L. (2019). Characterization of the bone marrow adipocyte niche with three-dimensional electron microscopy. In (Vol. 118, pp. 89–98): Elsevier.

Robling, A. G., & Bonewald, L. F. (2020). The Osteocyte: New Insights. *Annu Rev Physiol*, *82*, 485–506. https://doi.org/10.1146/annurev-physiol-021119-034332

Rodda, S. J., & McMahon, A. P. (2006). Distinct roles for Hedgehog and canonical Wnt signaling in specification, differentiation and maintenance of osteoblast progenitors. *Development*, *133*(16), 3231–3244. https://doi.org/10.1242/dev.02480

Romagnani, P., Remuzzi, G., Glassock, R., Levin, A., Jager, K. J., Tonelli, M., Massy, Z., Wanner, C., & Anders, H. J. (2017). Chronic kidney disease. In (Vol. 3, pp. 1–24): Nature Publishing Group.

Roohani, I., Yeo, G. C., Mithieux, S. M., & Weiss, A. S. (2022). Emerging concepts in bone repair and the premise of soft materials. *Curr Opin Biotechnol*, *74*, 220–229. https://doi.org/10.1016/j.copbio.2021.12.004

Rosen, C. J., Ackert-Bicknell, C., Rodriguez, J. P., & Pino, A. M. (2009). Marrow fat and the bone microenvironment: developmental, functional, and pathological implications. *Crit Rev Eukaryot Gene Expr*, *19*(2), 109–124. https://doi.org/10.1615/critreveukargeneexpr.v19.i2.20

Rosen, E. D., Hsu, C. H., Wang, X., Sakai, S., Freeman, M. W., Gonzalez, F. J., & Spiegelman, B. M. (2002). C/EBPalpha induces adipogenesis through PPARgamma: a unified pathway. *Genes Dev*, *16*(1), 22–26. https://doi.org/10.1101/gad.948702

Ross, S. E., Hemati, N., Longo, K. A., Bennett, C. N., Lucas, P. C., Erickson, R. L., & MacDougald, O. A. (2000). Inhibition of adipogenesis by Wnt signaling. *Science*, *289*(5481), 950–953. https://doi.org/10.1126/science.289.5481.950

Rossini, M., Gatti, D., & Adami, S. (2013). Involvement of WNT/beta-catenin signaling in the treatment of osteoporosis. *Calcif Tissue Int*, *93*(2), 121–132. https://doi.org/10.1007/s00223-013-9749-z

Rui, S., Kubota, T., Ohata, Y., Yamamoto, K., Fujiwara, M., Takeyari, S., & Ozono, K. (2022). Phosphate promotes osteogenic differentiation through non-canonical Wnt signaling pathway in human mesenchymal stem cells. *Bone*, *164*, 116525. https://doi.org/10.1016/j.bone.2022.116525

Saag, K. G., Petersen, J., Brandi, M. L., Karaplis, A. C., Lorentzon, M., Thomas, T., Maddox, J., Fan, M., Meisner, P. D., & Grauer, A. (2017). Romosozumab or Alendronate for Fracture Prevention in Women with Osteoporosis. *N Engl J Med*, *377*(15), 1417–1427. https://doi.org/10.1056/NEJMoa1708322

Sabaghian, T., Delkash, P., Rahmannia, M., Shahidi Bonjar, A. H., Centis, R., D'Ambrosio, L., Sotgiu, G., Nasiri, M. J., & Migliori, G. B. (2024). Efficacy and Safety of Anti-Osteoporotic Agents across CKD Stages: A Meta-Analysis of Randomized Clinical Trials. *Kidney Blood Press Res*, *49*(1), 581–587. https://doi.org/10.1159/000540235

Sabbagh, Y., Graciolli, F. G., O'Brien, S., Tang, W., dos Reis, L. M., Ryan, S., Phillips, L., Boulanger, J., Song, W., Bracken, C., Liu, S., Ledbetter, S., Dechow, P., Canziani, M. E., Carvalho, A. B., Jorgetti, V., Moyses, R. M., & Schiavi, S. C. (2012). Repression of osteocyte Wnt/beta-catenin signaling is an early event in the progression of renal osteodystrophy. *J Bone Miner Res*, *27*(8), 1757–1772. https://doi.org/10.1002/jbmr.1630

Sadick, J. S., Boutin, M. E., Hoffman-Kim, D., & Darling, E. M. (2016). Protein characterization of intracellular target-sorted, formalin-fixed cell subpopulations. *Sci Rep*, *6*, 33999. https://doi.org/10.1038/srep33999

Sagmeister, M. S., Harper, L., & Hardy, R. S. (2022). Cortisol excess in chronic kidney disease - A review of changes and impact on mortality. *Front Endocrinol (Lausanne)*, *13*, 1075809. https://doi.org/10.3389/fendo.2022.1075809

Salera, D., Merkel, N., Bellasi, A., & de Borst, M. H. (2025). Pathophysiology of chronic kidney disease-mineral bone disorder (CKD-MBD): from adaptive to maladaptive mineral homeostasis. *Clin Kidney J*, *18*(Suppl 1), i3–i14. https://doi.org/10.1093/ckj/sfae431

Scheller, E. L., Doucette, C. R., Learman, B. S., Cawthorn, W. P., Khandaker, S., Schell, B., Wu, B., Ding, S. Y., Bredella, M. A., Fazeli, P. K., Khoury, B., Jepsen, K. J., Pilch, P. F., Klibanski, A., Rosen, C. J., & MacDougald, O. A. (2015). Region-specific variation in the properties of skeletal adipocytes reveals regulated and constitutive marrow adipose tissues. *6*. https://doi.org/10.1038/NCOMMS8808

Scheller, E. L., Troiano, N., Vanhoutan, J. N., Bouxsein, M. A., Fretz, J. A., Xi, Y., Nelson, T., Katz, G., Berry, R., Church, C. D., Doucette, C. R., Rodeheffer, M. S., MacDougald, O. A., Rosen, C. J., & Horowitz, M. C. (2014). Use of Osmium Tetroxide Staining with Microcomputerized Tomography to Visualize and Quantify Bone Marrow Adipose Tissue In Vivo. *537*, 123–139. https://doi.org/10.1016/B978-0-12-411619-1.00007-0

Schellinger, D., , Lin, C. S., , Hatipoglu, G., , Fertikh, D., & (2001). Potential Value of Vertebral Proton MR Spectroscopy in Determining Bone Weakness. In (Vol. 22, pp. 1620–1627).

Schena, F. P., & Gesualdo, L. (2005). Pathogenetic mechanisms of diabetic nephropathy. *J Am Soc Nephrol*, *16 Suppl 1*, S30–33. https://doi.org/10.1681/asn.2004110970

Schill, R. L., Visser, J., Ashby, M. L., Li, Z., Lewis, K. T., Morales-Hernandez, A., Hoose, K. S., Maung, J. N., Uranga, R. M., Hariri, H., Hermsmeyer, I. D. K., Mori, H., & MacDougald, O. A. (2024). Deficiency of glucocorticoid receptor in bone marrow adipocytes has mild effects on bone and hematopoiesis but does not influence expansion of marrow adiposity with caloric restriction. *Front*

Endocrinol (Lausanne), *15*, 1397081. https://doi.org/10.3389/fendo.2024.1397081

Schlesinger, P. H., Blair, H. C., Beer Stolz, D., Riazanski, V., Ray, E. C., Tourkova, I. L., & Nelson, D. J. (2020). Cellular and extracellular matrix of bone, with principles of synthesis and dependency of mineral deposition on cell membrane transport. *Am J Physiol Cell Physiol*, *318*(1), C111–C124. https://doi.org/10.1152/ajpcell.00120.2019

Schwartz, A. V., Sigurdsson, S., Hue, T. F., Lang, T. F., Harris, T. B., Rosen, C. J., Vittinghoff, E., Siggeirsdottir, K., Sigurdsson, G., Oskarsdottir, D., Shet, K., Palermo, L., Gudnason, V., & Li, X. (2013). Vertebral bone marrow fat associated with lower trabecular BMD and prevalent vertebral fracture in older adults. *J Clin Endocrinol Metab*, *98*(6), 2294–2300. https://doi.org/10.1210/jc.2012-3949

Seeman, E. (2013). Age- and menopause-related bone loss compromise cortical and trabecular microstructure. *J Gerontol A Biol Sci Med Sci*, *68*(10), 1218–1225. https://doi.org/10.1093/gerona/glt071

Setiawati, R., & Rahardjo, P. (2018). Bone Development and Growth. *Osteogenesis and Bone Regeneration*.

Shahnazari, M., Wronski, T., Chu, V., Williams, A., Leeper, A., Stolina, M., Ke, H. Z., & Halloran, B. (2012). Early response of bone marrow osteoprogenitors to skeletal unloading and sclerostin antibody. *Calcif Tissue Int*, *91*(1), 50–58. https://doi.org/10.1007/s00223-012-9610-9

Shao, J. S., Cheng, S. L., Pingsterhaus, J. M., Charlton-Kachigian, N., Loewy, A. P., & Towler, D. A. (2005). Msx2 promotes cardiovascular calcification by activating paracrine Wnt signals. *J Clin Invest*, *115*(5), 1210–1220. https://doi.org/10.1172/JCI24140

Shen, W., Chen, J., Punyanitya, M., Shapses, S., Heshka, S., & Heymsfield, S. B. (2007). MRI-measured bone marrow adipose tissue is inversely related to DXA-measured bone mineral in Caucasian women. *Osteoporos Int*, *18*(5), 641–647. https://doi.org/10.1007/s00198-006-0285-9

Shi, Y., Yadav, V. K., Suda, N., Liu, X. S., Guo, X. E., Myers, M. G., Jr., & Karsenty, G. (2008). Dissociation of the neuronal regulation of bone mass and energy metabolism by leptin in vivo. *Proc Natl Acad Sci U S A*, *105*(51), 20529–20533. https://doi.org/10.1073/pnas.0808701106

Shigematsu, T., Fukagawa, M., Yokoyama, K., Akiba, T., Fujii, A., Odani, M., & Akizawa, T. (2018). Effects of the Intravenous Calcimimetic Etelcalcetide on Bone Turnover and Serum Fibroblast Growth Factor 23: Post Hoc Analysis of an Open-label Study. *Clin Ther*, *40*(12), 2099–2111. https://doi.org/10.1016/j.clinthera.2018.10.016

Shimada, T., Hasegawa, H., Yamazaki, Y., Muto, T., Hino, R., Takeuchi, Y., Fujita, T., Nakahara, K., Fukumoto, S., & Yamashita, T. (2004). FGF-23 is a potent regulator of vitamin D metabolism and phosphate homeostasis. *J Bone Miner Res*, *19*(3), 429–435. https://doi.org/10.1359/JBMR.0301264

Shimada, T., Mizutani, S., Muto, T., Yoneya, T., Hino, R., Takeda, S., Takeuchi, Y., Fujita, T., Fukumoto, S., & Yamashita, T. (2001). Cloning and characterization of FGF23 as a causative factor of tumor-induced osteomalacia. *Proc Natl Acad Sci U S A*, *98*(11), 6500–6505. https://doi.org/10.1073/pnas.101545198

Shyu, J. F., Liu, W. C., Zheng, C. M., Fang, T. C., Hou, Y. C., Chang, C. T., Liao, T. Y., Chen, Y. C., & Lu, K. C. (2021). Toxic Effects of Indoxyl Sulfate on Osteoclastogenesis and Osteoblastogenesis. *Int J Mol Sci*, *22*(20). https://doi.org/10.3390/ijms222011265

Siddiqui, J. A., & Partridge, N. C. (2016). Physiological Bone Remodeling: Systemic Regulation and Growth Factor Involvement. *Physiology (Bethesda)*, *31*(3), 233–245. https://doi.org/10.1152/physiol.00061.2014

Silva, B. C., & Bilezikian, J. P. (2015). Parathyroid hormone: anabolic and catabolic actions on the skeleton. *Curr Opin Pharmacol*, *22*, 41–50. https://doi.org/10.1016/j.coph.2015.03.005

Simkin, P. A. (2018). Marrow fat may distribute the energy of impact loading throughout subchondral bone. In (Vol. 57, pp. 414–418): Rheumatology (Oxford).

Sims, N. A., & Martin, T. J. (2015). Coupling Signals between the Osteoclast and Osteoblast: How are Messages Transmitted between These Temporary Visitors to the Bone Surface? *Front Endocrinol (Lausanne)*, *6*, 41. https://doi.org/10.3389/fendo.2015.00041

Sirimongkolchaiyakul, O., Pereira, R. C., Gales, B., Bacchetta, J., Salusky, I. B., & Wesseling-Perry, K. (2021). Bone marrow adiposity inversely correlates with bone turnover in pediatric renal osteodystrophy. *Bone Rep*, *15*, 101104. https://doi.org/10.1016/j.bonr.2021.101104

Slatopolsky, E., Weerts, C., Thielan, J., Horst, R., Harter, H., & Martin, K. J. (1984). Marked suppression of secondary hyperparathyroidism by intravenous administration of 1,25-dihydroxy-cholecalciferol in uremic patients. *J Clin Invest*, *74*(6), 2136–2143. https://doi.org/10.1172/jci111639

Slee, A. D. (2012). Exploring metabolic dysfunction in chronic kidney disease. *Nutr Metab (Lond)*, *9*(1), 36. https://doi.org/10.1186/1743-7075-9-36

Song, L., Liu, M., Ono, N., Bringhurst, F. R., Kronenberg, H. M., & Guo, J. (2012). Loss of wnt/beta-catenin signaling causes cell fate shift of preosteoblasts from osteoblasts to adipocytes. *J Bone Miner Res*, *27*(11), 2344–2358. https://doi.org/10.1002/jbmr.1694

Song, S. H., Oh, T. R., Choi, H. S., Kim, C. S., Ma, S. K., Oh, K. H., Ahn, C., Kim, S. W., & Bae, E. H. (2020). High serum adiponectin as a biomarker of renal dysfunction: Results from the KNOW-CKD study. *Sci Rep*, *10*(1), 5598. https://doi.org/10.1038/s41598-020-62465-2

Spath, S. S., Andrade, A. C., Chau, M., Baroncelli, M., & Nilsson, O. (2018). Evidence That Rat Chondrocytes Can Differentiate Into Perichondrial Cells. *JBMR Plus*, *2*(6), 351–361. https://doi.org/10.1002/jbm4.10056

Sprague, S. M., Bellorin-Font, E., Jorgetti, V., Carvalho, A. B., Malluche, H. H., Ferreira, A., D'Haese, P. C., Drüeke, T. B., Du, H., Manley, T., Rojas, E., & Moe, S. M. (2016). Diagnostic accuracy of bone turnover markers and bone histology in patients with CKD treated by dialysis. In (Vol. 67, pp. 559–566): W.B. Saunders.

Srisuwarn, P., Eastell, R., & Salam, S. (2024). Clinical Utility of Bone Turnover Markers in Chronic Kidney Disease. *J Bone Metab*, *31*(4), 264–278. https://doi.org/10.11005/jbm.24.789

Staiger, J., Lueben, M. J., Berrigan, D., Malik, R., Perkins, S. N., Hursting, S. D., & Johnson, P. F. (2009). C/EBPbeta regulates body composition, energy balance-

related hormones and tumor growth. *Carcinogenesis*, *30*(5), 832–840. https://doi.org/10.1093/carcin/bgn273

Stern, J. H., Rutkowski, J. M., & Scherer, P. E. (2016). Adiponectin, Leptin, and Fatty Acids in the Maintenance of Metabolic Homeostasis through Adipose Tissue Crosstalk. *Cell Metab*, *23*(5), 770–784. https://doi.org/10.1016/j.cmet.2016.04.011

Stern, J. H., Rutkowski, J. M., Scherer, P. E., & (2016). Adiponectin, Leptin, and Fatty Acids in the Maintenance of Metabolic Homeostasis through Adipose Tissue Crosstalk. *23*, 770–784. https://doi.org/10.1016/J.CMET.2016.04.011

Suchacki, K. J., Cawthorn, W. P., & Rosen, C. J. (2016). Bone marrow adipose tissue: formation, function and regulation. *28*, 50–56. https://doi.org/10.1016/J.COPH.2016.03.001

Suchacki, K. J., Thomas, B. J., Ikushima, Y. M., Chen, K. C., Fyfe, C., Tavares, A. A. S., Sulston, R. J., Lovdel, A., Woodward, H. J., Han, X., Mattiucci, D., Brain, E. J., Alcaide-Corral, C. J., Kobayashi, H., Gray, G. A., Whitfield, P. D., Stimson, R. H., Morton, N. M., Johnstone, A. M., & Cawthorn, W. P. (2023). The effects of caloric restriction on adipose tissue and metabolic health are sex- and age-dependent. *Elife*, *12*. https://doi.org/10.7554/eLife.88080

Suki, W. N., Zabaneh, R., Cangiano, J. L., Reed, J., Fischer, D., Garrett, L., Ling, B. N., Chasan-Taber, S., Dillon, M. A., Blair, A. T., & Burke, S. K. (2007). Effects of sevelamer and calcium-based phosphate binders on mortality in hemodialysis patients. *Kidney Int*, *72*(9), 1130–1137. https://doi.org/10.1038/sj.ki.5002466

Sulston, R. J., & Cawthorn, W. P. (2016). Bone marrow adipose tissue as an endocrine organ: close to the bone? In (Vol. 28, pp. 21–38): Horm Mol Biol Clin Investig.

Sun, D., Wang, J., Shao, W., Wang, J., Yao, L., Li, Z., & Ohno, S. (2020). Pathogenesis and Damage Targets of Hypertensive Kidney Injury. *J Transl Int Med*, *8*(4), 205–209. https://doi.org/10.2478/jtim-2020-0033

Sun, X., Bolster, M. B., Leder, B. Z., & Fan, W. (2025). Dose-Specific Effects of Denosumab on Serum Calcium Levels in Patients With Osteoporosis and Various Renal Functions. *J Clin Endocrinol Metab*, *110*(7), 1915–1922. https://doi.org/10.1210/clinem/dgae721

Sun, Y., Li, J., Xie, X., Gu, F., Sui, Z., Zhang, K., & Yu, T. (2021). Recent Advances in Osteoclast Biological Behavior. *Front Cell Dev Biol*, *9*, 788680. https://doi.org/10.3389/fcell.2021.788680

Szeri, F., Niaziorimi, F., Donnelly, S., Fariha, N., Tertyshnaia, M., Patel, D., Lundkvist, S., & van de Wetering, K. (2022). The Mineralization Regulator ANKH Mediates Cellular Efflux of ATP, Not Pyrophosphate. *J Bone Miner Res*, *37*(5), 1024–1031. https://doi.org/10.1002/jbmr.4528

Takegahara, N., Kim, H., & Choi, Y. (2024). Unraveling the intricacies of osteoclast differentiation and maturation: insight into novel therapeutic strategies for bone-destructive diseases. *Exp Mol Med*, *56*(2), 264–272. https://doi.org/10.1038/s12276-024-01157-7

Takei, R., Rosenthal, A., Pascart, T., Reynolds, R. J., Neogi, T., Terkeltaub, R., Tedeschi, S. K., & Merriman, T. R. (2025). Genome-wide association study in chondrocalcinosis reveals ENPP1 as a candidate therapeutic target in calcium

pyrophosphate deposition disease. *Ann Rheum Dis*, *84*(6), 1023–1032. https://doi.org/10.1016/j.ard.2025.04.002

Takito, J., & Nakamura, M. (2020). Heterogeneity and Actin Cytoskeleton in Osteoclast and Macrophage Multinucleation. *Int J Mol Sci*, *21*(18). https://doi.org/10.3390/ijms21186629

Tariq, M. H., & Sulaiman, S. A. S. (2020). Prevalence of Osteopenia and Osteoporosis among Chronic Kidney Disease Patients: A Systematic Review. *The Open Urology & Nephrology Journal*, *13*(1), 5–12. https://doi.org/10.2174/1874303x02013010005

Tavassoli, M. (1976). Marrow adipose cells. Histochemical identification of labile and stable components. *100*, 16–18.

Teitelbaum, S. L. (2007). Osteoclasts: what do they do and how do they do it? *Am J Pathol*, *170*(2), 427–435. https://doi.org/10.2353/ajpath.2007.060834

Tencerova, M., Figeac, F., Ditzel, N., Taipaleenmaki, H., Nielsen, T. K., & Kassem, M. (2018). High-Fat Diet-Induced Obesity Promotes Expansion of Bone Marrow Adipose Tissue and Impairs Skeletal Stem Cell Functions in Mice. *J Bone Miner Res*, *33*(6), 1154–1165. https://doi.org/10.1002/jbmr.3408

Tencerova, M., & Kassem, M. (2016). The Bone Marrow-Derived Stromal Cells: Commitment and Regulation of Adipogenesis. *Frontiers in Endocrinology*, *7*. https://doi.org/10.3389/fendo.2016.00127

Teven, C. M., Liu, X., Hu, N., Tang, N., Kim, S. H., Huang, E., Yang, K., Li, M., Gao, J. L., Liu, H., Natale, R. B., Luther, G., Luo, Q., Wang, L., Rames, R., Bi, Y., Luo, J., Luu, H. H., Haydon, R. C.,…He, T. C. (2011). Epigenetic regulation of mesenchymal stem cells: a focus on osteogenic and adipogenic differentiation. *Stem Cells Int*, *2011*, 201371. https://doi.org/10.4061/2011/201371

Thapa, S., Nandy, A., & Rendina-Ruedy, E. (2022). Endocrinal metabolic regulation on the skeletal system in post-menopausal women. *Front Physiol*, *13*, 1052429. https://doi.org/10.3389/fphys.2022.1052429

Thi Do, D., Phan, N. N., Wang, C. Y., Sun, Z., & Lin, Y. C. (2016). Novel regulations of MEF2-A, MEF2-D, and CACNA1S in the functional incompetence of adipose-derived mesenchymal stem cells by induced indoxyl sulfate in chronic kidney disease. *Cytotechnology*, *68*(6), 2589–2604. https://doi.org/10.1007/s10616-016-9983-0

Thomas, T. (2006). Intermittent parathyroid hormone therapy to increase bone formation. *Joint Bone Spine*, *73*(3), 262–269. https://doi.org/10.1016/j.jbspin.2005.11.007

Thomas, T., Gori, F., Khosla, S., Jensen, M. D., Burguera, B., & Riggs, B. L. (1999). Leptin acts on human marrow stromal cells to enhance differentiation to osteoblasts and to inhibit differentiation to adipocytes. *Endocrinology*, *140*(4), 1630–1638. https://doi.org/10.1210/endo.140.4.6637

Thompson, E., Tashman, A., & Scialla, J. J. (2025). Chronic Kidney Disease-Mineral and Bone Disorder Management in 4D: The Case for Dynamic Treatment Regime Methods to Optimize Care. *Curr Osteoporos Rep*, *23*(1), 16. https://doi.org/10.1007/s11914-025-00911-8

Tikhonova, A. N., Dolgalev, I., Hu, H., Sivaraj, K. K., Hoxha, E., Cuesta-Dominguez, A., Pinho, S., Akhmetzyanova, I., Gao, J., Witkowski, M., Guillamot, M., Gutkin, M. C., Zhang, Y., Marier, C., Diefenbach, C., Kousteni, S., Heguy, A., Zhong, H.,

Fooksman, D. R.,…Aifantis, I. (2019). The bone marrow microenvironment at single-cell resolution. *Nature*, *569*(7755), 222–228. https://doi.org/10.1038/s41586-019-1104-8

Tominaga, H., Maeda, S., Hayashi, M., Takeda, S., Akira, S., Komiya, S., Nakamura, T., Akiyama, H., & Imamura, T. (2008). CCAAT/enhancer-binding protein beta promotes osteoblast differentiation by enhancing Runx2 activity with ATF4. *Mol Biol Cell*, *19*(12), 5373–5386. https://doi.org/10.1091/mbc.e08-03-0329

Touaitahuata, H., Blangy, A., & Vives, V. (2014). Modulation of osteoclast differentiation and bone resorption by Rho GTPases. *Small GTPases*, *5*, e28119. https://doi.org/10.4161/sgtp.28119

Turner, C. H., Warden, S. J., Bellido, T., Plotkin, L. I., Kumar, N., Jasiuk, I., Danzig, J., & Robling, A. G. (2009). Mechanobiology of the skeleton. *Sci Signal*, *2*(68), pt3. https://doi.org/10.1126/scisignal.268pt3

Turner, R. T., Kalra, S. P., Wong, C. P., Philbrick, K. A., Lindenmaier, L. B., Boghossian, S., & Iwaniec, U. T. (2013). Peripheral leptin regulates bone formation. *J Bone Miner Res*, *28*(1), 22–34. https://doi.org/10.1002/jbmr.1734

Tyanova, S., Temu, T., Sinitcyn, P., Carlson, A., Hein, M. Y., Geiger, T., Mann, M., & Cox, J. (2016). The Perseus computational platform for comprehensive analysis of (prote)omics data. *Nat Methods*, *13*(9), 731–740. https://doi.org/10.1038/nmeth.3901

Ucer, S., Iyer, S., Bartell, S. M., Martin-Millan, M., Han, L., Kim, H. N., Weinstein, R. S., Jilka, R. L., O'Brien, C. A., Almeida, M., & Manolagas, S. C. (2015). The Effects of Androgens on Murine Cortical Bone Do Not Require AR or ERalpha Signaling in Osteoblasts and Osteoclasts. *J Bone Miner Res*, *30*(7), 1138–1149. https://doi.org/10.1002/jbmr.2485

Udani, S., Lazich, I., & Bakris, G. L. (2011). Epidemiology of hypertensive kidney disease. *Nat Rev Nephrol*, *7*(1), 11–21. https://doi.org/10.1038/nrneph.2010.154

Urakawa, I., Yamazaki, Y., Shimada, T., Iijima, K., Hasegawa, H., Okawa, K., Fujita, T., Fukumoto, S., & Yamashita, T. (2006). Klotho converts canonical FGF receptor into a specific receptor for FGF23. *Nature*, *444*(7120), 770–774. https://doi.org/10.1038/nature05315

Uslar, T., Newman, A. J., Tapia-Castillo, A., Carvajal, C. A., Fardella, C. E., Allende, F., Solari, S., Tsai, L. C., Milks, J., Cherney, M., Stouffer, D. G., Auchus, R., Brown, J. M., Baudrand, R., & Vaidya, A. (2025). Progressive 11beta-Hydroxysteroid Dehydrogenase Type 2 Insufficiency as Kidney Function Declines. *J Clin Endocrinol Metab*, *110*(4), 1037–1043. https://doi.org/10.1210/clinem/dgae663

Valdés-Flores, M., Velázquez Cruz, R., Orozco, L., & Parra-Torres, A. (2013). Molecular Aspects of Bone Remodeling. In M. Valdés-Flores (Ed.), *Topics in Osteoporosis*. IntechOpen. https://doi.org/10.5772/54905

van Lierop, A. H., Moester, M. J., Hamdy, N. A., & Papapoulos, S. E. (2014). Serum Dickkopf 1 levels in sclerostin deficiency. *J Clin Endocrinol Metab*, *99*(2), E252–256. https://doi.org/10.1210/jc.2013-3278

Vanhoenacker, F. M., Balemans, W., Tan, G. J., Dikkers, F. G., De Schepper, A. M., Mathysen, D. G., Bernaerts, A., & Hul, W. V. (2003). Van Buchem disease: lifetime evolution of radioclinical features. *Skeletal Radiol*, *32*(12), 708–718. https://doi.org/10.1007/s00256-003-0675-4

Vaziri, N. D., Wong, J., Pahl, M., Piceno, Y. M., Yuan, J., DeSantis, T. Z., Ni, Z., Nguyen, T. H., & Andersen, G. L. (2013). Chronic kidney disease alters intestinal microbial flora. *Kidney Int*, *83*(2), 308–315. https://doi.org/10.1038/ki.2012.345

Veldhuis-Vlug, A. G., & Rosen, C. J. (2018). Clinical implications of bone marrow adiposity. *J Intern Med*, *283*(2), 121–139. https://doi.org/10.1111/joim.12718

Wada, J., & Makino, H. (2013). Inflammation and the pathogenesis of diabetic nephropathy. *Clin Sci (Lond)*, *124*(3), 139–152. https://doi.org/10.1042/CS20120198

Walker, E. C., Poulton, I. J., McGregor, N. E., Ho, P. W., Allan, E. H., Quach, J. M., Martin, T. J., & Sims, N. A. (2012). Sustained RANKL response to parathyroid hormone in oncostatin M receptor-deficient osteoblasts converts anabolic treatment to a catabolic effect in vivo. *J Bone Miner Res*, *27*(4), 902–912. https://doi.org/10.1002/jbmr.1506

Wang, C. Y., Hsu, Y. J., Peng, Y. J., Lee, H. S., Chang, Y. C., Chang, C. S., Chiang, S. W., Hsu, Y. C., Lin, M. H., & Huang, G. S. (2017). Knee subchondral bone perfusion and its relationship to marrow fat and trabeculation on multi-parametric MRI and micro-CT in experimental CKD. *Sci Rep*, *7*(1), 3073. https://doi.org/10.1038/s41598-017-03059-3

Wang, L., You, X., Zhang, L., Zhang, C., & Zou, W. (2022). Mechanical regulation of bone remodeling. *Bone Res*, *10*(1), 16. https://doi.org/10.1038/s41413-022-00190-4

Wang, W., Liu, X., Wang, W., Li, J., Li, Y., Li, L., Wang, S., Zhang, J., Zhang, Y., & Huang, H. (2016). The Effects of Indoxyl Sulfate on Human Umbilical Cord-Derived Mesenchymal Stem Cells In Vitro. *Cell Physiol Biochem*, *38*(1), 401–414. https://doi.org/10.1159/000438639

Wang, Y., Sakata, T., Elalieh, H. Z., Munson, S. J., Burghardt, A., Majumdar, S., Halloran, B. P., & Bikle, D. D. (2006). Gender differences in the response of CD-1 mouse bone to parathyroid hormone: potential role of IGF-I. *The Journal of endocrinology*, *189*(2), 279–287. https://doi.org/10.1677/joe.1.06351

Wang, Y. K., Yu, X., Cohen, D. M., Wozniak, M. A., Yang, M. T., Gao, L., Eyckmans, J., & Chen, C. S. (2012). Bone morphogenetic protein-2-induced signaling and osteogenesis is regulated by cell shape, RhoA/ROCK, and cytoskeletal tension. *Stem Cells Dev*, *21*(7), 1176–1186. https://doi.org/10.1089/scd.2011.0293

Watanabe, H., Miyamoto, Y., Honda, D., Tanaka, H., Wu, Q., Endo, M., Noguchi, T., Kadowaki, D., Ishima, Y., Kotani, S., Nakajima, M., Kataoka, K., Kim-Mitsuyama, S., Tanaka, M., Fukagawa, M., Otagiri, M., & Maruyama, T. (2013). p-Cresyl sulfate causes renal tubular cell damage by inducing oxidative stress by activation of NADPH oxidase. *Kidney Int*, *83*(4), 582–592. https://doi.org/10.1038/ki.2012.448

Watanabe, K., Tominari, T., Hirata, M., Matsumoto, C., Hirata, J., Murphy, G., Nagase, H., Miyaura, C., & Inada, M. (2017). Indoxyl sulfate, a uremic toxin in chronic kidney disease, suppresses both bone formation and bone resorption. *FEBS Open Bio*, *7*(8), 1178–1185. https://doi.org/10.1002/2211-5463.12258

Webster, A. C., Nagler, E. V., Morton, R. L., & Masson, P. (2017). Chronic Kidney Disease. In (Vol. 389, pp. 1238–1252): Elsevier.

Whitlock, R., MacDonald, K., Tangri, N., Walsh, M., & Collister, D. (2024). The Efficacy and Safety of Bisphosphonate Therapy for Osteopenia/Osteoporosis in Patients With Chronic Kidney Disease: A Systematic Review and Individual Patient-Level Meta-Analysis of Placebo-Controlled Randomized Trials. *Can J Kidney Health Dis*, *11*, 20543581241283523. https://doi.org/10.1177/20543581241283523

Wijenayaka, A. R., Kogawa, M., Lim, H. P., Bonewald, L. F., Findlay, D. M., & Atkins, G. J. (2011). Sclerostin stimulates osteocyte support of osteoclast activity by a RANKL-dependent pathway. *PLoS One*, *6*(10), e25900. https://doi.org/10.1371/journal.pone.0025900

Wilson, R. J., & Copley, J. B. (2017). Elemental calcium intake associated with calcium acetate/calcium carbonate in the treatment of hyperphosphatemia. *Drugs Context*, *6*, 212302. https://doi.org/10.7573/dic.212302

Witcher, P. C., Miner, S. E., Horan, D. J., Bullock, W. A., Lim, K. E., Kang, K. S., Adaniya, A. L., Ross, R. D., Loots, G. G., & Robling, A. G. (2018). Sclerostin neutralization unleashes the osteoanabolic effects of Dkk1 inhibition. *JCI Insight*, *3*(11). https://doi.org/10.1172/jci.insight.98673

Wolf, M. (2012). Update on fibroblast growth factor 23 in chronic kidney disease. *Kidney Int*, *82*(7), 737–747. https://doi.org/10.1038/ki.2012.176

Wolock, S. L., Krishnan, I., Tenen, D. E., Matkins, V., Camacho, V., Patel, S., Agarwal, P., Bhatia, R., Tenen, D. G., Klein, A. M., & Welner, R. S. (2019). Mapping Distinct Bone Marrow Niche Populations and Their Differentiation Paths. In (Vol. 28, pp. 302–311.e305): Cell Press.

Woods, G. N., Ewing, S. K., Schafer, A. L., Gudnason, V., Sigurdsson, S., Lang, T., Hue, T. F., Kado, D. M., Vittinghoff, E., Rosen, C., Li, X., & Schwartz, A. V. (2022). Saturated and Unsaturated Bone Marrow Lipids Have Distinct Effects on Bone Density and Fracture Risk in Older Adults. *J Bone Miner Res*, *37*(4), 700–710. https://doi.org/10.1002/jbmr.4504

Woods, G. N., Ewing, S. K., Sigurdsson, S., Kado, D. M., Ix, J. H., Hue, T. F., Eiriksdottir, G., Xu, K., Gudnason, V., Lang, T. F., Vittinghoff, E., Harris, T. B., Rosen, C. J., Li, X., & Schwartz, A. V. (2018). Chronic Kidney Disease Is Associated With Greater Bone Marrow Adiposity. *J Bone Miner Res*, *33*(12), 2158–2164. https://doi.org/10.1002/jbmr.3562

Wu, H., Gordon, J. A., Whitfield, T. W., Tai, P. W., van Wijnen, A. J., Stein, J. L., Stein, G. S., & Lian, J. B. (2017). Chromatin dynamics regulate mesenchymal stem cell lineage specification and differentiation to osteogenesis. *Biochim Biophys Acta Gene Regul Mech*, *1860*(4), 438–449. https://doi.org/10.1016/j.bbagrm.2017.01.003

Wu, M., Wang, Y., Shao, J. Z., Wang, J., Chen, W., & Li, Y. P. (2017). Cbfbeta governs osteoblast-adipocyte lineage commitment through enhancing beta-catenin signaling and suppressing adipogenesis gene expression. *Proc Natl Acad Sci U S A*, *114*(38), 10119–10124. https://doi.org/10.1073/pnas.1619294114

Xu, J., Li, Z., Hou, Y., & Fang, W. (2015). Potential mechanisms underlying the Runx2 induced osteogenesis of bone marrow mesenchymal stem cells. *Am J Transl Res*, *7*(12), 2527–2535.

Xu, W., Mesa-Eguiagaray, I., Morris, D. M., Wang, C., Gray, C. D., Sjostrom, S., Papanastasiou, G., Badr, S., Paccou, J., Li, X., Timmers, P., Timofeeva, M., Farrington, S. M., Dunlop, M. G., Semple, S. I., MacGillivray, T., Theodoratou, E., & Cawthorn, W. P. (2025). Deep learning and genome-wide association meta-analyses of bone marrow adiposity in the UK Biobank. *Nat Commun*, *16*(1), 99. https://doi.org/10.1038/s41467-024-55422-4

Yadav, M. C., Bottini, M., Cory, E., Bhattacharya, K., Kuss, P., Narisawa, S., Sah, R. L., Beck, L., Fadeel, B., Farquharson, C., & Millan, J. L. (2016). Skeletal Mineralization Deficits and Impaired Biogenesis and Function of Chondrocyte-Derived Matrix Vesicles in Phospho1(-/-) and Phospho1/Pi t1 Double-Knockout Mice. *J Bone Miner Res*, *31*(6), 1275–1286. https://doi.org/10.1002/jbmr.2790

Yadav, M. C., Simao, A. M., Narisawa, S., Huesa, C., McKee, M. D., Farquharson, C., & Millan, J. L. (2011). Loss of skeletal mineralization by the simultaneous ablation of PHOSPHO1 and alkaline phosphatase function: a unified model of the mechanisms of initiation of skeletal calcification. *J Bone Miner Res*, *26*(2), 286–297. https://doi.org/10.1002/jbmr.195

Yamada, M. (1976). Ultrastructural and cytochemical studies on the calcification of the tendon-bone joint. *Arch Histol Jpn*, *39*(5), 347–378. https://doi.org/10.1679/aohc1950.39.347

Yan, C., Shi, Y., Yuan, L., Lv, D., Sun, B., Wang, J., Liu, X., & An, F. (2023). Mitochondrial quality control and its role in osteoporosis. *Front Endocrinol (Lausanne)*, *14*, 1077058. https://doi.org/10.3389/fendo.2023.1077058

Yang, M., Arai, A., Udagawa, N., Zhao, L., Nishida, D., Murakami, K., Hiraga, T., Takao-Kawabata, R., Matsuo, K., Komori, T., Kobayashi, Y., Takahashi, N., Isogai, Y., Ishizuya, T., Yamaguchi, A., & Mizoguchi, T. (2019). Parathyroid Hormone Shifts Cell Fate of a Leptin Receptor-Marked Stromal Population from Adipogenic to Osteoblastic Lineage. In (Vol. 34, pp. 1952–1963): John Wiley and Sons Inc.

Yang, Q., Su, S., Luo, N., & Cao, G. (2024). Adenine-induced animal model of chronic kidney disease: current applications and future perspectives. *Ren Fail*, *46*(1), 2336128. https://doi.org/10.1080/0886022X.2024.2336128

Yang, Y., Luo, X., Xie, X., Yan, F., Chen, G., Zhao, W., Jiang, Z., Fang, C., & Shen, J. (2016). Influences of teriparatide administration on marrow fat content in postmenopausal osteopenic women using MR spectroscopy. *Climacteric*, *19*(3), 285–291. https://doi.org/10.3109/13697137.2015.1126576

Yao, Y., Cai, X., Chen, Y., Zhang, M., & Zheng, C. (2025). Estrogen deficiency-mediated osteoimmunity in postmenopausal osteoporosis. *Med Res Rev*, *45*(2), 561–575. https://doi.org/10.1002/med.22081

Yee, C. S., Xie, L., Hatsell, S., Hum, N., Murugesh, D., Economides, A. N., Loots, G. G., & Collette, N. M. (2016). Sclerostin antibody treatment improves fracture outcomes in a Type I diabetic mouse model. *Bone*, *82*, 122–134. https://doi.org/10.1016/j.bone.2015.04.048

Yeung, D. K., Griffith, J. F., Antonio, G. E., Lee, F. K., Woo, J., & Leung, P. C. (2005). Osteoporosis is associated with increased marrow fat content and decreased marrow fat unsaturation: a proton MR spectroscopy study. *J Magn Reson Imaging*, *22*(2), 279–285. https://doi.org/10.1002/jmri.20367

Yokota, T., Meka, C. S., Medina, K. L., Igarashi, H., Comp, P. C., Takahashi, M., Nishida, M., Oritani, K., Miyagawa, J., Funahashi, T., Tomiyama, Y., Matsuzawa, Y., & Kincade, P. W. (2002). Paracrine regulation of fat cell formation in bone marrow cultures via adiponectin and prostaglandins. *J Clin Invest*, *109*(10), 1303–1310. https://doi.org/10.1172/JCI14506

Yokozawa, T., Zheng, P. D., Oura, H., & Koizumi, F. (1986). Animal model of adenine-induced chronic renal failure in rats. *Nephron*, *44*(3), 230–234. https://doi.org/10.1159/000183992

Yu, B., Zhao, X., Yang, C., Crane, J., Xian, L., Lu, W., Wan, M., & Cao, X. (2012). Parathyroid hormone induces differentiation of mesenchymal stromal/stem cells by enhancing bone morphogenetic protein signaling. *J Bone Miner Res*, *27*(9), 2001–2014. https://doi.org/10.1002/jbmr.1663

Yuan, H., Zheng, C., Zhu, L., Song, Z., Dai, L., Hu, Q., Wang, L., Chen, Y., & Xiong, J. (2021). Contribution of TFEB-mediated autophagy to tubulointerstitial fibrosis in mice with adenine-induced chronic kidney disease. In (Vol. 133, pp. 110949).

Zaidi, M., Blair, H. C., Moonga, B. S., Abe, E., & Huang, C. L. (2003). Osteoclastogenesis, bone resorption, and osteoclast-based therapeutics. *J Bone Miner Res*, *18*(4), 599–609. https://doi.org/10.1359/jbmr.2003.18.4.599

Zaimi, M., & Grapsa, E. (2024). Current therapeutic approach of chronic kidney disease-mineral and bone disorder. *Ther Apher Dial*, *28*(5), 671–689. https://doi.org/10.1111/1744-9987.14177

Zanotti, S., Stadmeyer, L., Smerdel-Ramoya, A., Durant, D., & Canalis, E. (2009). Misexpression of CCAAT/enhancer binding protein beta causes osteopenia. *The Journal of endocrinology*, *201*(2), 263–274. https://doi.org/10.1677/JOE-08-0514

Zhang, C., Bakker, A. D., Klein-Nulend, J., & Bravenboer, N. (2019). Studies on Osteocytes in Their 3D Native Matrix Versus 2D In Vitro Models. *Curr Osteoporos Rep*, *17*(4), 207–216. https://doi.org/10.1007/s11914-019-00521-1

Zhang, X., Tian, L., Majumdar, A., & Scheller, E. L. (2024). Function and Regulation of Bone Marrow Adipose Tissue in Health and Disease: State of the Field and Clinical Considerations. *Compr Physiol*, *14*(3), 5521–5579. https://doi.org/10.1002/cphy.c230016

Zhong, L., Yao, L., Tower, R. J., Wei, Y., Miao, Z., Park, J., Shrestha, R., Wang, L., Yu, W., Holdreith, N., Huang, X., Zhang, Y., Tong, W., Gong, Y., Ahn, J., Susztak, K., Dyment, N., Li, M., Long, F.,…Qin, L. (2020). Single cell transcriptomics identifies a unique adipose lineage cell population that regulates bone marrow environment. *Elife*, *9*. https://doi.org/10.7554/eLife.54695

Zhou, B. O., Yu, H., Yue, R., Zhao, Z., Rios, J. J., Naveiras, O., & Morrison, S. J. (2017). Bone marrow adipocytes promote the regeneration of stem cells and haematopoiesis by secreting SCF. In (Vol. 19, pp. 891–903): Nature Publishing Group.

Zhou, B. O., Yue, R., Murphy, M. M., Peyer, J. G., & Morrison, S. J. (2014). Leptin-receptor-expressing mesenchymal stromal cells represent the main source of bone formed by adult bone marrow. *Cell Stem Cell*, *15*(2), 154–168. https://doi.org/10.1016/j.stem.2014.06.008

Zhu, D., Mackenzie, N. C., Millan, J. L., Farquharson, C., & MacRae, V. E. (2011). The appearance and modulation of osteocyte marker expression during calcification of vascular smooth muscle cells. *PLoS One*, *6*(5), e19595. https://doi.org/10.1371/journal.pone.0019595

Zhu, G., Zhang, T., Chen, M., Yao, K., Huang, X., Zhang, B., Li, Y., Liu, J., Wang, Y., & Zhao, Z. (2021). Bone physiological microenvironment and healing mechanism: Basis for future bone-tissue engineering scaffolds. *Bioact Mater*, *6*(11), 4110–4140. https://doi.org/10.1016/j.bioactmat.2021.03.043

Zhu, S., Chen, W., Masson, A., & Li, Y. P. (2024). Cell signaling and transcriptional regulation of osteoblast lineage commitment, differentiation, bone formation, and homeostasis. *Cell Discov*, *10*(1), 71. https://doi.org/10.1038/s41421-024-00689-6

Zuccarini, M., Lambertucci, C., Carluccio, M., Giuliani, P., Ronci, M., Spinaci, A., Volpini, R., Ciccarelli, R., Iorio, P. D., & Bunnell, B. A. (2021). Multipotent Stromal Cells from Subcutaneous Adipose Tissue of Normal Weight and Obese Subjects: Modulation of Their Adipogenic Differentiation by Adenosine A1 Receptor Ligands. In (Vol. 10, pp. 3560): Multidisciplinary Digital Publishing Institute.

Zuo, Y., Qiang, L., & Farmer, S. R. (2006). Activation of CCAAT/enhancer-binding protein (C/EBP) alpha expression by C/EBP beta during adipogenesis requires a peroxisome proliferator-activated receptor-gamma-associated repression of HDAC1 at the C/ebp alpha gene promoter. *J Biol Chem*, *281*(12), 7960–7967. https://doi.org/10.1074/jbc.M510682200

Appendix

Appendix I: Primer sequences for qPCR

Gene	Forward, 5'→ 3'	Reverse, 5'→ 3'	Source
Adipoq	AAGAAGGACAAGGCCGTTCTCTT	GCTATGGGTAGTTGCAGTCAGTT	Sigma-Aldrich
Cebpa	TGGACAAGAACAGCAACGAG	TCACTGGTCAACTCCAGCAC	Sigma-Aldrich
Fabp4	TGGAAGCTTGTCTCCAGTGA	AATCCCCATTTACGCTGATG	Sigma-Aldrich
Lipe	CCTTGTGGCTTGCGCTCTGGA	CCGCGCGAACATGACCGAGT	Invitrogen
Lep	GACACCAAAACCCTCAT	CAGTGTCTGGTCCATCT	Sigma-Aldrich
Pparg2	CCAGAGCATGGTGCCTTCGC	TTCCGAAGTTGGTGGGCCAGA	Sigma-Aldrich
Pnpla2	CGGCTTCCTCGGGGTCTAC	CGCGCTCATGGCAATCAG	Invitrogen
Runx2	ACCATAACAGTCTTCACAAATCCT	CAGGCGATCAGAGAACAAACTA	Sigma-Aldrich
Sp7	ATGGCGTCCTCTCTGCTTG	TGAAAGGTCAGCGTATGGCTT	Sigma-Aldrich
Col1a1	ACATGTTCAGCTTTGTGGACC	TAGGCCATTGTGTATGCAGC	Sigma-Aldrich
Alpl	GGGACGAATCTCAGGGTACA	AGTAACTGGGGTCTCTCTC	Sigma-Aldrich
Mepe	AGAAATATCACGCAGCCTGTAA	GGAGACTTAGCATCATTGACATC	Invitrogen
Bglap	CCGGGAGCAGTGTGAGCTTA	TAGATGCGTTTGTAGGCGGTC	Sigma-Aldrich
Tnfrsf11b	CCTTGCCCTGACCACTCTTA	CACACACTCGGTTGTGGGT	Sigma-Aldrich
Tnfsf11	CAGCATCGCTCTGTTCCTGTA	CTGCGTTTTCATGGAGTCTCA	Sigma-Aldrich
Sost	TGAGAACAACCAGACCATGAAC	TCAGGAAGCGGGTGTAGTG	Sigma-Aldrich
Dkk1	CCGGGAACTACTGCAAAAAT	CCAAGGTTTTCAATGATGCTT	Invitrogen
Ctsk	GAAGAAGACTCACCAGAAGCAG	TCCAGGTTATGGGCAGAGATT	Sigma-Aldrich
Mmp9	CAAAGACCTGAAAACCTCCAAC	GACTGCTTCTCTCCCATCATC	Sigma-Aldrich
Acp5	AGCAGCCAAGGAGGACTACG	TGGCTAACAATGGTCGCAAG	Sigma-Aldrich
Nfatc1	GGCTGGTCTTCCGAGTTCACATC	GCTGTCTGTGCTCTGCTTCTCC	Sigma-Aldrich
Ppia	CACCGTGTTCTTCGACATCA	CAGTGCTCAGAGCTCGAAAGT	Sigma-Aldrich

Appendix II: R scripts using for bone and BMAT analysis along the tibial length (10-90% of tibia length) by R studio

R script for generating the percentage of bone and BMAT parameters along the 10% to 90% of the bone length from 2D analysis

```
## set working directory
setwd("C:/Users/s2226418/Desktop/2D cortical Scl study/porosity")

## (needs changing for each sample)Read data structure for each indivi
dual csv file.  File name needs to change for each csv file.
data1 <- read.csv("Po5192.csv",header=T)

## (needs changing for each sample)Define sample no
Label <- rep("5192",101)
```

```
## (need changing for each experimental group)Define variables (for ex
ample genotype & age and gender etc.)
Treatment <- rep("PBS",101)
#Age <- rep("5",101)
Disease <- rep("CKD", 101)

## check data structure
str(data1)

## 'data.frame':    3387 obs. of  16 variables:
##  $ X           : int  1 2 3 4 5 6 7 8 9 10 ...
##  $ X.1         : chr  "gu5192_rec0000_voi__tra_voi_3514.bmp" "gu519
2_rec0000_voi__tra_voi_3513.bmp" "gu5192_rec0000_voi__tra_voi_3512.bmp
" "gu5192_rec0000_voi__tra_voi_3511.bmp" ...
##  $ Pos.Z       : num  17.5 17.5 17.5 17.5 17.5 17.5 17.5 17.5 17.5
17.5 ...
##  $ Slice       : int  1 2 3 4 5 6 7 8 9 10 ...
##  $ X..of.length: num  0 0.0295 0.0591 0.0886 0.1181 ...
##  $ T.Ar        : num  0 0 0 0 0 0 0 0 0 0 ...
##  $ B.Ar        : num  0 0 0 0 0 0 0 0 0 0 ...
##  $ B.ArT.Ar    : num  0 0 0 0 0 0 0 0 0 0 ...
##  $ Po.N.cl     : int  0 0 0 0 0 0 0 0 0 0 ...
##  $ Po.Ar.cl    : num  0 0 0 0 0 0 0 0 0 0 ...
##  $ Po.Pm.cl    : num  0 0 0 0 0 0 0 0 0 0 ...
##  $ Po.cl       : num  0 0 0 0 0 0 0 0 0 0 ...
##  $ Po.Ar.op    : num  0 0 0 0 0 0 0 0 0 0 ...
##  $ Po.Ar.tot   : num  0 0 0 0 0 0 0 0 0 0 ...
##  $ Po.op       : num  0 0 0 0 0 0 0 0 0 0 ...
##  $ Po.tot      : num  0 0 0 0 0 0 0 0 0 0 ...

## generate sequence ID for the percentage 10-90
Seq <- seq(from=0,to=100,by=1)
## lower bound for the sequence
Seq1 <- rep(NA,101)
## upper bound of the sequence
Seq2 <- rep(NA,101)

## create data array for each parameter

Po.N.cl <- NA
Po.cl <- NA
Po.tot <- NA



## for loop to calculate the interpolated values at percentage 1-99

for (i in 1:99) {
```

```
  lowerX <- max(subset(data1,X..of.length<=i)$X..of.length)
  lowerid <- which(data1$X..of.length==lowerX)
  upperid <- lowerid+1
  upperX <- data1$X..of.length[lowerid+1]
  Seq1[i+1] <- lowerX
  Seq2[i+1] <- upperX
  k <- 1/(upperX-lowerX)*(i-lowerX)

 # T.Ar[i] <- data1$T.Ar[lowerid]+(data1$T.Ar[upperid]-data1$T.Ar[lowe
rid])*k
 # B.Ar[i] <- data1$B.Ar[lowerid]+(data1$B.Ar[upperid]-data1$B.Ar[lowe
rid])*k
 # B.ArT.Ar[i] <- data1$B.ArT.Ar[lowerid]+(data1$B.ArT.Ar[upperid]-dat
a1$B.ArT.Ar[lowerid])*k
  #P.Pm[i] <- data1$P.Pm[lowerid]+(data1$P.Pm[upperid]-data1$P.Pm[lowe
rid])*k
  #B.Pm[i] <- data1$B.Pm[lowerid]+(data1$B.Pm[upperid]-data1$B.Pm[lowe
rid])*k
  #E.Pm[i] <- data1$E.Pm[lowerid]+(data1$E.Pm[upperid]-data1$E.Pm[lowe
rid])*k
Po.N.cl[i] <- data1$Po.N.cl[lowerid]+(data1$Po.N.cl[upperid]-data1$Po.
N.cl[lowerid])*k
Po.cl[i] <- data1$Po.cl[lowerid]+(data1$Po.cl[upperid]-data1$Po.cl[low
erid])*k
Po.tot[i] <- data1$Po.tot[lowerid]+(data1$Po.tot[upperid]-data1$Po.tot
[lowerid])*k
 # MMI.polar[i] <- data1$MMI.polar[lowerid]+(data1$MMI.polar[upperid]-
data1$MMI.polar[lowerid])*k
 # MMI.max[i] <- data1$MMI.max[lowerid]+(data1$MMI.max[upperid]-data1$
MMI.max[lowerid])*k
 # MMI.min[i] <- data1$MMI.min[lowerid]+(data1$MMI.min[upperid]-data1$
MMI.min[lowerid])*k
  #Ecc[i] <- data1$Ecc[lowerid]+(data1$Ecc[upperid]-data1$Ecc[lowerid]
)*k
  #Th[i] <- data1$Th[lowerid]+(data1$Th[upperid]-data1$Th[lowerid])*k

}

## combine all the parameters together using cbind() function

temp <- cbind(Po.N.cl,Po.cl,Po.tot)

seq10 <- subset(data1, X..of.length==0)[9,12,16]
seq90 <- subset(data1, X..of.length==100)[9,12,16]

temp <- rbind(seq10,temp,seq90)

final <- cbind(Treatment,Disease,Label,Seq1,Seq2,Seq,temp)
```

```
## use this only the first time, after first use comment out by insert
ing a # sign before "write"
#write.table(final,file="wholeCortiPerimetersScl.csv",row.names = F,se
p=",")

## use this for all subsequent data by removing # sign
write.table(final,file="wholeCortiPorosityScl.csv",row.names = F,appen
d = T,sep=",",col.names=F)
```

R script for generating the line graph of bone and BMAT parameters from 10- 90% of the tibial length

```
#################################################################
### A) Loading required libraries
#################################################################
library(lattice)
library(latticeExtra)

## Warning: package 'latticeExtra' was built under R version 4.4.2

#library(xlsx)
library(openxlsx)
library(readxl)
library(Hart et al.)

## Warning: package 'phia' was built under R version 4.4.2

## Loading required package: car

## Loading required package: carData

library(gridExtra)
library(devEMF)
library(car)
library(ggplot2)

##
## Attaching package: 'ggplot2'

## The following object is masked from 'package:latticeExtra':
##
##     layer

library(Cairo)

#################################################################
### B) Defining different panels/functions
#################################################################
pgfun <- function(mark) function(n) grid.text(label = mark, gp = gpar(
```

```
fontface=2),check.overlap = T,
                                                x = unit(0.0235, "npc"),
y = unit(0.96, "npc"))
avg <- function ( v ) {
  mean(v, na.rm=TRUE)}
sem <- function ( v ) {
  sd(v, na.rm=TRUE)/sqrt(length ( v ) - sum ( is.na ( v ) ))}
stripwhite <- strip.custom(bg="white", cex=0.7)

polygon.bands <- function(x, y, upper, lower, fill, col,
                          subscripts, ..., font, fontface){
  upper <- upper[subscripts]
  lower <- lower[subscripts]
  panel.polygon(c(x, rev(x)), c(upper, rev(lower)),
                col = adjustcolor(col,alpha=0.4), border = FALSE, ...)
  panel.xyplot(x,y,type=c("l"),lwd=3,col=col,...)}

########################################
### C define colours used for different groups
########################################
col1 <- "black"
col2 <- "chartreuse4"
col3 <- "hotpink2"
col4 <- "darkcyan"
col5 <- "red4"
##col6 <- "navy"
##col7 <- "darkred"

### D) Read in final data and calculating mean, SEM
############################################################
setwd("C:/Users/s2226418/Desktop/2D cortical Scl study")

final <- read.csv("wholeCortiboneScl.csv", h=T, stringsAsFactors = T)
levels(final$Treatment) <- list("CON"="CON","CONAb"="CONAb","CKD"="CKD
", "CKDAb"="CKDAb")

## create a function "MeanSE" to calculate mean+/-SE
MeanSE <- function(x) {
  tmp.avg <- aggregate(get(paste(x))~ Treatment + Seq, FUN=avg, na.act
ion=na.pass, data=final)
  tmp.SE <- aggregate(get(paste(x))~ Treatment + Seq, FUN=sem, na.acti
on=na.pass, data=final)
  ## get the column number of the mean and SE
  loc <- ncol(tmp.avg)
  ## create output file with mean and +/- SE
  df <- cbind(tmp.avg, (tmp.avg[,loc]-tmp.SE[,loc]),(tmp.avg[,loc]+tmp
.SE[,loc]))
  names(Chouinard et al.) <- c("Treatment","Seq","mean","low","high")
  ## remove 0-9% and 91-100% sequences
  df <- subset(df, Seq>=10&Seq<=90)
```

```
  return(Chouinard et al.)
}

## calculate all the mean and SE
T.Ar <- MeanSE("T.Ar")
B.Ar <- MeanSE("B.Ar")
B.ArT.Ar <- MeanSE("B.ArT.Ar")
T.Pm <- MeanSE("T.Pm")
B.Pm <- MeanSE("B.Pm")
B.PmB.Ar <- MeanSE("B.PmB.Ar")
Po.N <- MeanSE("Po.N")
Po.cl <- MeanSE("Po.cl")
Po.tot <- MeanSE("Po.tot")
MMI.polar <- MeanSE("MMI.polar")
MMI.max <- MeanSE("MMI.max")
MMI.min <- MeanSE("MMI.min")
Ecc <- MeanSE("Ecc")
Th <- MeanSE("Th")

#############################################################
### D) Plotting individual parameters
#############################################################

# create a "LineGraph" function that will draw 6 lines
LineGraph <- function(data,ylab,ymin,ymax) {
  # subset the data for the 6 lines
  df1 <- subset(data, Treatment=="CON")
  df2 <- subset(data, Treatment=="CONAb" )
  df3 <- subset(data, Treatment=="CKD" )
  df4 <- subset(data, Treatment=="CKDAb" )
  ##df5 <- subset(data, Treatment=="CON" & Age=="5wk")
  ##df6 <- subset(data, Treatment=="CKD" & Age=="5wk")

  # define the size for xy-ticks and xy-labels
  cex.tick <- 2
  cex.lab <- 2

  xyplot(mean ~ Seq,data=df1, col=col2,type="a",
         ylim=c(ymin,ymax),
         ylab=list(label=ylab, cex=cex.lab),
         ylist=(cex=cex.tick),
         xlab=list(label="Tibia length (%)", cex=cex.lab),
         scale=list(col=1,tck=c(1,0),alternating=1,
                    x=list(at=c(10,20,30,40,50,60,70,80,90),cex=cex.ti
ck)),
         panel=function(...){
           panel.xyplot(...)
           panel.polygon(border=F,col=col2, alpha=0.3,
                         x =c(df1$Seq, rev(df1$Seq)),
                         y =c(df1$high, rev(df1$low)))
```

```
            })+
    xyplot(mean ~ Seq,data=df2, col=col4,type="a",
            panel=function(...){
              panel.xyplot(...)
              panel.polygon(border=F,col=col4, alpha=0.3,
                            x =c(df2$Seq, rev(df2$Seq)),
                            y =c(df2$high, rev(df2$low)))
            })+
    xyplot(mean ~ Seq,data=df3, col=col3,type="a",
            panel=function(...){
              panel.xyplot(...)
              panel.polygon(border=F,col=col3, alpha=0.3,
                            x =c(df3$Seq, rev(df3$Seq)),
                            y =c(df3$high, rev(df3$low)))
            })+
    xyplot(mean ~ Seq,data=df4, col=col5,type="a",
            panel=function(...){
              panel.xyplot(...)
              panel.polygon(border=F,col=col5, alpha=0.3,
                            x =c(df4$Seq, rev(df4$Seq)),
                            y =c(df4$high, rev(df4$low)))
            })
}


#### T.Ar
# use LineGraph()function to plot the data
plot_T.Ar <- LineGraph(data=T.Ar, ylab=expression(paste("T.Ar (mm"^{"2
"}, ")")), ymin=0, ymax=2)

svg("T.Ar.svg",width=14,height=7)
print(plot_T.Ar)
dev.off()

## png
##   2

#### B.Ar
plot_B.Ar <- LineGraph(data=B.Ar, ylab=expression(paste("B.Ar (mm"^{"2
"}, ")")), ymin=0.4, ymax=2)

svg("B.Ar.svg",width=14,height=7)
print(plot_B.Ar)
dev.off()

## png
##   2

#### B.ArT.Ar
plot_B.ArT.Ar <- LineGraph(data=B.ArT.Ar, ylab=("B.ArT.Ar (%)"), ymin=
98, ymax=100)
```

```
svg("B.ArT.Ar.svg",width=14,height=7)
print(plot_B.ArT.Ar)
dev.off()

## png
##   2

#### T.Pm
# use LineGraph()function to plot the data
plot_T.Pm <- LineGraph(data=T.Pm, ylab=("T.Pm (mm)"), ymin=-0.5, ymax=
10.5)

svg("T.Pm.svg",width=14,height=7)
print(plot_T.Pm)
dev.off()

## png
##   2

#### B.Pm
# use LineGraph()function to plot the data
plot_B.Pm <- LineGraph(data=B.Pm, ylab=("B.Pm (mm)"), ymin=-1, ymax=31
)

svg("B.Pm.svg",width=14,height=7)
print(plot_B.Pm)
dev.off()

## png
##   2

#### B.PmB.Ar
# use LineGraph()function to plot the data
plot_B.PmB.Ar <- LineGraph(data=B.PmB.Ar, ylab=("B.PmB.Ar (1/mm)"), ym
in=-1, ymax=40)

svg("B.PmB.Ar.svg",width=14,height=7)
print(plot_B.PmB.Ar)
dev.off()

## png
##   2

plot_Po.N <- LineGraph(data=Po.N, ylab=("Porosity number"), ymin=-5, y
max=120)

svg("Po.N.svg",width=14,height=7)
print(plot_Po.N)
dev.off()
```

```
## png
##   2

plot_Po.cl <- LineGraph(data=Po.cl, ylab=("Close Porosity (%)"), ymin=
-0.2, ymax=1)

svg("Po.cl.svg",width=14,height=7)
print(plot_Po.cl)
dev.off()

## png
##   2

plot_Po.tot <- LineGraph(data=Po.tot, ylab=("Total Porosity (%)"), ymi
n=0, ymax=2)

svg("Po.tot.svg",width=14,height=7)
print(plot_Po.tot)
dev.off()

## png
##   2

#### MMI.polar
# use LineGraph()function to plot the data
plot_MMI.polar <- LineGraph(data=MMI.polar, ylab=expression(paste(ital
ic(J), " (mm"^{"4"}, ")")), ymin=0, ymax=2)

svg("MMI.polar.svg",width=14,height=7)
print(plot_MMI.polar)
dev.off()

## png
##   2

#### MMI.max
# use LineGraph()function to plot the data
plot_MMI.max <- LineGraph(data=MMI.max, ylab=expression(paste("MMI.max
(mm"^{"4"}, ")")), ymin=0, ymax=1)

svg("MMI.max.svg",width=14,height=7)
print(plot_MMI.max)
dev.off()

## png
##   2

#### MMI.min
# use LineGraph()function to plot the data
plot_MMI.min <- LineGraph(data=MMI.min, ylab=expression(paste("MMI.min
(mm"^{"4"}, ")")), ymin=0, ymax=1)
```

```
svg("MMI.min.svg",width=14,height=7)
print(plot_MMI.min)
dev.off()

## png
##   2

#### Ecc
# use LineGraph()function to plot the data
plot_Ecc <- LineGraph(data=Ecc, ylab=("Eccentricity"), ymin=0.2, ymax=
1)

svg("Ecc.svg",width=14,height=7)
print(plot_Ecc)
dev.off()

## png
##   2

#### Th
# use LineGraph()function to plot the data
plot_Th <- LineGraph(data=Th, ylab=("Thickness (mm)"), ymin=0, ymax=0.
5)

svg("Th.svg",width=14,height=7)
print(plot_Th)
dev.off()

## png
##   2
```

R script for statistical testing and p-value heatmaps of bone and BMAT parameters along the tibial length from 2D analysis

```
### A) Loading required libraries
#################################################################
#library(xlsx)
library(readxl)
library(openxlsx)
library(car)

## Loading required package: carData

library(Hart et al.)

## Warning: package 'phia' was built under R version 4.4.2

library(gplots)
```

```
##
## Attaching package: 'gplots'

## The following object is masked from 'package:stats':
##
##     lowess

library(RColorBrewer)

#####################################################################
### B) Calculating 2-way ANOVA p values: main effects & interaction
###    Normality, post-hoc comparison
#####################################################################
setwd("C:/Users/s2226418/Desktop/2D cortical Scl study")

final <- read.csv("wholeCortiboneScl1.csv", h=T, stringsAsFactors = T)

levels(final$Treatment) <- list("Ab"="Ab","PBS"="PBS")
#final$Disease <- as.factor(final$Disease)
str(final)

## 'data.frame':    4040 obs. of  20 variables:
##  $ Treatment: Factor w/ 2 levels "Ab","PBS": 1 1 1 1 1 1 1 1 1 1 ..
.
##  $ Disease  : Factor w/ 2 levels "ckd","con": 1 1 1 1 1 1 1 1 1 1 .
..
##  $ Label    : int  5182 5182 5182 5182 5182 5182 5182 5182 5182 518
2 ...
##  $ Seq1     : num  NA 0.978 1.986 2.993 4 ...
##  $ Seq2     : num  NA 1.01 2.01 3.02 4.03 ...
##  $ Seq      : int  0 1 2 3 4 5 6 7 8 9 ...
##  $ T.Ar     : num  0 0.0812 0.4807 1.0943 1.2827 ...
##  $ B.Ar     : num  0 0.0808 0.4739 1.0706 1.2581 ...
##  $ B.ArT.Ar : num  0 99.5 98.6 97.8 98.1 ...
##  $ T.Pm     : num  0 2.18 13.41 28.77 34.63 ...
##  $ B.Pm     : num  0 2.3 15.3 35.3 40.8 ...
##  $ B.PmB.Ar : num  0 28.5 32.3 33 32.5 ...
##  $ Po.N     : num  0 2.5 30 100.8 88 ...
##  $ Po.cl    : num  0 0.309 0.502 0.872 0.529 ...
##  $ Po.tot   : num  0 0.503 1.424 2.167 1.917 ...
##  $ MMI.polar: num  0 0.00519 0.64944 1.71933 2.09344 ...
##  $ MMI.max  : num  0 0.00509 0.53608 1.03037 1.15673 ...
##  $ MMI.min  : num  0 0.000104 0.113367 0.688957 0.93671 ...
##  $ Ecc      : num  0 0.99 0.888 0.576 0.436 ...
##  $ Th       : num  0 0.0702 0.0619 0.0607 0.0616 ...

Traits <- c("B.Ar")

### setup dataframe to save the p-values
p.values <- list()
for (i in Traits) {
```

```
  p.values[[i]] <- data.frame(matrix(data=NA,nrow=100,ncol=9))
  p.values[[i]][,1] <- seq(1:100)
  names(p.values[[i]]) <- c("Seq","Treatment", "Disease", "Interaction
",
                            "Normality",
                            "Ab - PBS ckd",
                            "Ab - PBS con",
                            "con - ckd Ab",
                            "con - ckd PBS")
}

for(i in 10:90){
  for (j in Traits) {
    ## two-way ANOVA analysis using lm() function
    tmp <- lm(get(paste(j)) ~ Treatment + Disease + Treatment:Disease,
data=final,subset=(Seq==i))
    ## save p-values for effects of treatment, sex and their interacti
on
    p.values[[j]][i,2:4] <- Anova(tmp, type="II")$"Pr(>F)"[1:3]
    ## p-value for normality of residuals
    p.values[[j]][i,5]<- shapiro.test(resid(tmp))$p.value
    ## p-values for posthoc comparison
    # at specific age, what's he difference between control and PAE
    p.values[[j]][i,6:7] <- testInteractions(tmp, fixed=c("Disease"),p
airwise="Treatment", adjustment="none")$"Pr(>F)"[1:2]
    # at specific treatment condition what's the difference between ma
le and female
    p.values[[j]][i,8:9] <- testInteractions(tmp, fixed=c("Treatment")
,pairwise="Disease", adjustment="none")$"Pr(>F)"[1:2]
    rm(tmp)
  }
}

# save the p-values into Excel file
for (i in Traits) {
write.xlsx(p.values[[i]], "BArPValues.xlsx",sheetName=i,append=T)
}

############################################################
### C) Defining heatmap parameters
############################################################

## set up colour scheme
myCol2 <- c("red","yellow", "green", "blue")
myBreaks2 <- c(0,0.001,0.01,0.05, 1)


#### B.Ar
p_val <- read.xlsx("BArPValues.xlsx")
```

```
svg(file = "BAr_pvalueheatmap_LR.svg", width = 14, height = 2)
## p-value from the two-way ANOVA analysis (columns 3-6)
heatmap.2(t(as.matrix(p_val[10:90,2:4])),key=F,
          col=myCol2,breaks=myBreaks2,cexRow=1, cexCol=1,
          symm=F,dend="none",trace="none",scale="none",
          labCol="",labRow=c("Trt","Dis","Trt*Dis"),Colv=F,Rowv=F)
dev.off()

## png
##   2

svg(file = "BAr_pvalueheatmap_LR2.svg", width = 14, height = 2)
## p-values from post-hoc comparison (columns 7-10)
heatmap.2(t(as.matrix(p_val[10:90,6:9])),key=F,
          col=myCol2,breaks=myBreaks2,cexRow=1, cexCol=1,
          symm=F,dend="none",trace="none",scale="none",
          labCol="",labRow=c("ckd Ab - PBS",
                             "con Ab - PBS",
                             "con - ckd Ab",
                             "con - ckd PBS"),Colv=F,Rowv=F)
dev.off()

## png
##   2
```